



The  
University  
Of  
Sheffield.

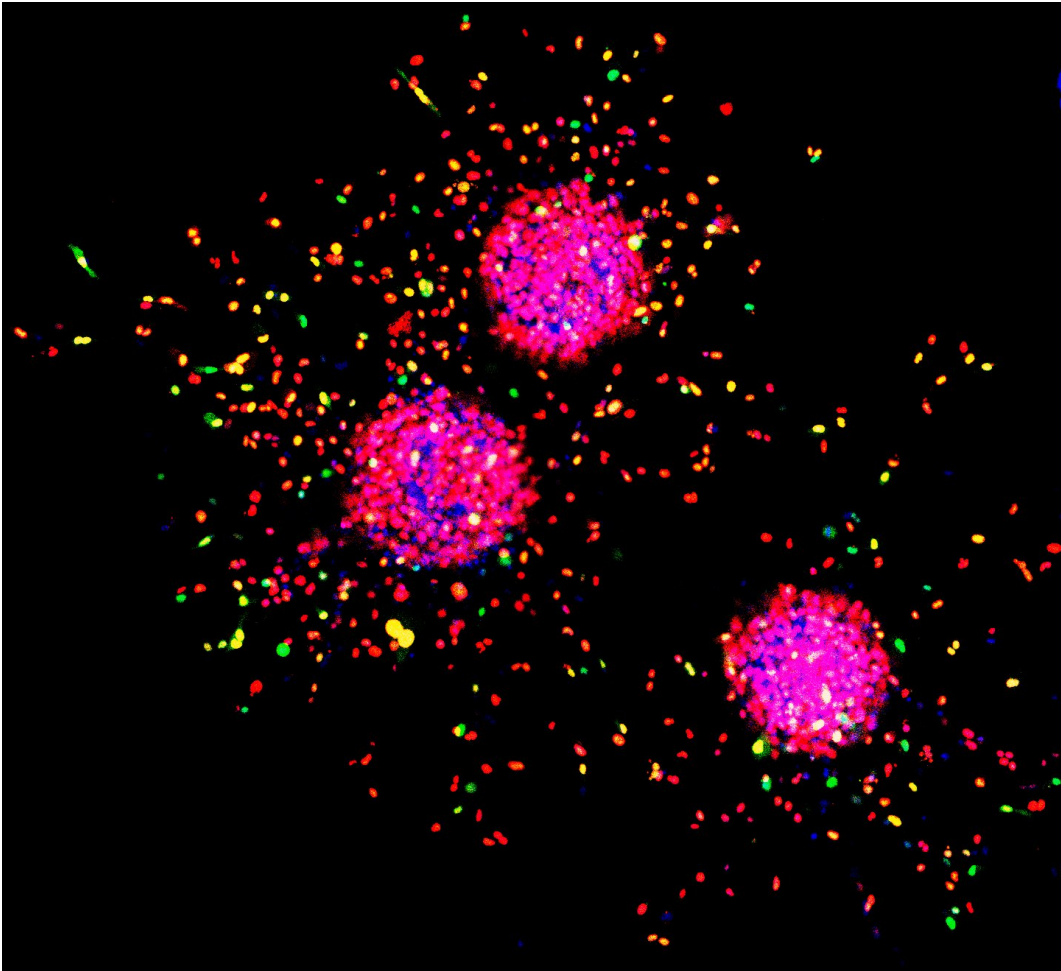
# **The role of ECM internalization in breast cancer cell migration and invasion**

**Keqian Nan**

A thesis submitted in partial fulfilment of the requirements for the degree of  
Doctor of Philosophy

The University of Sheffield  
Faculty of Science  
School of Bioscience

March 2022



## Abstract

The extracellular matrix (ECM) is an important component of the tumour microenvironment (TME) and comprised of a network of biochemically distinct components, including collagens, proteoglycans and glycoproteins. The ECM is continually undergoing a remodelling process, as a consequence of a fine balance between matrix synthesis, deposition and degradation. Increasing evidence demonstrates that dysregulated ECM remodelling is a key player in regulating the development of breast cancer. So far, two mechanisms are known to be participated in ECM degradation. One is extracellular degradation mainly mediated by matrix metalloproteases (MMPs). The other pathway is lysosomal degradation after receptor-mediated ECM uptake. Compared to proteolytic degradation, the role of ECM endocytosis and intracellular degradation in breast cancer is still poorly understood.

Here we revealed the contribution of integrin-dependent ECM endocytosis in breast cancer cell migration and invasion. We used two different, but complementary approaches showing that  $\alpha 2\beta 1$  integrin is required for the internalization of ECM in breast cancer cells. Moreover, the interactions between ECM components and  $\alpha 2\beta 1$  results in the internalization of  $\alpha 2\beta 1$  in breast cancer cells. Furthermore, we showed that the inhibition of  $\alpha 2\beta 1$  leads to a significant decrease both in breast cancer cell migration and invasion. We therefore suggest that  $\alpha 2\beta 1$ -dependent ECM endocytosis contributes to the migration and invasion of breast cancer cells. Additionally, we found that the internalization of laminin is upregulated in G1 phase in breast cancer cells. This cell cycle-dependent ECM internalization might be mediated by  $\beta 1$  integrin, contributing to the activation of mTORC1 in G1. Taken together, our findings highlight the contribution of integrin-dependent ECM internalization in the development of breast cancer, suggesting that ECM intracellular degradation might be one of the novel therapeutic targets in breast cancer treatment in the future.

## Acknowledgement

My gratitude goes first and foremost to my supervisor, Dr Elena Rainero, for her constant support, patience and exceptional expertise throughout my PhD. Most of this work would not have been completed without her help and for that, I am really grateful!

I want to thank my advisors Dr Kyra Campbell and Professor Andrew Furley for their advice. I would also like to warmly thank all the staff at Wolfson Light Microscopy Facility for their help with microscopy: Dr Darren Robinson, Dr Nick van Hateren and Dr Christa Walther. I want to thank Dr Mark Collins at Mass Spectrometry Centre, for his support to my mass spectrometry work. In addition, I would like to thank Susan Clark for her help to my cell cycle experiments.

I extend my gratitude to everyone from KA/SW/ER/HM group, for their emotional and moral support during my PhD. Special thanks go to Mona, Montse, Bian, Sherry, Shahd, Rechele, Haya, Stella. I am deeply indebted with you for your continued help, as much in the TC as outside of it, endless hours of jokes and friendships that I am pretty sure will last way beyond my time at B2 floor.

Finally, my thanks go to my family for their encourage and support throughout my PhD, and a big hug to my beautiful wife, Lan Hou, who is always by my side and organized important family schedules. I love you!

## **Declaration**

I, Keqian Nan, declare that this thesis is my own work and that where it is supported by others has been acknowledged. I confirm that this thesis has not been submitted for the award of a degree at the University of Sheffield. I confirm that where I have quoted from the work of others, the source is always given.

Keqian Nan

28/03/2022

# Table of content

<b>Abstract.....</b>	<b>2</b>
<b>Acknowledgement.....</b>	<b>2</b>
<b>Declaration.....</b>	<b>3</b>
<b>Table of content .....</b>	<b>4</b>
<b>List of Figures .....</b>	<b>7</b>
<b>List of tables .....</b>	<b>11</b>
<b>Abbreviations.....</b>	<b>12</b>
<b>1 Chapter 1: Introduction.....</b>	<b>15</b>
1.1 Breast Cancer .....	15
1.1.1 Epidemiology .....	15
1.1.2 Progression .....	15
1.1.3 Causative factors .....	18
1.1.3.1 Genetic predisposition .....	18
1.1.3.2 Acquired alterations.....	21
1.1.3.3 Lifestyle risk factors.....	23
1.1.4 Types of breast cancer.....	24
1.1.5 Treatment of breast cancer .....	26
1.1.5.1 Treatment for non-invasive breast cancer .....	26
1.1.5.2 Treatment for invasive breast cancer .....	26
1.2 Extracellular matrix .....	29
1.2.1 Primary components in ECM .....	29
1.2.1.1 Collagens .....	29
1.2.1.2 Fibronectin .....	31
1.2.1.3 Basement membrane.....	33
1.2.2 Receptors of ECM components .....	34
1.2.2.1 Integrins .....	34
1.2.2.2 Other receptors.....	37
1.2.3 Functions of the ECM.....	38
1.2.4 ECM remodelling in breast cancer .....	40
1.3 ECM internalization in cancer progression.....	44
1.3.1 Collagen I .....	44
1.3.2 Fibronectin.....	46
1.3.3 Laminin .....	47
1.4 The role of integrin endocytosis and trafficking in cell migration.....	48
1.5 Aims of the thesis.....	50

<b>2</b>	<b>Materials and methods .....</b>	<b>51</b>
2.1	Materials .....	51
2.1.1	Reagents .....	51
2.1.2	Solutions .....	54
2.2	Methods .....	54
2.2.1	Cell culture maintenance .....	54
2.2.2	2D ECM internalization assay .....	55
2.2.3	Cell-derived matrix generation .....	57
2.2.4	CDM internalization assay .....	57
2.2.5	siRNA-mediated knockdown of $\alpha 2$ integrin .....	58
2.2.6	Cell migration assay on CDM .....	60
2.2.7	3D spheroid invasion assay .....	60
2.2.8	Serum starvation .....	61
2.2.9	Double thymidine block .....	62
2.2.10	CDK4/6 inhibition .....	62
2.2.11	Cell cycle analysis by flow cytometry .....	62
2.2.12	Matrigel internalization with GM6001 .....	63
2.2.13	Measurement of macropinocytosis .....	63
2.2.14	Measurement of $\beta 1$ integrin internal pool .....	63
2.2.15	Measurement of mTORC1 activity .....	63
2.2.16	Immunofluorescence .....	64
2.2.17	Mass spectrometry analysis .....	65
2.2.17.1	Preparation of protein samples .....	65
2.2.17.2	Western blotting .....	66
2.2.17.3	Streptavidin-agarose beads pulldown and washing procedure .....	68
2.2.17.4	On-beads digestion .....	68
2.2.17.5	Desalting and drying of digested peptides .....	69
2.2.17.6	Data analysis .....	69
2.2.18	Imaging and analysis .....	70
2.2.18.1	2D ECM internalization assay .....	70
2.2.18.2	Colocalization assay .....	72
2.2.18.3	Measure the effectiveness of $\alpha 2$ knockdown .....	72
2.2.18.4	$\beta 1$ integrin and $\alpha 2$ integrin internalization assay .....	72
2.2.18.5	Cell migration assay .....	73
2.2.18.6	3D spheroids invasion assay .....	73
2.2.19	Statistical analysis .....	74
<b>3</b>	<b><math>\alpha 2\beta 1</math>-dependent ECM uptake promotes breast cancer cell migration and invasion ..</b>	<b>75</b>
3.1	Introduction .....	75
3.2	Results .....	77
3.2.1	CDM internalization is upregulated in invasive breast cancer cells .....	77
3.2.2	Collagen I internalization is not upregulated in invasive breast cancer cells .....	79
3.2.3	Matrigel internalization is upregulated in invasive breast cancer cells .....	81
3.2.4	Internalized Matrigel is trafficked through early and late endosomes/lysosomes .....	83
3.2.5	$\beta 1$ integrin is required for ECM internalization .....	88
3.2.6	$\alpha 2$ , but not $\alpha 3$ and $\alpha 6$ , is required for ECM uptake in invasive breast cancer cells .....	90
3.2.7	$\alpha 2\beta 1$ integrin knock-down reduced ECM uptake in invasive breast cancer cells .....	96
3.2.8	Collagen I and Matrigel binding induces $\alpha 2\beta 1$ integrin activation and endocytosis .....	99
3.2.9	$\alpha 2\beta 1$ integrin is required for MDA-MB-231 cell migration .....	103
3.2.10	$\alpha 2\beta 1$ integrin is required for MDA-MB-231 cell invasion .....	108

3.3	Discussion.....	116
<b>4</b>	<b>ECM component uptake is cell cycle-dependent in invasive breast cancer cells .....</b>	<b>121</b>
4.1	Introduction .....	121
4.2	Results .....	126
4.2.1	CDM internalization is upregulated in G1 phase MDA-MB-231 cells .....	126
4.2.2	Matrigel uptake is increased in G1 phase in invasive breast cancer cells .....	127
4.2.3	Matrigel uptake is not affected by the cell cycle in normal mammary epithelial cells.....	136
4.2.4	Laminin, but not collagen IV, uptake is upregulated in G1 invasive breast cancer cells .....	138
4.2.5	MMP inhibition might affect cell cycle-dependent ECM uptake .....	140
4.2.6	Macropinocytosis is slightly affected by the cell cycle in invasive breast cancer cells .....	142
4.2.7	$\beta$ 1 Integrin traffic is upregulated in the G1 phase in invasive breast cancer cells.....	143
4.2.8	Serum starvation regulates $\beta$ 1 integrin trafficking .....	145
4.2.9	Increased Matrigel uptake supports mTORC1 activity in G1 phase.....	146
4.3	Discussion.....	148
<b>5</b>	<b>A proteomic approach to identify internalized ECM components .....</b>	<b>153</b>
5.1	Introduction .....	153
5.2	Results .....	154
5.2.1	The detection of internalized CDM by western blotting .....	154
5.2.2	Detection of internalized proteins by streptavidin-agarose pulldown assay .....	156
5.2.3	Identification of internalized proteins by mass spectrometry.....	158
5.2.4	Identification of internalized proteins in MDA-MB-231 and MCF10A cells.....	172
5.3	Discussion.....	173
<b>6</b>	<b>General Discussion .....</b>	<b>178</b>
6.1	Summary of key findings .....	178
6.2	The identification of internalized ECM components in breast cancer cells .....	179
6.3	Cell cycle-dependent ECM uptake in breast cancer cells .....	182
6.4	Therapeutic opportunities.....	184
6.5	Conclusion and future directions .....	185
<b>7</b>	<b>References .....</b>	<b>187</b>

# List of Figures

## Chapter 1:

Figure 1.1 Anatomy of breast .....	16
Figure 1.2 Progression of ductal breast cancer .....	17
Figure 1.3 HER2 signalling and ER signalling pathway in breast cancer .....	23
Figure 1.4 Breast cancer survival rates in Canada .....	26
Figure 1.5 Breast cancer treatment among US female with invasive breast cancer by 2016	27
Figure 1.6 The process of collagen type I synthesis.....	31
Figure 1.7 Structure of fibronectin .....	32
Figure 1.8 Structure of laminin and the BM .....	34
Figure 1.9 Integrin heterodimers and interaction with ECM.....	35
Figure 1.10 Integrin endocytosis and trafficking pathways.....	37
Figure 1.11 Functions of the ECM .....	39
Figure 1.12 ECM remodelling in cancer development .....	42
Figure 1.13 The internalization pathways of main ECM components.....	44

## Chapter 2:

Figure 2.1 Schematic representation of CDM internalization protocol.....	58
Figure 2.2 Schematic representation of siRNA-mediated $\alpha 2$ knockdown.....	59
Figure 2.3 Schematic representation of 3D spheroids invasion assay protocol .....	61
Figure 2.4 Schematic representation of mass spectrometry proteomics protocol .....	66
Figure 2.5 Schematic representation of transfer stack structure.....	67
Figure 2.6 Schematic representation of ECM internalization analysis protocol.....	71
Figure 2.7 Schematic representation of cell invasion analysis protocol.....	73

## Chapter 3:

Figure 3.1 CDM internalization is upregulated in MDA-MB-231 cells .....	78
Figure 3.2 CDM internalization is upregulated in PyMT#1 cells .....	79
Figure 3.3 Collagen I uptake is not upregulated in MDA-MB-231 cells .....	80
Figure 3.4 Collagen I uptake is not upregulated in PyMT#1 cells .....	81
Figure 3.5 Matrigel uptake is increased in MDA-MB-231 cells.....	82

Figure 3.6 Matrigel uptake is upregulated in PyMT#1 cells .....	83
Figure 3.7 Internalized Matrigel is delivered and exited of the early endosomes .....	85
Figure 3.8 Internalized Matrigel is delivered to the late endosomes/lysosomes.....	87
Figure 3.9 $\beta 1$ integrin is trafficked together with internalized Matrigel in breast cancer cells .....	89
Figure 3.10 $\beta 1$ integrin is required for Matrigel uptake in breast cancer cells.....	90
Figure 3.11 The $\alpha 2\beta 1$ integrin is required for CDM and collagen I internalization in breast cancer cells .....	92
Figure 3.12 The $\alpha 2\beta 1$ integrin is required for Matrigel, laminin and collagen IV internalization in breast cancer cells .....	94
Figure 3.13 $\alpha 3$ integrin is not required for collagen I and Matrigel internalization in breast cancer cells .....	95
Figure 3.14 $\alpha 6$ integrin is not required for Matrigel internalization in breast cancer cells....	96
Figure 3.15 The $\alpha 2\beta 1$ integrin is required for collagen I and Matrigel internalization in breast cancer cells .....	98
Figure 3.16 The $\alpha 2\beta 1$ integrin is trafficked together with Matrigel in breast cancer cells.....	99
Figure 3.17 Collagen I and Matrigel binding can induce $\alpha 2\beta 1$ integrin endocytosis in breast cancer cells .....	100
Figure 3.18 Collagen I and Matrigel binding might induce $\alpha 2\beta 1$ integrin activation and uptake in breast cancer cells .....	103
Figure 3.19 $\alpha 2\beta 1$ integrin contributes to MDA-MB-231 cell migration.....	105
Figure 3.20 $\alpha 2\beta 1$ integrin promotes MDA-MB-231 cell migration.....	107
Figure 3.21 3D model supports the invasion of MDA-MB-231 cells in matrices .....	109
Figure 3.22 $\alpha 2\beta 1$ integrin facilitates MDA-MB-231 cell invasion .....	110
Figure 3.23 $\alpha 2\beta 1$ integrin contributes to MDA-MB-231 cell invasion.....	112
Figure 3.24 $\alpha 2\beta 1$ integrin facilitates MDA-MB-231 cell invasion .....	113
Figure 3.25 Green cell tracker staining makes MDA-MB-231 cells less invasive .....	115
Figure 3.26 Schematic to summarize $\alpha 2\beta 1$ integrin-dependent ECM endocytosis.....	116

## Chapter 4:

Figure 4.1 Diagram of cell cycle progression .....	122
--	-----

Figure 4.2 Dynamic colour change of FUCCI-MDA-MB-231 cells .....	125
Figure 4.3 CDM uptake is enhanced in serum starved MDA-MB-231 cells .....	127
Figure 4.4 Matrigel, but not collagen I, internalization is upregulated in serum starved MDA-MB-231 cells .....	128
Figure 4.5 Matrigel, but not collagen I, uptake is upregulated in serum starved PyMT#1 cells .....	130
Figure 4.6 Matrigel, but not collagen I, uptake is increased in Palbociclib (Pb) treated MDA-MB-231 cells .....	132
Figure 4.7 Matrigel, but not collagen I, uptake is upregulated in DTB synchronized MDA-MB-231 cells.....	134
Figure 4.8 Matrigel uptake is increased in G1 phase FUCCI-MDA-MB-231 cells .....	136
Figure 4.9 Matrigel internalization is not cell cycle dependent in NMuMG cells.....	137
Figure 4.10 Laminin and collagen IV internalization is enhanced in serum starved MDA-MB-231 cells.....	139
Figure 4.11 The internalization of laminin is promoted in DTB synchronized MDA-MB-231 cells.....	140
Figure 4.12 MMP inhibition does not affect increased Matrigel uptake in serum starved MDA-MB-231 cells.....	141
Figure 4.13 MMP activity affects upregulated Matrigel internalization in Pb treated MDA-MB-231 cells .....	142
Figure 4.14 Macropinocytosis is slightly upregulated in DTB synchronized MDA-MB-231 cells .....	143
Figure 4.15 $\beta$ 1 integrin endocytosis is upregulated in serum starved MDA-MB-231 cells...	144
Figure 4.16 $\beta$ 1 integrin endocytosis is upregulated in Pb treated MDA-MB-231 cells.....	145
Figure 4.17 $\beta$ 1 integrin endocytosis is increased in MDA-MB-231 cells after a 2-hour serum starvation .....	146
Figure 4.18 mTORC1 activity is increased in serum starved MDA-MB-231 cells on Matrigel .....	147
Figure 4.19 mTORC1 activity is increased in Pb treated MDA-MB-231 cells on Matrigel ....	148
Figure 4.20 Schematic to summarize the cell cycle-dependent ECM uptake.....	149

## Chapter 5:

Figure 5.1 Internalized CDM can be detected by western blotting using streptavidin .....	155
Figure 5.2 Detection of internalized proteins using streptavidin-agarose pulldown assay..	157
Figure 5.3 Identification of internalized proteins and integrins using mass spectrometry ..	158
Figure 5.4 Identification of internalized ECM proteins using mass spectrometry.....	160
Figure 5.5 Identification of integrins using mass spectrometry .....	162
Figure 5.6 Internalized CDM components are accumulated in the late endosomes/lysosomes .....	163
Figure 5.7 Western blotting results of internalized CDM in MDA-MB-231 cells and MCF10A cells.....	172
Figure 5.8 Integrins may be the major receptors responsible for the endocytosis of CDM.....	173

## Chapter 6:

Figure 6.1 Mechanism of $\alpha 2\beta 1$ -dependent ECM internalization in regulating breast cancer cell migration and invasion.....	179
--	-----

## List of tables

### Chapter 1:

Table 1.1 TNM breast cancer staging system .....	18
Table 1.2 Breast cancer susceptibility genes .....	21
Table 1.3 Major therapy of metastatic breast cancer .....	28

### Chapter 2:

Table 2.1 Reagents and suppliers .....	51
Table 2.2 Recipes of solutions .....	54
Table 2.3 List of integrin subunit inhibitors/function blocking antibodies.....	56
Table 2.4 siRNA participating in $\alpha 2$ integrin knockdown.....	59
Table 2.5 List of antibodies in immunofluorescence.....	64
Table 2.6 List of antibodies in western blotting .....	68

### Chapter 5:

Table 5.1 List of upregulated ECM proteins in biotinylated CDM .....	161
Table 5.2 List of ECM proteins presented in the screen.....	164

## Abbreviations

ACN	Acetonitrile
ADH	Atypical ductal hyperplasia
ALH	Atypical lobular hyperplasia
BCS	Breast-conserving surgery
BM	Basement membrane
CAF	Cancer-associated fibroblast
CDK	Cyclin-dependent kinase
CDKs	Cyclin-dependent kinases
CDM	Cell-derived matrix
CIE	Clathrin-independent endocytosis
CME	Clathrin-mediated endocytosis
CTCs	Circulating tumour cells
DCIS	Ductal carcinoma <i>in situ</i>
DDRs	Discoidin domain receptors
DMEM	Dulbecco's modified Eagle medium
DQ-collagen IV	Dye-quenched collagen IV
DTB	Double thymidine block
EEA1	Early endosomal antigen 1
EEs	Early endosomes
EGF	Epidermal growth factor
EMILIN-1	Elastin microfibril interface-1
EMT	Epidermal growth factor
ESCRT	Endosomal sorting complex required for transport
FA	Focal adhesion
FACITs	Fibril-associated collagens with interruptions in triple helices
FBS	Foetal bovine serum
FEA	Flat epithelial atypia
FGFs	Fibroblast growth factors

FMNL2	formin-like 2
FRET	Fluorescence Resonance Energy Transfer
FUCCI	Fluorescent Ubiquitin Cell Cycle Indicator
GAPs	GTPases activating-proteins
GEFs	Guanine nucleotide exchange factors
GFs	Growth factors
GWAS	Genome wide association studies
HA	Hyaluronic acid
HS	Horse serum
IAA	Iodoacetamide
ICAT	Isotope-coded affinity tags
IDC	Invasive ductal carcinoma
ILC	Invasive lobular carcinoma
ILVs	Intraluminal vesicles
LAMP1/2	Lysosomal-associated membrane protein 1/2
LCIS	Lobular carcinoma <i>in situ</i>
LF 2000	Lipofectamine 2000
LIMP-2	Lysosome integral membrane protein 2
LOX	Lysyl oxidase
MAPK	Mitogen-activated protein kinase
MesNa	Sodium 2-mercaptoethanesulfonate
MMPs	Matrix metalloproteinases
MMTV-PyMT	Mammary tumour virus-polyoma middle T antigen
MMTV	Mouse mammary tumour virus
MT1-MMP	Membrane type 1 MMP
mTOR	Mechanistic target of Rapamycin
mTORC1	Mammalian Target of Rapamycin Complex 1
MVBs	Multivesicular bodies
N-WASP	neural-Wiskott-Aldrich Syndrome protein
PARP	Poly (ADP-ribose) polymerase

Pb	Palbociclib
PBS <sup>++</sup>	PBS containing CaCl <sub>2</sub> and MgCl <sub>2</sub>
PDAC	Pancreatic ductal adenocarcinoma
Pen/Strep	Penicillin/Streptomycin
PFA	Paraformaldehyde
PFS	Progression-free survival
PI	Propidium Iodide
PNRC	Perinuclear recycling compartment
PR	Progesterone receptor
PyMT	Polyoma virus middle T antigen
Rb	Retinoblastoma
ROCK	RHO-associated protein kinase
RT	Radiation therapy
RTKs	Receptor tyrosine kinases
S6	Ribosomal subunit S6
S6K	Ribosomal S6 kinase
SAPA	Streptavidin-agarose pulldown assay
TCA	Tricarboxylic acid
TCEP	Tris(2-carboxyethyl) phosphine hydrochloride
TFA	Trifluoroacetic acid
TGF-β	Transforming growth factor-β
TGFBI	Transforming growth factor beta-induced
TIFs	Telomerase-immortalised human dermal fibroblasts
TME	Tumour microenvironment
TNBC	Triple negative breast cancer
TNC	Tenascin-C
TNfn	Fibronectin type III-like repeats
TSP-1	Thrombospondin 1
YAP	Yes-associated protein
ZO-1	Zonula occludens-1

# Chapter 1: Introduction

## 1.1 Breast Cancer

### 1.1.1 Epidemiology

Breast cancer is one of the three most common cancers, along with lung and colon cancers. In 2019, approximately 2.1 million new breast cancer cases were diagnosed worldwide, about one new case diagnosed each 18 seconds (Harbeck et al., 2019). Breast cancer rates are higher among women in more developed countries, but rates are increasing almost in all countries. Breast cancer survival rates are significantly higher in developed countries, with an estimated 5-year survival of 80% for high-income regions compared to below 40% in low-income regions (Akram et al., 2017). These data reflect both the risk factors of breast cancer and the standard of care for disease diagnosis and treatment. In North America and European countries, breast cancer is usually diagnosed at an early stage. Over the past 5 years, mortality in European countries has dropped by 5% for patients with an early-stage diagnosis. Nevertheless, breast cancer is one of the most common causes of cancer-related death among women in countries with advanced care. In contrast, breast cancer is generally diagnosed at a later stage in Africa and developing Asian countries, which is accompanied by poorer survival. Consequently, breast cancer is still the first leading cause of cancer-related death among women in less developed regions (Harbeck and Gnant, 2017).

### 1.1.2 Progression

The mammary gland is the functional unit of the breast, surrounded by adipose tissue. Female mammary gland has 12-20 lobes located beneath the nipple-areola complex which are further divided into smaller lobules. These lobes and lobules are connected by ducts. The ducts and lobules are composed of two cell types: an inner layer of luminal epithelial cells and an outer layer of myoepithelial cells. These cells are surrounded by a laminin-rich basement membrane (BM) (Figure 1.1) (Akram et al., 2017). As a specialized sheet-like extracellular matrix (ECM), the BM not only serves as physical barrier to the potential pathogenic cell migration, but also provides signals to the epithelium to regulate its morphogenesis and proliferation. Luminal epithelial cells are typically characterized by apical-basal polarity. The apical membrane lines

the lumen whereas basal surface interacts with ECM through plasma membrane receptors, including members of the integrin family (see below 1.2.2.1). Luminal cells are bound laterally to neighbours by tight and adherens junctions. Epithelial cell polarity is fundamental for tissue architecture and function (Roignot et al., 2013).

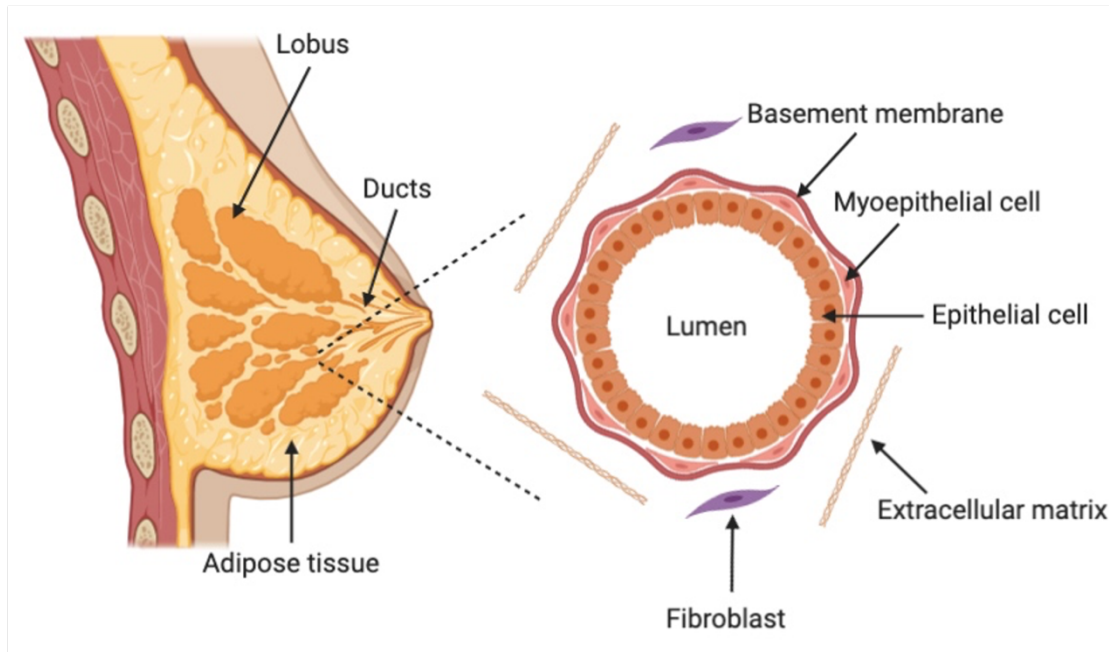


**Figure 1.1 Anatomy of breast.** The ducts and lobules consist of epithelial cells and myoepithelial cells. These cells are separated from surrounding stroma by basement membrane. Figure is adapted from (Harbeck et al., 2019).

Approximately 90-95% of breast cancers appear to evolve from the luminal epithelial cells, with the ductal subtype accounting for 60-85% of all diagnosed cases. Less commonly, breast cancer can arise from the stromal cells, such as myofibroblasts and blood vessel cells (Feng et al., 2018). In the model of ductal subtype progression, breast carcinomas originate as benign lesions including flat epithelial atypia (FEA) and atypical ductal hyperplasia (ADH), evolve to ductal carcinoma *in situ* (DCIS) and culminate as invasive ductal carcinoma (IDC) (Figure 1.2). FEA lesion is characterized by variably dilated ducts lined with one or more epithelial cell layers while ADH exhibits disorganized multi-layered ducts. The progression from ADH to DCIS involves the loss of ductal lumen and the proliferation of non-polarized malignant cells. The transition from localized DCIS to IDC is the first step for metastasis formation, which involves the detachment of cancer cells from the primary tumour mass, invasion and migration of the cells through the ECM surrounding the tumour epithelium, and subsequent breaking down the BM of local blood vessels, allowing stroma invasion and intravasation. The following steps

of metastasis are the survival transport through the circulation and arresting at the luminal side of the normal blood vessel endothelium in a distant organ such as the liver, brain, bone and lung. After transmigration of the endothelial barrier (extravasation), breast cancer cells need to adapt to the new microenvironment and re-initiate their proliferative programs at metastatic sites (Sökeland and Schumacher, 2019).

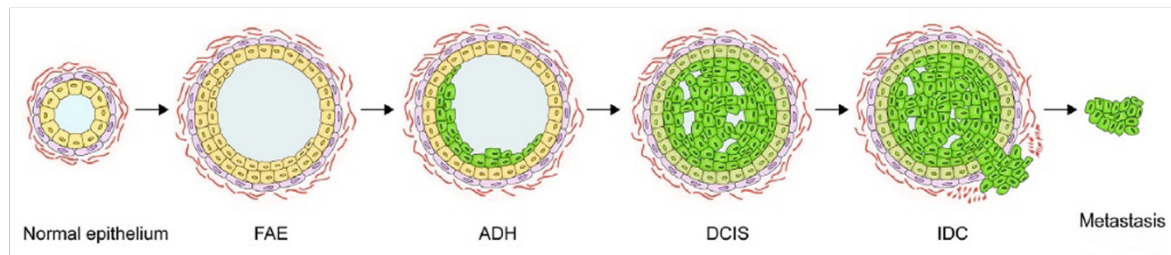


**Figure 1.2 Progression of ductal breast cancer.** The model of ductal subtype contains a multi-step progression from normal epithelium to FEA, ADH, DCIS and IDC (Rejon et al., 2016).

Lobular carcinoma is the second most common breast cancer. The progression of lobular carcinoma recognizes atypical lobular hyperplasia (ALH) and lobular carcinoma *in situ* (LCIS) as the non-obligate precursors to invasive lobular carcinoma (ILC) (Bombonati and Sgroi, 2011). *CDH1* gene encodes for the E-cadherin protein, which is a principal protein of adherens junctions, maintaining epithelial cells polarity. Approximately 90% of ILCs are associated with mutations in *CDH1* gene. Thus, compared with IDC, ILC is normally diagnosed as small, non-cohesive cells growing in a single-file pattern (Barroso-Sousa and Metzger-Filho, 2016).

The TNM is one of the most commonly used systems for staging breast cancer. This system provides information about the tumour size (T), involvement of nodes (N) and metastasis of tumour (M) (Table.1.1). DCIS is an example of stage 0 cancer. LCIS is generally considered as a benign condition associated with an enhanced risk of tumour thus removed from the TNM breast cancer staging system (Amin et al., 2017).

**Table 1.1. TNM breast cancer staging system**

Stage	Definition
Stage 0	Non-invasive stage of breast cancer (e.g. DCIS)
Stage I	IA – tumor ≤ 2cm, has not spread outside of breast IB – tumor ≤ 2cm, has spread to lymph nodes
Stage II	IIA – tumor ≤ 2cm, has spread to no more than 3 axillary lymph nodes; or 2cm < tumor ≤ 5cm, has not spread to axillary lymph nodes IIB – tumor 2cm < tumor ≤ 5cm, has spread to no more than 3 axillary lymph nodes; or tumor > 5cm, has not spread to axillary lymph nodes
Stage III	IIIA – tumor > 5cm, has spread to axillary lymph nodes; or any size of tumors have been found in 4-9 axillary lymph nodes or in sentinel lymph nodes IIIB – tumor has spread into the chest wall or the skin of breast and caused breast swelling IIIC – tumor has spread to 10 or more than 10 axillary lymph nodes
Stage IV	Tumor has spread not only to the nearby axillary lymph nodes but also to distant organs of the body

TNM staging system is published by the American Joint Committee on Cancer (AJCC) (Amin et al., 2017).

### 1.1.3 Causative factors

Many risk factors have been identified in the development and progression of breast cancer. However, two certain major risk factors, gender and age, are both beyond individual's control. For instance, breast cancer can affect both women and men, but the prevalence in female is about 100 times than in male (Gucalp et al., 2019). Breast cancer can affect women at the any age, but more than 50% of all breast cancers are diagnosed in women who are older than the age of 50 years (Kamińska et al., 2015).

#### 1.1.3.1 Genetic predisposition

It is estimated that about 10% of all breast cancers are hereditary forms, caused by inherited germ-line mutations in “high-penetrance”, “moderate-penetrance” and “low-penetrance” breast cancer susceptibility genes. High-penetrance genes account for up to 25% of inherited forms. Less than 5% of cases are due to mutations in moderate-risk genes. The remaining 70% of inherited breast cancers might be induced by low-penetrance alleles and other unknown genetic factors. Most of high- and moderate-penetrance breast carcinoma genes participate in the repair of DNA damage and cell-cycle regulation. Low-penetrance breast cancer genes are mainly identified through genome wide association studies (GWAS) (Shiovitz and Korde, 2015). This approach can scan most of the genome for genetic variants without any requirement of biological location or function. Several breast cancer susceptibility single

nucleotide polymorphisms (SNPs) have been identified, but their contribution in breast carcinoma are quite small (Feng et al., 2018).

Efficient double-strand DNA repair mechanisms are important to prevent the accumulation of genetic mutations and protect against genomic instability, leading to the development of breast cancer. This reflects the upregulated risk of breast cancer caused by mutations in breast cancer susceptibility gene 1 and 2 (*BRCA1* and *BRCA2*). *BRCA1&2* are the most important genes associated with hereditary breast carcinomas. Among women with a family history of breast cancer, up to 30% of them have a mutation in either *BRCA1* or *BRCA2*. Moreover, *BRCA1&2* mutations are reported to be responsible for 3-8% of all breast cancer cases (Shiovitz and Korde, 2015). *BRCA1* and *BRCA2* are located on human chromosome 17q21 and 13q12, respectively. *BRCA1* and *BRCA2* serve as tumour suppressors by promoting DNA double-stranded breaks repair by homologous recombination. In addition, *BRCA1* is a multi-functional protein and thereby repairs DNA damage through various pathways (particularly single-strand annealing and non-homologous end-joining) and checkpoint regulation (Orr and Savage, 2015). In the UK, about one in eight women will suffer breast cancer in her lifetime. The lifetime risks of developing breast cancer in women who carried *BRCA1* and *BRCA2* mutations increase from 12% to 60% and 45%, respectively. Furthermore, females with one of these two mutations have nearly 75% chance of developing breast cancer by the age of 70 years, compared to a 33% chance in the absence of these mutations (Harbeck et al., 2019). The prevalence of breast cancer in male is less than 1% worldwide. Men who are *BRCA2* mutation carriers have around 6-8% lifetime risk of breast cancer (Gucalp et al., 2019).

Phosphatase and tensin homolog (*PTEN*) is another well characterized high-penetrance breast cancer susceptibility gene. The phosphatidylinositol 3-kinase (PI3K)/AKT/mTOR pathway is known to be one of the most frequently enhanced oncogenic pathways in breast cancer (Elizalde et al., 2016). The PI3K family is a group of lipid kinases divided into three classes based on their structure. PI3K is generally activated by extracellular stimuli including insulin, cytokines and growth factors. Upon activation, PI3K phosphorylates the phosphatidylinositol 4,5-bisphosphate (PIP2) to the phosphatidylinositol 3,4,5-triphosphate (PIP3), resulting in the activation of AKT (Carbognin et al., 2019). *PTEN* acts as a tumour suppressor gene that is known to inhibit AKT activation through dephosphorylating the 3'-

group of PIP3 to PIP2 (Yang et al., 2019). At the same time, germ-line mutations in *PTEN* can lead to Cowden syndrome, an autosomal dominant disorder in which patients have an increased risk of both benign and malignant breast cancers. *PTEN* germ-line mutations are found in around 80% of patients reported with Cowden syndrome. In the UK, women patients with Cowden syndrome have a higher risk (25-50%) of developing breast cancer than the average incidence rate for women (12%) (Kimura et al., 2017).

Checkpoint kinase 2 (*CHEK2*) is an example of moderate-penetrance susceptibility gene. *CHEK2* germ-line mutation has been linked to a twofold increase in female breast cancer (Feng et al., 2018). Furthermore, *CHEK2* germ-line mutation causes a tenfold increase in male breast cancer. DNA damage leads to the activation of intracellular ATM kinase. CHK2 (encoded by *CHEK2* gene) is activated by ATM through a series of phosphorylation reaction. Activated CHK2 is involved in a number of pathways such as DNA repair, cell cycle regulation and apoptosis in response to the initial damage (Shiovitz and Korde, 2015). Moreover, CHK2 protein is known to function in *BRCA1* or *BRCA2* pathways. However, no additional increase risk of breast cancer is observed among co-carriers of *CHEK2* and *BRCA1* or *BRCA2* mutations (Apostolou and Papatotiriou, 2017).

In addition to the genes above, germ-line mutations in the high-penetrance and moderate-penetrance genes illustrated in table 1.2 can increase risk of developing breast cancer as well (Harbeck et al., 2019; Shiovitz and Korde, 2015).

**Table 1.2. Breast cancer susceptibility genes**

High-penetrance gene	Functions	Syndrome	Lifetime risk of breast cancer
<i>STK11</i>	Tumor suppressor genes, regulates cell growth	Peutz-Jeghers	30-50% by age 70
<i>TP53</i>	Tumor suppressor genes, controls cell-cycle and DNA repair	Li Fraumeni	25-50% by age 70
<i>CDH1</i>	Encodes for E-cadherin, maintains cell-cell adhesion	Hereditary diffuse gastric cancer	35-55% risk of getting ILC by age 70
Moderate-penetrance gene	Functions	Syndrome	Lifetime risk of breast cancer
<i>ATM</i>	Help DNA damage through p53, BRCA 1 and CHEK2 pathways	Ataxia telangiectasia	Lower than 20% by age 70
<i>PALB2</i>	Works with BRCA 2 proteins to repair DNA damage	Fanconi's anemia	33%-58% by age 70

### 1.1.3.2 Acquired alterations

In addition to hereditary form, the development and progression of the majority of breast cancers is mainly caused by acquired somatic genetic and molecular alterations. These alterations can result either in the activation of oncogenic pathways or inactivation of tumour suppressor genes, promoting breast cancer (Ottini et al., 2011).

As mentioned above, the PI3K/AKT/mTOR pathway is a key intracellular signalling pathway in breast cancer. Class I PI3K is the primary class of PI3K implicated in cancer (Feng et al., 2018). Class I PI3K is composed of p85 regulatory subunit and p110 catalytic subunit. *PIK3CA* encodes for the  $\alpha$ -isoform of catalytic subunit (p110 $\alpha$ ). The interaction between p85 and p110 $\alpha$  stabilizes and inhibits p110 $\alpha$  catalytic activity in the absence of activating signals. *PIK3CA* mutations are mainly located in two hot spots: E545K in exon 9 relieves the inhibition of p110 $\alpha$  while H1047 in exon 20 increases the interaction of p110 $\alpha$  with lipid membrane, contributing to p110 $\alpha$  activation. *PIK3CA* mutations occur in about 20-40% of all breast cancers, leading to the activation of PI3K/AKT/mTOR pathway (Ortega et al., 2020; Shimoi et al., 2018).

*HER2* (also known as *ERBB2*) is located on human chromosome 17q12. *HER2* amplification is found in around 15-20% of all breast cancers, leading to an activation of the *HER2* signalling pathways (Fallahpour et al., 2017). *HER2* belongs to the human epidermal growth factor receptor (*HER*) family. *HERs* are composed of an extracellular ligand-binding domain, a transmembrane domain and an intracellular catalytic domain. *HERs* exist as monomers on the cell surface. They undergo dimerization and transphosphorylation of their intracellular domains upon ligand binding. However, *HER2* does not have direct activating ligand and exists in a constitutively active conformation. Its signalling functions are triggered by the heterodimerisations with other family members like *HER1* and *HER3* (Iqbal and Iqbal, 2014). *HER2* signalling can promote tumour cell survival and proliferation through *PI3K/AKT/mTOR* and *RAS/MAPK* pathways (Figure 1.3A) (Elizalde et al., 2016).

Estrogen and estrogen receptor  $\alpha$  (*ER $\alpha$* ) play key roles in the development and progression of breast cancer (Wagner and Gil, 2020). Almost 75% of breast cancers are driven by *ER $\alpha$* -mediated transcriptional activity. As a ligand-binding-dependent transcriptional factor, estrogen-activated *ER $\alpha$*  translocates into the nucleus and regulates genes expression through interacting with estrogen response elements (*EREs*) located in the promoter region of target genes. *ER $\alpha$*  can also regulate genes expression without the involvement of *EREs* through tethering to other transcription factors such as *AP-1* and *RUNX1* (Williams and Lin, 2013). Deregulated cell cycle progression is a hallmark of cancer that enables limitless cell division. *CCND1* (encodes Cyclin D1) is an *ER $\alpha$*  targeted gene that plays a key role in regulating G1 to S phase transition. Cyclin D1 protein promotes the formation of cyclin D-*CDK4/6* complex that partly phosphorylates retinoblastoma (*Rb*), releasing its inhibition of *E2F* transcription factors. *E2F*-mediated transcription drives the expression of cyclin E. Cyclin E-*CDK2* complex in turn hyper-phosphorylates and completely inactivates *Rb*, promoting G1 to S phase transition (Figure 1.3B). *ER* positive (*ER<sup>+</sup>*) breast cancers exhibit enhanced *ESR1* expression (encodes *ER $\alpha$* ), contributing to breast cancer cell proliferation and tumour growth (Thu et al., 2018). *PIK3CA* mutations are frequently observed in *ER<sup>+</sup>* breast cancers, indicating that both pathways can co-ordinately facilitate breast cancer development. On the one hand, studies illustrated that *AKT* can activate *ER $\alpha$*  signalling via phosphorylating *ER $\alpha$*  in the absence of

estrogen. On the other hand, estrogen-bound ER $\alpha$  can activate PI3K/AKT/mTOR signalling directly through binding to p85 subunit of PI3K in the extranuclear area (Ciruelos Gil, 2014).

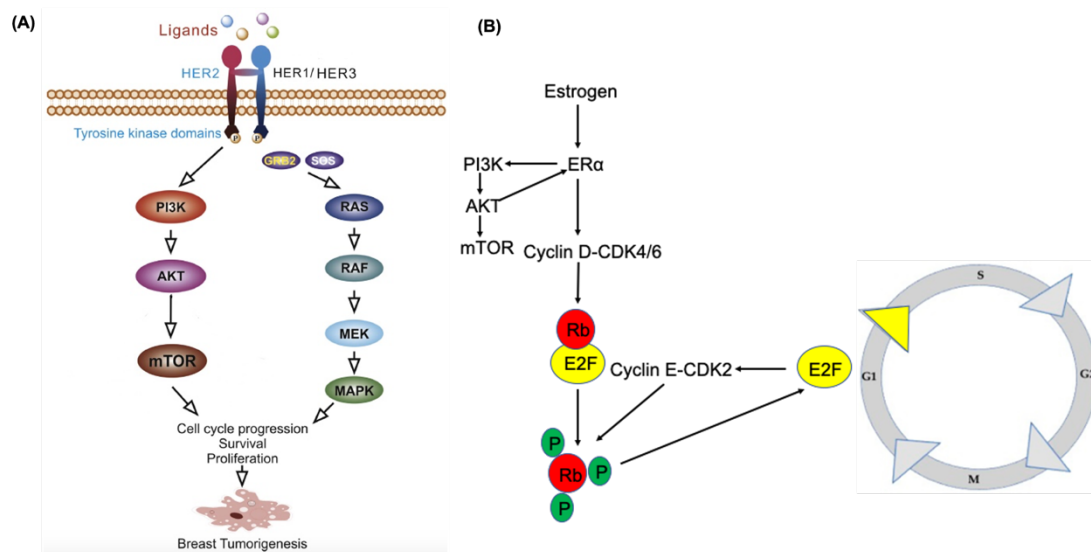


**Figure 1.3 HER2 signaling and ER signaling pathways in breast cancer. (A)** HER2 locates at the cell membrane and responds to a wide variety of ligands. Phosphorylation of the tyrosine kinase initiates PI3K/AKT and RAS pathways, promoting breast cancer cells proliferation. Figure is adapted from (Feng et al., 2018). **(B)** ER promotes cell proliferation through CDK4/6/Rb/E2F/CKD2 pathway. At the same time, this pathway can work coordinately with PI3K/AKT/mTOR pathway in breast cancer development. Figure is adapted from (Wagner and Gil, 2020).

The progesterone receptor (PR) is another key transcription factor involved in breast cancer development. PR exists in 2 isoforms: PR $\alpha$  and PR $\beta$ . PR $\alpha$  is located in the nucleus whereas PR $\beta$  shuttles between nuclear and cytoplasmic compartments continuously. PR can promote breast carcinoma through both genomic and non-genomic pathways (e.g., it can activate protein kinases like PI3K). Furthermore, PR is an upregulated target gene of ER signalling, and the high expression of PR is strongly dependent on estrogen. Therefore, it is rare to see the PR-positive (PR $^+$ ) and ER-negative (ER $^-$ ) cancer cells (Obr and Edwards, 2012).

### 1.1.3.3 Lifestyle risk factors

A number of lifestyle risk factors, including alcohol consumption and physical inactivity, have been described to promote the development and progression of breast cancer, indicating the contribution of a healthy lifestyle in inhibiting breast cancer.

Current researches show that women who have one alcoholic drink each day have about 7-10% higher prevalence of breast cancer compared to women who do not drink at all (Feng et

al., 2018). A possible association between alcohol consumption and breast cancer has been related to the concentration of estrogen. Firstly, studies showed that chronic alcohol consumption increases aromatase activity and that promotes conversion of testosterone to estrogen, increasing the levels of estrogen (Castro and Castro, 2014). In addition, a shorter menstrual cycle is observed in women with moderate alcohol consumption than women who do not consume alcohol, indicating high levels of estrogen exposure (Liu et al., 2015).

Obesity is another recognized risk factor for breast cancer. Recent studies demonstrated that obese women, defined as body mass index (BMI)  $\geq 25$  kg/m<sup>2</sup>, were more likely to develop breast cancer compared to normal-weight women. Obesity has been proved to cause chronic hyperinsulinemia. Hyperinsulinemia inhibits the synthesis of sex hormone-binding globulin leading to an enhanced estrogen level, increasing breast cancer risk (Li et al., 2018). Therefore, there is increasing evidence that regular physical activity may reduce breast cancer risk through its influence on weight loss and decreased level of body fat (Niehoff et al., 2019).

Women who have early menarche (before age 12) or late-onset menopause (after age 55) have a longer lifetime of hormonal exposure, leading to an enhanced risk of developing breast cancer. Similarly, breast feeding might decrease the risk of developing breast cancer due to a reduction in the total number of menstrual cycles (Feng et al., 2018).

#### **1.1.4 Types of breast cancer**

The histological and molecular characteristics of breast cancer strongly influence treatment decisions. Breast cancers are categorized into four intrinsic subtypes based on the expression of ER and/or PR (the luminal cluster), nuclear marker of proliferation Ki67 and HER2 (Tang and Tse, 2016).

**Luminal A** breast cancers are the most common subtype and account for 50-60% of all breast cancers. Luminal A breast cancers are defined as ER<sup>+</sup> and PR<sup>+</sup>, HER2<sup>-</sup> and have low levels of the protein Ki67. These cancers have a good prognosis, and the relapse rate is significantly lower than other subtypes. Recurrence is normally observed in bone (Yersal and Barutca, 2014).

**Luminal B** breast cancers make up about 10-20% of all breast cancers. These cancers have lower expression of ER and higher expression of Ki67 than luminal A subtype. Additionally, luminal B breast cancers can be either HER2<sup>+</sup> or HER2<sup>-</sup>. Compared to luminal A subtype, they have a more aggressive characteristic and a worse prognosis (Dai et al., 2015).

**HER2-enriched (non-luminal)** breast cancers are defined by the lack of expression for ER and PR, high expression of HER2 and high Ki67 index. HER2-enriched tumours account for 15-20% of all breast cancers. HER2-enriched breast cancers are more aggressive and characterized by a poorer prognosis than luminal-type tumours (Dai et al., 2015).

**Triple negative breast cancers (TNBCs)** account for around 8-35% of all cases. TNBCs are characterized by lacking the expression of ER, PR and HER2. TNBCs are considered to be more aggressive and have the worst prognosis than the other subtypes. TNBCs have a high rate of metastasis to the lung and brain. Most of *BRCA1* mutation tumours are TNBCs. In addition, TNBCs are normally diagnosed among females younger than the age of 50 years (Dai et al., 2015).

A recent research extracted around 30000 breast cancer cases diagnosed between 2010 and 2012 in Canada and tested survival rates among the different subtypes (Figure 1.4). Luminal A breast carcinoma accounted for 59% of all cases, followed by TNBC (16%), luminal B breast cancer (13%) and HER2-enriched subtype (12%). Although some factors are known to affect survival such as age and stage at diagnose, patients with luminal A breast cancer exhibit the longest survival overall. The worst survival rate was observed among patients with TNBC (Fallahpour et al., 2017).

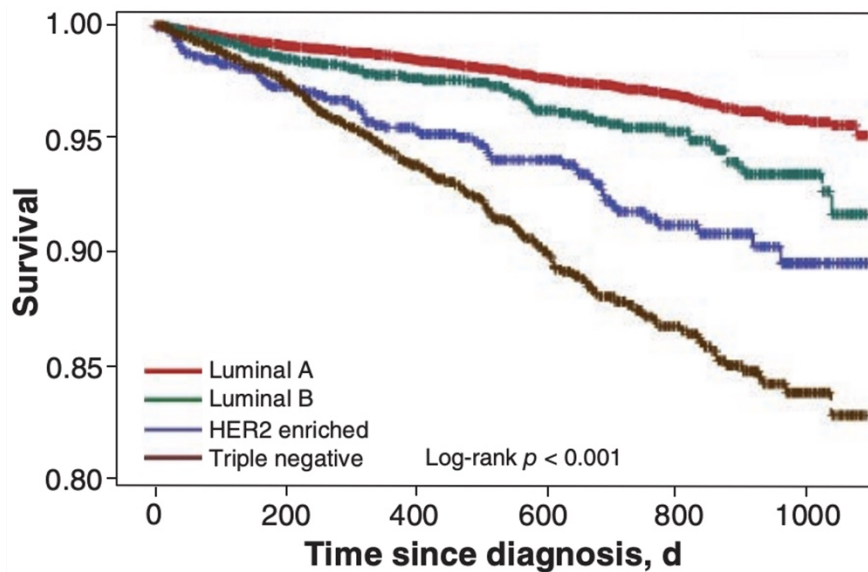


**Figure 1.4 Kaplan-Meier plot of breast cancer survival rates among different intrinsic subtypes from 2010-2012 in Canada (Fallahpour et al., 2017).**

## 1.1.5 Treatment of breast cancer

### 1.1.5.1 Treatment for non-invasive breast cancer

The primary goals of non-invasive breast cancer treatment are removing the tumour from the breast and preventing metastasis. Breast-conserving surgery is the most common treatment for non-invasive breast cancer, which is normally followed by postoperative radiotherapy to kill the remaining cancer cells. Mastectomy (removal of entire breast) may be required if there are several sites of DCIS. In addition, systemic therapy, including preoperative (neoadjuvant) and postoperative (adjuvant), might be required, which mainly depends on the expression of predictive biomarkers of breast cancer such as ER, PR, HER2, Ki67, *PIK3CA* mutations and germ-line *BRCA1/2* mutations. For example, patients who have ER<sup>+</sup> breast cancer normally receive a 10-12 weeks endocrine therapy after surgery to block the ER activity. The overall survival rates of DCIS in developed countries have reached to approximately 100% (Waks and Winer, 2019).

### 1.1.5.2 Treatment for invasive breast cancer

For invasive breast cancer, the main therapeutic goals are symptom palliation and prolonging quality-adjusted life expectancy. As illustrated in figure 1.5, the most common treatment for stage I/II is still breast-conserving surgery (BCS), followed by radiation therapy (RT) as the

standard procedure (Harbeck and Gnant, 2017). For stage III, the combination of mastectomy and chemotherapy (including targeted therapy and immunotherapy) has been commonly used in the last decade. For instance, trastuzumab is a monoclonal antibody targeting the extracellular domain of HER2. Mastectomy is generally followed by 12 months trastuzumab (Herceptin) treatment for patients who have HER2<sup>+</sup> breast cancer (Waks and Winer, 2019). Systemic therapy is preferentially used for advanced stages, and depends on the specific intrinsic subtype, rate of tumour progression and patients' choices. Chemotherapy is the major treatment for stage IV, in association with targeted therapy, contributing to slow down the growth of cancer. Additionally, surgery could be used to treat pain and other symptoms caused by metastasis, such as broken bones and spinal cord compression (DeSantis et al., 2019). Compared with other subtypes, TNBC patients normally have a poorer outcome due to the lack of effective targeted therapies (Maughan et al., 2010; Waks and Winer, 2019). Cytotoxic chemotherapy is currently the major care therapy for patients with TNBC (Lebert et al., 2018). However, approximately one-third of TNBC patients are known to develop distant metastases, and there is no standard of treatment for patients with metastatic TNBC (Li et al., 2019). It is illustrated that around 25-35% of TNBC patients have a proven *BRCA1/2* mutations. Moreover, about 70% of *BRCA1*-mutated breast cancers display a triple-negative phenotype (Liu et al., 2021). Hence, poly (ADP-ribose) polymerase (PARP) inhibitors have been developed for TNBC treatment by disrupting DNA damage repair (Han et al., 2020), significantly enhancing therapeutic effectiveness in TNBC.

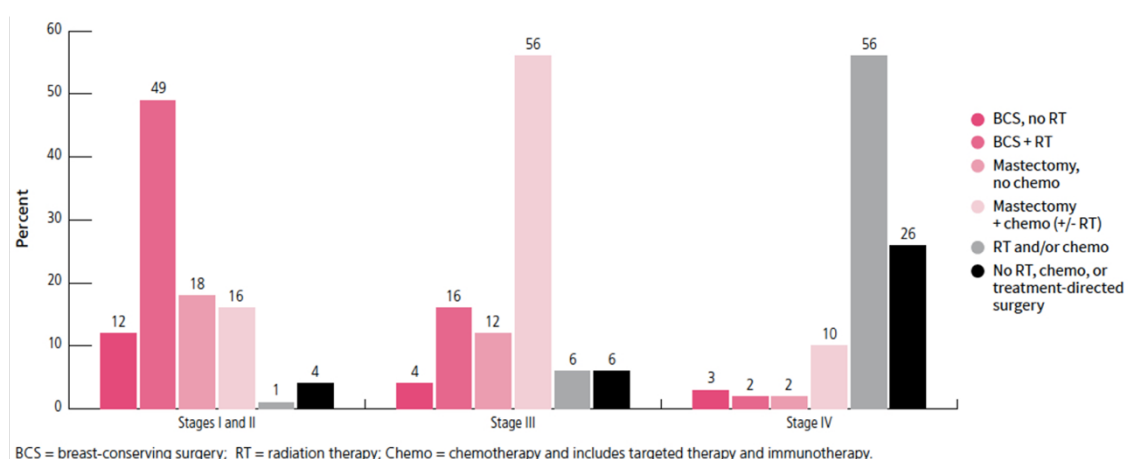


**Figure 1.5 Breast cancer treatment pattern among US female with invasive breast cancer by 2016.** Most of female with early-stage breast cancer (stage I-III) will have different types of surgery, which is often followed by other treatments, including chemotherapy, radiation therapy and targeted therapies. Women with metastatic breast cancer are mainly treated with systemic therapies such as chemotherapy, targeted therapies, radiation therapy (DeSantis et al., 2019).

Compared with non-invasive breast cancers, invasive breast cancers are still considered as incurable based on current treatments (Table 1.3). Thanks to rapid progression in molecular biology and genome science, the therapeutic effectiveness of invasive breast cancers has significantly increased in the past two decades (Feng et al., 2018). For example, dysregulated cellular proliferation is heralded as a ‘hallmark of cancer’. The cyclin D and its partner kinases, cyclin-dependent kinase 4/6 (CDK4/6) are known to play a key role in regulating the proliferation of breast cancer cells. Three CDK4/6 inhibitors have been used for the treatment of patients with ER-positive metastatic breast cancer, resulting in an increasing tendency in both overall survival and progression-free survival (PFS) in this subtype of breast cancer (Pernas et al., 2018). However, the median overall survival for patients with metastatic breast cancer is still only 2-3 years (Swain et al., 2015). Furthermore, long-term survivors since 1996 account for less than 5% for all metastatic breast cancer patients (Harbeck and Gnant, 2017). Additionally, almost all treatments for invasive breast cancer result in substantial side effects, impairing quality of patients’ life. For instance, chemotherapy is able to cause both chronic toxicities (including cardiotoxicity, cognitive dysfunction and infertility) and acute toxicities (like fatigue and nausea). Radiation therapy can induce a systemic immune response, leading to swelling, fatigue and lymphedema. Endocrine therapy is often accompanied by hot flushes. Some of these side effects are difficult to treat (Harbeck et al., 2019; Waks and Winer, 2019). Thus, although significant progress has been achieved in term of invasive breast cancer outcomes, more and better therapies are still required. In the past several decades, there is increasing evidence showing that the ECM promotes the development and progression of breast cancer, suggesting that targeting cell-ECM interaction could represent a novel strategy for therapeutic intervention.

**Table 1.3. Major therapy of metastatic breast cancer**

Breast cancer subtype	Major therapeutic approach	Median overall survival rate
Hormone receptor positive (HR <sup>+</sup> )	Endocrine therapy until disease is endocrine resistant, then followed by single-agent chemotherapy e.g. Aromatase inhibitor + CDK4/6 inhibitor; Fulvestrant ± everolimus	24.8 months
HER2 <sup>+</sup>	HER2-targeted agent combined with mastectomy, chemotherapy or endocrine therapy if HR <sup>+</sup> e.g. Mastectomy + Trastuzumab; Trastuzumab + endocrine therapy	9.6-18.5 months
TNBC	Single-agent chemotherapy e.g. Platinum; Taxane	3.1-4.5 months

Data is from (Waks and Winer, 2019)

## **1.2 Extracellular matrix**

### **1.2.1 Primary components in ECM**

The ECM is a highly specialized three-dimensional macromolecular network. The ECM not only serves as a physical scaffold to maintain tissue structural integrity, but also provides cells with proper biomechanical and biochemical signals for regulating cell survival, proliferation, migration and differentiation (Pickup et al., 2014). The ECM is composed of a highly dynamic and complex network of secreted proteins whose precise composition and specific structure vary with tissues. At the same time, the ECM is constantly remodelled during physiological conditions, as a consequence of a fine balance between matrix replacement and degradation (Rainero, 2016). Following the ECM composition classification described in the mammalian matrisome project, almost 300 components are identified as the 'core matrisome' elements, which consist of 43 collagen subunits, proteoglycans and glycoproteins (Naba et al., 2012). Collagens are the most abundant proteins which provide structural strength to all forms of the extracellular matrices (Mouw et al., 2014). Proteoglycans are characterized as proteins that have one or more glycosaminoglycans (GAGs) covalently bonded to them. Proteoglycans can interact with a number of ECM molecules, cell surface receptors and growth factors either through their core proteins or via their GAGs side chains, contributing to the formation of ECM scaffold and cell embedding within it (Theocharis et al., 2016). Glycoproteins are found on the surface of cell membrane that not only link structural molecules between each other, but also link cells and structural molecules (e.g., collagen) to add strength and stability to a tissue. Fibronectins and laminins are two most important components of glycoproteins (Hynes and Naba, 2012). In addition, the ECM is classified into two groups that vary in structure and composition: the interstitial matrix and BM. The interstitial matrix fills in the interstitial space between cells, whereas the BM is a specific thin layer of ECM that can physically separate the epithelial cells from surrounding stroma (Horejs, 2016). Here I discuss the roles of three most abundant ECM components, collagens, fibronectin and laminins, in maintaining the structural and functional integrity of the ECM.

#### **1.2.1.1 Collagens**

Collagens are the most abundant component in the interstitial ECM but are found in the BM as well, accounting for almost 30% of total proteins in human. There are 28 different subtypes

of collagen, and each subtype is composed of three  $\alpha$  chains that form a triple helical structure. Collagens are categorized into fibrillar collagens (e.g. collagen type I and II), network-forming collagen (e.g. collagen type IV) and fibril-associated collagens with interruptions in their triple helices (FACITs) (e.g. collagen type IX and XII) (Theocharis et al., 2016). The fibrillar collagen molecule is characterized by the repeating triplets of amino acids Gly-X-Y in central region of  $\alpha$  chains, where X and Y are generally occupied by proline and hydroxyproline, respectively. This region is flanked by amino- and carboxyl-terminal non-collagenous domains. The FACITs do not assemble into fibrils but associate with other collagen fibrils (Yue, 2014).

Collagen type I is the most common fibrillar collagen that is primarily produced by fibroblasts. The  $\alpha$  chains are assembled into the triple helical structure in the endoplasmic reticulum (ER). Following the hydroxylation of proline and lysine, the molecule is glycosylated to initiate the formation of procollagen triple helix. The procollagen is transported to the Golgi apparatus where it is modified and packaged for cellular export. During or following exocytosis, the C- and N-terminal propeptides are cleaved off by specific matrix metalloproteinases (MMPs); excision of both propeptides allows the following formation of collagen microfibrils in the extracellular space. Next, short microfibrils grow into large fibrils with the help of other ECM components such as FACITs and small leucine-rich repeat proteoglycans (SLRPs). Lysyl oxidase (LOX) can induce the crosslinking between triple-helical molecules during collagen assembly, providing collagen fibres with stability and enhanced mechanical properties (Figure 1.6) (Mouw et al., 2014; Riso et al., 2016). As the major structural element of ECM, collagen type I not only provides tissues with tensile strength, but also regulates cell migration, adhesion and wound healing (Xu et al., 2019).

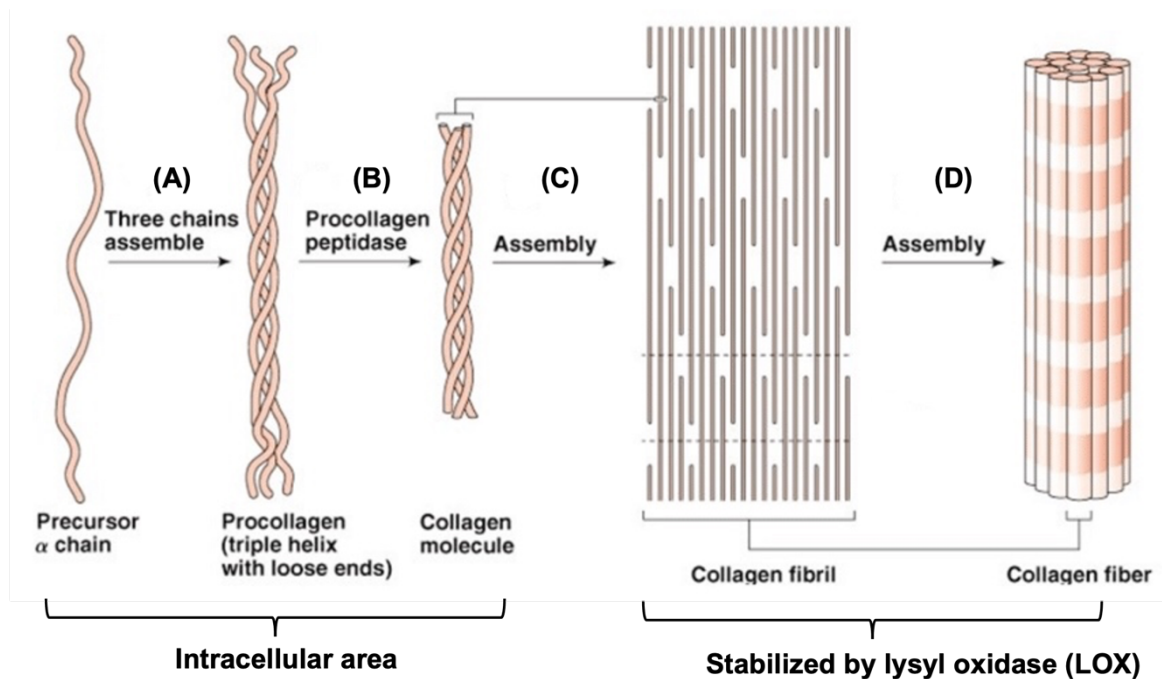


**Figure 1.6 The process of collagen type I synthesis. (A)** The  $\alpha$  chains assemble to form procollagen. **(B)** and **(C)** Procollagen peptidase removes loose termini and self-assemble to form a growing collagen fibril. **(D)** Self-assembly of collagen fibrils forms collagen type I fiber. Figure is adapted from (Riso et al., 2016).

### 1.2.1.2 Fibronectin

Fibronectin is a ubiquitous glycoprotein in the ECM that assembles into fibrillar structures via a cell-mediated process. Secreted fibronectin molecule exists as a dimer that is covalently connected by a pair of disulfide bonds at the C-terminus of each subunit. Fibronectin subunit is composed of type I, II and III repeating units. The folded fibronectin is formed through ionic interactions between type III repeats of neighbouring molecules. Type II repeats have the binding domains for collagens while type III repeats contain the amino acid sequence responsible for integrin-binding and heparin-binding sites (Figure 1.7) (Mouw et al., 2014).

Fibronectin assembly is primarily initiated by binding its RGD (Arg-Gly-Asp) domain to  $\alpha 5\beta 1$  integrins. Fibronectin binding leads to integrin clustering and activation, promoting continued deposition of fibronectin at the cell surface. Contractile force from actin cytoskeleton in turn stimulates the self-association of fibronectin that mediated by N-terminal assembly domain. Fibronectin conformational change reveals cryptic binding sites that promote fibril formation and in conversion of soluble plasma fibronectin into insoluble fibronectin molecules (Singh et al., 2010). In addition, syndecan-4 is transmembrane proteoglycan that is involved in the

assembly of fibronectin as well via binding to heparin-binding domain at the C-terminal of fibronectin. The interaction between syndecan-4 and fibronectin regulates  $\alpha 5\beta 1$  integrin recycling and enhances integrin-mediated cell migration, indicating that syndecan-4 acts as co-receptor in fibronectin fibril formation (Bass et al., 2011; Morgan et al., 2007). Once assembled, fibronectin contributes to tissue organization through regulating the assembly of other ECM components. For instance, fibronectin-null embryonic fibroblasts were cultured in the absence and presence of exogenous fibronectin, and the deposition of collagen fibrils was assessed by indirect immunofluorescence microscopy. Accumulation of endogenous collagen type I and III was not detected in cells cultured in the absence of fibronectin, suggesting that fibronectin serves as a key regulator in collagen assembly and deposition (Sottile et al., 2007). Moreover, fibronectin-treated wounds had an increased fascicular and horizontal collagen deposition compared to control wounds (without fibronectin treatment), indicating that fibronectin might act as a scaffold that aids in alignment of collagen fibrils, facilitating wound healing (Johnson et al., 2017).

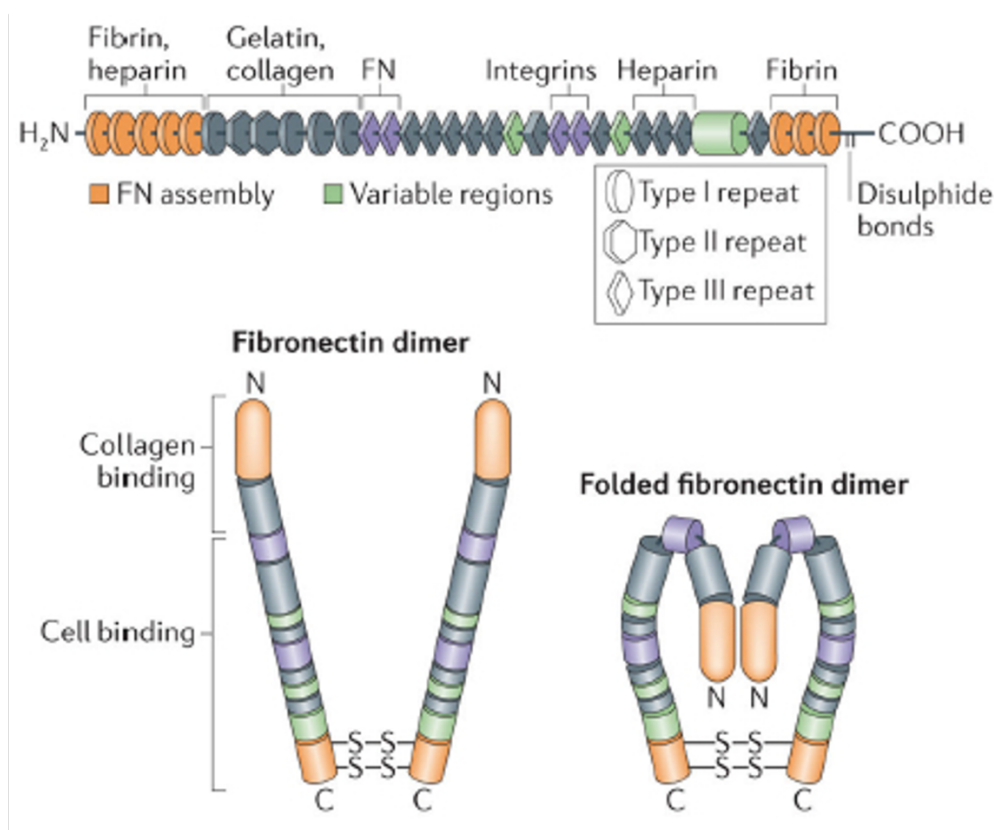


**Figure 1.7 Structure of fibronectin.** Fibronectin subunit is composed of type I, II and III repeats. These repeats contain the binding sites for other ECM components and cell surface receptors. Fibronectin molecule is stabilized through disulphide bonds between each type I and type II repeat. Type III repeats lack disulfide bonds and thus can undergo conformational change (Mouw et al., 2014).

### 1.2.1.3 Basement membrane

The BM is mainly composed of laminin, collagen type IV and nidogen. Laminins are trimeric glycoproteins consisting of  $\alpha$ ,  $\beta$  and  $\gamma$  chains that are located in the basal lamina. The 12 different mammalian laminin chains can form 16 distinct isoforms with differences in chain length and domain architecture (Theocharis et al., 2016). These chains form a characteristic cross structure, which contains three short arms and one long arm. Laminin deposits on the cell surfaces and assembles into sheet through interactions among the N-terminus of short arms (LN). Laminin sheet is linked to cells through interactions between the 5 laminin G-like (LG) domains at the distal end of the long arm and cell surface molecules including integrins, sulphated glycolipids and  $\alpha$ -dystroglycan (Figure 1.8A) (Hohenester and Yurchenco, 2013). Secreted collagen type IV heterotrimers form triple helical via disulfide bonds at the N-terminal 7S domains and further oligomerize into cross-linked tetramers. The interactions between the two trimeric C-terminal NC1 domains lead to polymeric collagen type IV formation (Mak and Mei, 2017).

Laminin network and collagen type IV is mainly connected via nidogen. Nidogen is composed of two N-terminal globules (G1 and G2) and one C-terminal globules (G3) that are connected by a rod-like domain made of epidermal growth factor (EGF)-like repeats. Nidogen C-terminus G3 globule binds to the  $\gamma$  chain of laminin molecule, while its G2 domain can bind to the triple helical region of collagen type IV (Mak and Mei, 2017). Heparan sulfate proteoglycans (HSPG) is a member of proteoglycans with multiple heparan sulfate (HS) side chains covalently coupled to the core protein. HSPGs present in the matrix such as perlecan, agrin and glypicans. It has been shown that the G2 domain of nidogen can bind to perlecan and agrin. At the same time, HSPG domain on perlecan and agrin can bind to the 7S and NC1 domains of collagen type IV as well as to the  $\alpha$  chain of laminin. Thus, perlecan and agrin can provide additional connection between laminin and collagen type IV networks via multiple binding interactions (Figure 1.8B) (Walker et al., 2018).

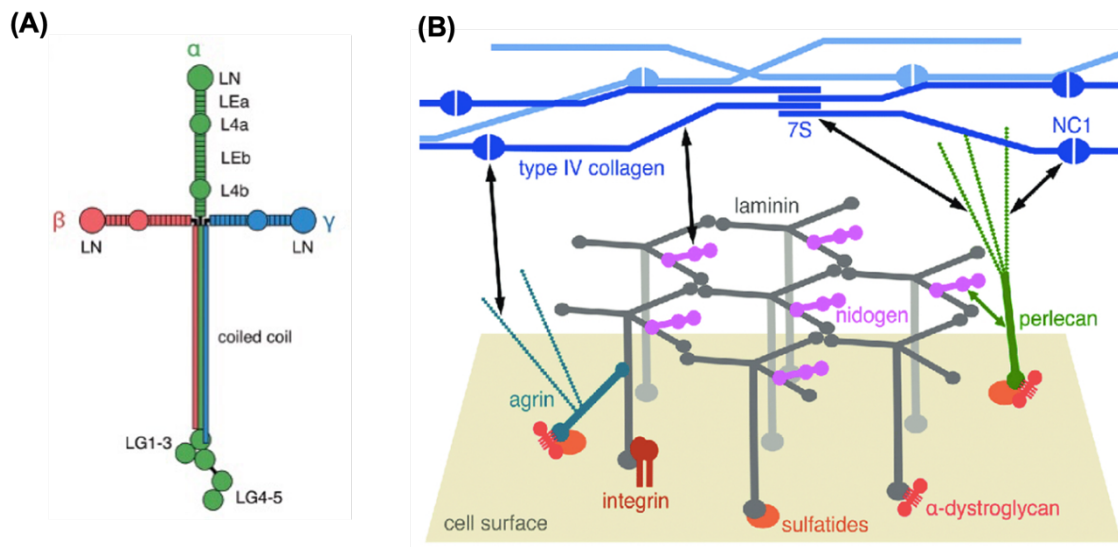


**Figure 1.8 Structure of laminin and the BM.** (A) Laminin is composed of  $\alpha$ ,  $\beta$  and  $\gamma$  chains. Laminins link to each others through their N-terminal domains (LN). Laminin binds to cells via interactions among the 5 laminin G-like (LG) domain and cell surface receptors. Figure is adapted from (Hohenester and Yurchenco, 2013). (B) The laminin and collagen networks are mainly linked by nidogen. Perlecan and agrin can provide additional linkage between two networks (Hohenester and Yurchenco, 2013).

## 1.2.2 Receptors of ECM components

### 1.2.2.1 Integrins

Cells are known to bind to the ECM via specialized receptors. Integrins are the principal adhesion receptors for the ECM. Integrin-ECM engagement not only links the ECM to the cell cytoskeleton but is also involved in the regulation of a number of cellular processes, such as cell migration, growth, proliferation and differentiation. In mammals, the combinations of the 18  $\alpha$ - and eight  $\beta$ -subunits generate 24 distinct heterodimeric receptors, the majority of which contain the  $\beta 1$ -subunit (Figure 1.9A) (Barczyk et al., 2010). The  $\alpha$ - and  $\beta$ -subunits are both type I transmembrane proteins that have a large extracellular domain, a single-pass transmembrane helix and a short cytoplasmic tail (Bridgewater et al., 2012). Integrin heterodimers can exist in a non-clustered (inactive) conformation that exhibits a low affinity for ligands or a clustered (active) conformation that exhibits a high affinity for ECM components. Integrins can transmit signals bidirectionally. Intracellular signals initiate by recruiting talin to the cytoplasmic tail of  $\beta$ -subunits. This interaction induces separation of the cytoplasmic domains of  $\alpha$ - and  $\beta$ -subunits, leading to a conformational change of the integrin and increased ligand binding affinity in the extracellular domain (inside-out signalling).

Alternately, the interactions between integrins and ECM ligands trigger the recruitment of additional scaffolding proteins, kinases and phosphatases, such as focal adhesion kinase (FAK), vinculin and paxillin, promoting the maturation of nascent adhesions to fully activated focal adhesions (FAs) which can transmit the signals (outside-in signalling) (Figure 1.9B) (Kinbara et al., 2003; Moreno-Layseca et al., 2019).

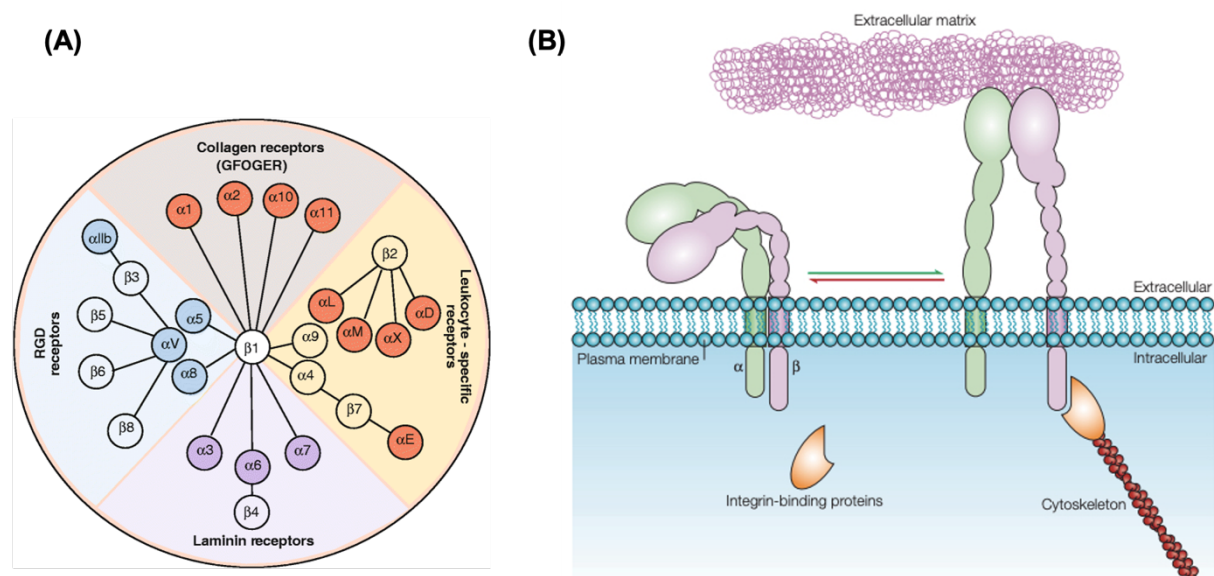


**Figure 1.9 Integrin heterodimers and interaction with ECM.** (A) In vertebrates, the integrin family consists of 24 heterodimers (Barczyk et al., 2010). (B) Integrins contain  $\alpha$  and  $\beta$  subunits that span the cell membrane and reach into the extracellular space. Non-covalent interactions between their extracellular and membrane-proximal regions bring  $\alpha$  and  $\beta$  subunits together in a heterodimer. The short cytoplasmic tails of both  $\alpha$  and  $\beta$  subunits interact with different intracellular proteins. These intracellular integrin-binding proteins link to the cytoskeleton (Kinbara et al., 2003).

Cell surface integrins are constantly trafficked in cells and undergo endosomal sorting that determines recycling or degradation of the receptors. Integrins can be endocytosed via either clathrin-mediated endocytosis (CME) or clathrin-independent endocytosis (CIE), whereby CIE contains several distinct integrin endocytic routes, including internalization through clathrin-independent carriers, caveolae and macropinocytosis from circular dorsal ruffles in response to growth factor stimulation (Moreno-Layseca et al., 2019). After endocytosis, the Rab and Arf family of GTPases play important roles in integrin trafficking through the endolysosomal system and are regulated by a cycle of GTP binding and GTP hydrolysis, which is catalysed by guanine nucleotide exchange factors (GEFs) and GTPases activating-proteins (GAPs), respectively (Donaldson et al., 2016). Integrins are firstly endocytosed and delivered to Rab5-positive early endosomes (EEs) to be sorted for recycling or degradation. A large proportion

of integrins are recycled back to the plasma membrane via either a Rab4-dependent short-loop or a Rab11 and Arf6-mediated long-loop pathway through the perinuclear recycling compartment (PNRC) (Bridgewater et al., 2012). EEs undergo maturation to late endosomes, where integrins sorted for degradation are retained and compartmentalized into low pH intraluminal vesicles (ILVs). Integrins sorted to ILVs are finally degraded via the fusion of multivesicular bodies (MVBs) with lysosomes (Rainero and Norman, 2013). Besides being degraded, late endosomes and MVBs can be re-secreted to the cell surface by fusing with the plasma membrane. The retrieval of integrins is an emerging mechanism regulating receptor recycling that is linked to the migration of cancer cells (Figure 1.10) (Wilson et al., 2018). In addition, inactive  $\beta 1$  integrin on the plasma membrane could be internalized as well. After internalization, inactive  $\beta 1$  is rapidly recycled back to the plasma membrane in a Rab4- and Arf6-dependent pathway (De Franceschi et al., 2015). However, the internalization rate of the active  $\beta 1$  is much higher than the inactive conformation. Thus, the active  $\beta 1$  is predominantly cytoplasmic, whereas the inactive conformation is primarily found on the plasma membrane (Arjonen et al., 2012).

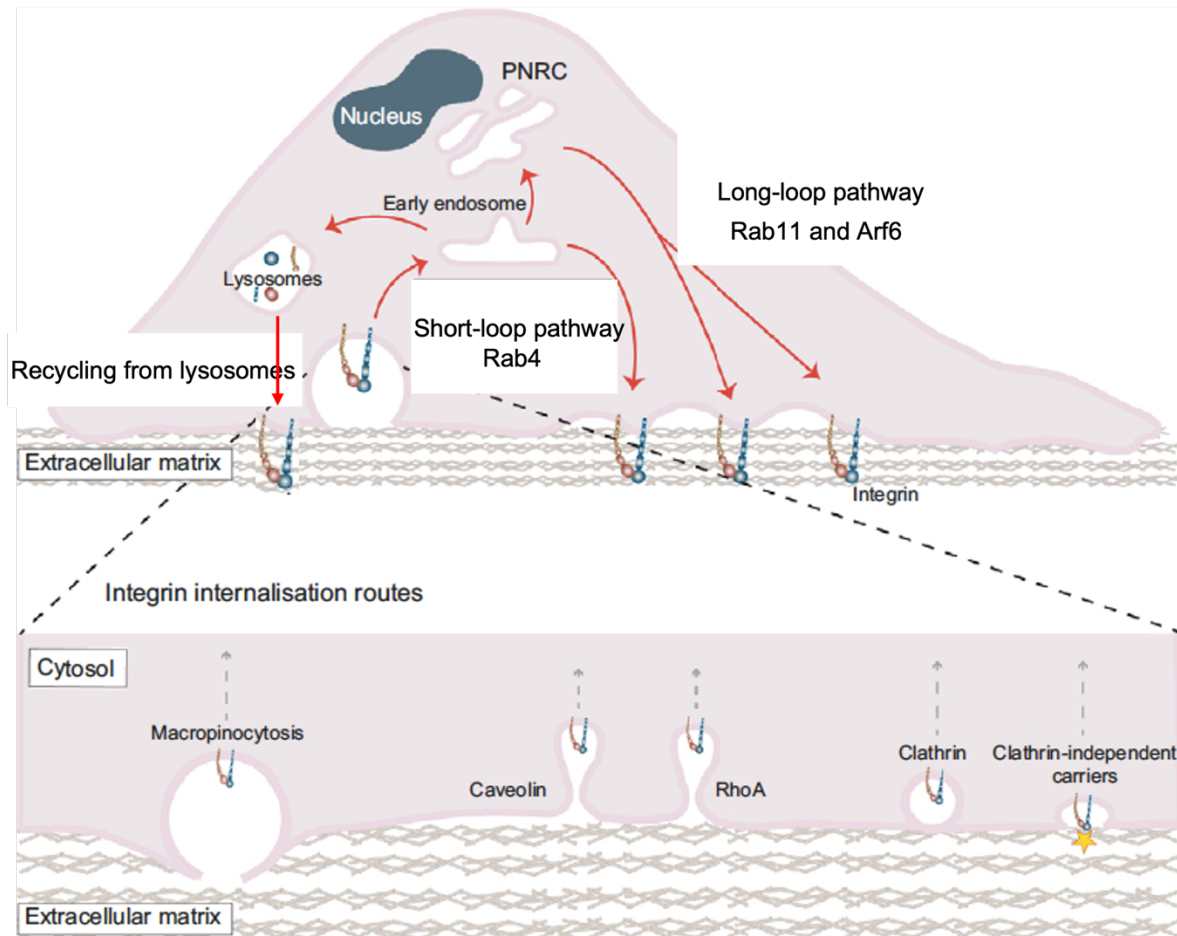


**Figure 1.10 Integrin endocytosis and trafficking pathways.** Integrins could be endocytosed through clathrin-mediated or clathrin-independent pathway. Most internalized integrins are recycled back to cell surface via either short-loop or long-loop pathway. A small proportion of integrins are degraded in lysosomes. In addition, integrins can also be recycled from lysosomes. Figure is adapted from (De Franceschi et al., 2015).

### 1.2.2.2 Other receptors

In addition to integrins, cells can also bind to the ECM via other receptors including syndecans, discoidin domain receptors (DDR), uPARAP/Endo180 and CD44. The syndecan family is a class of transmembrane proteoglycans containing four members (syndecan 1-4). Syndecan 1-3 are mainly expressed in the brain while syndecan 4 is expressed ubiquitously. Syndecan-4 normally acts as co-receptor with  $\alpha 5 \beta 1$  integrins for fibronectin (Kerrisk et al., 2014). DDRs are receptor tyrosine kinases that are activated via interaction with collagens. There are two forms of DDRs. DDR1 is primarily expressed in epithelial cells and immune cells and is activated by collagen type I and IV, whereas DDR2 is mainly found in mesenchymal cells and binds to collagen type I-III, but not to collagen type IV. Upon collagen binding via their extracellular domain, the cytoplasmic regions of the DDRs undergo autophosphorylation and

provide docking sites for various signalling molecules, including PI3K and Erk, that regulate distinct cellular behaviours such as migration and proliferation (Itoh, 2018). uPARAP/Endo180 is a member of the mannose receptor family that serves as endocytic receptor for collagen type I, II and IV. uPARAP/Endo180 not only plays key roles in tissue homeostasis but is also involved in pathological disruptions of the ECM structure during cancer progression (see below 1.3.1). CD44 is transmembrane glycoprotein that binds to different ECM components including osteopontin (OPN), collagens and especially hyaluronic acid (HA) (Senbanjo and Chellaiah, 2017). HA-induced CD44 signalling increases the expression of MMPs that promote breast cancer cells invasion (Montgomery et al., 2012).

### **1.2.3 Functions of the ECM**

The ECM serves distinct functions that can affect physical, biochemical and biomechanical processes, regulating a wide range of cellular behaviours. The ECM is best characterized as inert scaffold that provides physical support for tissue architecture and integrity (Figure 1.11A). In addition, the ECM can play either negative or positive roles in regulating cell migration. On the one hand, the ECM acts as a physical barrier and anchorage site that not only maintains cell polarity but also blocks pathological cell migration (Figure 1.11B and C). On the other hand, the ECM can function as a movement track for migration through changing its physical properties including topography, density and rigidity (Figure 1.11D). For example, collagen forms cross-links to align in a single direction parallel to the skin in scars rather than a random formation in normal tissue, indicating that collagen contributes to direct cell migration to promote wound healing (Sharma et al., 2017). At the same time, the ECM components can also promote cell migration through regulating turnover of FAs (Kai et al., 2019). As a highly charged protein network, the ECM also provides binding sites for a myriad of growth factors, including fibroblast growth factors (FGFs), epidermal growth factors (EGFs) and hedgehogs, inhibiting their free diffusion and controlling their release in certain situations (Figure 1.11E). For example, researches illustrated that proteoglycans can bind to FGFs and serve as their reservoir (Lu et al., 2012). At the same time, some ECM components not only bind to certain growth factors but also serve as low-affinity co-receptors, enhancing the binding affinity between these growth factors and their receptors (Figure 1.11F) (Lu et al., 2011). Additionally, the ECM can act as signal presenters to target cells (Figure 1.12G). For

example, the NC1, a fragment of collagen type IV which is processed by membrane type 2 (MT2)-MMP, has been demonstrated to promote epithelial proliferation and branching morphogenesis through binding to  $\beta$ 1-integrin and activating intracellular PI3K/AKT signalling pathway (Rebustini et al., 2009). Furthermore, the ECM regulates genome organization and gene expression through utilizing its biomechanical properties. These mechanical signals are sensed by integrins and transduced to the nucleus through the cytoskeleton networks (Figure 1.11H) (Uhler and Shivashankar, 2017). Finally, extracellular degradation of ECM components by MMPs is known to be a principal mechanism in the turnover of the ECM. Additionally, a number of ECM components can be internalized and degraded in the lysosomes as well (see below 1.3) (Rainero, 2016). These two mechanisms are considered to be collaborative rather than mutually exclusive during ECM remodelling (Figure 1.11I) (Shi and Sottile, 2008a). A balanced ECM remodelling plays an important role in maintaining epithelial morphogenesis and tissue homeostasis, and deregulated ECM remodelling is often associated with tumour progression (Quail and Joyce, 2013).

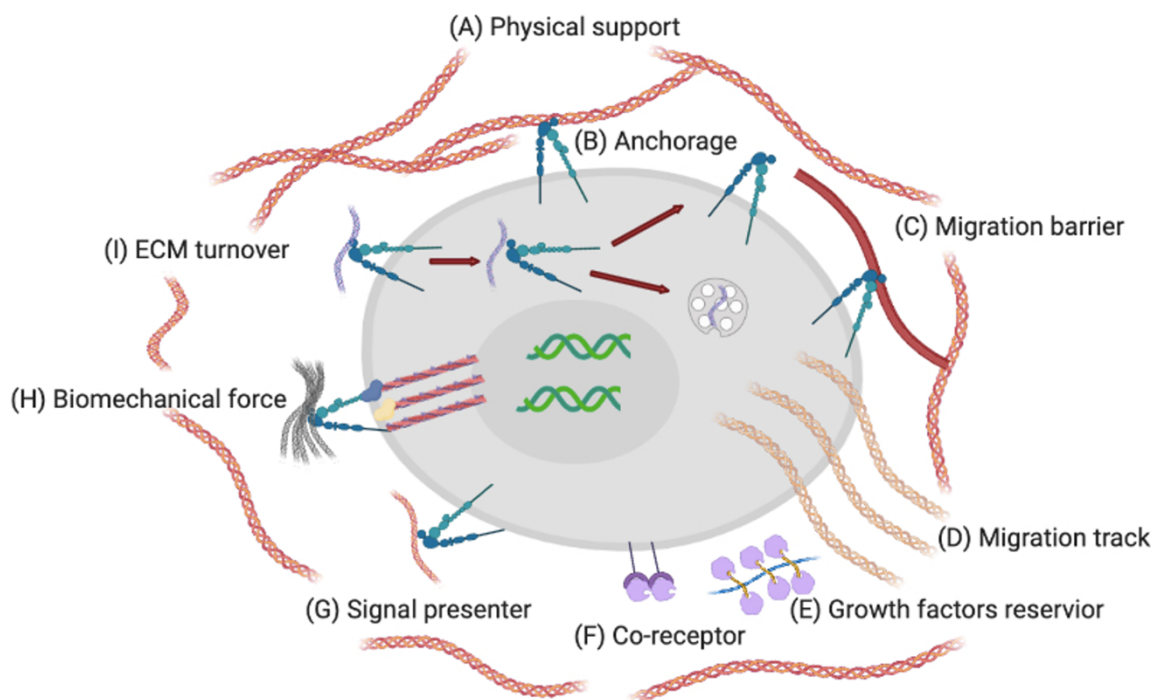


**Figure 1.11 Functions of the ECM.** (A) The ECM provides physical support for tissue. (B) and (C) The ECM serves as binding site for cells that inhibits cell migration. (D) The ECM acts as migration track in certain conditions. (E) The ECM can provide binding sites for growth factors, as well as act as low-affinity co-receptor (F). (G) The ECM serves as signal presenter to activate intracellular signals. (H) The physical properties of the ECM could be sensed by integrins, which control gene expression. (I) ECM internalization and lysosome degradation involves in ECM turnover. Image is 'Created with BioRender.com'.

#### 1.2.4 ECM remodelling in breast cancer

The continuous remodelling of ECM during physiological conditions is regulated by a fine balance between matrix synthesis, deposition and degradation. This tight regulation of the ECM remodelling process is disrupted in cancer. Increasing evidence demonstrates that the deregulated ECM remodelling has been implicated in almost every step of cancer development and progression (Lu et al., 2012). Here I will focus on the remodelling of primary ECM components and their contribution in breast cancer progression.

Breast cancer is characterized by a dense and desmoplastic tumour microenvironment (TME) owing to the excessed deposition and altered organization of ECM proteins. The desmoplastic reaction is generally associated with therapy resistance and tumorigenesis (Willumsen et al., 2019). As the most abundant ECM component, elevated deposition of collagen I is frequently observed in breast cancer (Insua-Rodríguez and Oskarsson, 2016). Additionally, the structural and physical properties of the ECM are continually changing in breast cancer as well. Collagen I surrounding normal epithelial structures is generally tangled and disorganized, whereas collagen I within breast carcinoma is stiffened, thickened and aligned perpendicularly to the tumour boundary (Figure 1.12) (Walker et al., 2018). Breast cancer cells are demonstrated to migrate faster on stiffer substrates and their persistent migration is directed up a stiffness gradient (Kai et al., 2016). Hence, collagen could be served as a scaffold to facilitate breast cancer cell migration. Consistently, local invasion of breast cancer cells has been illustrated to be oriented along aligned collagen fibres, suggesting the contribution of increased collagen alignment in tumour invasion (Conklin et al., 2011). These changes are not restricted to breast cancer. The majority of desmoplastic reaction in pancreatic ductal adenocarcinoma (PDAC) is attributed to enhanced production and crosslinking of collagen I. Increased levels of collagen I deposition in PDAC have been associated with poor prognosis and reduced overall survival (Whatcott et al., 2015). The abnormal collagen remodelling in breast cancer is mainly carried out by cancer associated fibroblasts (CAFs) (Lu et al., 2011). CAFs are activated forms of fibroblasts and one of the most abundant cellular components of the TME. Compared to fibroblasts, CAFs are able to enhance the release of MMPs and LOX proteins, contributing to the cross-linking and re-alignment of collagen (Pankova et al., 2016). Integrins are major mechanoreceptors on cells. Increased ECM stiffness has been proved to facilitate the

proliferation and migration of breast cancer cells via integrin-dependent mechanisms. Increased stiffness encourages  $\beta$ 1 integrins clustering, resulting in the elevated activated form of FAK (pY397 FAK). Subsequently, enhanced levels of pY397 FAK could result in a higher intracellular contractility through a RHO-associated protein kinase (ROCK)-dependent pathway, allowing cancer cells to pull on the matrix during invasion (Kaushik et al., 2016). Moreover, increased FAK activates mitogen-activated protein kinase (MAPK) pathway, contributing to the proliferation of breast cancer cells (Provenzano et al., 2009). Furthermore, nuclear yes-associated protein (YAP) and its transcriptional co-activator with PDZ-binding motif (TAZ) are key regulators of multiple cellular behaviours such as survival and proliferation. The YAP/TAZ proteins actively shuttle between the nucleus and the cytoplasm. In mammals, the core Hippo pathway can induce the phosphorylation of YAP in the cytoplasm, stimulating cytoplasmic retention or proteolytic degradation (Boopathy and Hong, 2019). Mechanosensing transmitted by the integrins and cytoskeleton inhibits YAP phosphorylation and thus promotes YAP nuclear translocation and transcriptional activation, facilitating breast cancer proliferation (Dobrokhotov et al., 2018). Increased ECM stiffness has been strongly linked to a poor prognosis for breast carcinoma patients, regardless of tumour stage, size and subtype (Xu et al., 2019).

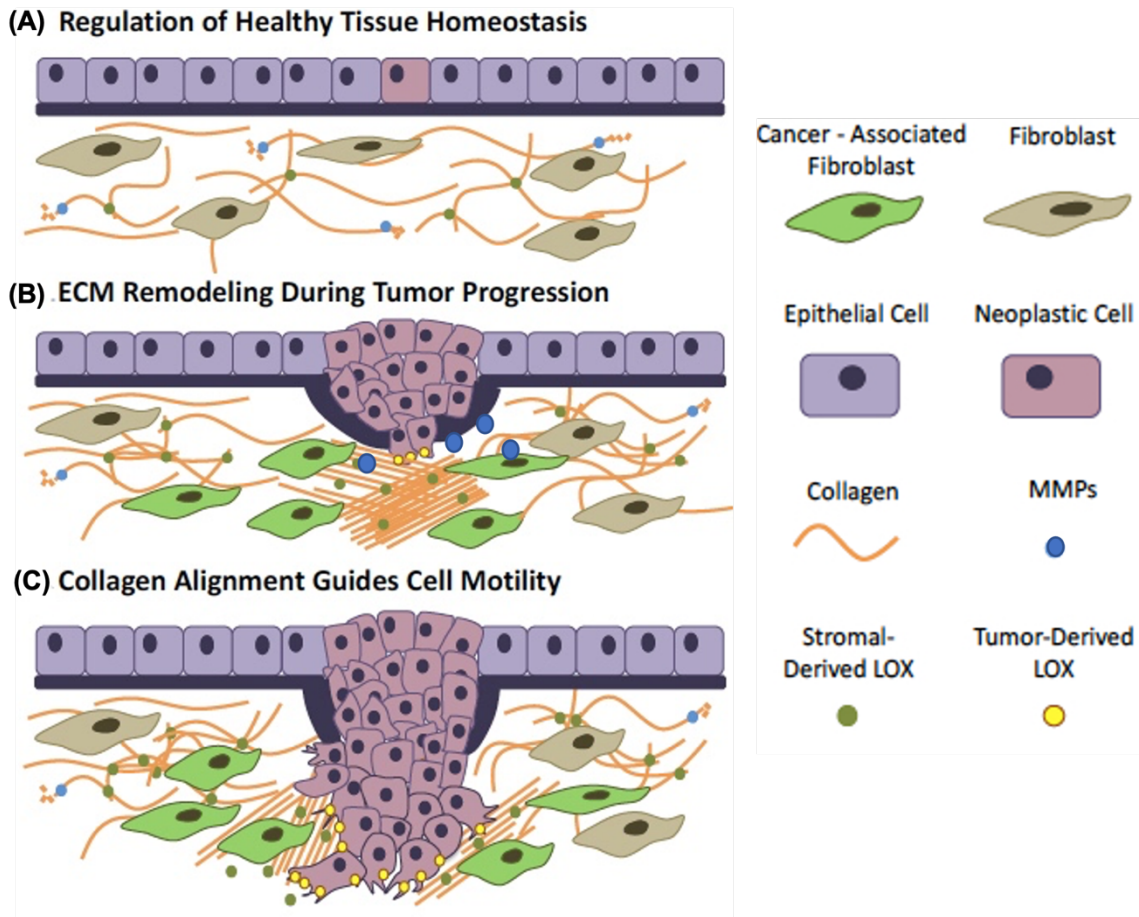


**Figure 1.12 ECM remodeling in cancer development.** (A) In normal tissue, collagen is generally tangled and disorganized. BM physically separates the epithelial cells and surrounding stroma. (B) and (C) During breast cancer development, collagen deposition is increased. Upregulated LOX aligns collagen. Cancer cells breach the BM with help of MMPs and migrate along aligned collagen. Figure is adapted from (Walker et al., 2018).

In addition to collagen I, deposition of fibronectin is strongly increased during desmoplasia. Upregulated fibronectin has been shown to facilitate breast cancer via distinct mechanisms (Oskarsson, 2013). At the primary tumour site, upregulated fibronectin deposition is required for the enhanced incorporation of collagens into the ECM, contributing to the formation of an organized fibrillar matrix architecture (Oskarsson, 2013). Epithelial-mesenchymal transition (EMT) is an important process in breast cancer development in which epithelial cells lose apical-basal polarity and cell-cell contacts and gain a migratory mesenchymal phenotype (Horejs, 2016). Fibronectin is a well-known mesenchymal marker that contributes to transforming growth factor  $\beta$  (TGF $\beta$ )-mediated EMT via binding to  $\beta$ 1 integrins (Park and Schwarzbauer, 2014). Additionally, zonula occludens-1 (ZO-1) is a tight junction adaptor that preferentially binds to the cytoplasmic tail of  $\alpha$ 5 integrin subunits.  $\alpha$ 5 $\beta$ 1/ZO-1 complexes have been proved to increase the recruitment of fibronectin- $\alpha$ 5 $\beta$ 1 complexes at the leading edge

of migrating cells, promoting breast cancer cells migration (González-Tarragó et al., 2017). Besides binding to integrins, increased fibronectin can bind to EGFRs as well to activate signal transducer and activator of transcription 3 (STAT3) signalling pathway, contributing to the proliferation and migration of breast tumour cells (Balanis et al., 2013). Moreover, fibronectin plays important roles in extravasation. The attachment of circulating tumour cells (CTCs) to the blood vessels of secondary sites is a key step in metastasis. Researchers illustrated that plasma fibronectin complexed with fibrin activates  $\alpha\beta3$  on the CTCs, promoting breast cancer cell adhesion to the endothelium to foster extravasation in a talin1-dependent pathway (Malik et al., 2010). Furthermore, increased deposition of fibronectin is frequently observed in the premetastatic niche as well. Primary melanoma tumour cells stimulate fibronectin generation in resident pulmonary fibroblasts that promotes the recruitment of both vascular endothelial growth factor receptor 1 (VEGFR1)<sup>+</sup> bone-marrow-derived hematopoietic cells and tumour cells to the premetastatic lung, promoting the metastasis of cancer cells (Kaplan et al., 2005). Lastly, metastatic breast cancer cells can remain in a dormant state at disseminated sites due to the lack of key growth-promoting signals. Fibronectin has been illustrated to induce the switch of breast cancer cells from quiescence to proliferation by promoting the phosphorylation of myosin light chain (Barkan et al., 2008), suggesting a role for fibronectin in the recurrence of breast cancer.

In non-malignant tissue, epithelial BM acts as a physical barrier to the potential pathogenic local invasion of cells, while endothelial BM inhibits intravasation and extravasation during metastasis. Laminins and collagen type IV are two important components in the BM (Mak and Mei, 2017). In early stage of breast carcinoma, expression of laminins and collagen type IV is significantly decreased because of increased BM degradation. MMPs are the most dominant proteases in the degradation of BM. Overexpressed MMP2 and MMP9 are mainly secreted by the CAFs for collagen type IV degradation, contributing to the formation of 'micro-tracks' during mesenchymal invasion (Chang and Chaudhuri, 2019). The degradation of BM not only weakens its barrier function but also contributes to cancer cell migration through signals induced by the cleaved products. For example, laminin-332 has previously been illustrated to be processed by MMP2 via cleaving the  $\gamma$ -2 chain of laminin-332, releasing an 80kDa fragment ( $\gamma$ 2x). This  $\gamma$ 2x-fragment has been proved to promote migration of breast cancer cells (Duffy et al., 2000).

### 1.3 ECM internalization in cancer progression

Currently, two major mechanisms are described to be participated in the turnover of the ECM. One is extracellular degradation, which is mainly mediated by MMPs and proteases. The other pathway is lysosomal degradation after receptor-dependent ECM endocytosis (Rainero, 2016). These two pathways are considered not mutually exclusive but to work collaboratively in the turnover of the ECM (Shi and Sottile, 2008a). Compared to proteolytic degradation, the role of ECM internalization and intracellular degradation in breast cancer is still poorly understood. In this part, I will introduce the pathways regulating main ECM component internalization and their contribution in the development and progression of different cancers (Figure 1.13).

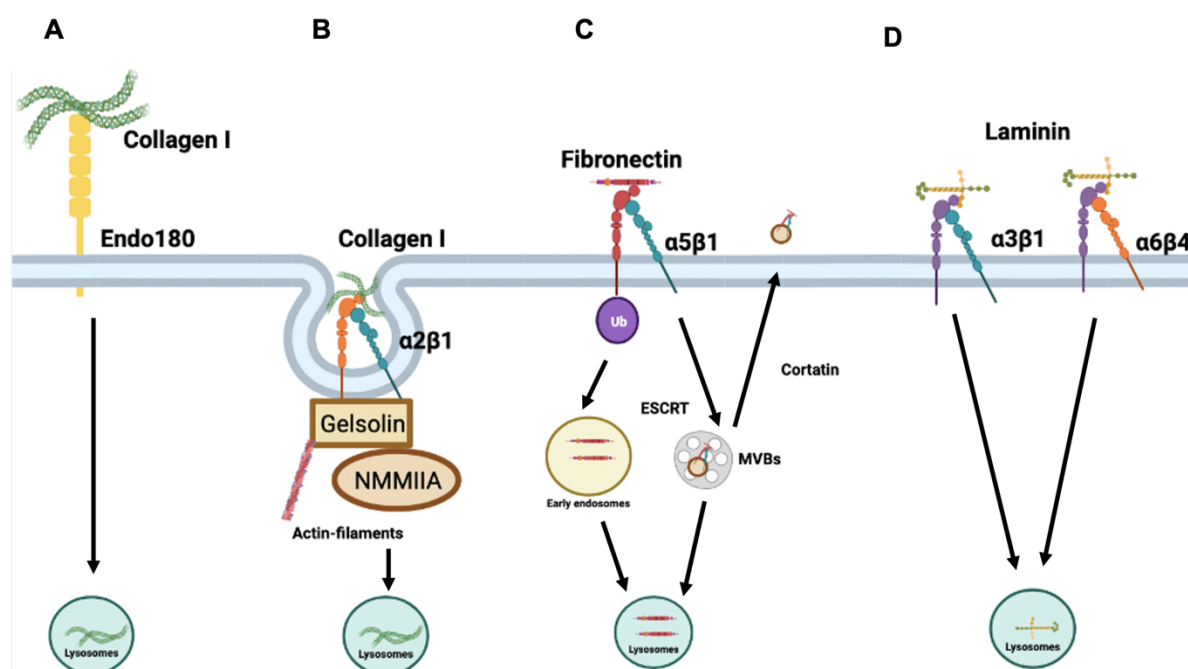


**Figure 1.13 The internalization pathways of main ECM components.** Collagen I can be internalized by (A) Endo180 and (B)  $\alpha 2\beta 1$ . (C)  $\alpha 5\beta 1$  is responsible to fibronectin endocytosis. Internalized fibronectin could be either degraded or re-secreted back to the plasma membrane. (D) Laminin is suggested to be internalized via  $\alpha 3\beta 1$ - or  $\alpha 6\beta 4$ -dependent pathway for degradation. Figure is adapted from (Rainero, 2016).

#### 1.3.1 Collagen I

Collagen I internalization is mainly regulated by two endocytic receptors: uPARAP/Endo180 and  $\alpha 2\beta 1$  integrin (Melander et al., 2015). uPARAP/Endo180 is composed of an N-terminal cysteine-rich domain, a fibronectin type II domain and 8 C-type lectin-like domains, and a transmembrane domain followed by a small cytoplasmic region (Wienke et al., 2003). Upon

binding to fibronectin type II domain, collagen is internalized through a clathrin-dependent endocytosis pathway and is delivered to late endosomes/lysosomes for degradation, while receptors are rapidly recycled back to the cell surface from early endosomes (Figure 1.13A) (Kjøller et al., 2004; Wienke et al., 2003). In addition, researchers found that, while both the soluble (cleaved) and the insoluble (intact) collagen could be endocytosed by uPARAP/Endo180, the endocytosis of MT1-MMP pre-cleaved collagen is much more efficient in uPARAP/Endo180 positive fibroblasts, highlighting that MMPs-dependent extracellular degradation and intracellular degradation after receptor-mediated internalization work collaboratively in regulating ECM turnover (Madsen et al., 2007). In fibroblasts, collagen can be internalized through binding to  $\alpha 2\beta 1$  integrin as well (Arora et al., 2000). Binding between topologically complex collagen substrate and  $\alpha 2\beta 1$  integrin induces the activation of stretch-activated  $Ca^{2+}$  channels, which can promote the interactions of the non-muscular myosin II A (NMMIIA) with the actin-binding protein gelsolin at the adhesion site. This interaction enhances gelsolin-dependent nucleation of actin-filaments, leading to collagen phagocytosis and intracellular degradation (Figure 1.13B) (Arora et al., 2013). However, it is less clear how fibroblasts select between uPARAP/Endo180- and  $\alpha 2\beta 1$ -dependent mechanisms for collagen internalization. On the one hand, it has previously been shown that MT1-MMP is required for the uptake of collagen I through uPARAP/Endo180-dependent pathway (Madsen et al., 2007), whereas the presence of MMP-1 inhibitor significantly decreases  $\alpha 2\beta 1$ -dependent collagen I endocytosis (Arora et al., 2013). Hence, there is the possibility that the pathways of collagen I internalization are dependent on the expression levels of different MMPs. On the other hand,  $\alpha 2\beta 1$ -dependent collagen phagocytosis is strongly dependent on the morphology of collagen substrate (Arora et al., 2013), suggesting a role for ECM organization in controlling collagen endocytosis.

uPARAP/Endo180-dependent collagen endocytosis has been illustrated to promote breast cancer growth. For example, uPARAP/Endo180 is overexpressed on mesenchymal stromal cells in mammary tumours. Increased stroma collagen accumulation from the invasive front and diminished tumour burden are observed *in vivo* due to a targeted deletion in the *Endo180* gene. This increased collagen accumulation is not caused by an increase in collagen synthesis,

indicating that uPARAP/Endo180-dependent intracellular collagen degradation is functionally important to mammary tumour growth (Curino et al., 2005). Besides fibroblasts, increasing evidence shows that uPARAP/Endo180 can be expressed in tumour cells as well. For example, MCF-7 cells are able to be uPARAP/Endo180-positive after TFG- $\beta$  treatment. Overexpressed uPARAP/Endo180 in MCF-7 cancer cells is shown to promote tumour growth. In contrast, no growth advantage is found in tumours containing Endo180 (Ala<sup>1468</sup>/Ala<sup>1469</sup>) mutant, which can be expressed at the cell surface but unable to undergo endocytosis. Consistently, upregulated accumulation of extracellular collagen is observed in endocytosis-deficient tumours (Wienke et al., 2007). These findings highlight the contribution of collagen uptake to tumour growth *in vivo*. Additionally, recent findings from the Rainero lab demonstrated that under amino acid starvation, internalized collagen I contributes to the growth of invasive breast cancer cells in a metabolism-dependent manner, suggesting a role for collagen I internalization in controlling tumor growth under nutrient starvation (Nazemi et al., 2021). Altogether, the internalization of collagen I in both stroma and tumour cells plays an important role in the growth of breast cancer cells.

### 1.3.2 Fibronectin

Fibronectin turnover has been shown to occur through a cavin-1-dependent endocytosis pathway, followed by lysosomal degradation (Sottile and Chandler, 2005). Additionally, it has been proved that  $\alpha 5\beta 1$  integrin, but not  $\alpha v\beta 3$  integrin, is responsible to the endocytosis of both soluble and matrix fibronectin by myofibroblasts (Shi and Sottile, 2008a). Fibronectin binding induced rapid ubiquitination of  $\alpha 5$  integrin at cytoplasmic domain and accelerated internalization of fibronectin-bound  $\alpha 5\beta 1$  integrin. Endosomal acidification contributes to dissociation of majority  $\alpha 5\beta 1$  integrin from fibronectin, as well as USP9x-mediated deubiquitination of  $\alpha 5\beta 1$  integrin, facilitating  $\alpha 5\beta 1$  integrin recycling to the cell surface (Kharitidi et al., 2015). The ubiquitinated fibronectin-bound  $\alpha 5\beta 1$  integrin can be delivered to ILVs of MVBs via an endosomal sorting complex required for transport (ESCRT) machinery, leading to lysosomal degradation (Figure 1.13C). This degradation is required for the migration of fibroblasts (Lobert et al., 2010). Moreover, this  $\alpha 5\beta 1$ -dependent fibronectin endocytosis has been shown to be regulated by MT1-MMP activity (Shi and Sottile, 2011), suggesting that extracellular proteolysis and endocytosis can co-ordinately regulate the

turnover of fibronectin. In addition to being degraded, internalized fibronectin could be re-secreted from the late endosomes/lysosomes as well. Cortactin is a well-known regulator in controlling membrane trafficking and exocytosis, focal adhesion assembly and lamellipodia formation (Kirkbride et al., 2011). In fibrosarcoma and breast cancer cells, cortactin is required for the secretion and the deposition of fibronectin at the basal cell surface through interactions with branched actin networks (Sung et al., 2011). A potential explanation for this fibronectin trafficking is that re-secreted fibronectin is insoluble compared to newly synthesized fibronectin from the Golgi. Therefore, targeted deposition of assembled fibronectin from late endosomes/lysosomes might be faster to regulate FAs formation at the leading edge of cells, promoting cell migration (Sung and Weaver, 2011).

### **1.3.3 Laminin**

Laminin-111 is a major component in the BM. Researchers illustrated that dystroglycan is the dominant receptor in regulating laminin internalization and lysosomal degradation in normal epithelial cells (Leonoudakis et al., 2014). Both soluble and assembled laminin could be internalized via a dystroglycan-dependent pathway (Leonoudakis et al., 2014). However, dystroglycan is known to be functionally compromised in many aggressive tumours, including MDA-MB-231 breast cancer cells, which leads to the disruption of dystroglycan-dependent laminin endocytosis (Leonoudakis et al., 2014). This suggests that altered laminin trafficking is required to facilitate cancer progression. In breast cancers, laminin-bound  $\alpha 3\beta 1$  integrin has been shown to promote the phagocytosis of both Matrigel and gelatin, followed by their lysosomal degradation, indicating that  $\alpha 3\beta 1$ -mediated laminin endocytosis might be involved in breast cancer progression (Figure 1.13D) (Coopman et al., 1996). This result is consistent with the increased expression of  $\alpha 3\beta 1$  integrin in MDA-MB-231 cells, contributing to cancer cell migration (Morini et al., 2000). A recent study showed that in normal mammary epithelial cells laminin could be internalized by  $\alpha 6\beta 4$  integrin under dietary restriction and nutrient deprivation conditions (Figure 1.13D). Internalized laminin was delivered to late endosomes/lysosomes for degradation, resulting in an increase in essential intracellular amino acid levels and enhanced mammalian target of rapamycin complex 1 (mTORC1) signalling, thus supporting starved epithelial cell survival (Muranen et al., 2017). These data suggest that laminin acts as the fuel for anabolism. Although this study did not illustrate if

breast cancer cells could internalize laminin through  $\alpha6\beta4$  integrin-dependent mechanism for cell growth and proliferation under nutrient stress, elevated  $\alpha6\beta4$  integrin expression has been found in basal-like breast cancer cells that leads to a decreased 5-year relapse-free survival in patients with TNBC (Bierie et al., 2017; Lu et al., 2008). Desmoplasia results in hypoxia and nutrient limitation. In this microenvironment, internalized laminin via  $\alpha6\beta4$  integrin-dependent manner may be a potential nutrient source in promoting breast cancer growth.

#### **1.4 The role of integrin endocytosis and trafficking in cell migration**

Cell migration is a ubiquitously observed physiological process in mammalian systems which supports embryogenesis, wound healing, immune responses and the metastatic progression of cancer (Horwitz and Webb, 2003). Cell migration is thought of as a cyclic process including four important stages: polarisation to form distinct front and rear edges (Lauffenburger and Horwitz, 1996); forward protrusion of the front edge (Mogilner and Oster, 1996); adhesion to the substratum using integrins (Hynes, 1987); and retraction and forward propulsion of the cell rear (Riento and Ridley, 2003). Increasing evidence demonstrates that integrin trafficking is an important player in regulating cell migration and invasion, due to its contribution to the turnover of FAs (Caswell and Norman, 2008; Paul et al., 2015). The classic hypothesis is that integrins are predominantly internalized from the cell rear and transported to the cell front. However, this original hypothesis has been disproved by increasing evidence showing that integrins trafficking in migrating cells could be directed towards the cell rear and endocytosis and recycling have been shown to occur at the leading edge. For example, kinesin family member 1C (Kif1C)-dependent  $\alpha5\beta1$  integrin trafficking from the perinuclear domain along microtubules to the rear of migrating epithelial cells contributes to adhesions maturation that stabilizes cell tails, supporting the persistent migration (Theisen et al., 2012).

The role of integrin endocytosis and trafficking in cell migration and invasion depends on the availability of ECM ligands. Increasing body of evidence has implicated the trafficking of two fibronectin-binding integrins,  $\alpha\beta3$  and  $\alpha5\beta1$ , in driving invasive cell migration. In the absence of fibronectin,  $\alpha\beta3$  integrin is internalized and recycled in a Rab4-dependent pathway by binding to vitronectin. This Rab4-dependent  $\alpha\beta3$  recycling can inhibit the recycling of  $\alpha5\beta1$ ,

facilitating breast cancer cell invasive migration in a  $\alpha v\beta 3$ -dependent manner. In the presence of fibronectin,  $\alpha v\beta 3$  inhibition can result in an increased recycling of  $\alpha 5\beta 1$ , contributing to cancer cell invasion (Christoforides et al., 2012). The recycling of  $\alpha 5\beta 1$  is regulated by several different pathways, depending on its activation status. Inactive  $\alpha 5\beta 1$  integrin has been shown to be recycled to the leading edge via a Rab11/Rab coupling protein (RCP)-dependent pathway. This pathway can be stimulated by the inhibition of  $\alpha v\beta 3$  (Caswell et al., 2008) or by the expression gain-of-function mutants of the tumour suppressor p53 in cancer cells (Muller et al., 2009). RCP and  $\alpha 5\beta 1$  can recruit receptor tyrosine kinases (RTKs), promoting their trafficking and stimulating their signalling (Muller et al., 2013). Localized RTK signalling is able to activate AKT that inhibits Rac and subsequently increase RhoA activity, resulting in the formation of filopodial protrusions (Jacquemet et al., 2013; Rainero et al., 2012). These protrusions have been shown to drive metastatic cancer cell migration both *in vitro* (3D matrix) and *in vivo* (zebrafish) (Wilson et al., 2018). Additionally, Rab25 is a member of the Rab11 family of small GTPases, which can drive the recycling of ligand-bound  $\alpha 5\beta 1$  from chloride intracellular channel protein 3 (CLIC3)-positive late endosomes/lysosomes to the cell surface at the rear of the cells. This recycling mechanism drives localized Src activity that is required for ovarian cancer cell invasive migration (Dozynkiewicz et al., 2012).

Tensins 1-3 and Arf4 can coordinate the internalization of fibronectin-bound  $\alpha 5\beta 1$  integrin from adhesions located in the subnuclear area in ovarian cancer cells over-expressing Rab25, eventually leading to fibronectin lysosomal degradation. This pathway stimulates the activation of the key nutrient sensing regulator mTORC1 to promote cancer cell migration. Moreover, when mTOR1 activity is inhibited,  $\alpha 5\beta 1$  integrin-dependent fibronectin endocytosis is significantly increased (Rainero et al., 2015). These data suggest that internalized fibronectin can fuel cancer cells invasive migration in low nutrient conditions. Additionally, re-secreted fibronectin is able to facilitate directional migration via stabilizing protrusions at the leading edge of fibrosarcoma cells.  $\alpha 5\beta 1$  Integrin is functionally required for fibronectin endocytosis in this process (Sung et al., 2015). These findings indicate that internalized ECM components during integrin trafficking can regulate cell migration as well.

## 1.5 Aims of the thesis

Dysregulated ECM degradation is related to the migration and invasion of breast cancer cells. Two major ECM degradation pathways have been described: MMPs-dependent pericellular degradation and lysosomal degradation after integrin-mediated endocytosis. Currently, the role of extracellular ECM degradation in breast cancer is widely recognized. For example, enhanced MMP-13 expression by  $\alpha 2\beta 1$ -mediated activation of p38 mitogen-activated protein kinase (MAPK) promotes MDA-MB-231 cell migration (Ibaragi et al., 2011). There is increasing evidence showing that integrin-dependent ECM endocytosis is also a key regulator in cancer cell migration and invasion. For example,  $\alpha 5\beta 1$ -dependent fibronectin uptake is shown to be required for the migration of invasive ovarian cancer cells (Rainero et al., 2015). However, the contribution of ECM endocytosis in breast cancer is still overlooked, compared with extracellular degradation. Hence, this project aims to characterize the contribution of ECM internalization in breast cancer cell migration and invasion. In addition, the Gligorijevic lab recently demonstrated the coordination of cell cycle progression with the extracellular degradation of ECM (Bayarmagnai et al., 2019b). The Humphries lab revealed that cell adhesion complexes were regulated during cell cycle progression (Jones et al., 2018). These findings suggest the potential role of cell cycle in ECM internalization, but the molecular basis of the connection is unknown. Therefore, this project will identify whether ECM components endocytosis in breast cancer cells is controlled by the cell cycle as well.

The aims of this study are as follow:

- To compare the endocytosis of different types of ECM (cell-derived matrices, collagen I, Matrigel and laminin) between normal mammary epithelial and breast cancer cells.
- To characterize which integrins are required for ECM endocytosis in breast cancer cells.
- To further investigate internalized ECM components and their receptors through an unbiased mass spectrometry screen.
- To examine the role of integrin-mediated ECM internalization in breast cancer cell migration and invasion.
- To explore the possible connection between ECM uptake and cell cycle progression.

## 2 Materials and methods

### 2.1 Materials

#### 2.1.1 Reagents

Table 2.1	Reagents and suppliers	
	Reagents	Supplier
	0.45µm syringe filter	Gilson
	10cm <sup>2</sup> petri dishes	Greiner bio-one
	12-well tissue culture plates	Greiner bio-one
	24-well glass bottom tissue culture plates	Greiner bio-one
	3.5cm <sup>2</sup> glass-bottom dishes	SPL Life Science
	6-well tissue culture plates	Greiner bio-one
	Alexa Fluor™ 488 Phalloidin	Invitrogen
	Alexa Fluor™ 555 Phalloidin	Invitrogen
	Alexa Fluor™ 647 NHS Ester	Invitrogen
	Ammonium hydroxide (NH <sub>4</sub> OH)	Sigma-Aldrich
	Bovine serum albumin (BSA)	Sigma-Aldrich
	Cell tracker™ Green CMFDA	Thermo Scientific
	Cell tracker™ Red CMTPX	Thermo Scientific
	Collagen type I (Rat tail high concentration)	Corning
	Dimethyl sulfoxide (DMSO)	Fisher Scientific
	DMEM, high glucose, pyruvate	Gibco
	DN25 (DNase)	Sigma
	DQ™-collagen, type IV from human placenta	Thermo Fisher Scientific
	Dulbecco's Modified Eagle Medium/Nutrient Mixture F-12	Gibco
	E64d (Aloxistatin)	AdooQ Bioscience

<b>Reagents</b>	<b>Supplier</b>
Epidermal growth factor (EGF)	Sigma
Ethylenediaminetetraacetic acid (EDTA)	Sigma
EZ-Link™ Sulfo-NHS-SS-Biotin	Thermo Scientific
Fetal Bovine Serum (FBS)	Gibco
Gelatin	Sigma
Glutaraldehyde solution	Sigma Aldrich
Glycine	Sigma
GM6001	Millipore
Horse Serum (HS)	Gibco
Hydrocortisone	Sigma
Insulin solution human	Sigma
Iodoacetamide (IAA)	Sigma Aldrich
L-Ascorbic acid	Sigma
Laminin/entactin complex	Corning
Lipofectamine™ 2000 (LF 2000) transfection reagent	Invitrogen
Matrigel	Corning
Methylcellulose	Sigma
NHS-Fluorescein	Thermo Fisher
NuPAGE™ LDS Sample Buffer	Thermo Fisher
Opti-MEM® I (1X), reduce serum medium	Gibco
Palbociclib	Cayman Chemical
Paraformaldehyde (PFA)	Fluka Chemika
PBS containing calcium and magnesium	Sigma
Penicillin/Streptomycin (P/S)	Life Technologies

<b>Reagents</b>	<b>Supplier</b>
Pierce™ C18 spin columns	Thermo Fisher
Propidium Iodide (PI)	Merck
Protease inhibitor cocktail	Cell signaling
PVDF membrane	IMMOBILON-FL
Qia-shredder columns	QIAGEN
Rhodamine-dextran	Life Tech
Ribonuclease	Thermo Scientific
RNase free water	Cleaver Scientific
Sodium 2-mercaptoethanesulfonate (MesNa)	Sigma Aldrich
Sodium hydroxide (NaOH)	Fisher Chemical
Soluble collagen I	Bio Engineering
Streptavidin, agarose conjugate beads	Merck
Streptavidin, Alexa Fluor™ 488	Thermo Scientific
Thymidine	Sigma
Triton-X100	Sigma
Trypan blue stain 0.4%	Gibco by life technologies
Trypsin EDTA solution 1x	Sigma
Tween-20	Sigma
Vectashield mounting reagent containing DAPI	VECTOR
Wizard® Minicolumns	Promega

## 2.1.2 Solutions

<b>Table 2.2</b>	<b>Recipes of solutions</b>
------------------	-----------------------------

Solutions	Recipe
Ammonium bicarbonate solution	50mM Ammonium bicarbonate prepared in HPLC-grade dH <sub>2</sub> O
Cell extraction buffer	20mM NH <sub>4</sub> OH, 0.5% Triton X-100 (v/v) in PBS with calcium and magnesium
Sample running buffer	1% SDS (V/V), 50mM Tris-HCl pH 7.0
TBS	10mM Tris-HCl pH7.4, 150mM NaCl
TBS-T	TBS, 0.1% Tween-20 (v/v)
TCEP	0.5M Tris (2-carboxyethyl) phosphine hydrochloride prepared in HPLC-grade dH <sub>2</sub> O
TFA	0.1% TFA (Trifluoroacetic acid) prepared in HPLC-grade dH <sub>2</sub> O
TFA/ACN	0.1% TFA, 50% ACN (acetonitrile) prepared in HPLC-grade dH <sub>2</sub> O
Towbin buffer 10x	1.92M Glycine, 0.25M Tris
Transfer buffer	10% 10X Towbin buffer, 20% methanol
Urea buffer	2M Urea prepared in HPLC-grade dH <sub>2</sub> O

## 2.2 Methods

### 2.2.1 Cell culture maintenance

MDA-MB-231 cells, fluorescent ubiquitination-based cell cycle indicator (FUCCI)-MDA-MB-231 cells and telomerase-immortalised human dermal fibroblasts (TIFs) were thawed and grown in Dulbecco's modified Eagle medium (DMEM) supplemented with 10% (v/v) foetal bovine serum (FBS) and 1% (v/v) penicillin/streptomycin (Pen/Strep), here referred to as complete medium. FUCCI-MDA-MB-231 cells were kindly provided by Dr Gligorijevic lab (Temple University, US). MCF10A cells were grown in DMEM/F-12 medium containing 5% (v/v) horse serum (HS), 1% (v/v) Pen/Strep, 20ng/ml epidermal growth factor (EGF), 10µg/ml insulin and 0.2µg/ml hydrocortisone. The MMTV-PyMT (mammary tumour virus-polyoma middle T antigen) mouse model is well characterized and widely used for breast cancer study. In this model, the oncogenesis is induced by expressing the polyoma virus middle T antigen

(PyMT) under the control of mouse mammary tumour virus (MMTV) promoter and therefore is restricted to the mammary epithelium (Lin et al., 2003). PyMT#1 were invasive breast cancer cells generated from MMTV-PyMT tumours in Dr Norman group (CR-UK Beatson Institute, Glasgow UK). PyMT#1 cells were grown in complete medium supplemented with 20ng/ml EGF and 10µg/ml insulin. NMuMG cells were cultured in complete medium containing 10µg/ml insulin. Cells were maintained at 37 °C in 5% CO<sub>2</sub>.

The cells were passaged twice a week when they reached 80% confluence. Firstly, cells were washed once with PBS and 0.25% (w/v) of trypsin was added to detach the cells. Next, cells were incubated at 37 °C for 3-5 minutes. After visualising cell detachment by light microscopy, cells were resuspended in full growth medium and plated in new tissue culture dishes at the required density. Cell lines were routinely tested for the contamination of mycoplasma.

The cells were cryopreserved when they reached 80%-90% confluence in a 10cm<sup>2</sup> dish. Cells were detached and collected in a falcon tube as described above. Next, cell suspension was centrifuged at 1000rpm for 5 minutes. The medium was then aspirated, and the cell pellet was suspended in 500µl of cryopreserving solution containing 50% (v/v) normal medium and 50% (v/v) FBS/HS. Cell suspension was then dispensed into 1ml cryopreservation vial followed by adding 500µl solution containing 80% (v/v) FBS/HS and 20% (v/v) DMSO. The vial was kept at -80 °C for at least 24 hours before transferring to liquid nitrogen.

To recover cells from cryopreservation, the cryo-vial containing cells were immersed into a water bath until nearly fully thawed. The cell suspension was transferred into a 10cm<sup>2</sup> dish containing 10ml of pre-warmed growth medium and allowed to attach overnight. Medium was removed in the following day, and the cells were washed once with PBS before being placed in 10ml fresh growth medium.

### **2.2.2 2D ECM internalization assay**

Collagen I (0.5mg/ml), Matrigel (1mg/ml) and laminin/entactin (2mg/ml) solutions were prepared in ice-cold PBS and coated on 3.5cm<sup>2</sup> glass-bottom dishes (100µl each dish). The dishes were kept at 37 °C for 1 hour for polymerisation. Afterwards, 300µl of 10µg/ml NHS-

fluorescein was added to the matrix-coated dishes for a 1-hour incubation at room temperature with gentle rocking. NHS-fluorescein is a labelling reagent which could react with primary amino groups in the matrix, forming stable amide bonds. For ECM endocytosis assays in Fucci-MDA-MB-231 cells and colocalization assays, the matrix-coated dishes were labelled with 10µg/ml Alexa Fluor 647 NHS Ester for 1 hour at room temperature. The fluorescently labelled matrix dishes were washed once with PBS before seeding the cells. For DQ-collagen IV internalization assays, 25µg/ml of DQ-collagen IV was mixed into 1mg/ml Matrigel and polymerised at 37 °C for 1 hour. The gel mixture was washed once with PBS before seeding the cells.

Cells were plated on labelled matrix dishes and incubated at 37 °C to allow the endocytosis of ECM in the presence of DMSO (Control) or 20µM E64d. E64d is a membrane-permeable cysteine protease inhibitor which prevents lysosomal protein degradation. For MDA-MB-231 and MCF10A cells, 3 x 10<sup>5</sup> cells were seeded on fluorescently labelled matrix dishes for 8 hours, while 2.5 x 10<sup>5</sup> PyMT#1 and NMuMG cells were plated for 12 hours, before being fixed and stained by immunofluorescence.

In order to measure the endocytosis of ECM in the presence of inhibitor/functional blocking antibodies against α-integrin subunits and β1 integrin, 3 x 10<sup>5</sup> MDA-MB-231 cells were plated onto 3.5cm<sup>2</sup> glass-bottomed dishes coated with NHS-fluorescein-labelled matrices and left for 2 hours at 37 °C in 5% CO<sub>2</sub> to fully adhere. Cells were treated with integrin inhibitor/blocking antibodies and DMSO/control IgG antibodies in the presence of 20µM E64d (Table 2.3). MDA-MB-231 cells were incubated for 24 hours (β1 integrin function blocking antibody) or 6 hours (α integrin subunits inhibitor/function blocking antibodies), before being fixed and stained by immunofluorescence.

**Table 2.3** List of integrin subunit inhibitor/function blocking antibodies

Integrin	Antibody/Inhibitor	Concentration	Supplier
α2	BTT-3033	10µM	Torcis (4724)
	DMSO		Fisher Scientific
α3	Purified Mouse Anti-Human (IgG1) Integrin α3 Antibody	5µg/ml	Merck (MAB19522)
	Purified Mouse (IgG1) Ctrl Antibody		BioLegend (401401)
α6	Purified Rat Anti-Human/Mouse (IgG2a) CD49f Antibody	10µg/ml	BioLegend (313637)
	Purified Rat (IgG2a) Ctrl Antibody		BioLegend (400543)
β1	Purified Rat Anti-Human (IgG1) β1 Antibody	3µg/ml	Merck (MABT409)
	Purified Rat (IgG1) Ctrl Antibody		BioLegend (400543)

### 2.2.3 Cell-derived matrix generation

The cell-derived matrix (CDM) was generated as described before (Kaukonen et al., 2017a). Tissue culture dishes were coated with 0.2% (v/v) gelatin for 1 hour at 37 °C. Afterwards, the dishes were washed twice with PBS and cross-linked with 1% (v/v) sterile glutaraldehyde for 30 minutes at room temperature. Subsequently, the dishes were washed twice with PBS and quenched with 1M sterile glycine for 20 minutes at room temperature. Following two more PBS washes, the tissue culture dishes were equilibrated for 30 minutes in complete medium at 37 °C. TIFs were grown up to 70-80% confluence and seeded onto gelatin coated dishes in complete medium. The following day, TIFs were fed with complete medium supplemented with 50µg/ml ascorbic acid, contributing to induce collagen production and render the CDM adherent to the tissue culture dishes. The medium was refreshed every other day for 8 days. To denude the matrix from intact cells, cells were washed once with PBS containing CaCl<sub>2</sub> and MgCl<sub>2</sub> (PBS<sup>++</sup>) followed by a 2-minute incubation in extraction buffer (20mM NH<sub>4</sub>OH, 0.5% (v/v) Triton X-100 in PBS<sup>++</sup>). After visualising all the cells had been removed by light microscopy, the extraction buffer was aspirated and the CDM was washed twice with PBS<sup>++</sup>. The remaining DNA residues were then digested with 15µg/ml DNase I in PBS<sup>++</sup> for 1 hour at 37 °C. Finally, the CDM was washed two times with PBS<sup>++</sup> and stored in PBS<sup>++</sup> supplemented with Pen/Strep (1:100 dilution) at 4°C for no more than two weeks.

### 2.2.4 CDM internalization assay

To measure the endocytosis of CDM, the CDM was incubated with 0.13mg/ml NHS-SS-biotin in PBS<sup>++</sup> for 30 minutes with gentle rocking at 4°C. NHS-SS-biotin is a cell-impermeable biotinylating reagent which contains a reducible disulphide bond. NHS-SS-biotin reacts with the amine groups of CDM proteins. Labelled CDM was washed once in PBS<sup>++</sup> and 3.5 x 10<sup>5</sup> cells/3.5cm<sup>2</sup> dish were seeded in the presence of 20µM E64d for an 8-hour (MDA-MB-231 and MCF10A cells) or a 12-hour (PyMT#1 and NMuMG cells) incubation. Following this, cells were washed once with ice-cold PBS<sup>++</sup> followed by a 90-minute incubation in a cell-impermeable reducing agent (15mg/ml MesNa, 15µM NaOH in PBS<sup>++</sup>) with gentle rocking at 4°C to cleave the extracellular biotin. This reaction was then quenched by adding 17mg/ml iodoacetamide (IAA) for a further 10-minute incubation at 4°C. Cells were fixed with 4% (w/v) paraformaldehyde (PFA) for 15 minutes and permeabilised with 0.25% (v/v) Triton X-100 for

5 minutes. After two washes with PBS, the cells were incubated with Streptavidin Alexa Fluor 488 (1:1000) at room temperature for 1 hour. Streptavidin can specifically associate with biotin. Next, cells were washed twice with PBS and incubated with Phalloidin Alexa Fluor 555 (1:400) for 10 minutes at room temperature to label the actin filaments. Following two more washes with PBS and one wash with sterilized water, vectashield containing DAPI was added for nucleus staining and sample preservation (Figure 2.1).

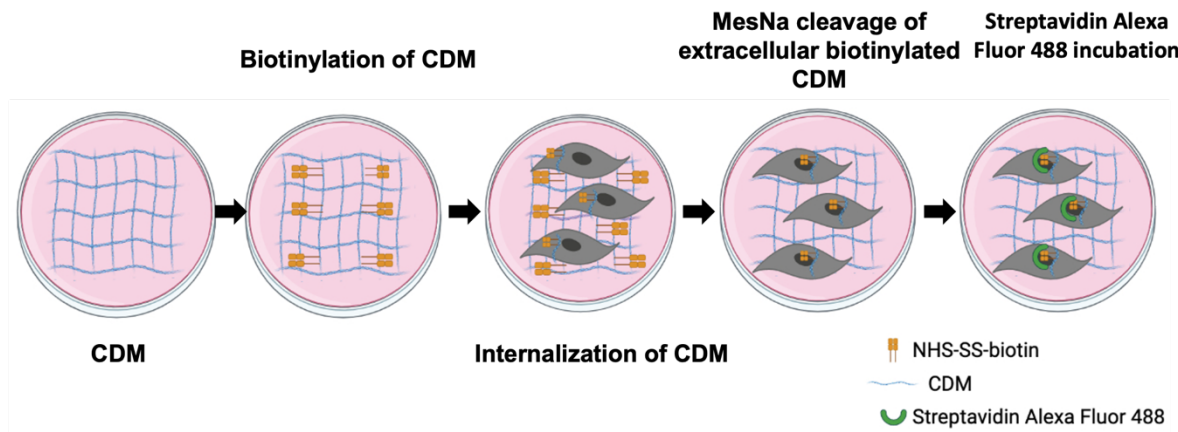


**Figure 2.1. Schematic representation of CDM internalization protocol.** CDM was biotinylated with NHS-SS-Biotin. Cells were plated on CDM for incubation in the presence of 20 $\mu$ M E64d or DMSO. The extracellular biotin was cleaved by treatment with a cell-impermeable reducing agent (MesNa). The reaction was then quenched by iodoacetamide (IAA). Cells were fixed and internalized CDM was detected by incubation with Streptavidin Alexa Fluor 488. Phalloidin Alexa Fluor 555 and DAPI were added for actin filaments and nucleus staining. Image is 'Created with BioRender.com'.

### 2.2.5 siRNA-mediated knockdown of $\alpha$ 2 integrin

MDA-MB-231 cells were seeded into 2 wells of a 6-well plate to reach 70%-80% confluence in 24 hours. 10 $\mu$ l of Lipofectamine 2000 (LF 2000) was firstly diluted in 500 $\mu$ l Opti-MEM medium. At the same time, 5 $\mu$ l of 20 $\mu$ M siRNA-targeting integrin  $\alpha$ 2 (si- $\alpha$ 2) (ON-TARGETplus SMARTpool Human ITGA2 siRNA, which contains an equal mix of different 4 siRNAs direct against the same transcript) and 5 $\mu$ l of 20 $\mu$ M non-targeting siRNA (si-nt) (ON-TARGETplus Non-targeting Control siRNA#4) were diluted into 250 $\mu$ l of Opti-MEM medium (Table 2.4). Subsequently, 250 $\mu$ l of diluted LF 2000 solution was added to each siRNA solution, referred to as transfection solution, and incubated for 20 minutes inside the tissue culture hood at room temperature. Next, cells were washed once with PBS and 500 $\mu$ l of Opti-MEM medium was added. 500 $\mu$ l of transfection solution was transferred to each well. After a 6-hour

incubation, the transfection solution was replaced with full growth medium and cells were incubated at 37 °C in 5% CO<sub>2</sub> for 48 hours (Figure 2.2).

<b>Table 2.4</b>		
<b>siRNA participating in <math>\alpha 2</math> integrin knockdown</b>		
<b>siRNA</b>	<b>Sequence</b>	<b>Supplier</b>
ON-TARGETplus SMARTpool Human ITGA2 siRNA (Catalog number: L-004566-00-0005)	GAACGGGACUUUCGCAUCA GAAACGCCCUUGAUACUAA GUUCAGACCUACUAAGCAA AAACAAGGCUGAUAAUUUG	Dharmacon™
ON-TARGETplus Non-targeting Control siRNAs (Catalog number: D-001810-04)	UGGUUUACAUGUUUUCCUA	Dharmacon™

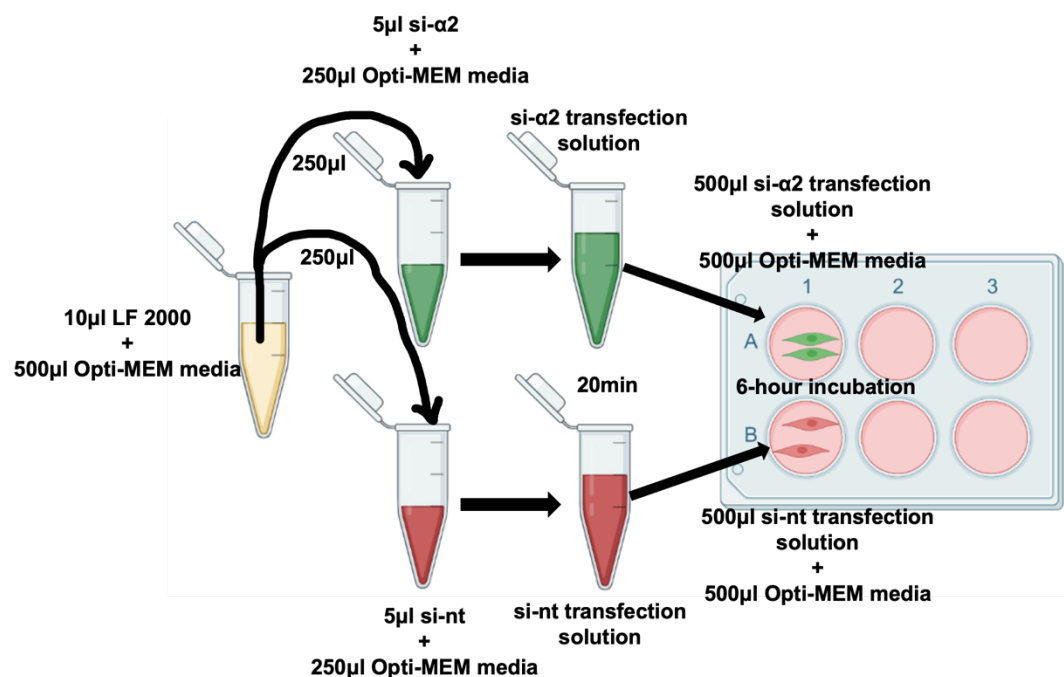


**Figure 2.2. Schematic representation of siRNA-mediated  $\alpha 2$  knockdown.** 10  $\mu$ l of Lipofectamine 2000 (LF 2000) was diluted in 500  $\mu$ l Opti-MEM media followed by adding into siRNA-target (si- $\alpha 2$ ) solution and non-targeting siRNA (si-nt) solution. si- $\alpha 2$  transfection solution and si-nt transfection solution were incubated for 20 minutes at room temperature. Cells were washed once with PBS and 500  $\mu$ l of Opti-MEM media was added. 500  $\mu$ l of transfection solution was then transferred to each well for a 6-hour incubation. Cells were then incubated in full growth media for 2 days before using. Image is 'Created with BioRender.com'.

### 2.2.6 Cell migration assay on CDM

MDA-MB-231 cells were seeded onto CDM at a density of  $5 \times 10^4$  cells/well in a 12-well plate. Where indicated, cells were allowed to attach for 4 hours and  $10\mu\text{M}$  BTT-3033 or DMSO (control) were then added. For  $\alpha 2$  knockdown experiments, cells were plated onto CDM for 4 hours to fully adhere before imaging. At the same time,  $2.5 \times 10^5$  si- $\alpha 2$  and si-nt MDA-MB-231 cells were seeded onto  $3.5\text{cm}^2$  glass-bottomed dishes and fixed at the end of migration assays.  $\alpha 2$  integrin was then stained to check the effectiveness of  $\alpha 2$  knockdown (section 2.2.16).

### 2.2.7 3D spheroid invasion assay

MDA-MB-231 and MCF10A spheroids were generated using the hanging-drop method described previously (Bayarmagnai et al., 2019a). Firstly, cells were washed once with PBS and stained with green/red cell tracker ( $2\mu\text{M}$ ) in serum-free medium for 45 minutes at  $37^\circ\text{C}$ . Next,  $3 \times 10^5$  cells were harvested and resuspended in 2ml spheroid compaction medium containing  $4.8\text{mg/ml}$  methylcellulose and  $20\mu\text{g/ml}$  soluble collagen I in full growth medium. Afterwards,  $20\mu\text{l}$  of cell suspension was seeded onto the inner surface of  $10\text{cm}^2$  culture dish lid with 3000 cells in each droplet. To prevent the suspended drops from drying out during the formation of the spheroids, the culture dish was filled with 5ml of PBS to create a humid environment. Spheroids formed in 48 hours at  $37^\circ\text{C}$  in 5%  $\text{CO}_2$ .

To avoid breaking the structures, spheroids were gently flushed with  $500\mu\text{l}$  of full growth medium to concentrate the spheroids in the lower part of the lid. Spheroid suspension was transferred into a 1.5ml microcentrifuge tube. Growth medium was then removed when all spheroids settled at the bottom by gravity. The spheroids were washed once with  $500\mu\text{l}$  of fresh growth medium before being embedded into a 1:1 mixture of  $2\text{mg/ml}$  Matrigel and  $2\text{mg/ml}$  collagen I. Following this, 2-3 spheroids were aspirated and mixed homogeneously with  $60\mu\text{l}$  of Matrigel/collagen I mixture, depositing  $45\mu\text{l}$  of gel mixture and spheroids onto the center of each well of a glass-bottomed 24 well-plate. In order to prevent the embedded spheroids from reaching the bottom of the wells, the plate was slowly turned upside-down and incubated for 5 minutes at  $37^\circ\text{C}$ . Next, the plate was slowly inverted right-side-up and incubated for 1 minute. The last two steps were repeated for 4 times and the plate was then

incubated for 20 minutes at 37 °C while keeping it upside-down. Lastly, 1ml of fresh growth medium was added slowly on the surrounding of the well, avoiding the detachment of the gel droplets. The spheroids were incubated at 37 °C in 5% CO<sub>2</sub> and imaged live after 0, 40, 48 and 64 hours (Figure 2.3). For α2 knockdown experiments, 1.5 x 10<sup>5</sup> si-α2 and si-nt MDA-MB-231 cells were seeded on 3.5cm<sup>2</sup> glass-bottomed dishes after red cell tracker staining. Cells were incubated at 37 °C in 5% CO<sub>2</sub> and fixed at the end of the invasion assay. α2 integrin was stained (section 2.2.16) to measure the effectiveness of α2 knockdown.

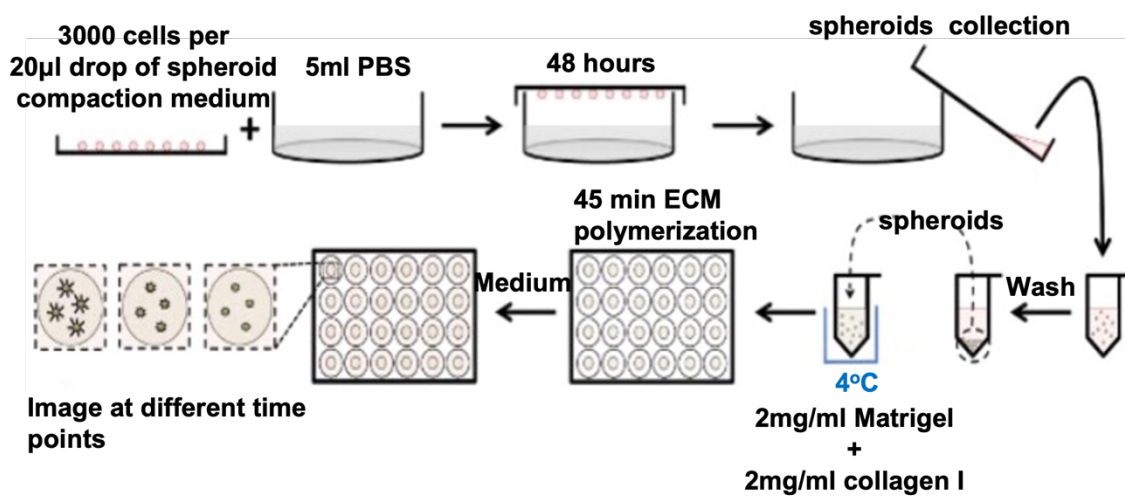


**Figure 2.3. Schematic representation of 3D spheroids invasion assay protocol.** Every 20µl spheroid compaction medium contains 3000 cells. The spheroids were formed in 48 hours. The spheroids were collected and embedded into a 1:1 mixture of 2mg/ml Matrigel and 2mg/ml collagen I. 45µl of ECM mixture containing 2-3 spheroids were deposited into each well. After 45 minutes polymerization, 1ml of fresh growth medium was added to each well. The spheroids were kept in the incubator and imaged live after 0, 40, 48 and 64 hours. Figure is adapted from (Berens et al., 2015).

### 2.2.8 Serum starvation

Cells were seeded in 10cm<sup>2</sup> culture dishes to reach around 60-70% confluency after 24 hours. The following day, the culture medium was aspirated, the cells were washed once with PBS and cell culture medium without serum was added. After a 24-hour incubation at 37 °C, the cells were washed once with PBS and 10ml of standard culture medium with serum was added into the dishes. This releases the cells from the G1 block and they progress through the cell cycle. The samples were then harvested at the indicated time points for flow cytometry analysis (section 2.2.11).

### **2.2.9 Double thymidine block**

Cells were plated onto 10cm<sup>2</sup> culture dishes to reach ~50% confluency within 24 hours. The following day, the culture medium was removed and the cells were washed once with PBS. Afterwards, 10ml of standard culture medium supplemented with 2mM thymidine was added to the dishes. Cells were grown at 37 °C for 18 hours. Cells were washed once with PBS followed by a 9-hour incubation in standard culture medium at 37 °C to release the block. After this the medium was removed, cells were washed once with PBS and 10ml of standard culture medium containing 2mM thymidine was added to dishes for a second block, which was performed at 37 °C for 18 hours. Subsequently, cells were washed once with PBS and released into standard culture medium. The samples were harvested at the indicated time points for flow cytometry analysis (section 2.2.11).

### **2.2.10 CDK4/6 inhibition**

Cells were seeded in 10cm<sup>2</sup> culture dishes to reach ~70% confluency with 24 hours. The cells were washed once with PBS and incubated in standard culture medium supplemented with 1µM Palbociclib for 24 hours at 37 °C. After this, the cells were washed with PBS and released into standard culture medium. The samples were harvested at the indicated time points for flow cytometry analysis (section 2.2.11).

### **2.2.11 Cell cycle analysis by flow cytometry**

The cells were detached in 0.25% (w/v) trypsin and collected in 4.5ml PBS. The trypsin/PBS solution was centrifuged at 1000\*g for 5 minutes. Afterwards, the supernatant was aspirated and the pellet was re-suspended in 0.5ml of ice-cold PBS supplemented with 2mM EDTA. The re-suspended cells were added dropwise into 4.5ml ice-cold 70% (v/v) ethanol with shaking by fingers, to fix the samples and prevent cell clumping. The samples were kept at 4°C for no more than three months.

To quantify the number of cells in the different stages of the cell cycle, propidium iodide (PI) staining was used to quantitatively assess the amount of DNA within cells. The samples were centrifuged at 1000\*g for 10 minutes. The ethanol was then removed and the cells washed twice with 3ml PBS, vortexed gently and spun at 800\*g for 5 minutes. Subsequently, the cell

pellet was re-suspended and incubated in 500µl of PBS containing 200µg/ml ribonuclease RNase for 5 minutes on ice to avoid RNA staining. Following this, 5µl 2mg/ml PI was added to the samples and left to incubate in the cold room for 3 hours. The levels of fluorescence emitted by the samples were measured and analysed by Susan Clark (Flow Cytometry Core Facility of the University of Sheffield, UK).

### **2.2.12 Matrigel internalization with GM6001**

1mg/ml Matrigel was polymerized and labelled with NHS-fluorescein as described in section 2.2.2. Following this,  $3 \times 10^5$  synchronized and asynchronous MDA-MB-231 cells were seeded onto NHS-fluorescein-labelled Matrigel dishes either with DMSO (control) or 10µM GM6001, which is a broad spectrum MMP inhibitor, in the presence of 20µM E64d, for 6 hours. Cells were fixed and stained by immunofluorescence.

### **2.2.13 Measurement of macropinocytosis**

0.1mg/ml collagen I was polymerized as described in section 2.2.2. Afterwards,  $3 \times 10^5$  synchronized and asynchronous MDA-MB-231 cells were seeded onto 0.1mg/ml collagen I coated dishes for 6 hours to fully adhere. Subsequently, 0.25mg/ml rhodamine-dextran was added for 1 hour incubation. Cells were fixed and stained by immunofluorescence.

### **2.2.14 Measurement of $\beta$ 1 integrin internal pool**

1mg/ml Matrigel was polymerized as described in section 2.2.2. Next,  $3 \times 10^5$  synchronized and asynchronous MDA-MB-231 cells were seeded for a 6-hour incubation in the presence of 20µM E64d. Cells were fixed and stained for  $\beta$ 1 integrin (section 2.2.16).

### **2.2.15 Measurement of mTORC1 activity**

3.5cm<sup>2</sup> glass-bottomed dishes were coated with 1mg/ml of Matrigel, 0.1mg/ml of Matrigel and 0.1mg/ml of collagen I as described in section 2.2.2. Following this,  $3 \times 10^5$  synchronized and asynchronous MDA-MB-231 cells were seeded in full growth medium. Cells were incubated at 37 °C and 5% CO<sub>2</sub> for 6 hours before being fixed and stained for p-S6 (section of 2.2.16).

## 2.2.16 Immunofluorescence

Cells were fixed using 4% (w/v) PFA in PBS for 15 minutes and permeabilized with 0.25% (v/v) Triton X-100 in PBS for 5 minutes at room temperature. Next, cells were washed two times with PBS.

For 2D ECM internalization assay, cells were incubated with Phalloidin Alexa Fluor 555 (1:400 dilution) or Phalloidin Alexa Fluor 488 (1:500 dilution; ECM internalization in FUCCI-MDA-MB-231 cells) for 10 minutes at room temperature to label the actin filaments.

For integrin staining, cells were blocked in 1% (w/v) BSA for 1 hour at room temperature followed by one wash in PBS. The cells were then incubated in Alexa Fluor 488 anti-human  $\beta$ 1 integrin antibody (1:300 dilution) or FITC anti-human CD49b antibody (1:200 dilution) in 1% (w/v) BSA for 1 hour at room temperature. For EEA1, LAMP2 and p-S6 staining, cells were firstly incubated in primary antibodies in 1% (w/v) BSA for 1 hour (EEA1 and LAMP2) or 90 minutes (p-S6) at room temperature after BSA blocking. The cells were then washed three times with PBS and incubated with secondary antibodies in 1% (w/v) BSA (1:1000 dilution) for 45 minutes at room temperature (Table 2.5). Afterwards, cells were washed two times with PBS and incubated with Phalloidin Alexa Fluor 555 for 10 minutes as described above.

Following twice washes with PBS and one wash with sterilized water, vectashield containing DAPI was added for nucleus staining and sample preservation. The sample dishes were sealed with parafilm and kept at 4 °C for no more than two weeks.

**Table 2.5** List of antibodies in immunofluorescence

<b>Integrin Antibody</b>	<b>Dilution ratio</b>	<b>Supplier</b>
Alexa Fluor® 488 Anti-Human (IgG1) CD29 Antibody	1:300	BioLegend (303015)
FITC-Anti Human CD49b Antibody	1:200	BioLegend (359306)
<b>Primary Antibody</b>	<b>Dilution ratio</b>	<b>Supplier</b>
Purified Mouse Anti-EEA1 (IgG1) Antibody	1:100	BD Bioscience (610457)
Purified Mouse Anti-Human LAMP-2 (IgG1) Antibody	1:100	BioLegend (354303)
Rabbit Phospho-S6 Ribosomal Protein (Ser235/236) Antibody	1:100	Cell Signaling (2211)
<b>Secondary Antibody</b>	<b>Dilution ratio</b>	<b>Supplier</b>
Alexa Fluor® 488 Donkey-Anti Mouse (IgG H+L) Antibody	1:1000	Fisher Scientific (A-21202)
Alexa Fluor® 488 Donkey-Anti Rabbit (IgG H+L) Antibody	1:1000	Fisher Scientific (A-21206)

## **2.2.17 Mass spectrometry analysis**

### **2.2.17.1 Preparation of protein samples**

As described in the section of 2.2.3, CDM was generated in 10cm<sup>2</sup> dish and followed by biotinylation with 0.13mg/ml NHS-SS-biotin. After biotinylation, 12 x 10<sup>5</sup> cells were plated on CDM in the presence of 20μM E64d for 16 hours. Subsequently, cells were washed once with cold PBS<sup>++</sup> and the extracellular biotin was then cleaved by treating cells with reducing agent (15mg/ml MesNa, 15μM NaOH in PBS<sup>++</sup>) for a 90-minute incubation at 4°C. This reaction was quenched by adding 17mg/ml IAA for a further 10-minute incubation at 4°C. Following this, 400μl of ice-cold extraction buffer (20mM NH<sub>4</sub>OH, 0.5% (v/v) Triton X-100 in PBS<sup>++</sup>) containing a protease inhibitor cocktail (1:100 dilution) was added into each dish. Cells were then lysed on ice for 10-15 minutes until most of cells were not visualised by light microscopy. Next, cell lysates were transferred into Qia-shredder columns (Qiagen) and spun in a small desk centrifuge at full speed for two minutes. Homogenized cell lysates were then spun at 13000rpm for 10 minutes at 10°C. The supernatant containing the total protein was collected while the cell debris remaining in the pellet were discarded. Subsequently, cell lysates were mixed with sample buffer, heated at 70°C for 10 minutes and then stored at -20°C for western blotting, whereas the remaining of the lysates were used for Streptavidin-agarose beads pull-down assay (Figure 2.4).

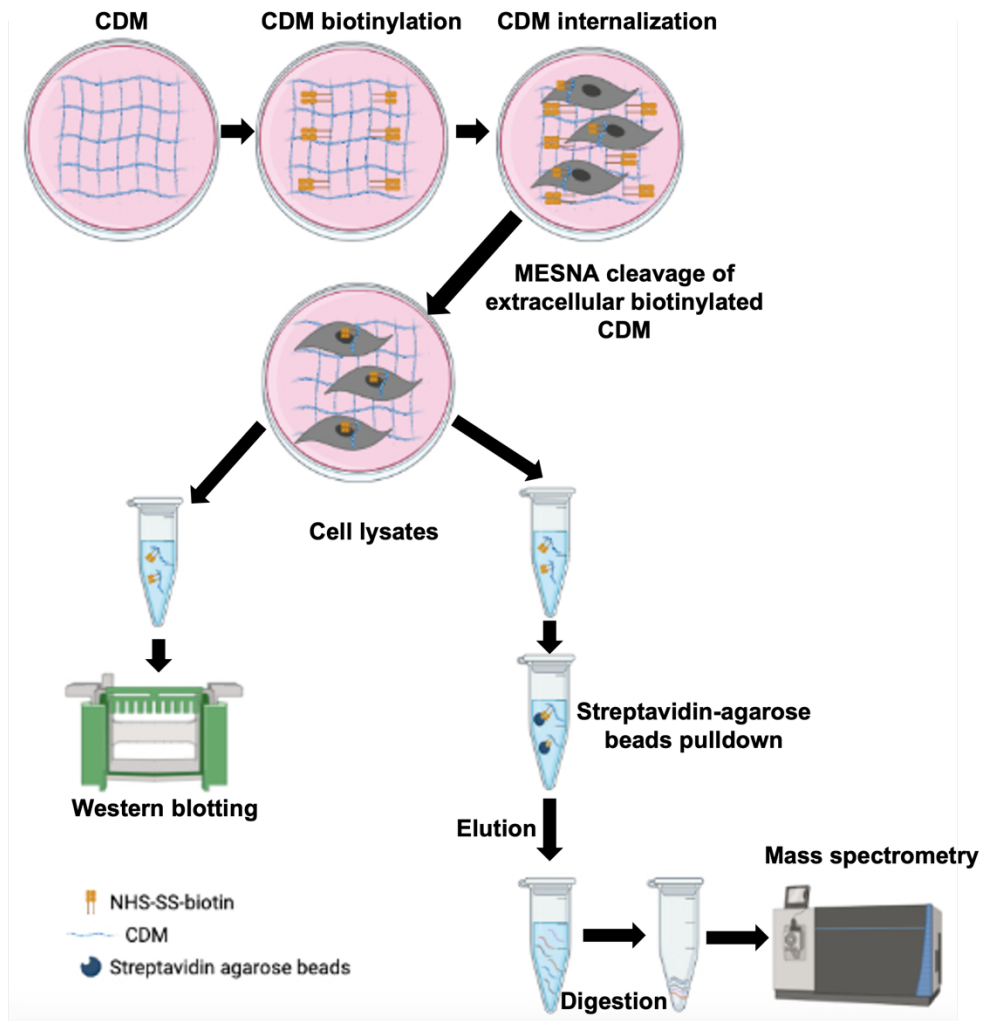


**Figure 2.4. Schematic representation of mass spectrometry proteomics protocol.** Biotinylated CDM was internalized by cells. After the cleavage of extracellular biotin, cell lysates were collected. 50 $\mu$ l of cell lysates were used for western blotting, The left cell lysates were used for streptavidin-agarose beads pull-down and following mass spectrometry assay. Image is 'Created with BioRender.com'.

### 2.2.17.2 Western blotting

The cell lysates/sample buffer mixture was fully thawed, 30 $\mu$ l of each sample and 4 $\mu$ l of protein ladder were then loaded into a Bio-Rad 4-15% Mini-PROTEAN precast polyacrylamide gel (separates polypeptides from 5kDa-200kDa) in running buffer (3g Tris base, 14.4g glycine and 1g SDS in 1L H<sub>2</sub>O). The gel was run at 100 volts constant voltage for 2 hours until the dye reached the bottom of the gel. Following this, the proteins were transferred from gel onto a FL-PVDF membrane (IMMOBILON-FL) assembled into a cassette (Figure 2.5). The membrane was pre-wet with 100% methanol to activate the chemical groups in the membrane, allowing the interactions between membrane and proteins and contributing to transfer efficiency. The

transferring process was performed in Towbin transferring buffer (25mM Tris, 192mM glycine, 20% methanol (v/v) pH 8.3) for 75 minutes at 100 volts. The membrane was then blocked in 5% (w/v) BSA in TBS-T (50mM Tris, pH 7.5, 150mM NaCl and 0.5% (w/v) Tween-20) for 1 hour at room temperature. Afterwards, the primary antibody against GAPDH (1:1000 dilution) was applied to the membrane in 5% (w/v) BSA in TBS-T overnight at 4°C. Afterwards, the membrane was washed three times in TBS-T for 10 minutes with gentle rocking before the secondary LiCor IR Dye 800 antibody (anti mouse IgG; 1:30000 dilution) and IR Dye 680LT streptavidin (1:20000 dilution) (Table 2.6) supplemented with 0.01% (w/v) SDS were applied for a 1-hour incubation at room temperature. Lastly, three more TBS-T washes were carried out followed by three washes in distilled water. A LiCor Odyssey Sa system was used for imaging. The intensity of bands was quantified using ImageStudioLite by normalizing the intensity of Streptavidin bands to the intensity of GAPDH band.

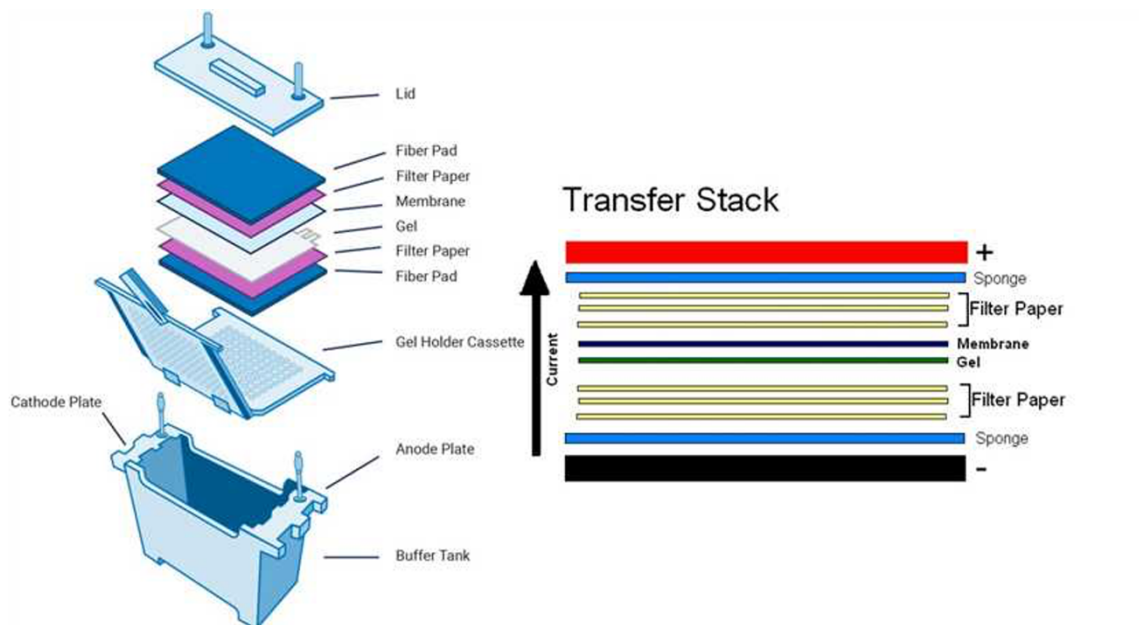


**Figure 2.5. Schematic representation of transfer stack structure.** The protein transfer is organized in the direction that allows negatively charged protein move out of gel and toward membrane in the positively charged electrode. Figure is adapted from <https://www.antibody-creativebiolabs.com/protein-transfer-from-gel-to-membrane-in-western-blot-assay.htm>.

<b>Table 2.6</b>	<b>List of antibodies in western blotting</b>
------------------	---

<b>Primary Antibody</b>	<b>Dilution ratio</b>	<b>Supplier</b>
GAPDH	1:1000	Cell signaling
<b>Secondary Antibody</b>	<b>Dilution ratio</b>	<b>Supplier</b>
IR Dye®680LT Streptavidin	1:20000	LI-COR
IR Dye®800 anti-Mouse Antibody	1:30000	LI-COR

### 2.2.17.3 Streptavidin-agarose beads pulldown and washing procedure

Streptavidin-agarose beads were firstly washed three times with 1ml of PBS<sup>++</sup> at 14000rpm for 15 seconds (cell lysates volume : beads volume = 10 : 1). The supernatant was removed after the last wash (to not disrupt the beads pellet). Subsequently, cell lysates were incubated with the equilibrated beads at 4°C overnight under constant rotation. Following this, the mixture of lysates and beads was transferred to a Wizard minicolumn, which has a filter that allows the lysis buffer to flow through, whereas the agarose beads remain in the column. The beads were washed with 10ml of 2% (w/v) SDS, 10ml of 2M urea+50mM ammonium bicarbonate and 10ml of 50mM ammonium bicarbonate in turn, removing non-specific bound proteins. All flow-through solution was discarded.

### 2.2.17.4 On-beads digestion

The proteins bound to streptavidin-agarose beads were then digested with trypsin. Firstly, proteins bound beads were collected in 100µl of ammonium bicarbonate. 1µl of 0.5M TCEP (Tris(2-carboxyethyl) phosphine hydrochloride) was then added to denature the disulphide bonds. The tube was incubated at 800 rpm for 15 mins at 37°C in a Thermomixer. Afterwards, 2 µl of 0.5M freshly made IAA was added to the sample followed by a 15-minute incubation in a Thermomixer at 800 rpm at 37°C, covered with aluminium foil to protect from light. Lastly, 2 µl 1µg/ml trypsin was added and incubated at 800 rpm for 3 hours at 37°C. The supernatant was collected. At this step, the sample can be stored at -20°C.

#### **2.2.17.5 Desalting and drying of digested peptides**

Because salt and urea traces from the digestion solution might affect the following analysis, peptides were desalted before Orbitrap injection. Firstly, the Pierce™ C18 spin columns were equilibrated and washed as the following order: 200µl of 100% acetonitrile (ACN), 200µl of 50% ACN/0.1% (v/v) trifluoroacetic acid (TFA), 200µl of TFA, acidifying the pH for better peptide binding. Next, the digested samples collected as described above were acidified by adding 4µl of neat TFA. Afterwards, the acidified samples were added to the acidified columns. The flow-through was collected for repeating the same procedure three times. Following this, the stage tips were washed three times with 100µl of 0.1% (v/v) TFA. The peptides were then eluted with 100µl of 50% ACN/0.1% (v/v) TFA into a clean Eppendorf. The desalted peptides were spun in SpeedVac (Eppendorf) for 90 mins at 45°C. The Eppendorf tube lid was opened to evaporate the solution and dry the sample. The dried peptides were reconstituted in 0.5% (v/v) formic acid and vortexed gently at the lowest speed for 10 mins followed by Orbitrap injection.

#### **2.2.17.6 Data analysis**

The peptide samples were analysed using Orbitrap Elite Hybrid Mass Spectrometer (Thermo Fisher). This procedure was operated by Dr Mark Collins (Senior Lecturer in the School of Biosciences and Deputy Director of the Biological Mass Spectrometry Facility, University of Sheffield). The mass spectrometry data were analysed using Perseus software version 2.0.3.0. In this study, we had two groups that each contained two technical repeats. Firstly, the data was transformed to a logarithmic scale by going to 'Basic-Transform' and specifying the  $\log_2(x)$  transformation function. Next, the 'Annot.rows-Categorical annotation rows' tool was used, making sure that the replicates belonging to the same condition received the same name in the following data frame. Afterwards, we moved to 'Filter rows-Filter rows based on valid values'. In this step, the minimum percentage of valid values in the expression columns that in at least one group needed to have to survive the filtering process was defined, which was 70% in this study. Subsequently, in 'Normalization-Subtract', the intensity of each condition was normalized by the median intensity of all the conditions in each sample/column. The missing values were then replaced from normal distribution. Lastly, T-test was performed between two groups of samples, comparing the differences between their internalized

contents. In the t-test,  $S_0$ , which defines the artificial within groups variance, was set to 0.1 and false discovery rate (FDR) was set to 0.05. Thus, test results below  $p < 0.05$  were shown as significant.

## **2.2.18 Imaging and analysis**

### **2.2.18.1 2D ECM internalization assay**

A Nikon A1 confocal microscope (Nikon Instruments Inc, Japan) with Plan-Apochromat 60X NA 1.4 oil immersion objective was used to image ECM internalization. The following channels were applied for the imaging of ECM internalization assays: DAPI ( $\lambda_{ex}=403.5\text{nm}$ ), FITC ( $\lambda_{ex}=480.0\text{nm}$ ) and Alexa Fluor 568 ( $\lambda_{ex}=562.0\text{nm}$ ). Cells were imaged at a resolution of 1024 X 1024 pixels, acquiring Z-stacks with 1 $\mu\text{m}$  interval through the whole depth of the cells. 80-120 cells were imaged and quantified in each experiment.

All images were analysed using image J software (Schindelin et al., 2012) as described before (Commisso et al., 2014). Firstly, the Z-stacks were maximum-projected. The outline of cells was then identified using the Phalloidin staining and recorded in the region of interest (ROI) manager. The area of each cell was measured before further processing (Figure 2.6 A). Next, the thresholds of images were adjusted to specifically select internalized ECM (black box in Figure 2.6B). Following this, the “Total Area” of internalized ECM in the ROI manager was measured (blue boxes in Figure 2.6B and C).

$$\text{ECM uptake index} = \text{Total area of internalized ECM} / \text{Cell area} \times 100$$

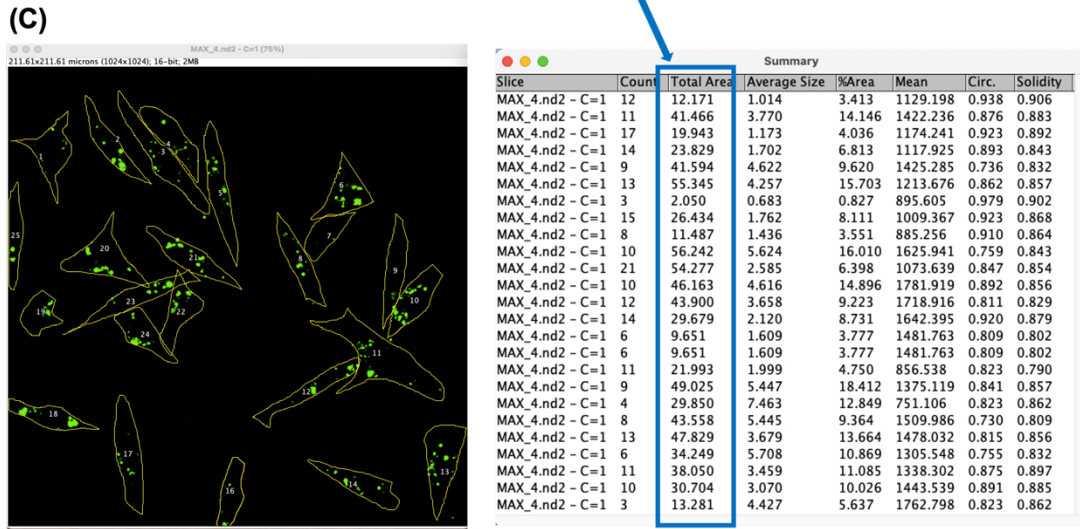
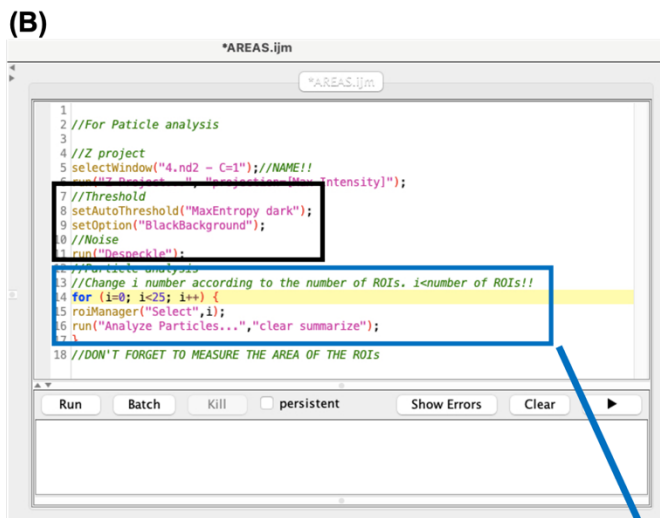
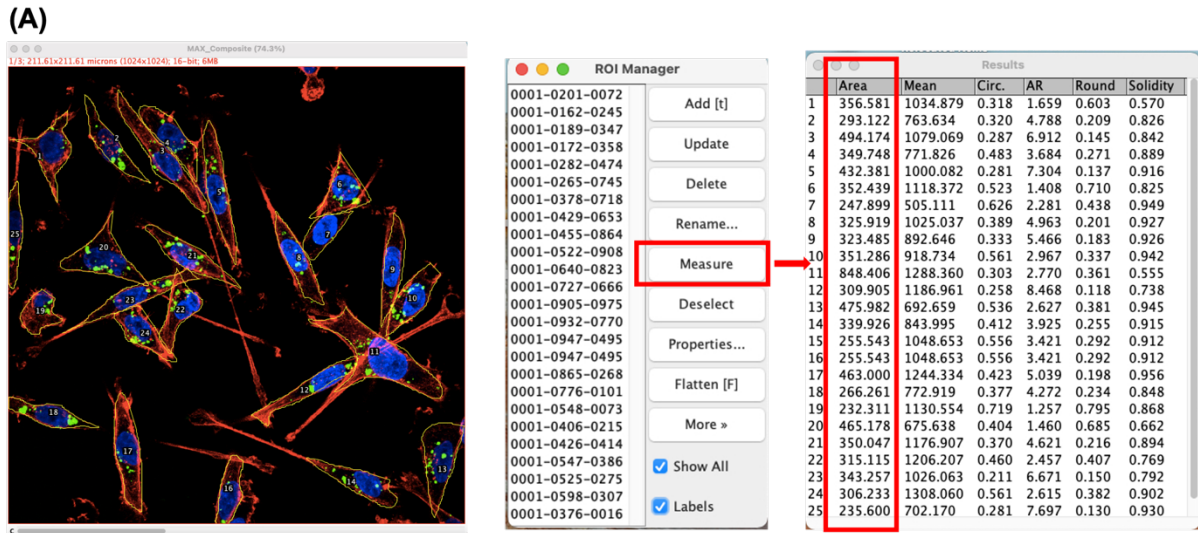


**Figure 2.6. Schematic representation of ECM internalization analysis protocol. (A)** Cells were identified individually using the Phalloidin staining in maximum projection images and recorded in ROI manager. The area of each cell was measured. **(B)** The black box illustrated the performance of background subtraction and the adjustment of thresholds on the images. The blue boxes in **(B)** and **(C)** showed the measurement of total area of internalized ECM in the ROI manager.

### **2.2.18.2 Colocalization assay**

The samples were imaged using the Nikon A1 confocal microscope as illustrated in section of 2.2.18.1. The following channels were applied for colocalization imaging: DAPI ( $\lambda_{ex}=403.5nm$ ), FITC ( $\lambda_{ex}=480.0nm$ ), Alexa Fluor 568 ( $\lambda_{ex}=562.0nm$ ) and Alexa Fluor 647 ( $\lambda_{ex}=620.0nm$ ). More than 10 cells were imaged and quantified in each experiment. The correlation of pairs of pixels was then characterised using the plugin of Colocalization Colormap in the ImageJ software (<https://sites.google.com/site/colocalizationcolormap>). This plugin can calculate normalized mean deviation product (nMDP) as a measure of correlation between corresponding pairs of pixels. The result of the algorithm is an image that contains distribution of calculated (nMDP) in a colour scale ranging from -1 to 1. Cold colours (toward blue) display to no-colocalization while warm colours (toward red) indicate co-localization, generating a spatial map of colocalization. Lastly, the method would compute index of correlation (Icorr), indicating the fraction of positively correlated (colocalized) pixel (Jaskolski et al., 2005).

### **2.2.18.3 Measure the effectiveness of $\alpha 2$ knockdown**

The samples were imaged using the Nikon A1 confocal microscope as illustrated in section of 2.2.18.1. The following channels were used for  $\alpha 2$  expression imaging: DAPI ( $\lambda_{ex}=403.5nm$ ), FITC ( $\lambda_{ex}=480.0nm$ ) and Alexa Fluor 568 ( $\lambda_{ex}=562.0nm$ ). For ECM uptake assays, the outline of cells was identified using the Phalloidin staining and recorded in ROI manager as well. The mean  $\alpha 2$  integrin intensity of each cell was measured in the FITC channel. More than 80 cells were imaged and quantified in each experiment. For cell invasion assays, cells were too confluent to quantify the intensity of individual cells at the end of the experiments. Thus, the mean intensity of  $\alpha 2$  of all cells was calculated in the FITC channel. More than five images were captured in each experiment.

### **2.2.18.4 $\beta 1$ integrin and $\alpha 2$ integrin internalization assay**

The samples were imaged using the Nikon A1 confocal microscope as illustrated in section of 2.2.18.1. The following channels were applied for  $\beta 1$  integrin and  $\alpha 2$  integrin uptake imaging: DAPI ( $\lambda_{ex}=403.5nm$ ), FITC ( $\lambda_{ex}=480.0nm$ )/ Alexa Fluor 488 ( $\lambda_{ex}=480.0nm$ ) and Alexa Fluor 568 ( $\lambda_{ex}=562.0nm$ ). Because both  $\beta 1$  integrin and  $\alpha 2$  integrin are expressed on plasma membrane, the outline of cells was carefully identified following the inner of the Phalloidin staining and

recorded in ROI manager. The internalization of integrins was then measured as described in 2.2.18.1. 80-120 cells were imaged and quantified in each experiment.

### 2.2.18.5 Cell migration assay

The plates were imaged live using Nikon widefield live-cell system with 10x/NA objective at 37 °C and 5% CO<sub>2</sub>. The images were taken every 10 minutes for 17 hours (more than 30 cells per well were quantified). Individual cell migration was manually tracked using the MTrack2 ImageJ plug-in. The velocity of migration was calculated using the plugin of Chemotaxis tool in ImageJ (<https://ibidi.com/chemotaxis-analysis/171-chemotaxis-and-migration-tool.html>). The protrusion was quantified by measuring the length between the nucleus and the end of the protrusive side of the cells (Caswell et al., 2008).

### 2.2.18.6 3D spheroids invasion assay

A Nikon A1 confocal microscope (Nikon Instruments Inc, Japan) with 10X objective was used that allowed visualization of the whole spheroids. The FITC ( $\lambda_{ex}=480.0\text{nm}$ ) and Alexa Fluor 568 ( $\lambda_{ex}=562.0\text{nm}$ ) channels were used for green cell tracker and red cell tracker staining imaging, respectively. The core spheroid area, total area, invasion distance and the number of invading cell strands were applied to measure the invasion of cells quantitatively (Figure 2.7).

Mean invasion distance ( $\mu\text{m}$ ) = Average of invasion distance (green)

Invasive area ( $\mu\text{m}^2$ ) = Total area (blue) – core spheroid area (yellow)

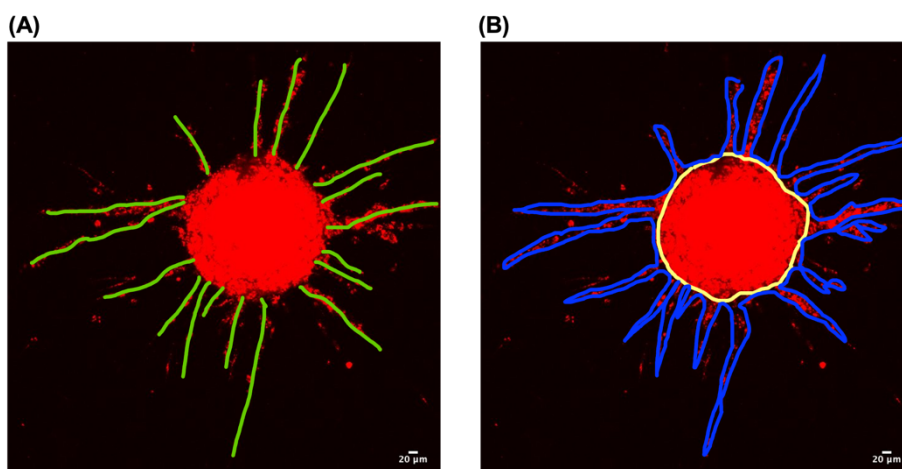


**Figure 2.7. Schematic representation of cell invasion analysis protocol. (A)** The invasion distance and the number of invading cell strands were identified (green lines). **(B)** The size of core area (yellow) and total area (blue) were measured.

### **2.2.19 Statistical analysis**

After acquiring quantitative data, graphs and statistical analysis were performed by Graphpad Prism (V.9.0) software. The method of statistical analysis was based on the dataset and indicated in each figure legend. Statistical analysis for the mass spectrometry approach was performed using Perseus software and Student t-test (described in section 2.2.17.6).

### **3 $\alpha 2\beta 1$ -dependent ECM uptake promotes breast cancer cell migration and invasion**

#### **3.1 Introduction**

The ECM is a highly dynamic and complex three-dimensional meshwork of secreted proteins surrounding cells within tissues. The ECM is continually undergoing a remodelling process where ECM components are synthesized, deposited and degraded (Pickup et al., 2014). Two principal mechanisms have been reported to be involved in the turnover of the ECM. One is extracellular degradation mediated by matrix metalloproteases (MMPs) and proteases. The other pathway is lysosomal degradation after receptor-mediated ECM internalization (Shi and Sottile, 2011). Many studies have demonstrated that abnormal extracellular ECM degradation reciprocally affects cellular functions to facilitates diverse aspects of tumour progression. For example, enhanced collagen degradation by MMP-14 promotes the formation of movement track for cancer cell migration (Friedl and Gilmour, 2009). Overexpressed MMP-9 in various cancer types not only contributes to BM breakdown at sites of origin (Winkler et al., 2020), but also facilitates awakening of dormant cancer cells and subsequent proliferation at sites of metastasis by degrading laminin (Winkler et al., 2020). Additionally, accumulating evidence is pointing that ECM internalization is important for tumour progression as well. Integrin are major receptors for ECM proteins. A recent research looking at ovarian cancer cells shows that the endocytosis of fibronectin-bound  $\alpha 5\beta 1$  integrins is required for tumour invasion (Rainero et al., 2015). Compared to proteolytic degradation, the roles of intracellular degradation in tumour progression are still poorly understood.

$\alpha 2\beta 1$  integrin is a major receptor for collagen I but can also bind to other types of collagens (III, IV and XI), laminins and some proteoglycans (Naci, 2015). Accumulating evidence suggests that  $\alpha 2\beta 1$  integrin serves as a crucial regulator in cancer development and progression either by promoting or inhibiting tumour metastasis. On the one hand, it has been shown that  $\alpha 2\beta 1$  integrin-mediated activation of p38 mitogen-activated protein kinase (MAPK) enhances the production of MMP-13, which contributes to MDA-MB-231 cell migration (Ibaragi et al., 2011). Moreover,  $\alpha 2\beta 1$  integrin can facilitate ovarian cancer cell invasion by increasing the activation of MMP-2/MMP-9 and through the disaggregation of tumour spheroids (Shield et al., 2007).

Furthermore, a recent research illustrates that downregulation of  $\alpha 2\beta 1$  integrin in MCF-7 cells strongly inhibits breast cancer metastasis (Zuo et al., 2019). On the other hand, in the mouse mammary tumour virus-*Neu* (MMTV-*Neu*) model of breast cancer,  $\alpha 2\beta 1$  integrin serves as a suppressor of cancer cell intravasation without altering tumour growth (Ramirez et al., 2011). However, despite these studies, the potential contribution of  $\alpha 2\beta 1$  integrin in breast cancer metastasis have not been addressed in detail yet.

In this chapter, we investigated the migration of breast cancer cells on cell-derived matrices (CDM). As the main cell type contributing to the synthesis of ECM *in vivo*, CDM generated by fibroblasts can mimic several properties of natural tissue (Kaukonen et al., 2017a). It has been reported that many cell lines can migrate both significantly quicker and in a more directionally persistent, less random, meandering manner on CDM compared to on traditional synthetic or polymerized 3D scaffolds or plastic (Kutys et al., 2013a; Petrie et al., 2009). Additionally, we established a 3D collagen and Matrigel mixture gel culture model to quantify the invasion of breast cancer cells. In comparison with 2D cell culture model, 3D spheroids accurately mimics the *in vivo* matrix architecture and microenvironment (Costa et al., 2016). The key differences between 2D system and 3D system are notably reflected in cellular morphology and migration speed. For example, MCF-7 cells exhibit a flat shape in 2D model, while maintain a circular and cluster conformation within the gels, similar to those *in vivo* (Cavo et al., 2016). Therefore, employing 3D models is a reliable relative and logical way to study cancer cell invasion.

In this chapter we show that the internalization of Matrigel, but not collagen I, is upregulated in breast cancer cells compared to normal mammary epithelial cells. Moreover, we point out that internalized Matrigel is delivered into late endosomes/lysosomes for degradation. At the same time, we illustrate that  $\alpha 2\beta 1$  integrin is involved in the uptake of ECM in invasive breast cancer cells. Finally, we reveal that  $\alpha 2\beta 1$  integrin is required for breast cancer cell migration and invasion. Taken together, our findings suggest that  $\alpha 2\beta 1$  integrin might be a promoter of breast cancer migration and invasion by regulating ECM internalization.

## 3.2 Results

### 3.2.1 CDM internalization is upregulated in invasive breast cancer cells

Extracellular degradation of several ECM components is strongly upregulated in breast cancer cells compared to normal mammary epithelial cells (Rebustini et al., 2009; Shi and Sottile, 2011). To assess whether invasive breast cancer cells can also uptake more ECM components compared to normal mammary epithelial cells, we firstly measured the internalization of CDM, generated by normal breast fibroblasts. CDMs are complex 3D matrices that can recapitulate several *in vivo* features of native collagen-rich matrices (Kaukonen et al., 2017a). The internalization of CDM was performed in MDA-MB-231 invasive breast cancer cells and MCF10A non-transformed mammary epithelial cells. There is growing evidence showing that internalized ECM components could be delivered to lysosomes for degradation (Rainero, 2016). Consequently, the cells were treated with DMSO (control) or 20 $\mu$ M E64d, which is a membrane-permeable cysteine protease inhibitor to prevent lysosomal protein degradation. The internalized CDM could be visualized as green signals in the cells. As illustrated in figure 3.1, in MCF10A only a small number of CDM positive vesicles were visualised inside the cells in the presence of DMSO, while E64d treatment resulted in the accumulation of more vesicles in some cells. By contrast, most of MDA-MB-231 cells displayed several CDM positive vesicles in the control group, and this was promoted after E64d treatment. Our analysis revealed that the internalization of CDM was much higher in MDA-MB-231 cells compared to MCF10A cells both in the presence and in the absence of E64d, indicating that CDM internalization was upregulated in invasive breast cancer cells compared to normal mammary epithelial cells. In addition, statistical results suggested that most of internalized CDM were degraded inside the lysosomes in both cell lines.

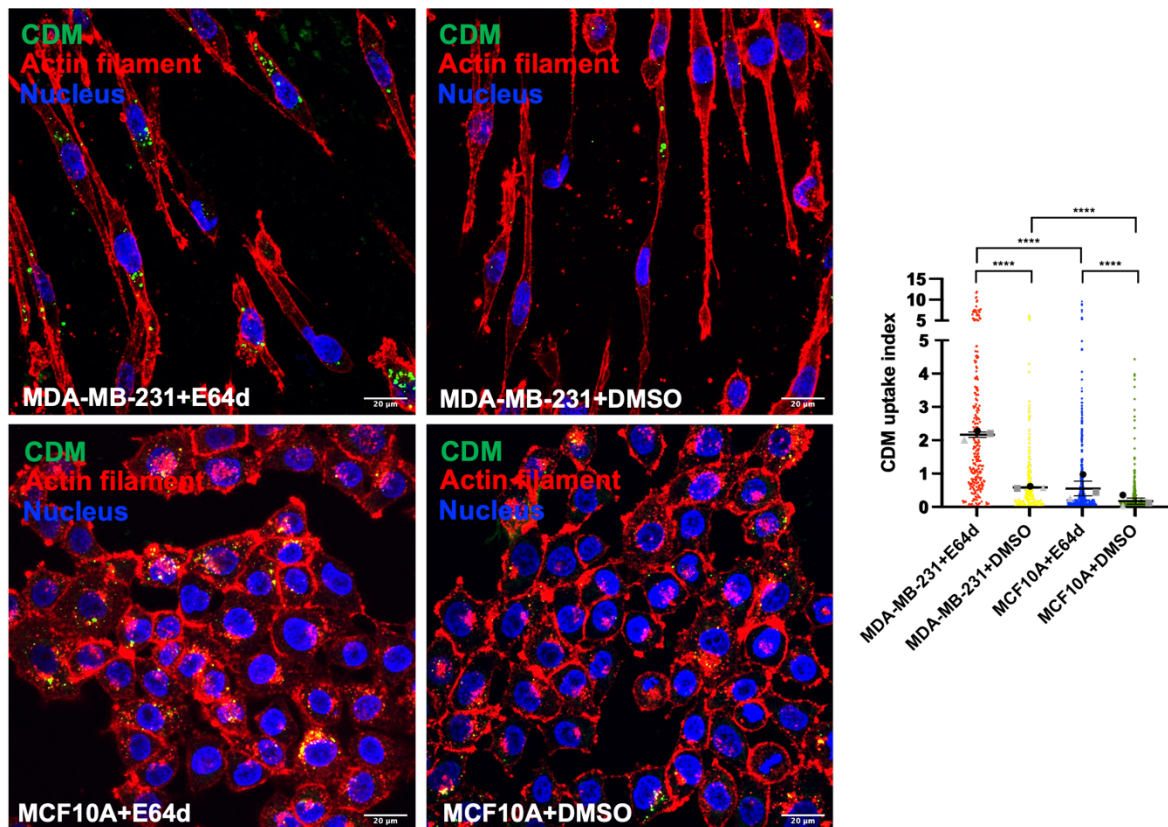


**Figure 3.1. CDM internalization is upregulated in MDA-MB-231 cells.** MDA-MB-231 and MCF10A cells were plated on biotinylated CDM for an 8-hour incubation in the presence of DMSO (control) or 20 $\mu$ M E64d. The extracellular biotin was removed by treatment with a cell-impermeable reducing agent (MesNa). Cells were fixed and stained for Streptavidin (green), actin (red) and nuclei (blue). Samples were imaged with a Nikon A1 confocal microscope and CDM uptake index was calculated with Image J. Bar=20 $\mu$ m. N=3 independent experiments. Mean  $\pm$  SEM, Kruskal-wallis with multiple comparisons (the big dots represent the mean of individual experiments). \*\*\*\*p<0.0001.

To confirm this, we performed CDM internalization assays in cells derived from mouse breast tumours, driven by the expression of the oncogene polyoma middle T (PyMT) in the mammary gland under the control of the mammary epithelial MMTV promoter (PyMT#1) and normal mouse mammary epithelial cells (NMuMG). Both cell lines were seeded on biotinylated CDM for 12 hours. Firstly, similarly to what we observed in MDA-MB-231 cells, increased accumulation of internalized CDM in the presence of the lysosomal inhibitor E64d was observed in PyMT#1 cells. However, E64d treatment did not affect CDM intracellular accumulation in NMuMG cells. Secondly, we found that, while in the control group we detected higher levels of internalized CDM in NMuMG cells, the presence of E64d resulted in a higher accumulation of internalized CDM in PyMT#1 cells, suggesting that CDM were readily

degraded in PyMT#1 cells (Figure 3.2). Altogether, our data show that the internalization of CDM is promoted in invasive breast cancer cells compared to normal mammary epithelial cells.

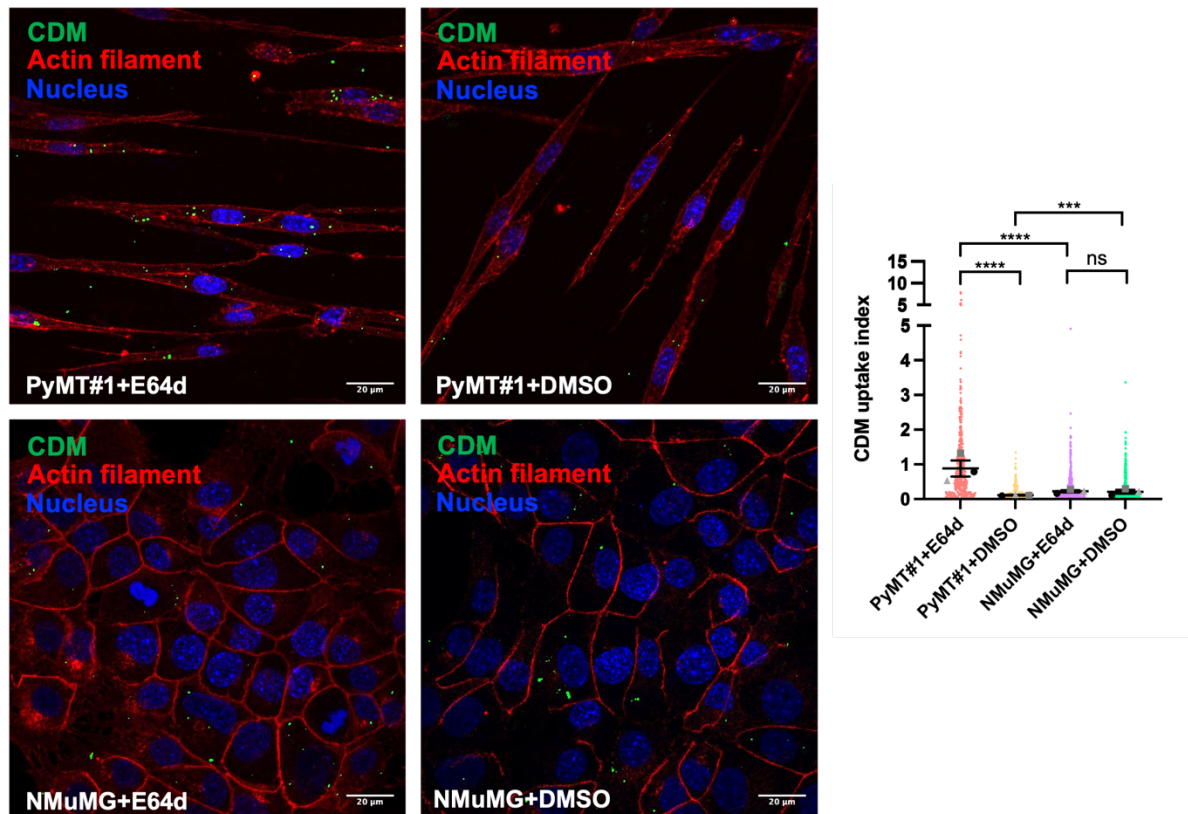


**Figure 3.2. CDM internalization is upregulated in PyMT#1 cells.** PyMT#1 and NMuMG cells were plated on biotin-labelled CDM a 12-hour incubation in the presence of 20 $\mu$ M E64d or DMSO (control). The extracellular biotin was removed by treatment with MesNa. Cells were fixed and stained for Streptavidin (green), actin (red) and nuclei (blue). Samples were imaged with a Nikon A1 confocal microscope and CDM uptake index was calculated with Image J. Bar=20 $\mu$ m. N=3 independent experiments. Mean  $\pm$  SEM, Kruskal-wallis with multiple comparisons (the big dots represent the mean of individual experiments). \*\*\*p<0.001, \*\*\*\*p<0.0001.

### 3.2.2 Collagen I internalization is not upregulated in invasive breast cancer cells

Following the ECM composition classification described in the mammalian matrisome project, almost 300 components are identified as the 'core matrisome' components (Hynes and Naba, 2012). To verify the internalisation of which ECM components is specifically upregulated in invasive breast cancer cells, we compared collagen I uptake between MDA-MB-231 cells and MCF10A cells. As the most common fibrillar collagen in ECM, increased deposition and cross-

linking of collagen I are frequently observed in breast cancer serving as a scaffold to facilitate tumour invasion (Conklin et al., 2011). Here MDA-MB-231 and MCF10A cells were seeded on fluorescently labelled collagen I for 8 hours of incubation. In the control group, we detected significantly higher collagen I internalization in MDA-MB-231 cells compared to MCF10A cells. However, internalized collagen I strongly accumulated in the presence of lysosomal inhibitor E64d in both cell lines, leading to higher accumulation in MCF10A cells (Figure 3.3).

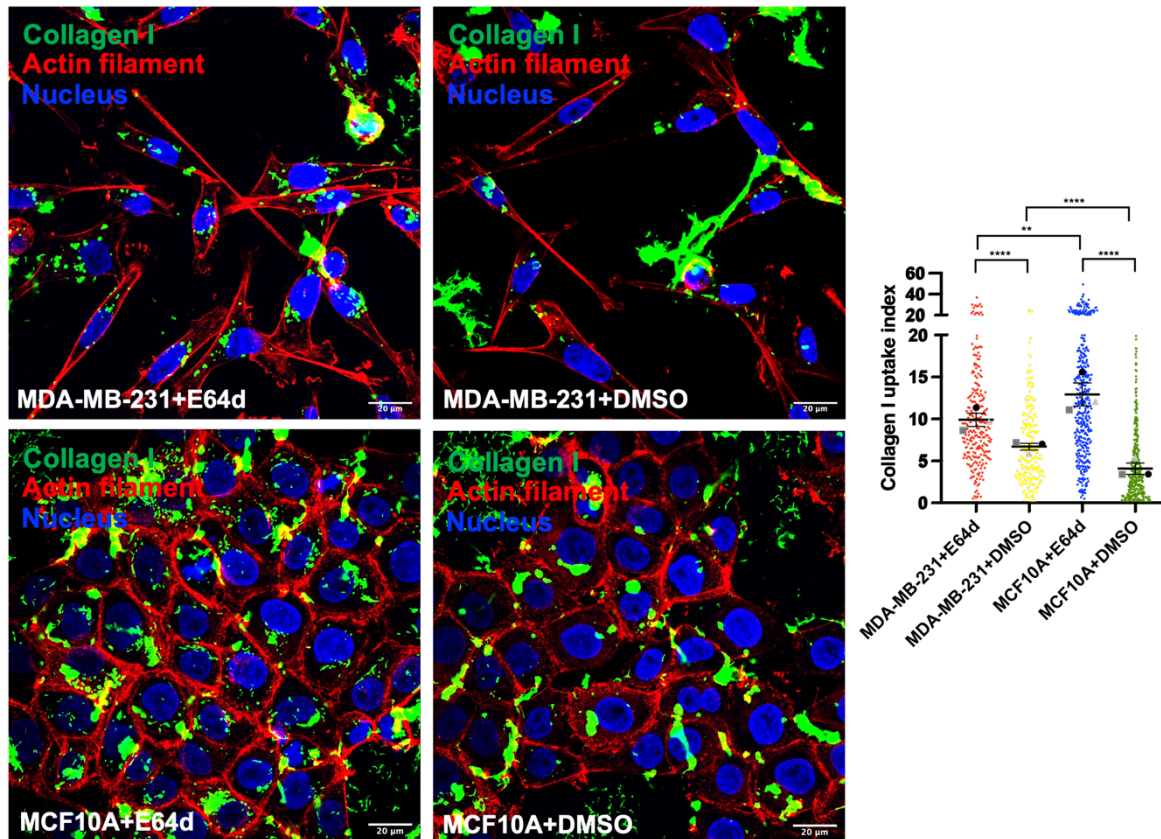


**Figure 3.3. Collagen I uptake is not upregulated in MDA-MB-231 cells.** MDA-MB-231 and MCF10A cells were plated on NHS-fluorescein labelled 0.5mg/ml collagen I dishes for 8 hours in the presence of 20µM E64d or DMSO (control). Cells were fixed and stained for actin (red) and nuclei (blue). Samples were imaged with a Nikon A1 confocal microscope and collagen I uptake index was calculated with Image J. Bar=20µm. More than 300 cells per condition in three independent experiments were analyzed. Mean ± SEM, Kruskal-wallis with multiple comparisons (the big dots represent the mean of individual experiments). \*\*p<0.01, \*\*\*\*p<0.0001.

Similarly, E64d treatment resulted in a strong accumulation of internalized collagen I in both PyMT#1 and NMuMG cells after a 12-hour incubation. Moreover, the presence of DMSO led to a small, but statically significant increased collagen I uptake in PyMT#1 cells compared to NMuMG cells. Furthermore, there was no significant difference in collagen I uptake between PyMT#1 and NMuMG cells in the presence of E64d (Figure 3.4). Taken together, these findings

demonstrate that the internalization of collagen I is not upregulated in invasive breast cancer cells.

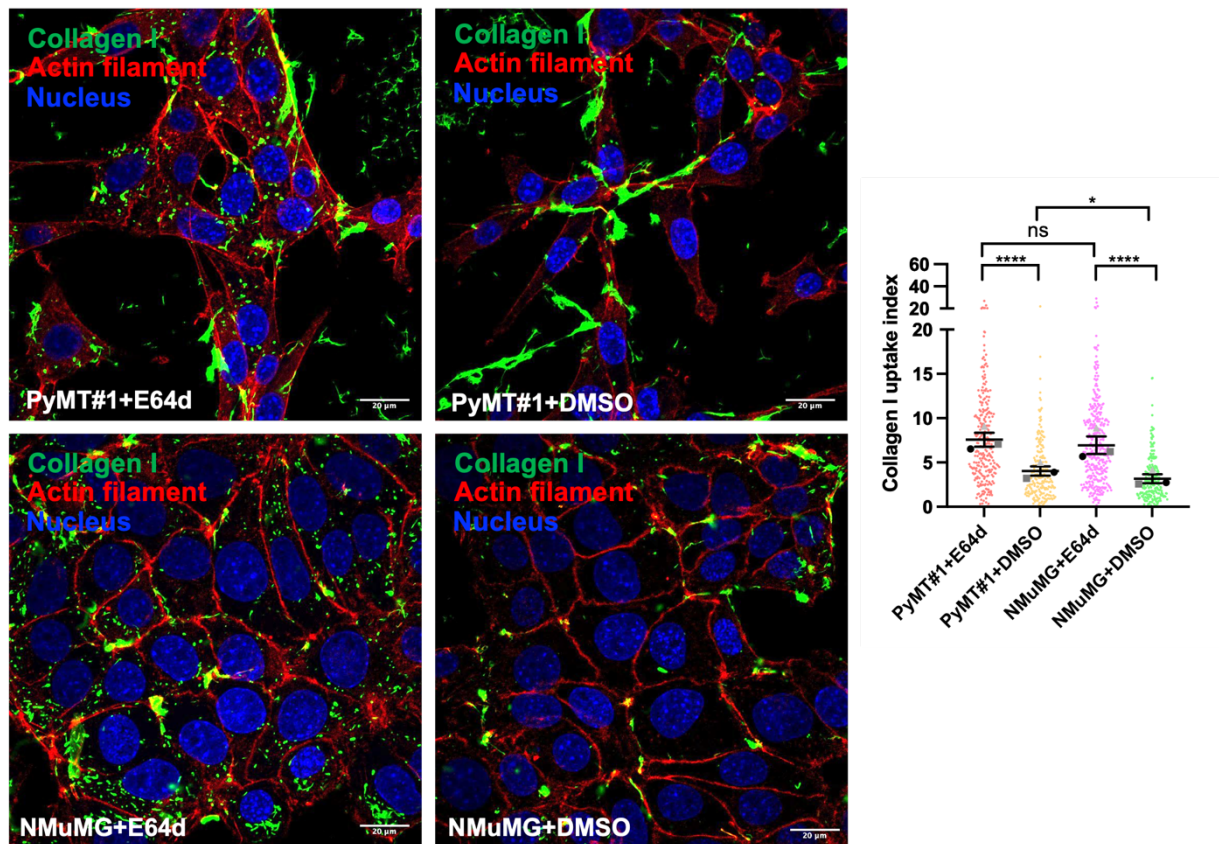


**Figure 3.4. Collagen I uptake is not upregulated in PyMT#1 cells.** PyMT#1 and NMuMG cells were plated on NHS-fluorescein labelled 0.5mg/ml collagen I dishes for a 12-hour incubation in the presence of 20μM E64d or DMSO (control). Cells were fixed and stained for actin (red) and nuclei (blue). Samples were imaged with a Nikon A1 confocal microscope and collagen I uptake index was calculated with Image J. Bar=20μm. N=3 independent experiments. Mean ± SEM, Kruskal-wallis with multiple comparisons (the big dots represent the mean of individual experiments). \*p<0.05, \*\*\*\*p<0.0001.

### 3.2.3 Matrigel internalization is upregulated in invasive breast cancer cells

Owing to the fact that increased degradation of BM is frequently observed in breast cancer, we sought to compare the internalization of Matrigel, a reconstituted BM preparation extracted from the Engelbreth-Holm-Swarm (EHS) mouse sarcoma, between MDA-MB-231 and MFC10A cells. As shown in figure 3.5, MDA-MB-231 and MFC10A cells were seeded on fluorescently labelled Matrigel for 8 hours, only a small number of MFC10A cells exhibited Matrigel positive vesicles in DMSO, while most of MDA-MB-231 cells displayed several Matrigel vesicles in the control group. As apparent from the quantification, the internalization of Matrigel was increased in MDA-MB-231 cells compared to MFC10A cells in the presence of

DMSO. Furthermore, E64d treatment resulted in an up-regulated Matrigel accumulation in both cell lines, leading to an increased Matrigel internalization in MDA-MB-231 cells (Figure 3.5).

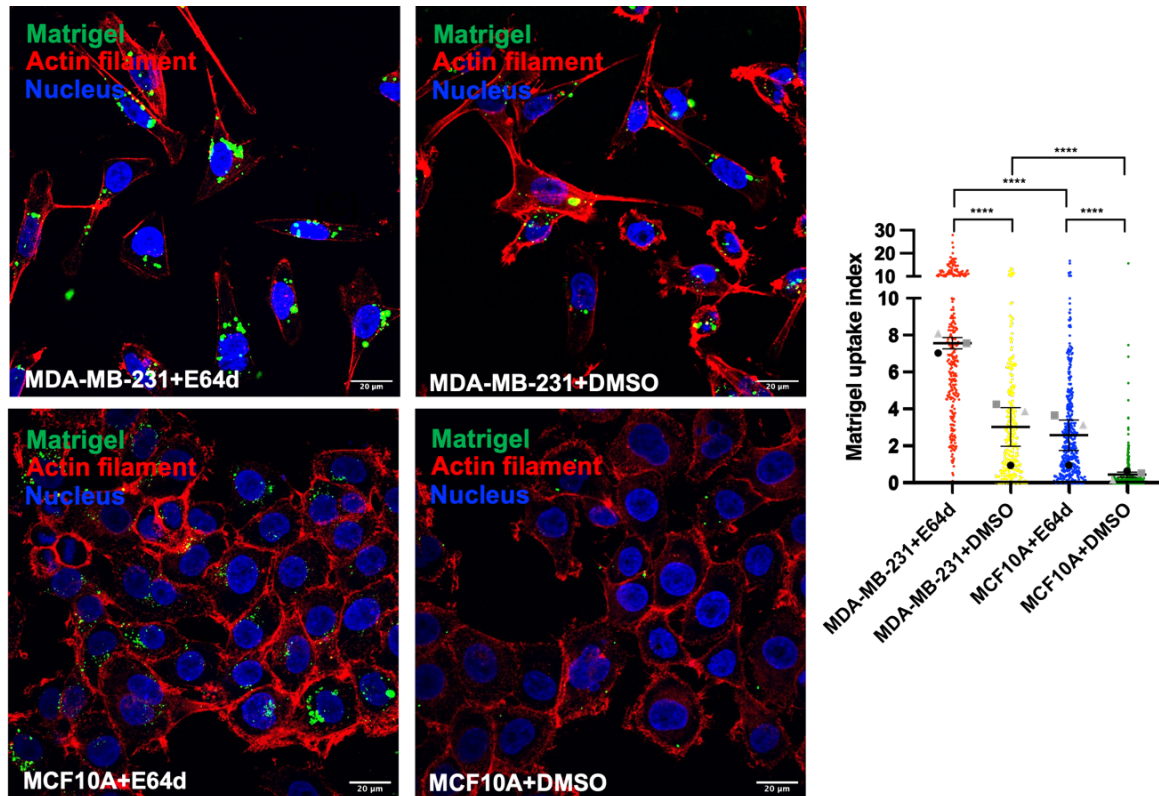


**Figure 3.5. Matrigel uptake is increased in MDA-MB-231 cells.** MDA-MB-231 and MCF10A cells were plated on NHS-fluorescein labelled 1mg/ml Matrigel dishes for an 8-hour incubation in the presence of 20 $\mu$ M E64d or DMSO (control). Cells were fixed and stained for actin (red) and nuclei (blue). Samples were imaged with a Nikon A1 confocal microscope and Matrigel uptake index was calculated with Image J. Bar=20 $\mu$ m. N=3 independent experiments. Mean  $\pm$  SEM, Kruskal-wallis with multiple comparisons (the big dots represent the mean of individual experiments). \*\*\*\*p<0.0001.

Similar results were observed in PyMT#1 cells and NMuMG cells as well. PyMT#1 cells and NMuMG cells were seeded on fluorescently labelled Matrigel for a 12-hour incubation. As illustrated in figure 3.6, in the control group, only a small number of internalized Matrigel vesicles were observed in few NMuMG cells, while most of PyMT#1 cells showed Matrigel-positive vesicles. Additionally, E64 treatment resulted in a dramatically increased accumulation of internalized Matrigel in both cell lines. The quantification demonstrated that Matrigel internalization was much higher in PyMT#1 cells compared to NMuMG cells in both conditions. In sum, our results suggest that the internalization of Matrigel is significantly promoted in invasive breast cancer cells compared to normal mammary epithelial cells.

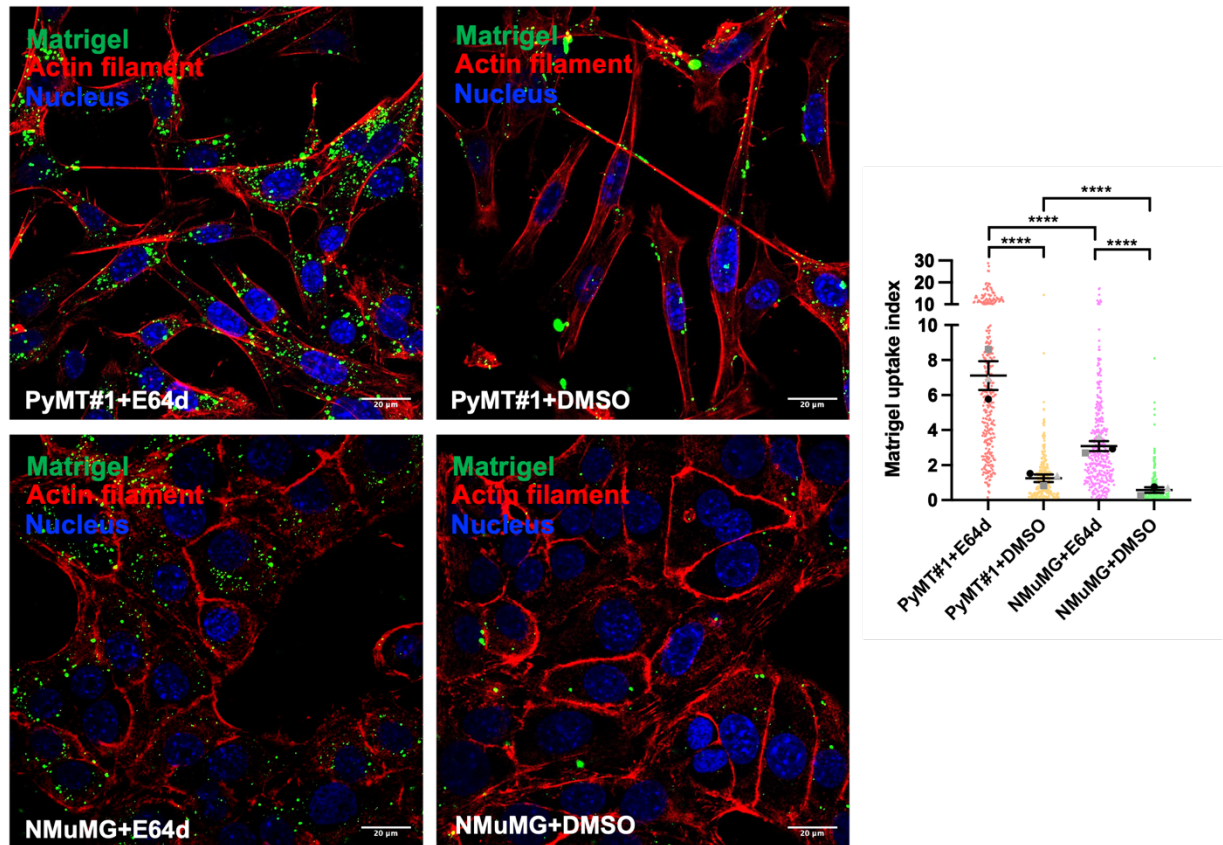


**Figure 3.6. Matrigel uptake is upregulated in PyMT#1 cells.** PyMT#1 and NMuMG cells were plated on NHS-fluorescein labelled 1mg/ml Matrigel dishes for 12 hours in the presence of 20 $\mu$ M E64d or DMSO (control). Cells were fixed and stained for actin (red) and nuclei (blue). Samples were imaged with a Nikon A1 confocal microscope and Matrigel uptake index was calculated with Image J. Bar=20 $\mu$ m. N=3 independent experiments were analyzed. Mean  $\pm$  SEM, Kruskal-wallis with multiple comparisons (the big dots represent the mean of individual experiments).\*\*\*\*p<0.0001.

### 3.2.4 Internalized Matrigel is trafficked through early and late endosomes/lysosomes

In order to determine the intracellular trafficking pathway of internalized Matrigel in MDA-MB-231 cells, we measured its colocalization with an early endosomal marker (EEA1) and a late endosomal/lysosomal marker (LAMP2) at different time points after seeding the cells on fluorescently labelled Matrigel. As illustrated in figure 3.7, internalized Matrigel exhibited a strong colocalization with EEA1 at the early time points, as indicated by the dark red spots in the co-localization map. As the time progressed, the overlap between Matrigel and EEA1 was progressively reduced, highlighted by the absence of dark red spots in the co-localization map.

The statistical results showed that the colocalization index between internalized Matrigel and EEA1 was constantly decreased from 3 hours to 12 hours in MDA-MB-231 cells, indicating the delivery and exit of internalized Matrigel from the early endosomes.

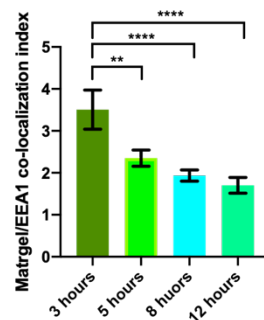
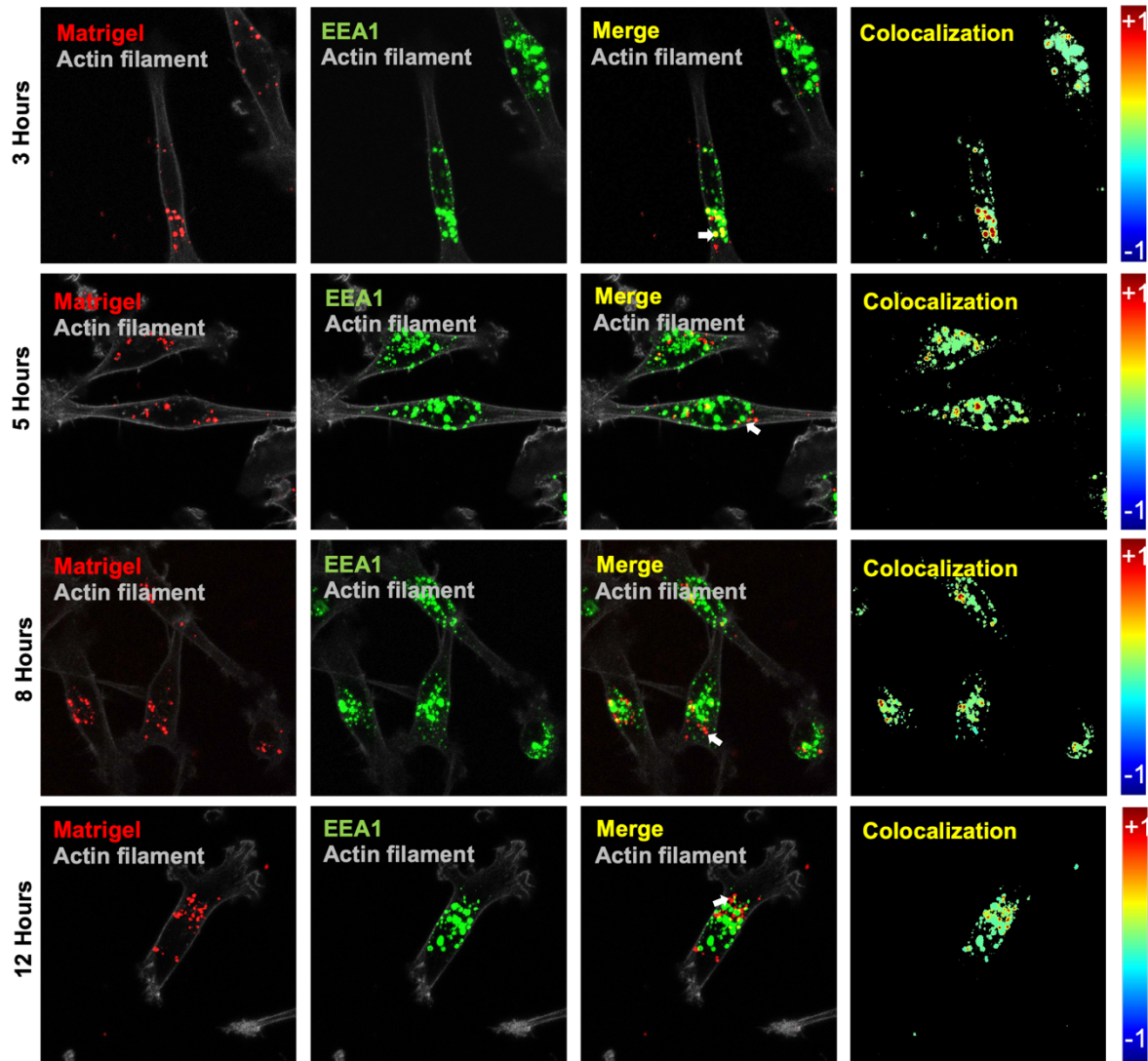


**Figure 3.7. Internalized Matrigel is delivered and exited of the early endosomes.** MDA-MB-231 cells were seeded on Alexa Fluor 647-labelled 1mg/ml Matrigel coated dishes in the presence of 20 $\mu$ M E64d. Cells were then fixed at 3, 5, 8 and 12 hours respectively. Samples were imaged with a Nikon A1 confocal microscope and analyzed by Colocalization Colormap through ImageJ. Briefly, the pixel-by-pixel colocalization of internalized Matrigel with EEA1 was determined using an algorithm in which areas of high colocalization are depicted by the red pseudocolor, and pixels in which the Matrigel and marker were present but not colocalized with one another are represented by the blue pseudocolor. The white arrows indicate a decrease of colocalization between EEA1 and internalized Matrigel in MDA-MB-231 cells. Colocalization index is the mean  $\pm$  SEM from five independent experiments, Kruskal-wallis with multiple comparisons. \*\* $p < 0.01$ , \*\*\*\* $p < 0.0001$ .

In contrast, internalized Matrigel illustrated a constant increased colocalization with the late endosomal/lysosomal marker LAMP2. At the early time points, some Matrigel exhibited little colocalization with the late endosomes/lysosomes, while most of Matrigel containing vesicles appeared to colocalize with LAMP2 at later time points. The quantification illustrated that the colocalization index between internalized Matrigel and LAMP2 was constantly enhanced as the time progressed (Figure 3.8), suggesting that Matrigel was internalized and delivered to late endosomes/lysosomes, consistent with what we observed in the Matrigel uptake assays (Figure 3.5 and 3.6), where inhibition of lysosomal function significantly increased the amount of intracellular Matrigel. Taken together, our data show that internalized Matrigel is delivered to the early and late endosomes in MDA-MB-231 cells.

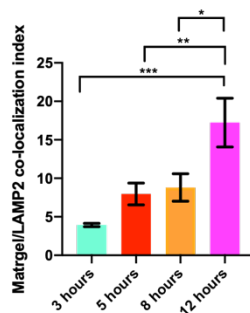
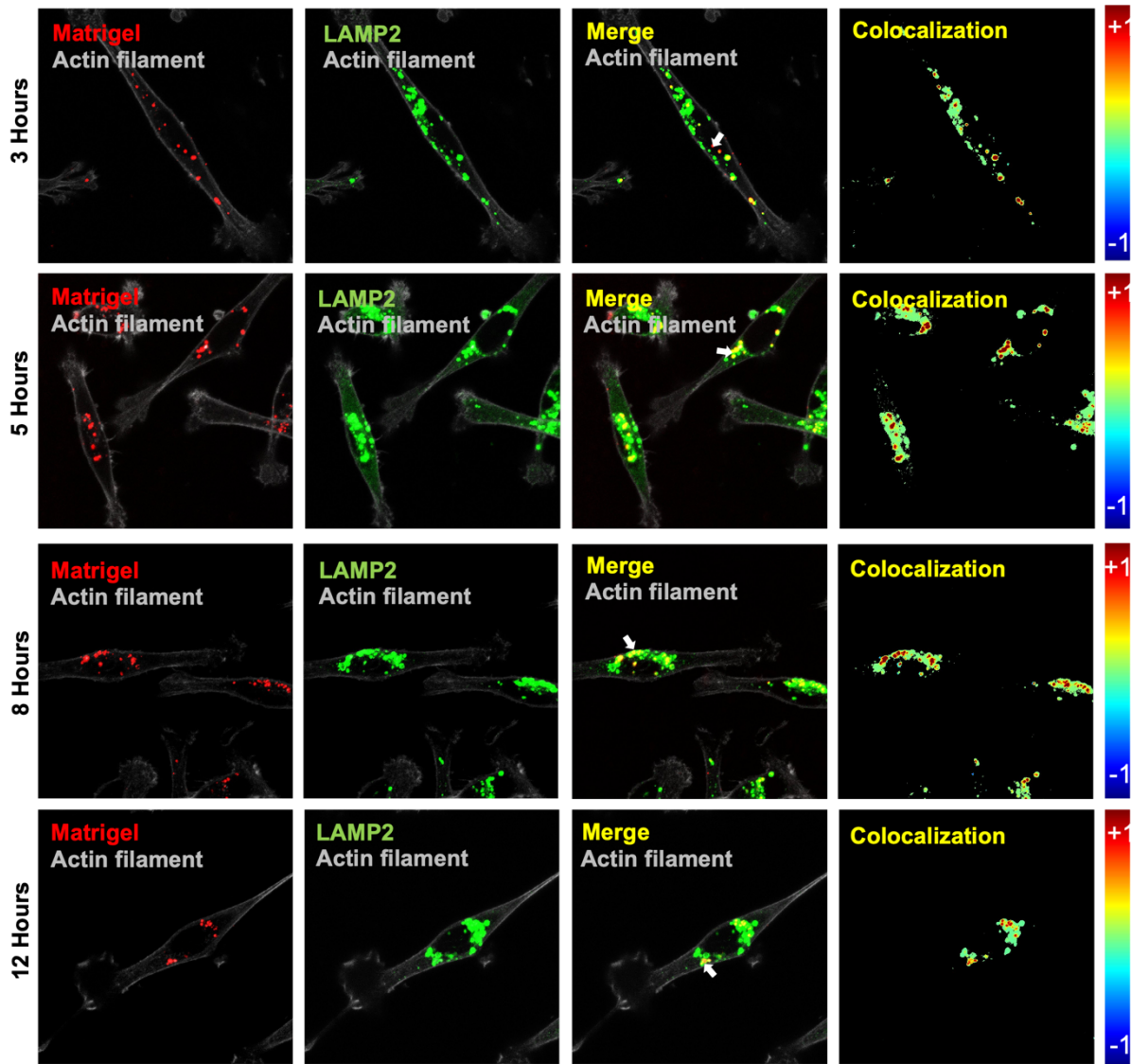


**Figure 3.8. Internalized Matrigel is delivered to the late endosomes/lysosomes.** MDA-MB-231 cells were seeded on Alexa Fluor 647-labelled 1mg/ml Matrigel coated dishes in the presence of 20 $\mu$ M E64d. Cells were then fixed at 3, 5, 8 and 12 hours respectively. Samples were imaged with a Nikon A1 confocal microscope and analyzed by Colocalization Colormap through ImageJ. Briefly, the pixel-by-pixel colocalization of internalized Matrigel with LAMP2 was determined using an algorithm in which areas of high colocalization are depicted by the red pseudocolor, and pixels in which the Matrigel and marker were present but not colocalized with one another are represented by the blue pseudocolor. The white arrows point out an increase of colocalization between LAMP2 and internalized Matrigel in MDA-MB-231 cells. Colocalization index is the mean  $\pm$  SEM from five independent experiments, Kruskal-wallis with multiple comparisons. \* $p < 0.05$ , \*\* $p < 0.01$ , \*\*\* $p < 0.001$ .

### 3.2.5 $\beta$ 1 integrin is required for ECM internalization

As the principal adhesion receptors for ECM, integrins have been reported to be involved in the internalization of different ECM components such as collagens, fibronectin and laminins (Rainero, 2016). In order to understand whether internalized Matrigel is trafficked together with integrins, we measured the colocalization between internalized Matrigel and ligand-bound  $\beta$ 1 integrin in MDA-MB-231 cells. In breast epithelium,  $\beta$ 1 integrin is able to form heterodimers with  $\alpha$ 1,  $\alpha$ 2,  $\alpha$ 3,  $\alpha$ 5 and  $\alpha$ 6 integrins (Nissinen et al., 2012). Importantly, overexpressed  $\beta$ 1 integrin in breast cancer correlates with enhanced metastatic ability, and in some cases with shortened patient survival (Lahlou and Muller, 2011; Yao et al., 2007). As demonstrated in figure 3.9, MDA-MB-231 cells were plated on fluorescently labelled Matrigel and fixed at different time points. To measure colocalization, cells were stained for active  $\beta$ 1 integrin. The overlap of Matrigel and  $\beta$ 1 integrin channels was observed at all time points, as illustrated by the dark red spots in the co-localization map. The quantification illustrated that the colocalization index between internalized Matrigel and  $\beta$ 1 integrin persisted throughout the time course, suggesting that  $\beta$ 1 integrin might be trafficked together with Matrigel in MDA-MB-231 cells.

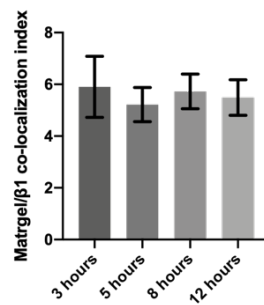
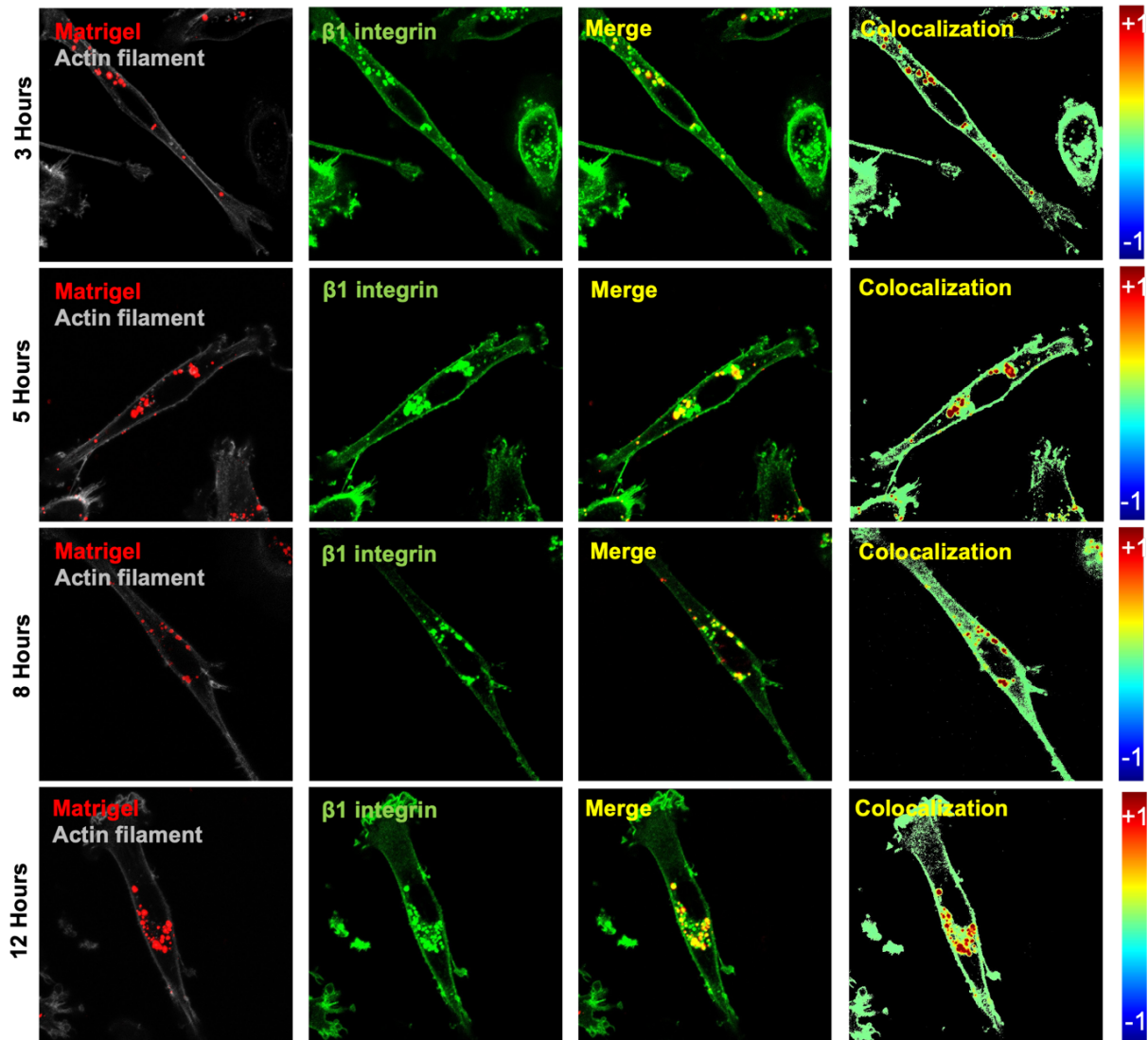


**Figure 3.9.  $\beta$ 1 integrin is trafficked together with internalized Matrigel in breast cancer cells.** MDA-MB-231 cells were seeded on Alexa Fluor 647-labelled 1mg/ml Matrigel coated dishes in the presence of 20 $\mu$ M E64d. Cells were then fixed at 3, 5, 8 and 12 hours respectively. Samples were imaged with a Nikon A1 confocal microscope and analyzed by Colocalization Colormap through ImageJ. The pixel-by-pixel colocalization of internalized Matrigel with  $\beta$ 1 integrin was determined using an algorithm in which areas of high colocalization are depicted by the red pseudocolor, and pixels in which the Matrigel and  $\beta$ 1 integrin were present but not colocalized with one another are represented by the blue pseudocolor. Colocalization index is the mean  $\pm$  SEM from five independent experiments, Kruskal-wallis with multiple comparisons.

To test whether  $\beta 1$  integrin was required for the internalization of Matrigel, we measured Matrigel uptake with and without a functional-blocking antibody against  $\beta 1$  integrin for 24 hours in MDA-MB-231 cells as the cells detached following the treatment with the blocking antibody. As illustrated in figure 3.10, internalized Matrigel containing vesicles were observed within the population in the control group. By contrast, in the presence of  $\beta 1$  integrin blocking antibody only few vesicles were visualised inside the cells. Furthermore, siRNA-mediated  $\beta 1$  integrin knock-down resulted in a significant reduction of Matrigel, collagen I and CDM uptake (data not shown, Rainero lab, unpublished). Overall, our findings demonstrate that  $\beta 1$  integrin is trafficked together with internalized Matrigel and is required for Matrigel internalization in MDA-MB-231 cells.

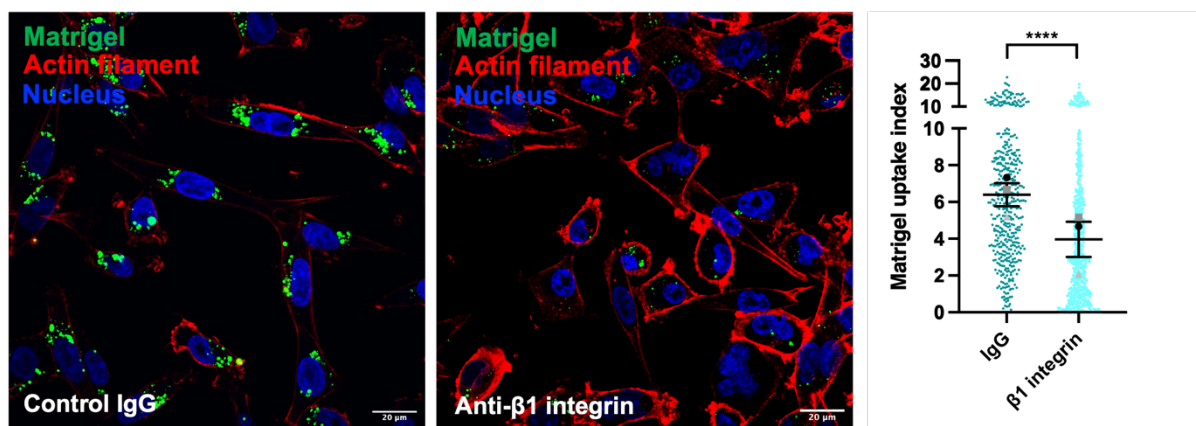


**Figure 3.10.  $\beta 1$  integrin is required for Matrigel uptake in breast cancer cells.** MDA-MB-231 cells were seeded on NHS-fluorescein labelled 1mg/ml Matrigel coated dishes for 2 hours to fully adhere.  $3\mu\text{g/ml}$   $\beta 1$  integrin blocking antibody and  $3\mu\text{g/ml}$  rat IgG control antibody were then added for a 24-hour incubation in the presence of  $20\mu\text{M}$  E64d. Cells were fixed and stained for actin (red) and nuclei (blue). Samples were imaged with a Nikon A1 confocal microscope. Matrigel uptake index was calculated with Image J. Bar= $20\mu\text{m}$ . N=3 independent experiments. Mean  $\pm$  SEM, Mann-Whitney test (the big dots represent the mean of individual experiments). \*\*\*\* $p < 0.0001$ .

### 3.2.6 $\alpha 2$ , but not $\alpha 3$ and $\alpha 6$ , is required for ECM uptake in invasive breast cancer cells

To assess which  $\beta 1$ -containing integrin heterodimers are responsible for ECM internalization in MDA-MB-231 cells, we then measured different ECM component uptake in the presence of inhibitor/functional blocking antibodies against  $\alpha$ -integrin subunits. The MDA-MB-231 cells express high levels of  $\alpha 2$ ,  $\alpha 3$ ,  $\alpha 5$  and  $\alpha 6$  integrin subunits (Lahlou and Muller, 2011). Among these heterodimers,  $\alpha 2\beta 1$  integrin is a well-characterized receptor of collagens and laminins

(Humphries et al., 2006a). In addition,  $\alpha 2\beta 1$  integrin-dependent collagen I internalization and intracellular degradation has been described in fibroblasts (Arora et al., 2013, 2000). Integrins  $\alpha 3\beta 1$  and  $\alpha 6\beta 1$  are considered as major receptors of laminin. Laminin-bound  $\alpha 3\beta 1$  has been shown to promote the phagocytosis and lysosomal degradation of Matrigel in MDA-MB-231 cells (Coopman et al., 1996). Although there is no evidence showing that  $\alpha 6\beta 1$  is involved in the internalization of ECM, the expression of  $\alpha 6\beta 1$  integrin has been linked to the metastatic and survival potential of human breast carcinoma cells (Mukhopadhyay et al., 1999; Wewer et al., 1997).

Because of the upregulated CDM internalization in invasive breast cancer cells compared to normal mammary epithelial cells, we compared CDM uptake with and without a selective  $\alpha 2\beta 1$  inhibitor BTT-3033. MDA-MB-231 cells were plated on biotinylated CDM for 2 hours to fully adhere, followed by a 6-hour incubation in the presence and in the absence of BTT-3033. As shown in figure 3.11A, most of MDA-MB-231 cells showed CDM positive vesicles in the DMSO group, while only a small number of CDM vesicles were visualised in some cells in the presence BTT-3033. Image analysis quantification demonstrated a significant reduction in the CDM internalization index in the presence of BTT-3033, suggesting that  $\alpha 2\beta 1$  integrin was required for the internalization of CDM in MDA-MB-231 cells. Notably, CDM are enriched in collagen I, an  $\alpha 2\beta 1$  integrin ligand (Kutys et al., 2013a). Thus, MDA-MB-231 cells were plated on fluorescently labelled collagen I for 2 hours, then treated with BTT-3033 or DMSO for 6 hours. Internalized collagen I positive vesicles were observed within the cells in the presence of DMSO, while in the presence of BTT-3033 fewer and smaller vesicles were visualized inside the cells (Figure 3.11B). The quantification analysis illustrated a statistically significant reduction in the collagen I internalization index in the presence of BTT-3033, indicating that  $\alpha 2\beta 1$  integrin contributed to collagen I internalization in MDA-MB-231 cells.

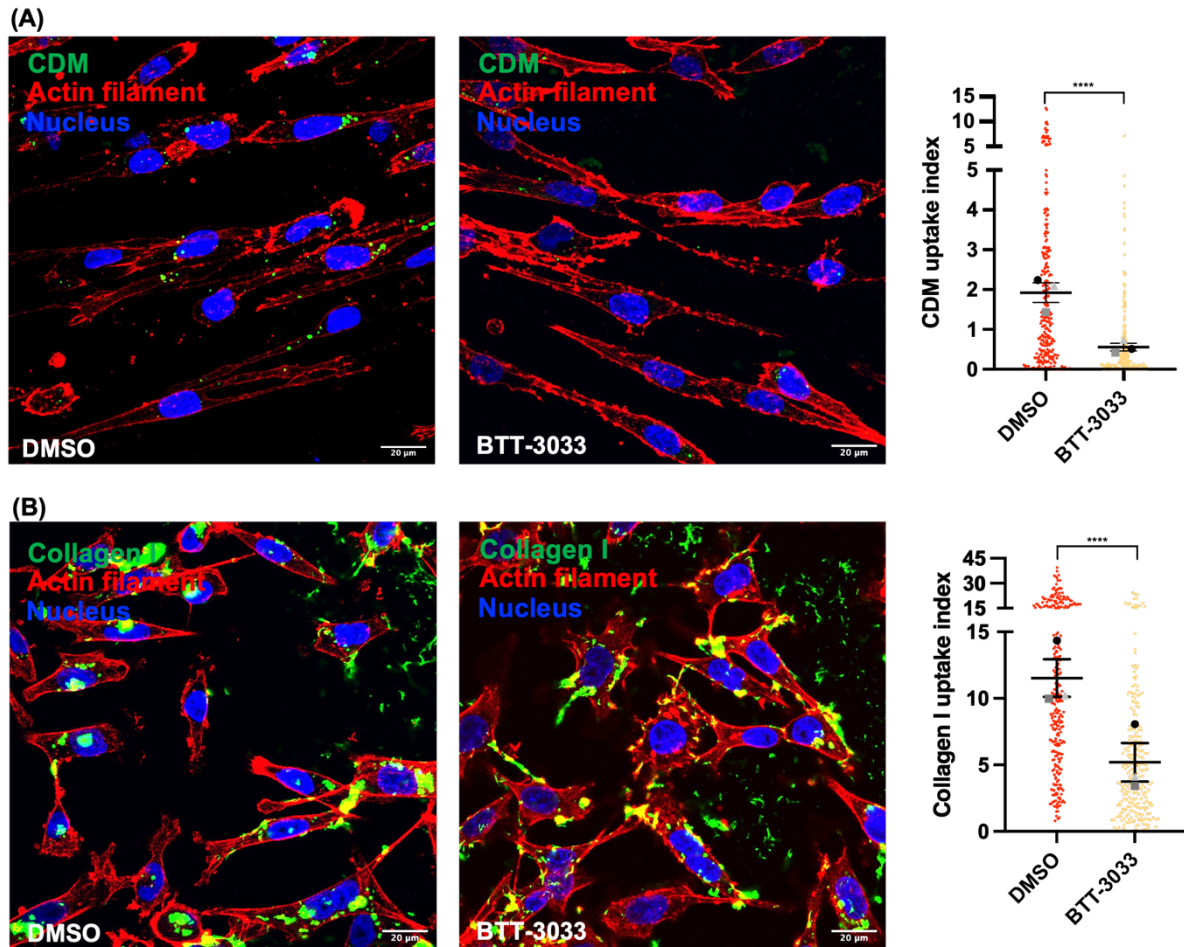


**Figure 3.11. The  $\alpha 2\beta 1$  integrin is required for CDM and collagen I internalization in breast cancer cells.** MDA-MB-231 cells were seeded on **(A)** biotin-labelled CDM and **(B)** NHS-fluorescein labelled 0.5mg/ml collagen I coated dishes for 2 hours to fully adhere. 10 $\mu$ M  $\alpha 2$  integrin inhibitor (BTT-3033) and DMSO (control) were added for a 6-hour incubation in the presence of 20 $\mu$ M E64d. For CDM internalization assay, cells were fixed and stained for Streptavidin (green), actin (red) and nuclei (blue). For collagen I uptake, cells were fixed and stained for actin (red) and nuclei (blue). Samples were imaged with a Nikon A1 confocal microscope. CDM and collagen I uptake index were calculated with Image J. Bar=20 $\mu$ m. N=3 independent experiments (the big dots represent the mean of individual experiments). \*\*\*\*p<0.0001. Mean  $\pm$  SEM, Mann-Whitney test.

It was previously shown that the internalization of Matrigel was promoted in invasive breast cancer cells compared to normal mammary epithelial cells. To examine whether  $\alpha 2\beta 1$  integrin contributes to the internalization of Matrigel, MDA-MB-231 cells were plated on fluorescently labelled Matrigel for 2 hours to fully adhere, followed by a 6-hour incubation with either BTT-3033 or DMSO.  $\alpha 2$  integrin inhibition led to a significant decrease in Matrigel internalization, fewer Matrigel positive vesicles were observed in the cells treated with BTT-3033 compared to the cells in the presence of DMSO (Figure 3.12A). To characterise which BM component uptake is regulated by  $\alpha 2\beta 1$  integrin, we compared the internalization of two major Matrigel

components in the presence and in the absence of BTT-3033: laminin/entactin and collagen IV. MDA-MB-231 cells were seeded on fluorescently labelled laminin or Matrigel containing dye-quenched collagen IV (DQ-collagen IV) for 2 hours to fully adhere, followed by a 6-hour incubation with and without BTT-3033. Consistent with our findings from the Matrigel uptake assay (Figure 3.12A),  $\alpha 2$  inhibition resulted in a significant reduction of laminin internalization; indeed, laminin containing vesicles were only visualised inside the cells in the control group but not in the cells in the presence of BTT-3033 (Figure 3.12B). Visualization of internalized collagen IV depends on the fluorescent characteristics of the DQ-substrates. The proximity of the dye molecules to each other renders native DQ-collagen IV fluorescently quenched because of a Fluorescence Resonance Energy Transfer (FRET) effect. The fluorescence is visualized due to the proteolytic hydrolysis of internalized DQ-collagen IV (Jedezsko et al., 2013). Here a small, but statically significant reduction in DQ-collagen IV internalization was observed in the cells in the presence of BTT-3033 compared to the cells in the control group (Figure 3.12C). However, the reduced collagen IV internalization after  $\alpha 2$  inhibition was not as significant as the difference we observed in the Matrigel and laminin uptake assays (Figure 3.12A and 3.12B). Taken together, our findings indicate that  $\alpha 2\beta 1$  integrin is required for the internalization of collagen I and laminin in the BM (Matrigel) in MDA-MB-231 cells.

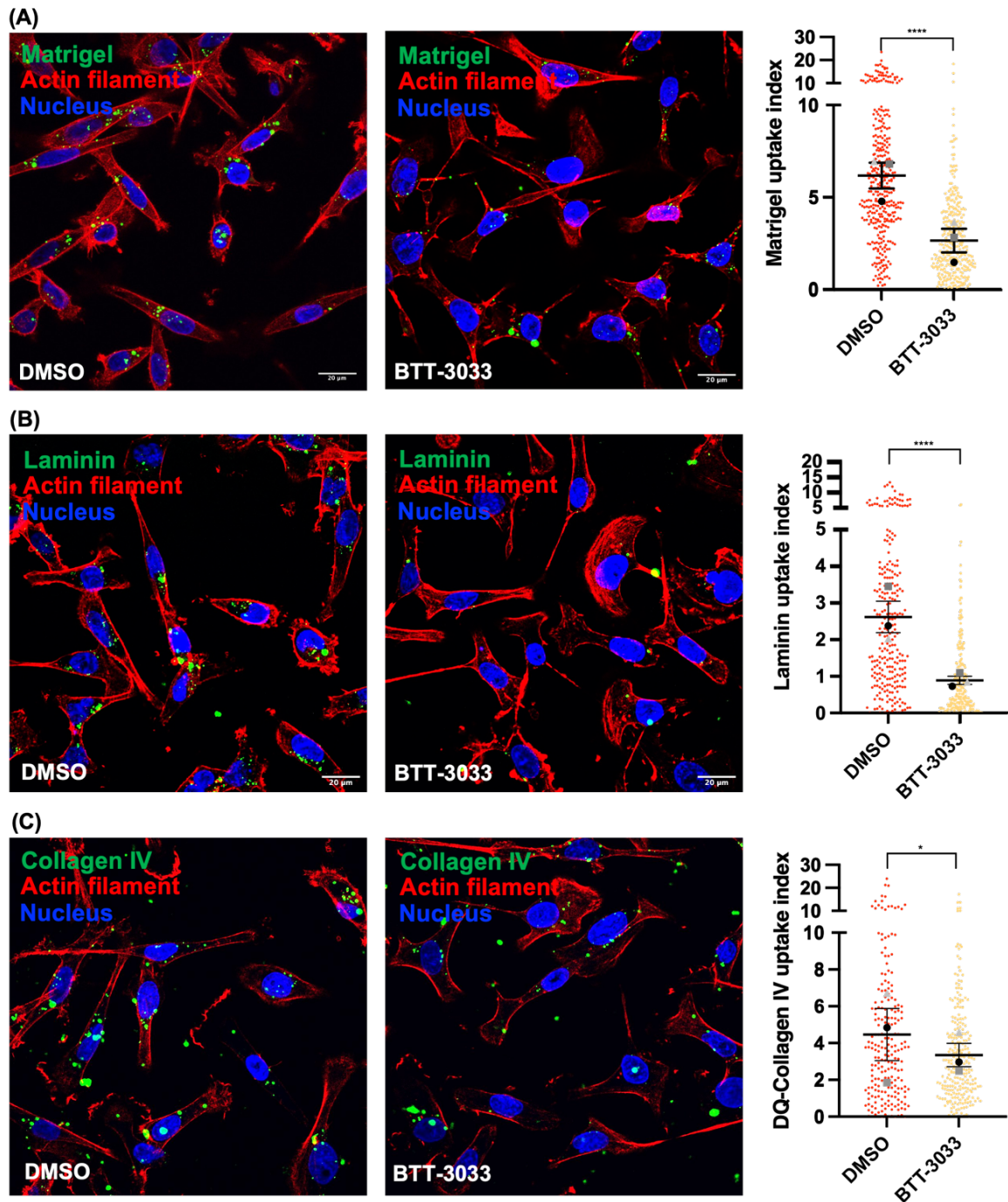


**Figure 3.12. The  $\alpha 2\beta 1$  integrin is required for Matrigel, laminin and collagen IV internalization in breast cancer cells.** MDA-MB-231 cells were seeded on (A) NHS-fluorescein labelled 1mg/ml Matrigel, (B) NHS-fluorescein labelled 2mg/ml laminin and (C) the mixture of 25 $\mu$ g/mL of DQ-collagen IV and 1mg/ml Matrigel coated dishes for 2 hours to fully adhere. 10 $\mu$ M  $\alpha 2$  integrin inhibitor (BTT-3033) and DMSO (control) were added for a 6-hour incubation in the presence of 20 $\mu$ M E64d. Cells were fixed and stained for actin (red) and nuclei (blue). Samples were imaged with a Nikon A1 confocal microscope. Matrigel, laminin and DQ-collagen IV uptake index were calculated with Image J. Bar=20 $\mu$ m. N=3 independent experiments (the big dots represent the mean of individual experiments). \* $p < 0.05$  \*\*\*\* $p < 0.0001$ . Mean  $\pm$  SEM, Mann-Whitney test.

We next tested whether  $\alpha 3$  integrin contributed to the internalization of ECM in invasive breast cancer cells. MDA-MB-231 cells were seeded on fluorescently labelled collagen I and Matrigel for 2 hours to fully adhere, followed by incubation for 6 hours in the presence and in the absence of an  $\alpha 3$  integrin blocking antibody or an IgG antibody control. As illustrated in figure 3.13A, the number of collagen I containing vesicles inside the cells in the control group was similar to the cells that received the  $\alpha 3$  integrin blocking antibody, and the image quantification illustrated that  $\alpha 3$  inhibition did not affect the collagen I uptake index in MDA-MB-231 cells. This is expected, as  $\alpha 3\beta 1$  does not bind to collagen I. Interestingly, there was no significant difference in Matrigel uptake with and without  $\alpha 3$  integrin blocking antibody (Figure 3.13B). Altogether, our data reveal that  $\alpha 3$  integrin is not required for the endocytosis of collagen I and Matrigel in MDA-MB-231 cells.

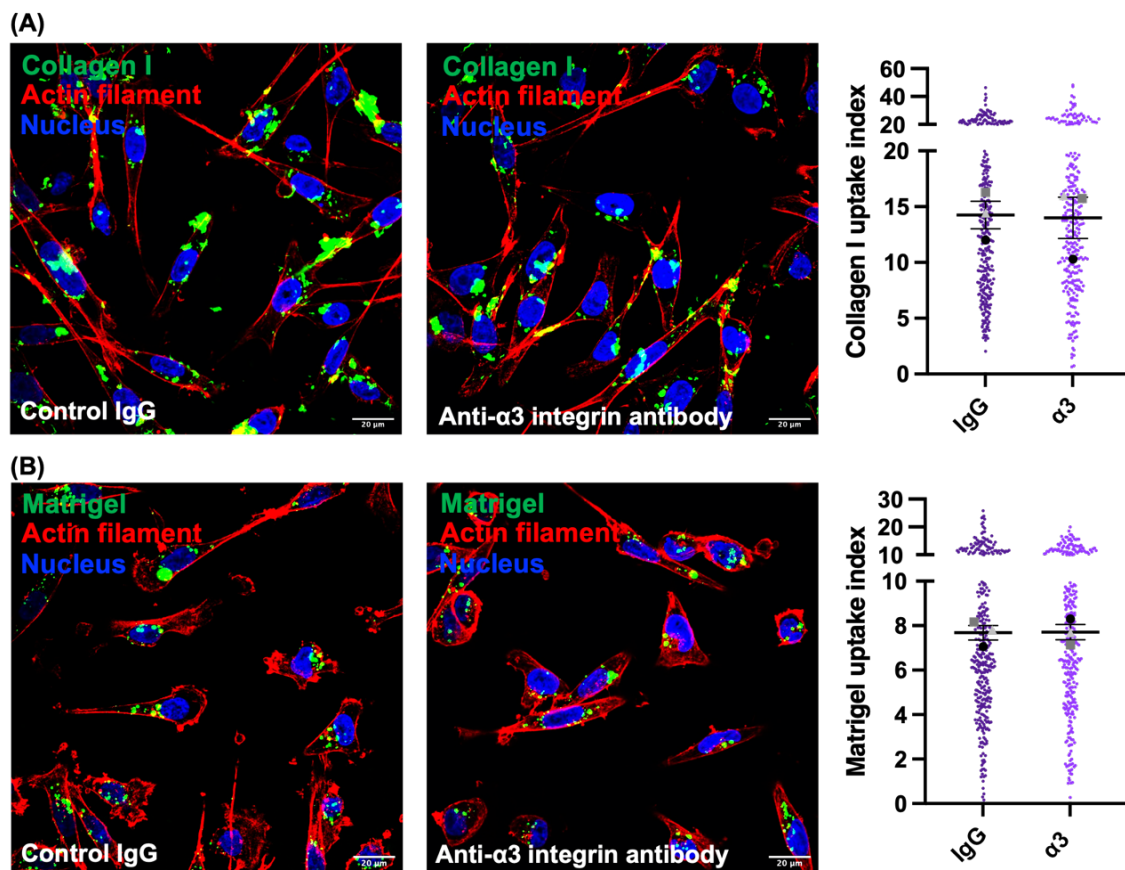


**Figure 3.13.  $\alpha 3$  integrin is not required for collagen I and Matrigel internalization in breast cancer cells.** MDA-MB-231 cells were seeded on NHS-fluorescein labelled (A) 0.5mg/ml collagen I and (B) 1mg/ml Matrigel coated dishes for 2 hours to fully adhere. 5 $\mu$ g/ml  $\alpha 3$  integrin blocking antibody and 5 $\mu$ g/ml mouse control IgG antibody were added for a 6-hour incubation in the presence of 20 $\mu$ M E64d. Cells were fixed and stained for actin (red) and nuclei (blue). Samples were imaged with a Nikon A1 confocal microscope. Collagen I and Matrigel uptake index were calculated with Image J. Bar=20 $\mu$ m. N=3 independent experiments (the big dots represent the mean of individual experiments). Mean  $\pm$  SEM, Mann-Whitney test.

To characterize the role of  $\alpha 6$  integrin in the internalization of ECM in invasive breast cancer cells, MDA-MB-231 cells were plated on fluorescently labelled Matrigel for 2 hours to fully adhere, followed by incubation for 6 hours with and without a blocking antibody against  $\alpha 6$  integrin. Surprisingly, more Matrigel containing vesicles were observed inside the cells in the presence of  $\alpha 6$  blocking antibody compared to the control IgG antibody (Figure 3.14).  $\alpha 6$  inhibition led to a small, albeit statistically significant, increase in Matrigel endocytosis. Thus, our data suggest that  $\alpha 6$  integrin is not required for Matrigel uptake in MDA-MB-231 cells.

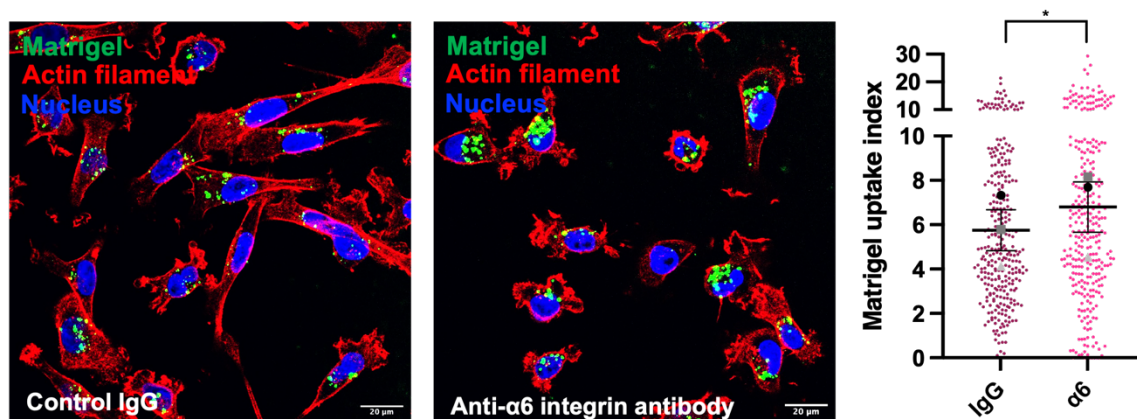
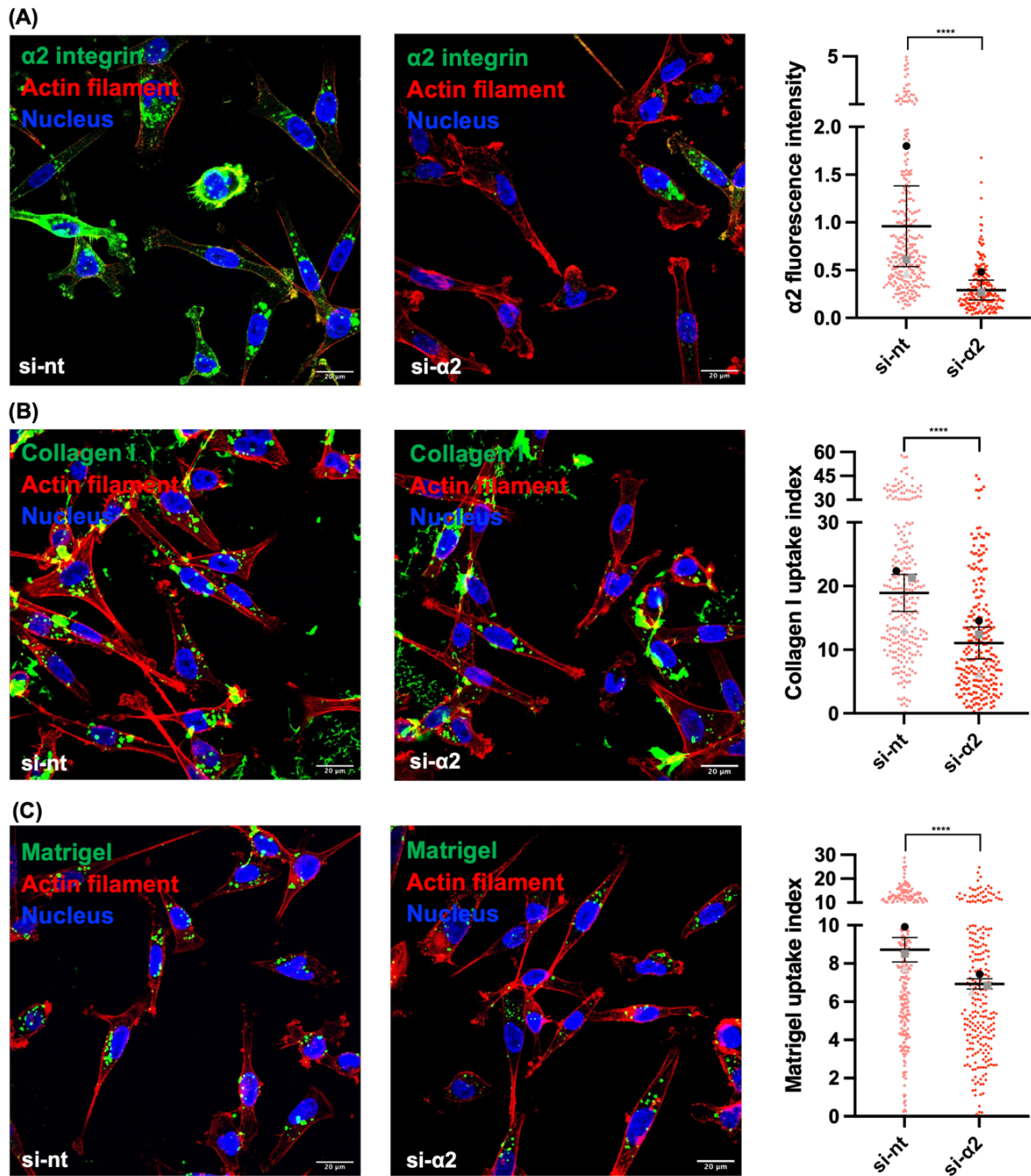


**Figure 3.14.  $\alpha 6$  integrin is not required for Matrigel internalization in breast cancer cells.** MDA-MB-231 cells were seeded on NHS-fluorescein labelled 1mg/ml Matrigel coated dishes for 2 hours to fully adhere. 10 $\mu$ g/ml  $\alpha 6$  integrin blocking antibody and 10 $\mu$ g/ml rat control IgG were added for a 6-hour incubation in the presence of 20 $\mu$ M E64d. Cells were fixed and stained for actin (red) and nuclei (blue). Samples were imaged with a Nikon A1 confocal microscope. Matrigel uptake index were calculated with Image J. Bar=20 $\mu$ m. N=3 independent experiments (the big dots represent the mean of individual experiments). \* $p$ <0.05. Mean  $\pm$  SEM, Mann-Whitney test.

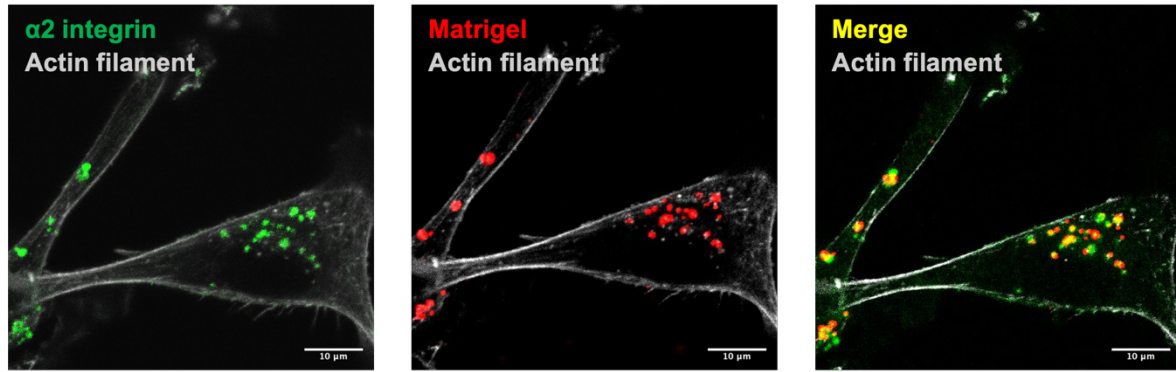
### 3.2.7 $\alpha 2\beta 1$ integrin knock-down reduced ECM uptake in invasive breast cancer cells

To confirm the contribution of  $\alpha 2\beta 1$  integrin in ECM internalization, MDA-MB-231 cells were treated with either a non-targeting siRNA control (si-nt) or an siRNA targeting  $\alpha 2$  integrin (si- $\alpha 2$ ) for 48 hours before seeding the cells on fluorescently labelled ECM for 6 hours. To assess the efficiency of the knock-down, cells were stained for  $\alpha 2$  integrin. We observed a significant reduction in  $\alpha 2$  integrin intensity in the si- $\alpha 2$  treated cells compared to the si-nt ones; indeed, the expression of  $\alpha 2$  integrin on both plasma membrane and intracellular vesicles was only visualized in a small proportion of cells after siRNA knock-down (Figure 3.15A). Consistent with our findings with the  $\alpha 2$  integrin inhibitor BTT-3033 (Figure 3.11B),  $\alpha 2$  integrin knock-

down decreased the internalization of collagen I in MDA-MB-231 cells (Figure 3.15B). In addition, fewer Matrigel positive vesicles were observed inside the cells as a result of  $\alpha 2$  integrin knock-down, and the image quantification demonstrated a significant reduction in Matrigel endocytosis index in the presence of the siRNA targeting  $\alpha 2$  integrin (Figure 3.15C). Moreover, we detected the colocalization between  $\alpha 2$  integrin and internalized Matrigel. The cells were plated on fluorescently labelled Matrigel and stained for  $\alpha 2$  integrin after a 6-hour incubation. Here we showed that a big fraction of internalized Matrigel exhibited a strong colocalization with  $\alpha 2$  integrin, as illustrated by the yellow spots in the merge channel (Figure 3.16), suggesting that  $\alpha 2\beta 1$  integrin was trafficked together with Matrigel. Taken together, our results indicate that  $\alpha 2\beta 1$  integrin contributes to the endocytosis of ECM in MDA-MB-231 cells.



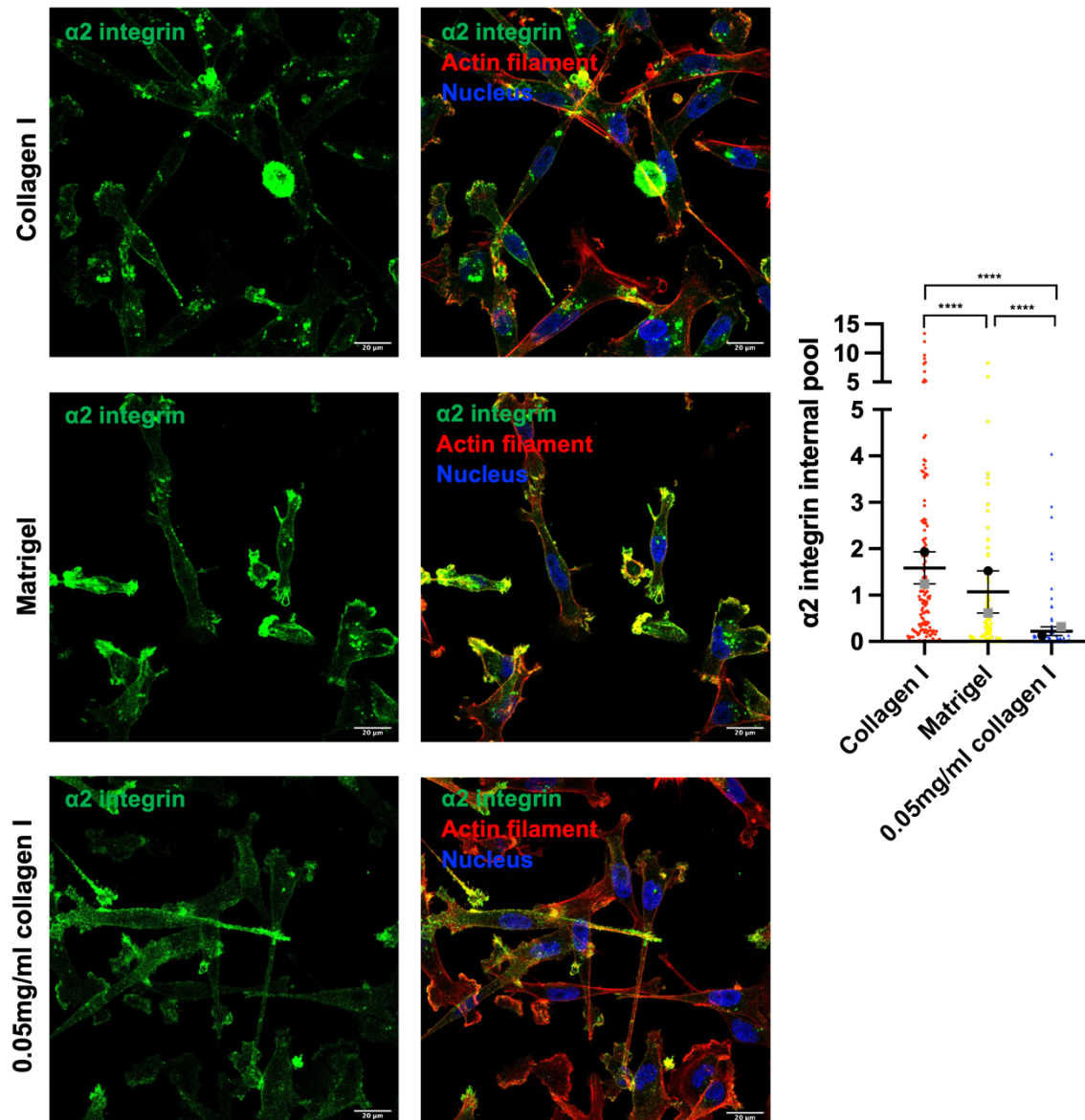
**Figure 3.15. The  $\alpha 2\beta 1$  integrin is required for collagen I and Matrigel internalization in breast cancer cells.** (A) MDA-MB-231 cells were transfected with siRNA targeting  $\alpha 2$  integrin (si- $\alpha 2$ ) or nontargeting control (si-nt). Cells were plated onto 0.1mg/ml collagen I coated dishes for 6 hours. Cells were fixed and stained for  $\alpha 2$  integrin (green), nuclei (blue) and actin (red). The mean  $\alpha 2$  fluorescence intensity were measured by ImageJ. Bar=20 $\mu$ m. N=3 independent experiments (the big dots represent the mean of individual experiments). \*\*\*\*p<0.0001. Mean  $\pm$  SEM, Mann-Whitney test. (B and C) MDA-MB-231 cells were transfected siRNA targeting  $\alpha 2$  integrin (si- $\alpha 2$ ) or nontargeting control (si-nt), plated on (B) NHS-fluorescein labelled 0.5mg/ml collagen I and (C) NHS-fluorescein labelled 1mg/ml Matrigel for 6 hours incubation in the presence of 20 $\mu$ M E64d. Cells were fixed and stained for actin (red) and nuclei (blue). Bar=20 $\mu$ m. N=3 independent experiments (the big dots represent the mean of individual experiments). \*\*\*\*p<0.0001. Mean  $\pm$  SEM, Mann-Whitney test.



**Figure 3.16. The  $\alpha 2\beta 1$  integrin is trafficked together with Matrigel in breast cancer cells.** MDA-MB-231 cells were plated on Alexa Fluor 647-labelled 1mg/ml Matrigel coated glass dishes in the presence of 20 $\mu$ M E64d. Cells were fixed at 6 hours and stained for  $\alpha 2$  integrin and actin filament. Samples were imaged with a Nikon A1 confocal microscope. Bar=10 $\mu$ m.

### 3.2.8 Collagen I and Matrigel binding induces $\alpha 2\beta 1$ integrin activation and endocytosis

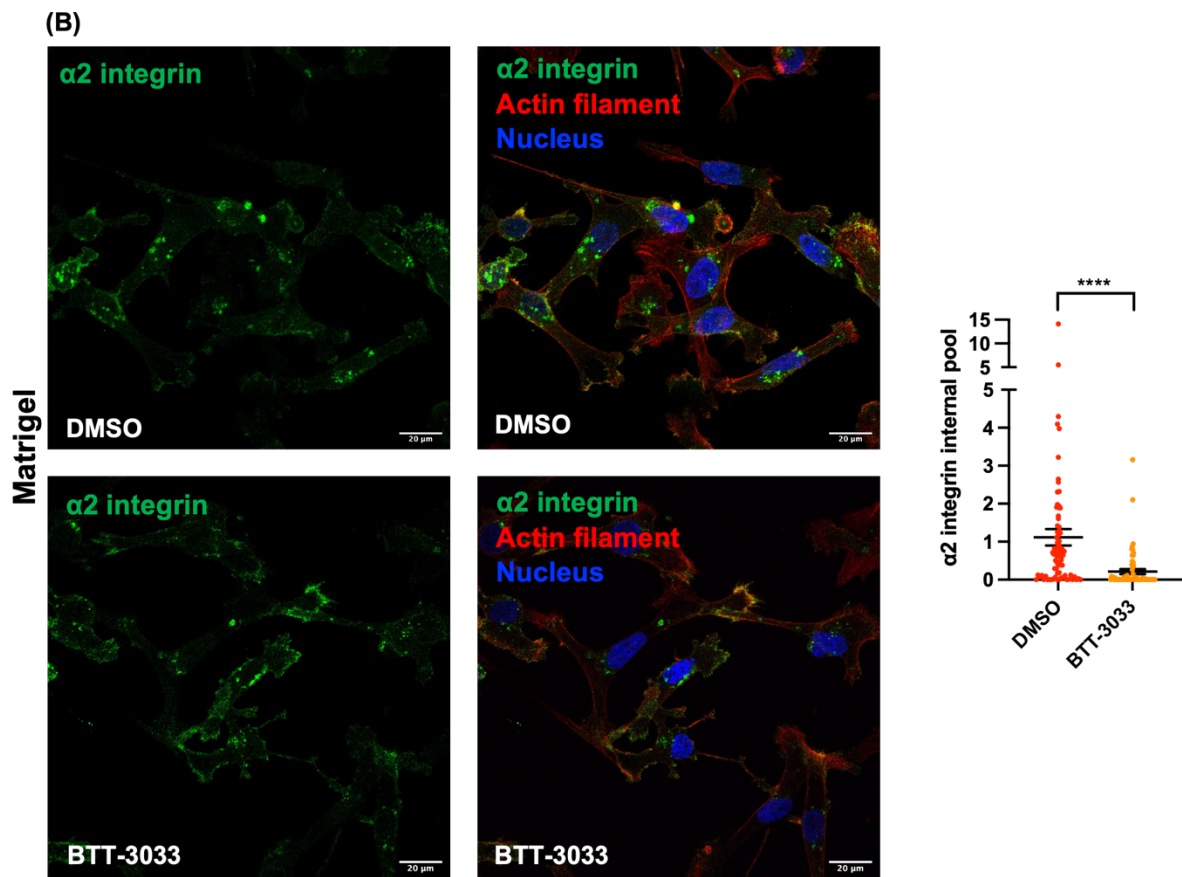
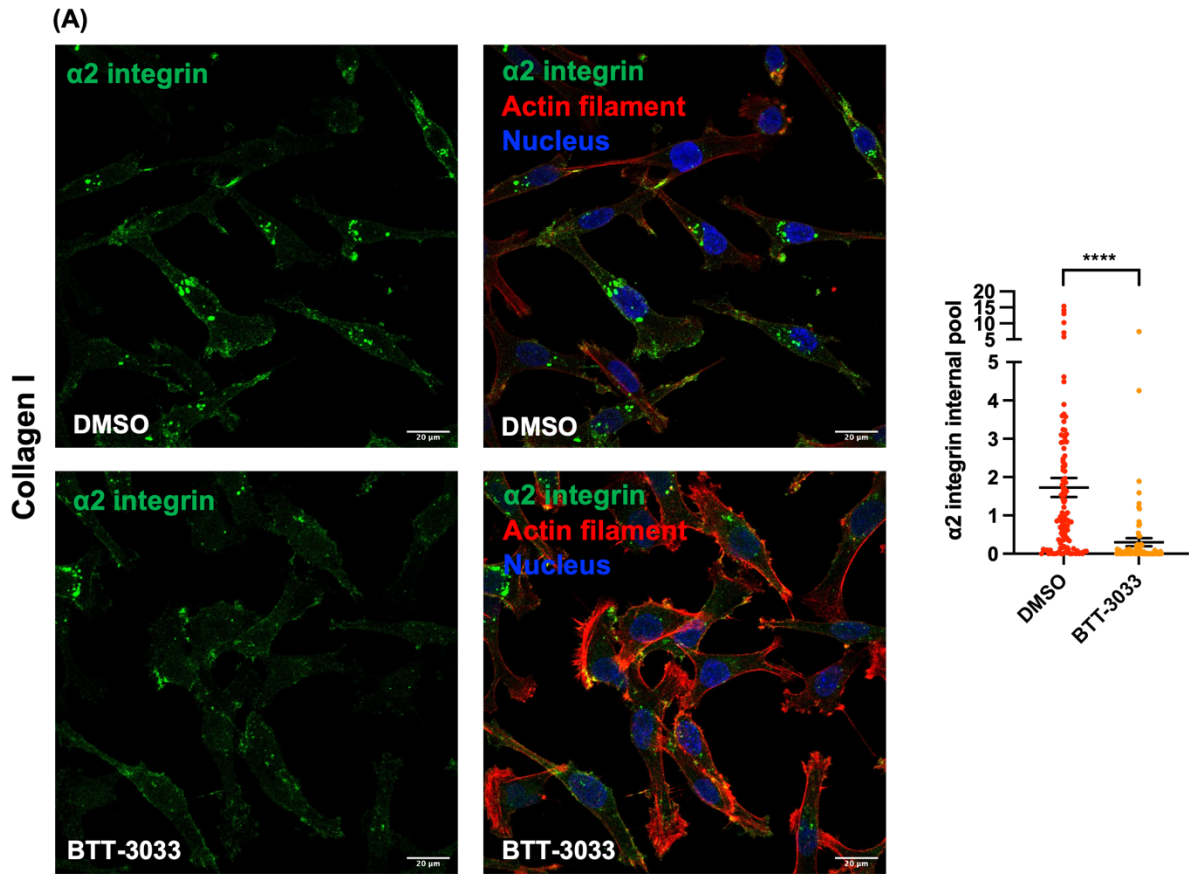
Interestingly,  $\alpha 2\beta 1$  integrin was detected as a receptor for collagen I and Matrigel endocytosis in MDA-MB-231 cells, promoting us to investigate whether these physiological ligands affected the distribution of  $\alpha 2\beta 1$  integrin. The MDA-MB-231 cells were plated onto collagen I (0.5mg/ml), Matrigel and a thin collagen I coating (0.05mg/ml) for 6 hours, and stained for  $\alpha 2$  integrin. As shown in figure 3.17, collagen I and Matrigel resulted in the redistribution of  $\alpha 2\beta 1$  to cytosolic vesicles. On thin collagen I coating, only a small number of MDA-MB-231 cells exhibited  $\alpha 2$  integrin-positive vesicles, while the presence of collagen I and Matrigel led to the accumulation of  $\alpha 2$  integrin vesicles in a big proportion of cells. The quantification of  $\alpha 2$  internal pool showed that collagen I and Matrigel promoted the endocytosis of  $\alpha 2$  integrin, as they resulted in a statistically significant increase in the amount of  $\alpha 2$  integrin in the internal pool. Moreover, our results revealed that exposure of cells to collagen I led to more intracellular  $\alpha 2$  integrin vesicles than Matrigel (Figure 3.17), consistent with previous findings that  $\alpha 2$  integrin displays a higher affinity for collagen I than laminin and collagen IV (Shi et al., 2012).



**Figure 3.17. Collagen I and Matrigel binding can induce  $\alpha 2\beta 1$  integrin endocytosis in breast cancer cells.** MDA-MB-231 cells were plated onto 0.5mg/ml collagen I, 1mg/ml Matrigel and 0.05mg/ml collagen coated confocal dishes for 6 hours. Cells were fixed and stained for  $\alpha 2$  integrin (green), nuclei (blue) and actin (red). The  $\alpha 2$  integrin internal pool was measured by ImageJ. Bar=20 $\mu$ m. N=2 independent experiments (the big dots represent the mean of individual experiments). Kruskal-wallis with multiple comparisons. \*\*\*\* $p < 0.0001$ .

BTT-3033 is a highly selective  $\alpha 2\beta 1$  integrin inhibitor for both active and inactive forms via binding to the  $\alpha 2$  domain of the recombinant  $\alpha 2$  subunit (Nissinen et al., 2012). We found that exposure of cells to ECM facilitated the accumulation of  $\alpha 2$  integrin vesicles. Hence, we hypothesized that preventing ligands binding by BTT-3033 would oppose  $\alpha 2\beta 1$  integrin uptake. Here MDA-MB-231 cells were plated onto collagen I (0.5mg/ml), Matrigel and a thin

collagen I coating (0.05mg/ml) for 2 hours to fully adhere, followed by a 6-hour incubation with BTT-3033 or DMSO. The blocking of  $\alpha 2 I$  domain on  $\alpha 2$  subunit by BTT-3033, which prevents the binding to collagens and laminin (Ivaska et al., 1999a), prevented the internalization of  $\alpha 2 \beta 1$  integrin. The quantification illustrated that the presence of BTT-3033 strongly decreased  $\alpha 2 \beta 1$  endocytosis inside the cells plated on collagen I and Matrigel (Figure 3.18A and B). In contrast,  $\alpha 2 I$  domain inhibition did not affect  $\alpha 2$  uptake in MDA-MB-231 cells planted onto thin collagen I coating. The localization of  $\alpha 2$  integrin was mainly observed on the plasma membrane, while only a small proportion of cells exhibited intracellular  $\alpha 2$  vesicles with and without BTT-3033 (Figure 3.18C). It has been illustrated that active  $\beta 1$  integrin preferentially appears to be accumulated in endosomes, whereas inactive  $\beta 1$  integrin is mainly localized at the plasma membrane (De Franceschi et al., 2015). Altogether, our data suggest that collagen I and Matrigel binding can induce  $\alpha 2 \beta 1$  integrin activation and endocytosis.



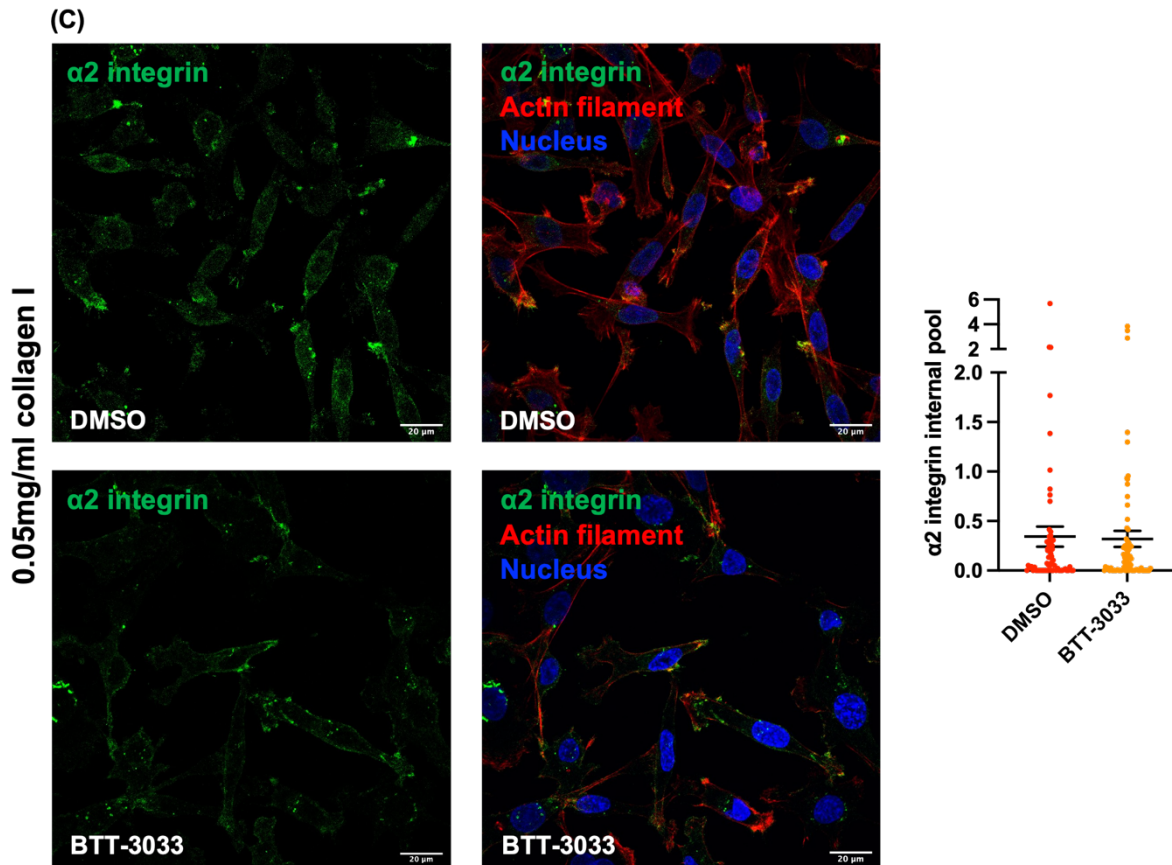


**Figure 3.18. Collagen I and Matrigel binding might induce  $\alpha 2\beta 1$  integrin activation and uptake in breast cancer cells.** MDA-MB-231 cells were plated on (A) 0.5mg/ml collagen I (B) 1mg/ml Matrigel and (C) 0.05m/ml collagen I coated dishes for 2 hours to fully adhere. 10 $\mu$ M  $\alpha 2$  integrin inhibitor (BTT-3033) and DMSO (control) were added for a 6-hour incubation. Cells were fixed and stained for  $\alpha 2$  integrin (green), nuclei (blue) and actin (red). Samples were imaged with a Nikon A1 confocal microscope. The  $\alpha 2$  integrin internal pool was measured by ImageJ. Bar=20 $\mu$ m. N=1 experiment. Mean  $\pm$  SEM, Mann-Whitney test, \*\*\*\*p<0.0001.

### 3.2.9 $\alpha 2\beta 1$ integrin is required for MDA-MB-231 cell migration

Interestingly, increased integrin trafficking correlates with enhanced migration and invasion *in vitro* and *in vivo* (Muller et al., 2009). We found that collagen I and Matrigel contributed to the internalization of  $\alpha 2\beta 1$  integrin. Therefore, we wanted to investigate whether  $\alpha 2\beta 1$  integrin is required for breast cancer cell migration. The cells were plated on CDM for 4 hours, treated with BTT-3033 or DMSO and their migration was recorded by time-lapse microscopy, acquiring images every 10 minutes for 17 hours. We found that MDA-MB-231 cells migrated directionally with and without BTT-3033. However, cells were small and round with highly variable protrusions in the presence of BTT-3033, whereas cells were significantly elongated

and exhibited traveling waves of protrusions in the control group. The quantification of velocity demonstrated that the cells in the presence of BTT-3033 displayed a decreased cell speed compared to the cells in the control group (Figure 3.19A). Additionally, we quantified the extension of protrusions called invasive pseudopods at the front of the cells (Caswell et al., 2008). We showed that pseudopod extension in the direction of migration was strikingly decreased by the inhibition of  $\alpha 2$  integrin (Figure 3.19B), indicating that  $\alpha 2$  integrin inhibition in MDA-MB-231 cells slowed migration on CDM.

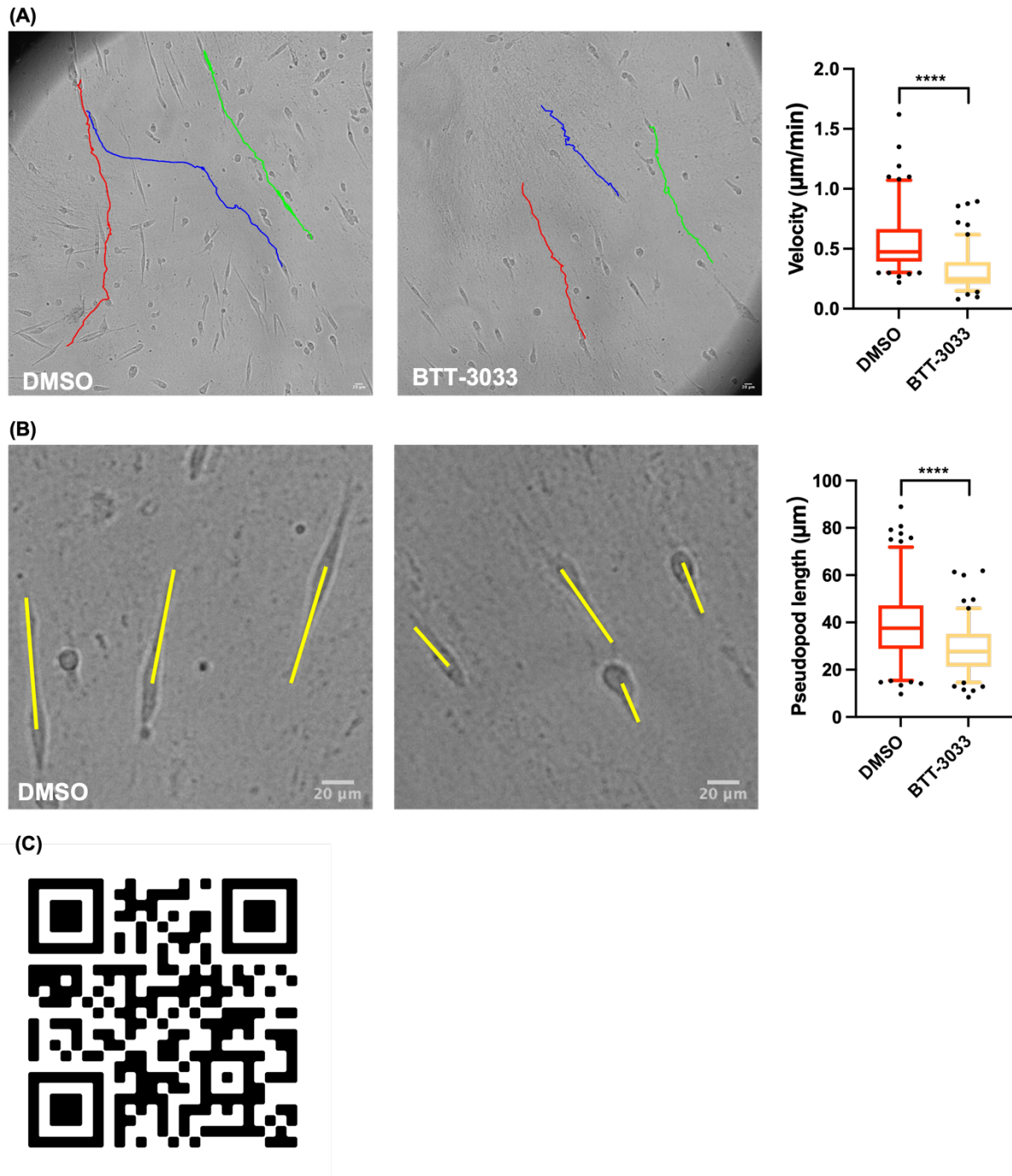


**Figure 3.19.  $\alpha 2\beta 1$  integrin contributes to MDA-MB-231 cell migration.** MDA-MB-231 cells were plated on CDM for 4 hours to fully adhere. Then 10 $\mu$ M of  $\alpha 2$  integrin inhibitor (BTT-3033) and DMSO (control) were added for migration. Cell migration was recorded by time-lapse microscopy every 10 minutes for 17 hours. **(A)** The velocity was calculated using Chemotaxis tool in ImageJ. **(B)** The pseudopod length was measured from the middle of the nucleus to the front of the cells in the direction of migration and analyzed using ImageJ. Time-lapse movies that correspond to the experiments present in **(A)** are available by scanning the QR code in **(C)**. N=2 independent experiments, box and whisker plot represents 5-95 percentile. \*\*\*\*p<0.0001. Mean  $\pm$  SEM, Mann-Whitney test.

We confirmed the impact of  $\alpha 2\beta 1$  integrin inhibition on cell migration by treating MDA-MB-231 cells with either a non-targeting siRNA control (si-nt) or an siRNA targeting  $\alpha 2$  (si- $\alpha 2$ ) for 48 hours before seeding the cells on CDM.  $\alpha 2$  integrin was stained to confirm the effectiveness of  $\alpha 2$  knockdown at the end of migration assays. As expected, the expression level of  $\alpha 2$  integrin was strongly decreased (Figure 3.20A). During cell migration, we noticed that the  $\alpha 2$  integrin knockdown cells exhibited shorter pseudopod extension in the direction of migration with a rounder shape. This phenomenon was consistent with our observations in the presence of BTT-3033. The quantitation analysis of velocity and pseudopod length demonstrated that knockdown of  $\alpha 2$  integrin inhibited MDA-MB-231 cell migration on CDM (Figure 3.20B and C). Taken together, our findings reveal that  $\alpha 2$  integrin promotes breast cancer cell migration.

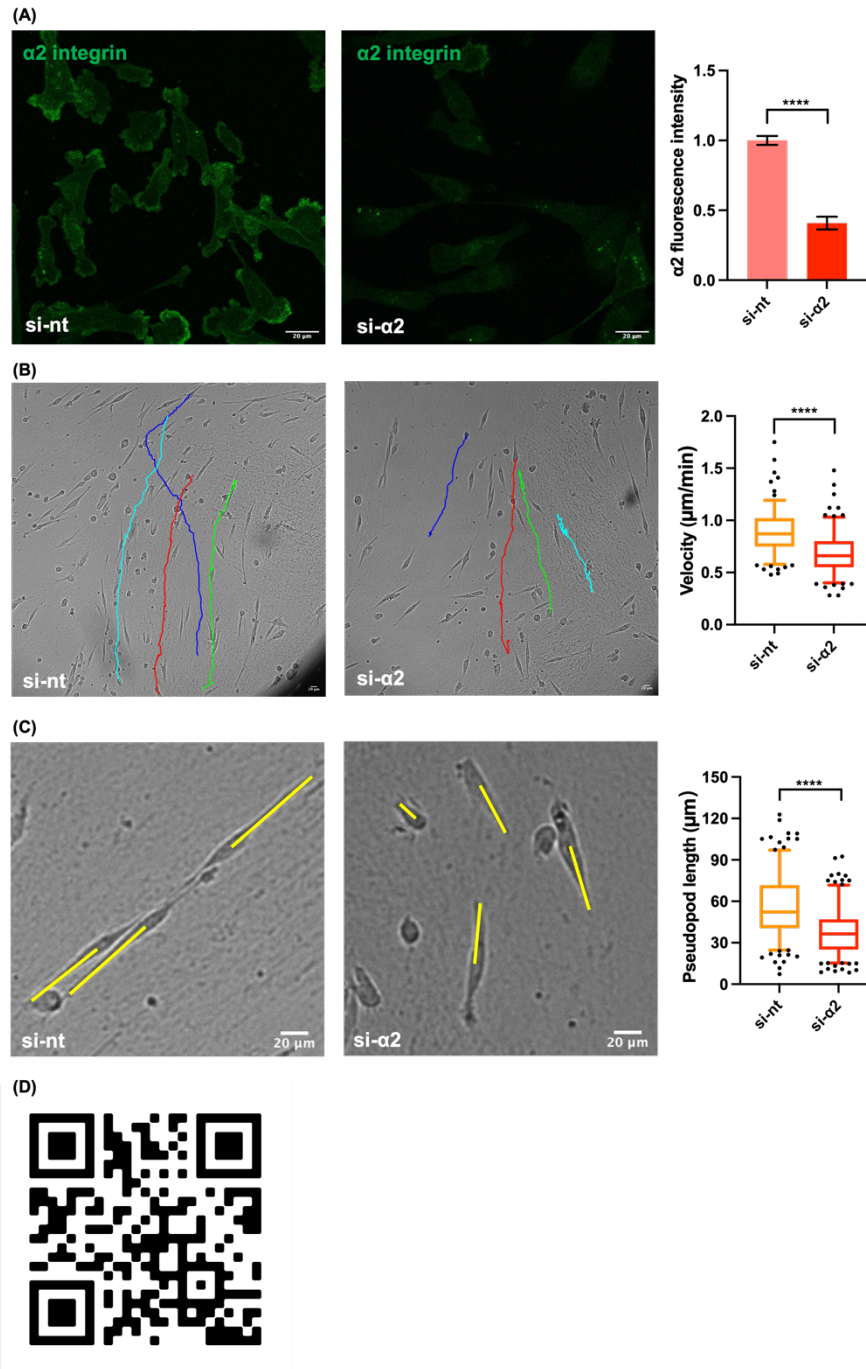


**Figure 3.20.  $\alpha 2\beta 1$  integrin promotes MDA-MB-231 cell migration.** MDA-MB-231 cells were transfected with siRNA targeting  $\alpha 2$  integrin (si- $\alpha 2$ ) or nontargeting control (si-nt) for 48 hours. **(A)** To assess the expression of  $\alpha 2$ , cells were plated glass-bottom dishes for 21 hours, fixed and stained for  $\alpha 2$  integrin (green). Bar=20 $\mu$ m. N=3 independent experiments. \*\*\*\*p<0.0001. Mean  $\pm$  SEM, Mann-Whitney test. MDA-MB-231 cells were plated on CDM for 4 hours to fully adhere. Cell migration was recorded by time-lapse microscopy every 10 minutes for 17 hours. **(B)** The velocity was calculated using Chemotaxis tool in ImageJ. **(C)** The pseudopod length was measured from the middle of the nucleus to the front of the cells in the direction of migration and analyzed using ImageJ. Time-lapse movies that correspond to the experiments present in **(A)** are available by scanning the QR code in **(D)**. N=3 independent experiments, box and whisker plot represents 5-95 percentile. \*\*\*\*p<0.0001. Mean  $\pm$  SEM, Mann-Whitney test.

### **3.2.10 $\alpha 2\beta 1$ integrin is required for MDA-MB-231 cell invasion**

Because  $\alpha 2\beta 1$  integrin was shown to contribute to MDA-MB-231 cells migration, we wanted to characterize whether  $\alpha 2\beta 1$  was required for MDA-MB-231 cell invasion as well. Thus, we measured the invasiveness of cells grown in 3D culture. In order to validate if our 3D model, fluorescently labelled MDA-MB-231 and MCF10A cell spheroids were embedded into a mixture of 1:1 collagen I and Matrigel for 64 hours. Images of cell invasion were obtained at hours 0, 40, 48 and 64 after embedding. The size of core spheroid and the average invasion distance were measured. As normal mammary epithelial cells, MCF10A cells grew around the core spheroids without any sign of invasion into the matrix (Figure 3.21). By contrast, there was no significant difference in the core area in MDA-MB-231 spheroids. However, MDA-MB-231 spheroids were able to gradually invade into the matrix in forms of either cellular sprouts or individual cell which detached from the original core of the spheroid. At 40 hours, it was possible to observe cells protruding out the spheroids, and subsequently, elongated strands of cells were shown around the core spheroids as the time progressed (Figure 3.21), indicating that invasive breast cancer cells, but not normal mammary epithelial cells, display invasive behaviours in these settings.

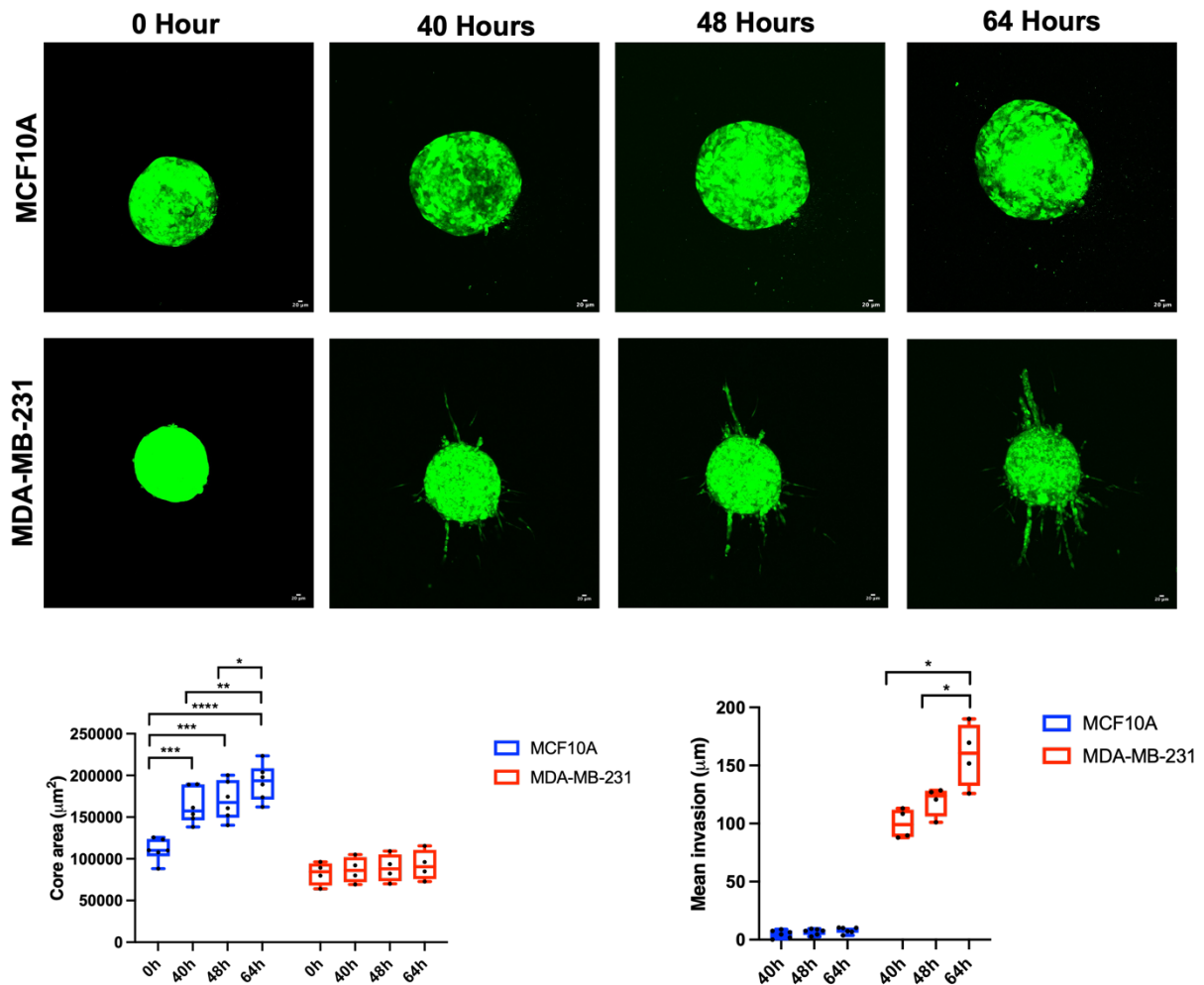


**Figure 3.21. 3D model supports the invasion of MDA-MB-231 cells in matrices.** MCF10A and MDA-MB-231 cells were stained with cell tracker (green) for 40 minutes before making spheroids. The spheroids were formed in 48 hours and embedded into the mixture of 2mg/ml collagen I and 2mg/ml Matrigel for 64 hours. The size of core area and mean invasion was measured at hours of 0, 40, 48 and 64. Spheroids were imaged with a Nikon A1 confocal microscope. Bar=20µm. N=2 independent experiments (the black dots represent each individual spheroid). \*p<0.05, \*\*p<0.01, \*\*\*p<0.001, \*\*\*\*p<0.0001. Mean ± SEM, two-way ANOVA test (Min to Max, show all points).

MDA-MB-231 spheroids were then embedded into the mixture of 1:1 collagen I:Matrigel and covered with medium with or without the  $\alpha 2$  integrin inhibitor BTT-3033. To characterize cell invasion inside the matrix, we employed the size of core area, the mean invasion distance and the invading area as three criteria for measuring invasion quantitatively. It has been reported that  $\alpha 2$  integrin deletion affects the proliferation of prostate cancer cells (Ojalill et al., 2018). Therefore, we firstly quantitatively assessed the proliferative capability of cells by measuring the size of core spheroid to understand whether  $\alpha 2\beta 1$  integrin also played a role in regulating breast cancer cell growth. We found that there was no significant difference in the core area

of MDA-MB-231 spheroids in the presence and in the absence of BTT-3033. Additionally, several strands of invading cells were observed at 40 hours in the presence of DMSO, more and longer cellular sprouts were presented in the following 24 hours. By contrast, the invasion has been significantly inhibited in the presence of BTT-3033. The  $\alpha 2$  integrin inhibition resulted in fewer and shorter strands of invading cells compared to what we observed in the control group. As apparent from the quantification, a nearly 2-fold increase in the mean invasion distance was obtained in the spheroids in the control group compared to the spheroids in the presence of BTT-3033 at all time points. Similarly, consistent with our observations in the mean invasive distance, the invading area was also strongly reduced because of  $\alpha 2$  integrin inhibition (Figure 3.22).

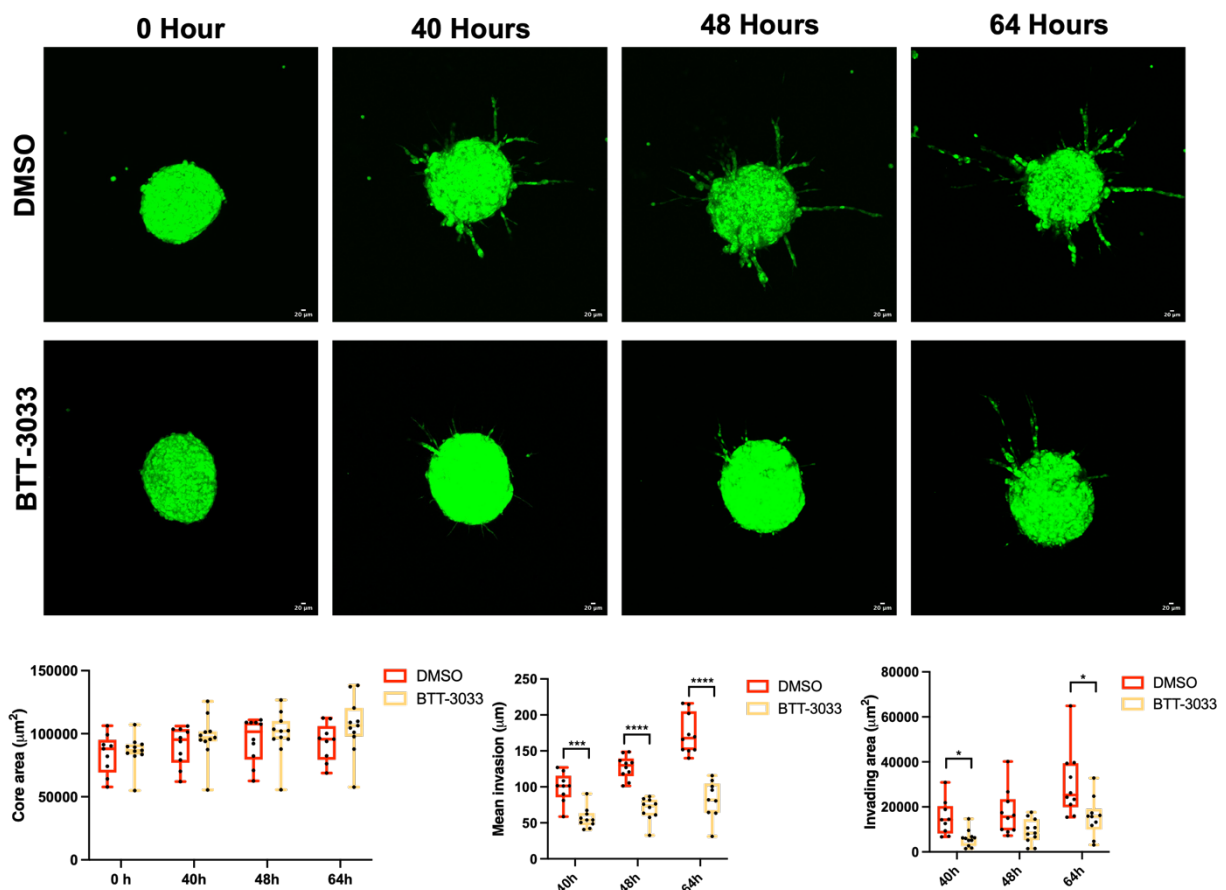


**Figure 3.22.  $\alpha 2\beta 1$  integrin facilitates MDA-MB-231 cell invasion.** MDA-MB-231 cells were stained with cell tracker (green). The spheroids were then formed in 48 hours and embedded into the mixture of 2mg/ml collagen I and 2mg/ml Matrigel for 64 hours in the presence of DMSO (control) or 10 $\mu$ M of  $\alpha 2$  integrin inhibitor BTT-3033. Spheroids were imaged with a Nikon A1 confocal microscope at hours of 0, 40, 48 and 64. The size of core area, mean invasion and invading area were calculated with Image J. Bar=20 $\mu$ m. 12 spheroids per condition in four independent experiments were analyzed. Mean  $\pm$  SEM, Multiple comparisons test (Min to Max, show all points). \* $p < 0.05$ , \*\*\* $p < 0.001$ , \*\*\*\* $p < 0.0001$ .

To confirm the contribution of  $\alpha 2\beta 1$  in promoting breast cancer cell invasion, we decreased the expression of  $\alpha 2$  integrin by siRNA and assessed the invasion of breast cancer cells in the 3D model. MDA-MB-231 cells were treated with either a non-targeting siRNA control (si-nt) or an siRNA targeting  $\alpha 2$  integrin (si- $\alpha 2$ ) for 48 hours before making cell spheroids. Confocal images demonstrated greater than 50% reduction of  $\alpha 2$  integrin expression at 64 hours after embedding, suggesting that RNA-mediated gene knockdown could be effective up to the last time point of the invasion assays (Figure 3.23A). Interestingly, we found that knockdown of  $\alpha 2$  integrin with siRNA resulted in a slight, but not significant, decrease in the core area size compared to control cell spheroids, suggesting that  $\alpha 2$  knockdown may have a marginal effect on cell growth (Figure 3.23B). In addition,  $\alpha 2$  knockdown resulted in fewer and shorter strands of invading cells at 40 hours. Subsequently, more and longer cellular sprouts were observed in the presence of non-targeting siRNA in the following time points (Figure 3.23B). The quantification showed that  $\alpha 2$  knockdown resulted in a nearly 2-fold decrease in both the mean invasion distance and the invading area at all time points (Figure 3.23B), consistent with our observations in the presence of BTT-3033 (Figure 3.22). Collectively, our data reveal that  $\alpha 2\beta 1$  integrin is necessary for the invasion of MDA-MB-231 cells.

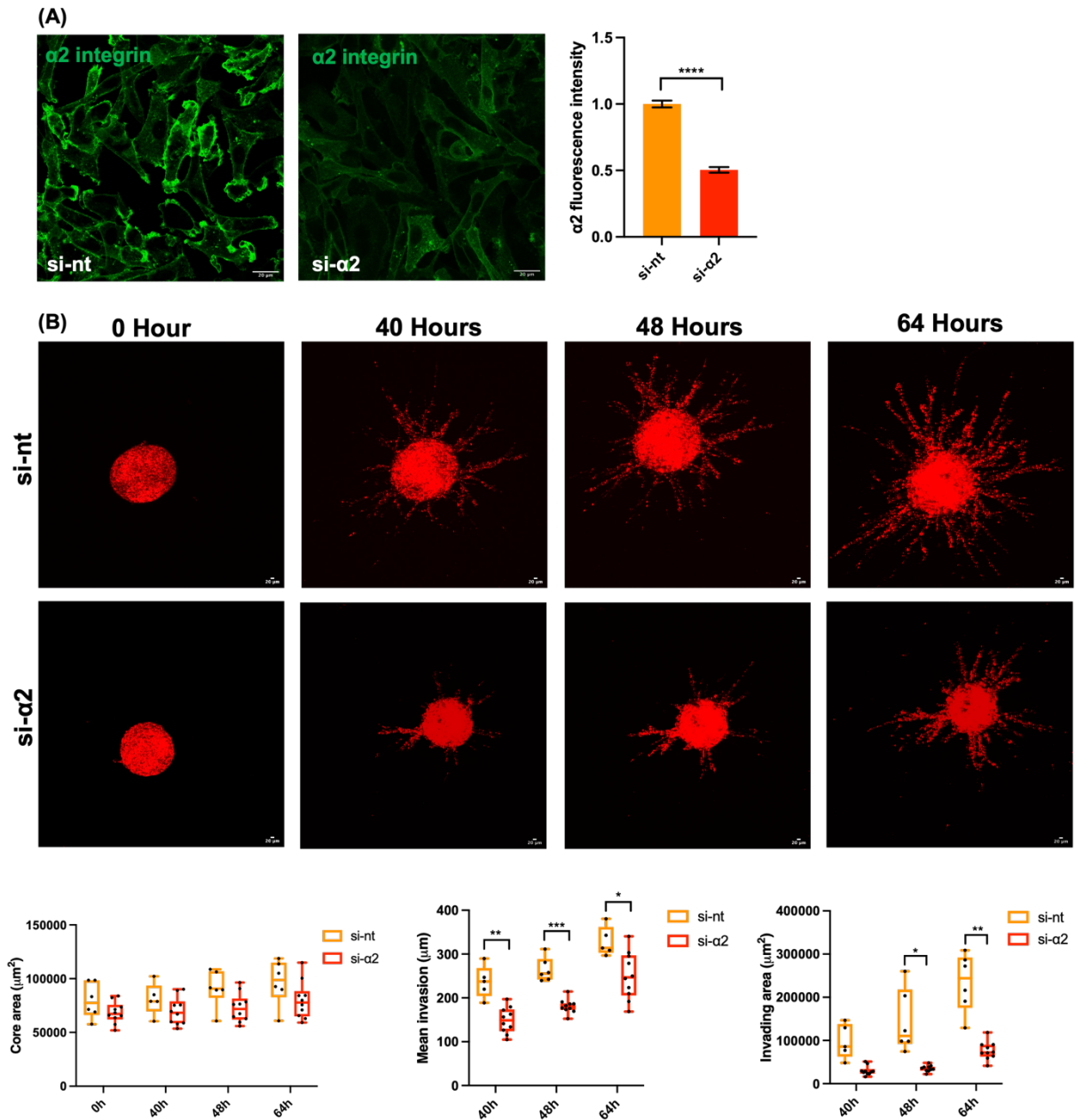


**Figure 3.23.  $\alpha 2\beta 1$  integrin contributes to MDA-MB-231 cell invasion.** MDA-MB-231 cells were transfected with siRNA targeting  $\alpha 2$  integrin (si- $\alpha 2$ ) or nontargeting control (si-nt) for 48 hours. Cells were then stained with cell tracker (red). **(A)** To assess the expression of  $\alpha 2$ , cells were plated glass-bottom dishes for 112 hours, fixed and stained for  $\alpha 2$  integrin (green). Bar= $20\mu\text{m}$ . N=2 independent experiments. \*\*\*\* $p < 0.0001$ . Mean  $\pm$  SEM, Mann-Whitney test. **(B)** To perform invasion assays, spheroids were formed in 48 hours and embedded into 2mg/ml collagen I and 2mg/ml Matrigel mixture for 64 hours. Spheroids were imaged with a Nikon A1 confocal microscope at hours of 0, 40, 48 and 64. The size of core area, mean invasion and invading area were calculated with Image J. Bar= $20\mu\text{m}$ . 6 si-nt spheroids and 10 si- $\alpha 2$  spheroids were obtained from two independent experiments. Mean  $\pm$  SEM, Multiple comparisons test (Min to Max, show all points). \* $p < 0.05$ , \*\* $p < 0.01$ , \*\*\* $p < 0.001$ .

Interestingly, a greater invasion ability was observed in MDA-MB-231 cell spheroids stained with red cell tracker compared to the spheroids stained with green cell tracker. It is possible that green dye inhibits MDA-MB-231 cell invasion. To test this in more detail, MDA-MB-231 cells were stained with red cell tracker, and spheroids were then embedded into 1:1 collagen I: Matrigel mixture with or without  $\alpha 2$  integrin inhibitor BTT-3033. Quantifying the mean invasion distance and the invading area, as expected, illustrated that  $\alpha 2$  inhibition resulted in a significant reduction in the invasion of MDA-MB-231 cells. At the same time, there was no difference in cell growth (Figure 3.24). These findings were consistent with our observations in green cell tracker staining that  $\alpha 2\beta 1$  contributed to breast cancer cell invasion (Figure 3.22).

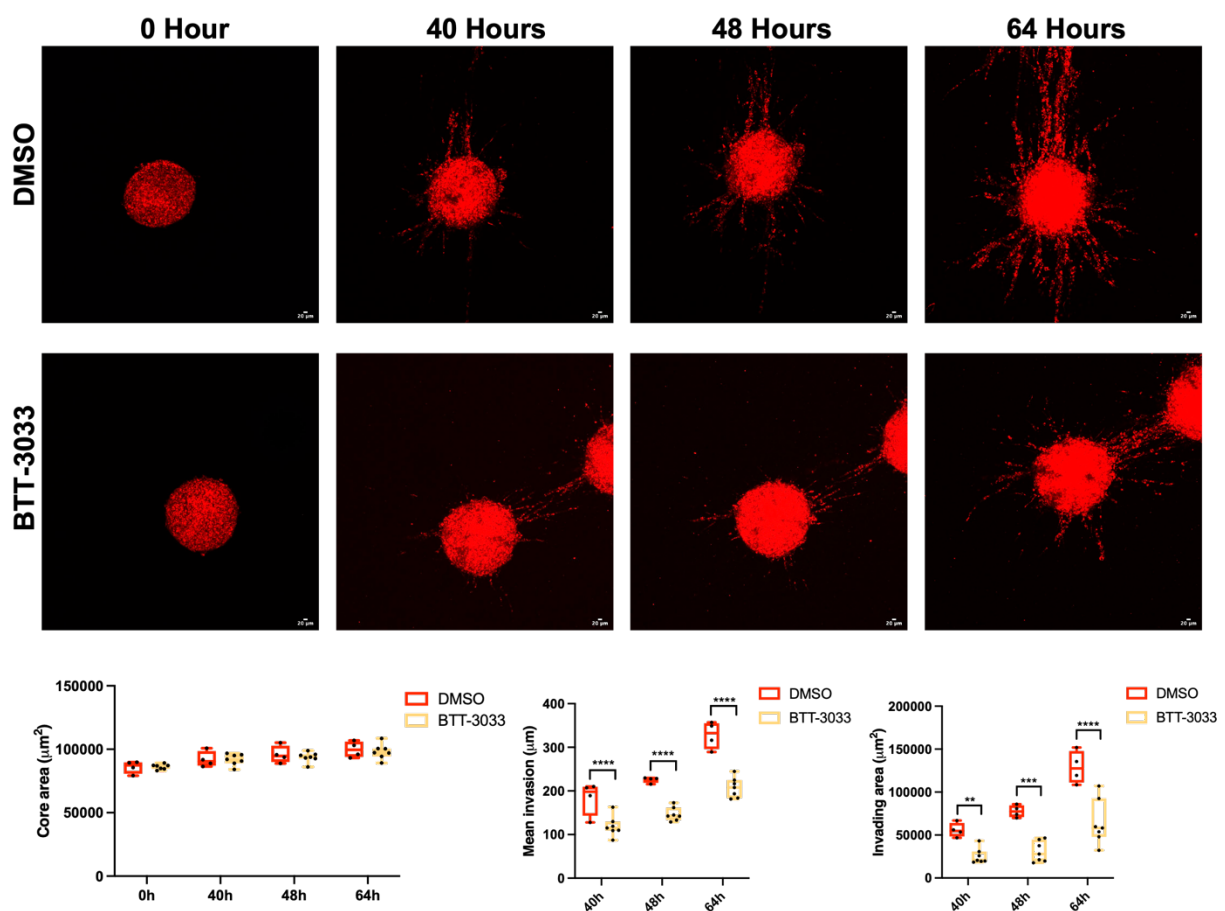


**Figure 3.24.  $\alpha 2\beta 1$  integrin facilitates MDA-MB-231 cell invasion.** MDA-MB-231 cells were stained with cell tracker (red). The spheroids were then formed in 48 hours and embedded into the mixture of 2mg/ml collagen I and 2mg/ml Matrigel for 64 hours in the presence of DMSO (control) or 10 $\mu$ M of  $\alpha 2$  integrin inhibitor BTT-3033. Spheroids were imaged with a Nikon A1 confocal microscope at hours of 0, 40, 48 and 64. The size of core area, mean invasion and invading area were calculated with Image J. Bar=20 $\mu$ m. 4 DMSO treated spheroids and 7 BTT-3033 treated spheroids were obtained from one experiment. Mean  $\pm$  SEM, Multiple comparisons test (Min to Max, show all points). \*\* $p < 0.01$ , \*\*\* $p < 0.001$ , \*\*\*\* $p < 0.0001$ .

At the same time, the quantification analysis of invading distance and invasion area showed that MDA-MB-231 cells stained by green cell tracker were less invasive compared to the cells stained with red cell tracker in the presence and in the absence of BTT-3033 (Figure 3.25). Moreover, our data showed that spheroids stained with green cell tracker had a significantly reduced number of protrusions compared to the spheroids stained with red cell tracker in the presence of DMSO (Figure 3.25A). Measuring the number of protrusions in the presence of BTT-3033 illustrated a similar trend in which cells stained with green cell tracker exhibited decreased invasion ability compared to the cells stained with red cell tracker (Figure 3.25B). Furthermore, our data showed that green cell tracker did not affect cell growth. No difference was observed in the size of core area in the presence and in the absence of BTT-3033 (Figure 3.25). Altogether, our findings suggest that green cell tracker at the concentration used in this study has an inhibitory effect on MDA-MB-231 cell invasion.

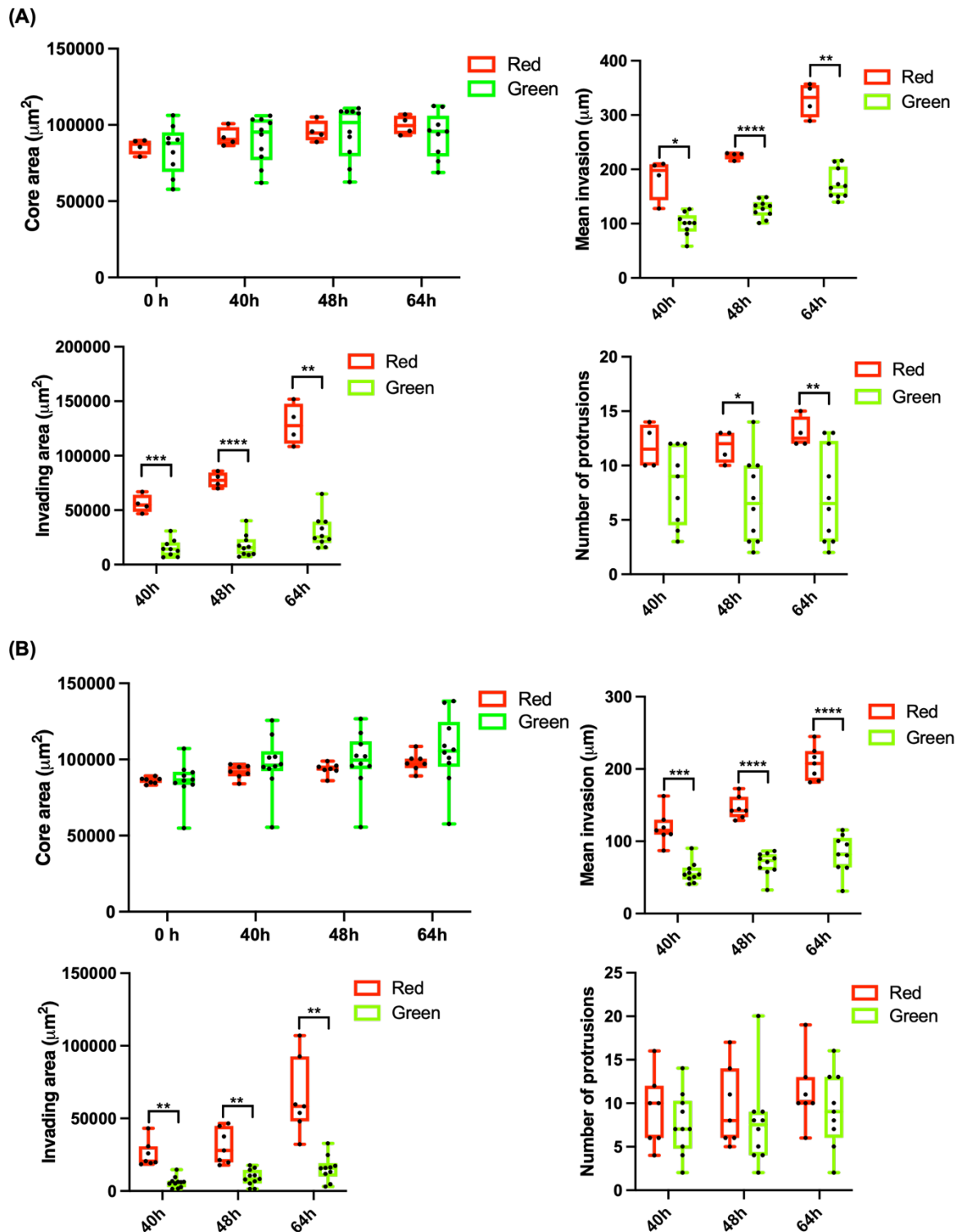


**Figure 3.25. Green cell tracker staining makes MDA-MB-231 cells less invasive.** The size of core area, mean invasion, invading area and the number of protrusions were measured at hours of 0, 40, 48 and 64 after embedding into the matrices in the presence of **(A)** DMSO and **(B)** 10 $\mu\text{M}$  of  $\alpha 2$  integrin inhibitor BTT-3033. For red dye staining invasion assay, N=1 experiment. For green cell tracker staining invasion assays, N=4 independent experiments. Mean  $\pm$  SEM, Multiple comparisons test (Min to Max, show all points). \* $p < 0.05$ , \*\* $p < 0.01$ , \*\*\* $p < 0.001$ , \*\*\*\* $p < 0.0001$ .

### 3.3 Discussion

$\alpha 2\beta 1$  has been implicated as a key target in cancer development and progression in a variety of cancers (Salemi et al., 2021). Here we characterize the role of  $\alpha 2\beta 1$  in the migration and invasion of breast cancer cells. We find that the binding of collagen I and Matrigel promotes the internalization of  $\alpha 2\beta 1$  integrin, which in turns contributes to collagen I and Matrigel endocytosis in breast cancer cells. In addition, our findings show  $\alpha 2\beta 1$  as a regulator for breast cancer cell migration and invasion (Figure 3.26).

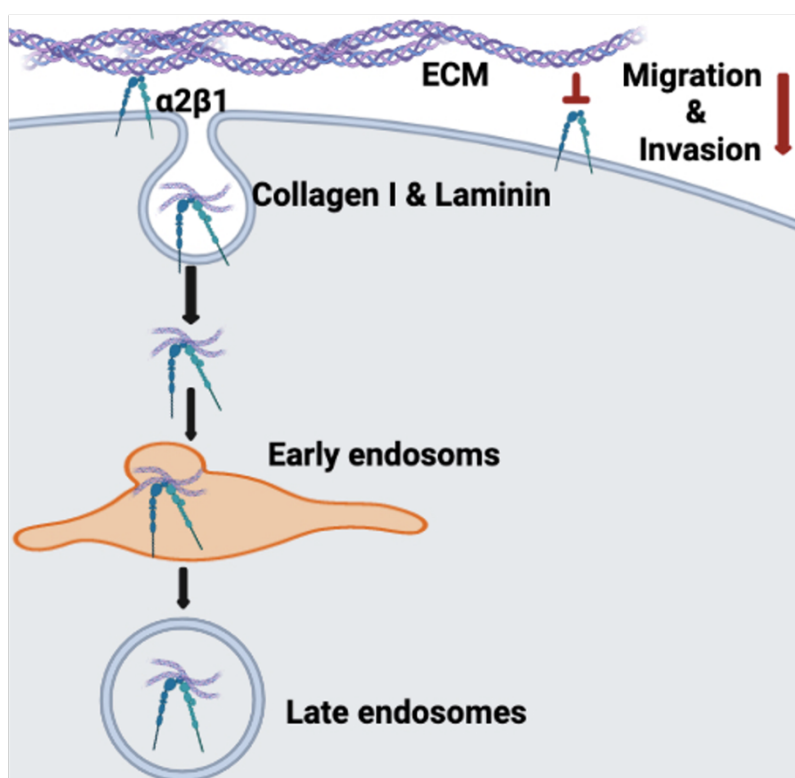


**Figure 3.26. Schematic to summarize  $\alpha 2\beta 1$  integrin-dependent ECM endocytosis.**  $\alpha 2\beta 1$  integrin is necessary for the endocytosis of collagen I and laminin in breast cancer cells. At the same time, internalized ECM components are degraded in lysosomes in the presence of the lysosomal inhibitor E64d. Moreover, ECM binding promotes  $\alpha 2\beta 1$  internalization. Furthermore, inhibition of  $\alpha 2$  or decrease the expression of  $\alpha 2$  by knockdown inhibits the migration and invasion of breast cancer cells.

We demonstrated that there is no significant difference in collagen I internalization between breast cancer cells and normal mammary epithelial cells. However, it should be noticed that in the absence of E64d, the internalization of collagen I is strongly increased in invasive breast cancer cells. E64d is an inhibitor of cathepsin B and L and calpain (Jung et al., 2015). One possible explanation is that collagen I internalization is inhibited as a result of the increased

collagen I accumulation in the lysosomes. Additionally, cathepsin B is known to be secreted in the extracellular space by MDA-MB-231 cells (Uhlman et al., 2017). There is also evidence that cathepsin B can degrade extracellular collagen I, contributing to breast cancer cell metastasis (Withana et al., 2012). Cleaved collagen could be endocytosed more efficiently than intact collagen (Rainero, 2016). Thus, the other possible explanation is that E64d might inhibit cathepsin B activity in the extracellular space, leading to a slower collagen I endocytosis rate in invasive breast cancer cells, but not in normal epithelial cells, where cathepsin secretion has not been observed. Recent results from the Rainero lab illustrated that E64d inhibited the internalization of higher concentration collagen I (1mg/ml) in breast cancer cells at shorter time point (6 hours), rather than longer time point (24 hours) or lower concentration collagen I internalization (0.5mg/ml) (data not shown). This is consistent with our second hypothesis.

In breast cancer, the disruption of BM is required for tumour cell invasion (Bonnans et al., 2014). The contribution of MMPs-dependent BM degradation has been widely recognised in this process (Insua-Rodríguez and Oskarsson, 2016). We found that Matrigel internalization is strongly upregulated in invasive breast cancer cells compared to normal mammary epithelial cells, indicating that lysosomal degradation might also promote the disruption of BM in breast cancer. Subsequently, we showed that internalized Matrigel is degraded in the cells. However, we examined the colocalization between internalized Matrigel and early and late endosomes in the presence of E64d, which might affect Matrigel trafficking. Therefore, more studies are required to assess the intracellular trafficking pathway of Matrigel in the absence of E64d.

$\beta$ 1 integrin, which can pair with 12 different  $\alpha$  integrin subunits, is known to be aberrantly expressed in human breast cancer and contribute to diverse malignant phenotypes, including proliferation and metastasis (Lahlou and Muller, 2011). Our findings indicated that  $\beta$ 1 integrin is responsible for the endocytosis of Matrigel in MDA-MB-231 cells. Interestingly, Matrigel containing vesicles are still observed in several cells in the presence of  $\beta$ 1 integrin blocking antibody. The evidence suggest that laminin could be internalized by  $\alpha$ 6 $\beta$ 4 integrin under dietary restriction and nutrient deprivation conditions (Muranen et al., 2017). At the same time, it has been demonstrated that the knockout of  $\beta$ 1 integrin resulted in an increased expression of  $\beta$ 4 integrin in MDA-MB-231 cells (Hou et al., 2016). Although dystroglycan is

known as another important receptor for laminin internalization (Leonoudakis et al., 2014), the dystroglycan expressed on MDA-MB-231 cells is not functionally glycosylated (de Bernabé et al., 2009). Thus, it is worth investigating whether  $\beta 4$  inhibition affects Matrigel endocytosis in breast cancer cells.

MDA-MB-231 cells express  $\alpha 1$ ,  $\alpha 2$ ,  $\alpha 3$  and  $\alpha 6$  integrin subunits (Lahlou and Muller, 2011).  $\alpha 1\beta 1$  and  $\alpha 2\beta 1$  integrins bind to both collages and laminin. However,  $\alpha 1\beta 1$  integrin displays a higher affinity for collagen IV, while  $\alpha 2\beta 1$  preferentially binds to collagen I (Shi et al., 2012). Both  $\alpha 3\beta 1$  and  $\alpha 6\beta 1$  integrins are highly selective laminin receptors (Humphries et al., 2006a). Here we showed that  $\alpha 2\beta 1$  inhibition leads to a decrease in collagen I internalization in MDA-MB-231 cells. Similar findings were observed in MCF10A-CA1 cells (derived from MCF10A cells by transformation with h-Ras followed by selecting aggressive tumour in mice xenografts) in Rainero lab as well (data not shown). Consistent with our results on breast cancer cells, there is also evidence suggesting that  $\alpha 2\beta 1$  contributes to the internalization of collagen I in human osteosarcoma cells (Rintanen et al., 2012). Additionally, we found that  $\alpha 3\beta 1$  is not necessary for collagen I endocytosis. Contrary to our findings, it is previously demonstrated that  $\alpha 3\beta 1$  participates in ECM phagocytosis in MDA-MB-231 cells. The stimulation of  $\alpha 3$  by treating cells with anti- $\alpha 3$  monoclonal antibodies contributes to gelatin endocytosis (Coopman et al., 1996). However, gelatin displays a less ordered macromolecular structure and poor mechanical properties compared to collagen I (Davidenko et al., 2016). Alongside, we demonstrated that collagen I is necessary for the activation and internalization of  $\alpha 2\beta 1$ . Therefore, here we could hypothesize that collagen I is preferentially binding to  $\alpha 2\beta 1$  integrin and internalized in  $\alpha 2\beta 1$ -dependent pathway under more physiological conditions.

$\alpha 2\beta 1$  integrin has been shown to be expressed in a panel of breast cancer cell lines *in vitro*. It has been illustrated that compared to ER-positive cell lines, ER-negative cells have a lower binding affinity to laminin. Because laminin is served as a physical barrier to potential local invasion, a possible explanation is that cells with higher invasive capacity are preferentially binding to collagen I (Maemura et al., 1995). Consistently, more intracellular  $\alpha 2$  integrin vesicles were observed on collagen I than on Matrigel. However, our data showed that  $\alpha 2\beta 1$  is still required for the internalization of Matrigel and laminin in MDA-MB-231 cells. Although DQ-collagen IV and Matrigel mixture has been widely used to investigate collagen IV uptake

in different cell types (Jevnikar et al., 2008; Sameni et al., 2003), the small, but significant, decrease in collagen IV endocytosis that was observed in the presence of BTT-3033 might be because DQ-collagen IV can bind to laminin in the Matrigel, as it might be internalized in a complex with laminin. We showed that neither  $\alpha 3$  nor  $\alpha 6$  inhibition decreases Matrigel endocytosis in MDA-MB-231 cells. However,  $\alpha 3$  inhibition resulted in a small reduction in cellular aspect ratio (data not shown). These data are in agreement with previous studies showing that  $\alpha 3$  displays a strongly colocalization with laminin at the leading edge of cellular protrusions in MDA-MB-231 cells (Scales et al., 2013). Additionally,  $\alpha 6$  inhibition significantly decreased cellular aspect ratio (data not shown). Thus, it is possible that changes in cellular morphology might be one of the reasons why Matrigel internalization index is higher in the presence of  $\alpha 6$  blocking antibody. Furthermore, a recent study demonstrated that  $\alpha 2\beta 1$  is a negative regulator for the expression of  $\alpha 6\beta 1$  and  $\alpha 6\beta 4$  (Dao et al., 2021). Therefore, the inhibition of  $\alpha 6$  might increase  $\alpha 2$  expression, facilitating  $\alpha 2\beta 1$ -dependent laminin uptake.

Integrin traffic is a key regulator of cell motility in many different contexts (Paul et al., 2015; Rainero et al., 2015). There is only limited data available on the endo/exocytic traffic of  $\alpha 2\beta 1$  integrin. Collagen I-occupied  $\alpha 2\beta 1$  integrin is demonstrated to be internalized through early endosomes to the PNRC in a Rab21-dependent pathway (Pellinen et al., 2008, 2006). Internalized  $\alpha 2\beta 1$  integrin could be recycled back to the plasma membrane in a p120RasGAP-dependent pathway (Mai et al., 2011). Moreover, virus clustered  $\alpha 2\beta 1$  integrin is internalized from the lipid rafts to the perinuclear cytoplasm, accumulating in  $\alpha 2$  integrin-enriched multivesicular bodies ( $\alpha 2$ -MVBs) (Upla et al., 2004). However, this route differs from typical integrin recycling as virus-induced clustering directs  $\alpha 2\beta 1$  integrin into a non-recycling, calpain-dependent degradative endosomal pathway (Mai et al., 2011; Rintanen et al., 2012). Inactive  $\alpha 2\beta 1$  integrin is illustrated to be internalized from the dorsal surface of cells in a clathrin-dependent pathway, generating an internal pool of  $\alpha 2\beta 1$  integrin that is subsequently recycled to form adhesions at the cell leading of cell (Teckchandani et al., 2009). Here we revealed that collagen I and Matrigel binding is necessary for the endocytosis of  $\alpha 2\beta 1$  integrin. In addition,  $\alpha 2\beta 1$  inhibition significantly decreases  $\alpha 2\beta 1$  internalization and MDA-MB-231 migration and invasion. It is possible that collagen I and Matrigel can promote the activation and endocytosis of  $\alpha 2\beta 1$  integrin. Cytoplasmic  $\alpha 2\beta 1$  integrin is recruited to EGFR by p120RasGAP at the cell front (Mai et al., 2011), facilitating breast cancer cell migration and

invasion. However, further studies are needed to fully characterise  $\alpha 2\beta 1$  integrin traffic in this condition.

In addition to integrin traffic, the attachment of cancer cells to collagen I by  $\alpha 2\beta 1$  has been demonstrated to activate p38 MAPK signalling (Ibaragi et al., 2011; Klekotka et al., 2001), which could accelerate tumour cell migration (Huth et al., 2017; Ojalill et al., 2018). The data are consistent with our observations. However, the mechanism of p38 MAPK signalling in tumour migration and invasion is still not well understood. On the one hand, MMP13 expression is reported to be upregulated as a result of  $\alpha 2\beta 1$ -dependent p38 MAPK activation, facilitating the migration of MDA-MB-231 cells (Ibaragi et al., 2011). On the other hand, p38 MAPK signalling has been demonstrated to regulate breast cancer invasion in association with other signalling proteins such as H-RAS (Kim et al., 2003). Therefore, future work will measure changes of p38 MAPK activation in MDA-MB-231 cells plated on both collagen I and Matrigel, to find whether  $\alpha 2\beta 1$  integrin can regulate breast cancer cell migration and invasion in this pathway.

Taken together, our results highlight a novel role of  $\alpha 2\beta 1$  integrin in regulating breast cancer progression via ECM endocytosis. This raise the possibility that targeting  $\alpha 2$  could be a viable strategy to slow down the migration and invasion of breast cancer cells, eventually leading to the generation of improved clinical outcomes.

## 4 ECM component uptake is cell cycle-dependent in invasive breast cancer cells

### 4.1 Introduction

Dysregulated cell cycle is a hallmark of cancer that leads to aberrant cellular proliferation with the continuing and excessive rounds of cell division (Hanahan and Weinberg, 2011). The cell cycle is mainly composed of four phases including the G1, S, G2 and M phase. The G1, S and G2 together are called interphase. The M phase is comprised of mitosis, which can be further divided into five subphases including the prophase, prometaphase, metaphase, anaphase and telophase (Figure 4.1) (Wang, 2021). The G1 phase is a decision window in which cells can either commit to initiate DNA replication or stay in the G1 phase. Additionally, the cells in the G1 phase can also exit the cell cycle into a non-proliferative state (Matthews et al., 2021). Specific cyclins expressed during different phases of the cell cycle regulate the activity of a family of cyclin-dependent kinases (CDKs), whose phosphorylation of key substrates promotes cell cycle progression. The transition from G1 to S phase is mainly regulated by D-type cyclins. Briefly, D-cyclins binds to CDK4/6, and cyclin D-CDK4/6 complexes then enter the nucleus to phosphorylate tumour suppressor protein retinoblastoma (RB), facilitating the expression of E2F target genes including A- and E-type cyclins. Cyclin E then binds to and activates CDK2, which can further hyperphosphorylate RB, contributing to E2F target genes expression that are critical for initiation of DNA synthesis and entry into S phase (Goel et al., 2018; Sherr and Bartek, 2017). Deregulated cyclin D-CDK4/6 complex activation is commonly observed in breast cancer. For example, cyclin D1 (*CCND1*) amplification has been shown in breast cancer. Increased expression of cyclin D leads to continuous phosphorylation of Rb and causes continuous proliferation of breast cancer cell, which is correlated with worse clinical outcomes (Lundgren et al., 2012). Additionally, increased levels of *CDK4* and *CDK6* also have been found in other human cancer types such as liposarcoma, upper gastrointestinal cancer and prostate carcinoma (Cerami et al., 2012). Thus, the inhibition of cell cycle progression by arresting the cells in G1 phase has become a new therapeutic frontier in the treatment of cancers.

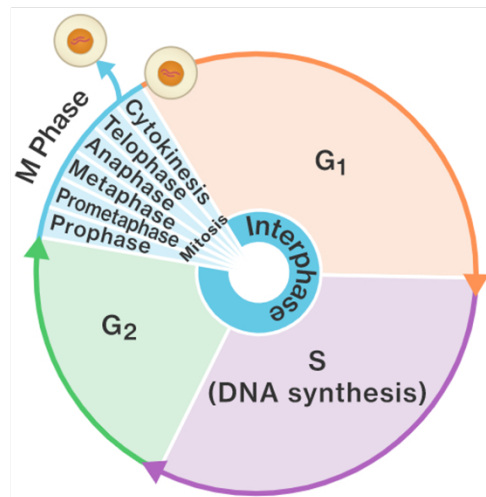


**Figure 4.1. Diagram of cell cycle progression.** The interphase comprises the G1, S and G2 phases. The M phase consists of mitosis, which is further divided into prophase, prometaphase, metaphase, anaphase and telophase. Figure adapted from (Wang, 2021).

During cell division, cell shape, adhesiveness and cytoskeletal architecture are changed in a highly conserved manner, which is necessary for chromosome segregation and cytokinesis (Taubenberger et al., 2020). Integrins are adhesion receptors that can interact with the ECM and the actin cytoskeleton inside the cells, indicating a primordial link between the cell cycle progression and integrin-dependent cell-ECM adhesion (Moreno-Layseca and Streuli, 2014). A recent study demonstrated that adhesion complexes are regulated during the cell cycle in a CDK1-dependent manner. CDK1 is a serine/threonine kinase that can phosphorylate a wide range of substrates during mitosis. It is shown that the interaction between CDK1 and cyclin A2 leads to an increased adhesion complex area from G1 to S phase, whereas the adhesion complex area then decreases in G2 phase as a result of the enhanced activation of cyclin B1-CDK1 complexes. At the same time, the changes in adhesion complex area are accompanied by the distribution of focal adhesion from the peripheral area in G1 and G2 phases to the central area in the S phase. These changes on focal adhesion are essential for cells entry into the M phase (Jones et al., 2019, 2018). Additionally, Dix and co-workers illustrated that while focal adhesion complexes are disassembled during mitotic rounding, the activated integrins remain at the tips and tails of retraction fibers that connect the cells to the substrate, guiding polarized cell migration following mitotic exit (Dix et al., 2018). Collectively, current evidence suggests that integrin-dependent ECM-adhesion is regulated during the cell cycle. In the previous chapter, we illustrated that  $\alpha 2\beta 1$  integrin is required for ECM endocytosis in breast

cancer cells. Therefore, we set out to investigate whether the endocytosis of ECM is cell cycle dependent as well.

As mentioned earlier, integrin-dependent ECM uptake is one of the mechanisms regulating the turnover of ECM. The other mechanism is extracellular degradation mediated by MMPs and proteases (Jabłońska-Trypuć et al., 2016). Invadopodia are actin-rich membrane protrusions formed by invasive cancer cells. The invadopodia precursors, including cortactin, cofilin and neural-Wiskott-Aldrich Syndrome protein (N-WASP), are formed at the cell periphery. These structures are then stabilized through binding to focal adhesions. In the early steps of invadopodia assembly, cortactin promotes the polymerization of actin filaments and MMP recruitment to the tip of nascent invadopodia, leading to further invadopodia maturation and ECM degradation (Jacob and Prekeris, 2015). The Gligorijevic lab recently demonstrated the coordination of cell cycle progression with the formation of invadopodia. They showed that MT1-MMP (MMP-14) is preferentially recruited to invadopodia in the G1 phase of the cell cycle, contributing to invadopodia maturation and extracellular ECM degradation, as well as increasing tumour cell invasion (Bayarmagnai et al., 2019b). Compared to proteolytic degradation, more studies are required to understand whether intracellular ECM degradation is regulated in the G1 phase as well.

The mammalian target of rapamycin complex 1 (mTORC1), in response to the energy status, nutrients, and growth factors stimulation of cells, plays a key role in regulating cell growth and proliferation. As reported, mTOR is aberrantly overactivated in more than 70% of cancers (Tian et al., 2019). On the one hand, there is increasing evidence demonstrating that mTORC1 regulates the G1 phase of cell cycle. The inhibition of mTORC1 activity, by both rapamycin and nutrient starvation, has been proved to arrest human osteosarcoma cells in the G1 phase (Fingar et al., 2004). Similar results were observed in ovarian cancer cells as well (Gao et al., 2004). Additionally, a recent study characterized that growth factors (GFs), amino acid and mTORC1 regulate distinct metabolic checkpoints in mammalian G1 phase. The GF-dependent checkpoint in the middle of G1 phase determines whether cells are appropriate to divide, while the checkpoints mediated by amino acids and mTOR in late G1 phase assess whether cells have sufficient nutrients to accomplish cell division progression (Saqcena et al., 2013). On the other hand, the internalization of an ECM component, fibronectin, has been shown to

stimulate the activation of mTORC1 and promote ovarian cancer cell invasion (Rainero et al., 2015). Thus, it is possible that internalized ECM components in G1 can trigger mTORC1 activity and cell division.

In this chapter we synchronized cells in G1 phase by serum starvation, double thymidine block (DTB) and palbociclib (Pb) treatment. The transition from G1 to S phase is regulated by growth factors present in the extracellular environment. Therefore, serum starvation has been widely used for synchronizing cells in G1 by removing mitogenic factors in the growth medium (Davis et al., 2001). However, serum starvation often reduces cell survival and increases the DNA fragmentation (Baghdadchi, 2013). As an inhibitor of DNA synthesis, thymidine arrests cells at G1/S boundary by binding to deoxyadenosine with double stranded DNA. Briefly, the first exposure to thymidine halts most of cells at the early S phase and G1/S boundary of the cell cycle. Those cells then progress through G2/M phases during the release. During the second exposure, the cells in G2/M phases will be synchronized at G1/S boundary. Additionally, some cells would be arrested in the late S phase after the first exposure. Those will progress to G1 phase following the release. These cells will then be synchronized at G1/S boundary as well after the second exposure (Chen and Deng, 2018). However, the stalled DNA replication forks tends to collapse due to the extended arrest, resulting in chromosomal rearrangements and damage after DTB release (Trotter and Hagan, 2020). Pb is the first FDA-approved CDK4/6 inhibitor for the treatment of metastatic ER<sup>+</sup>/HER2<sup>-</sup> breast cancer. Pb can hinder the transition from the G1 to S phase by inhibiting Rb phosphorylation and E2F release, inhibiting tumour cell growth (Liu et al., 2018). Moreover, we used nuclear labelled MDA-MB-231 cells with FUCCI (Fluorescent Ubiquitin Cell Cycle Indicator) system, which allows us to distinguish the G1 phase of the cell cycle from S, G2 and M phase. The FUCCI system utilizes the phase-dependent nature of replication licensing factors Cdt1 and Geminin. Cdt1 is a key DNA replication protein whose accumulation from the beginning of G1 phase to early S phase is required for the formation and replication of pre-replicative complexes in the following cell cycle phases. Geminin is known as an inhibitor of Cdt1, expressing from S phase to metaphase of M phase (Ballabeni et al., 2013). The reciprocal expression of Cdt1 and Geminin is regulated by the sequential activation of the E3 ligase complexes SCFskp2 and APCcdh1. The SCFskp2 ubiquitin ligase is known to be active from S to G2 phases and targets Cdt1 for degradation, whereas the APCcdh1 ubiquitin ligase is active from mid-mitosis throughout G1 and targets

Geminin for degradation (Zielke and Edgar, 2015). Therefore, a fusion protein of a fragment of Cdt1 with the fluorescent reporter Kusabira-Orange 2 (mKO2) can serve as an indicator of the G1 phase, while a fusion protein of a fragment of Geminin with the fluorescent protein Azami-Green (mAG1) can visualize the late S/G2/M phase. In the early S phase, both red and green colours are expressed, the cell nucleus appear yellow (Figure 4.2) (Prasedya et al., 2016; Sakaue-Sawano et al., 2008).

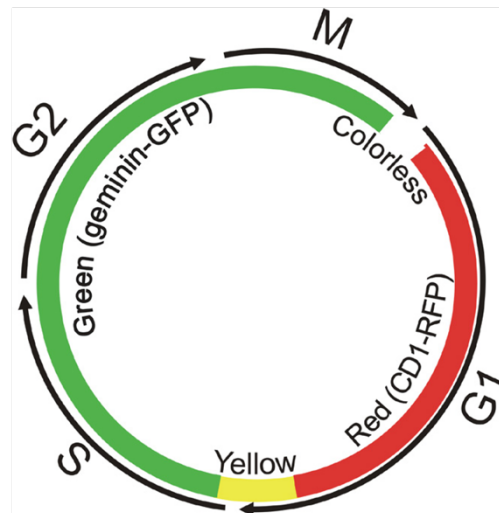


**Figure 4.2. Dynamic color change of Fucci-MDA-MB-231 cells.** Fucci is a fluorescent, two colour sensor of cell cycle progression and division in live cells. During early G1 phase there is no fluorescence as both Fucci reporters are downregulated. Cells change from red in the G1 to yellow in the G1/S interphase and green in S, G2, and M phases (Prasedya et al., 2016).

In the previous chapter, we demonstrated that the internalization of ECM promotes breast cancer cell migration and invasion. Meanwhile, it is illustrated that MDA-MB-231 cells in G1 phase are more invasive due to upregulated extracellular ECM degradation (Bayarmagnai et al., 2019b). Therefore, we hypothesized that breast cancer cells in G1 might uptake more ECM than cells in S/G2/M phases as well, contributing to cell migration and invasion. Here we synchronize cells in G1 via different methods and illustrate that ECM endocytosis is cell-cycle dependent in invasive breast cancer cells, but not in normal mammary epithelial cells. Our findings reveal that Matrigel internalization is promoted in G1, accompanied by increased  $\beta 1$  integrin endocytosis. Furthermore, our results suggest that this increased Matrigel uptake might not be only regulated by the enhanced MMP expression in the G1 phase. Finally, our data highlight a potential role of Matrigel in promoting mTORC1 activity in G1.

## 4.2 Results

### 4.2.1 CDM internalization is upregulated in G1 phase MDA-MB-231 cells

In order to investigate whether the internalization of ECM components is affected by the cell cycle, we firstly compared CDM internalization in synchronized and asynchronous MDA-MB-231 cells. Here we synchronized cells in the G1 phase by a 24-hour serum starvation. As shown in figure 4.3A, there was a significant increase in the proportion of cells in G1 phase when cells were serum starved for 24 hours compared to the control non-starved cells. At the same time, we illustrated that cells were arrested in the G1 phase for around 12 hours following release in full growth medium. Next, serum-starved and control non-starved cells were plated in complete medium on biotinylated CDM for 8 hours in the presence of the lysosomal inhibitor E64d. The internalized CDM can be visualized as green signals inside the cells. A greater number of CDM containing vesicles were visualized in synchronized cells compared to what we observed in the asynchronous cells, and the image quantification showed that the internalization of CDM was strongly upregulated in G1 phase MDA-MB-231 cells (Figure 4.3B).

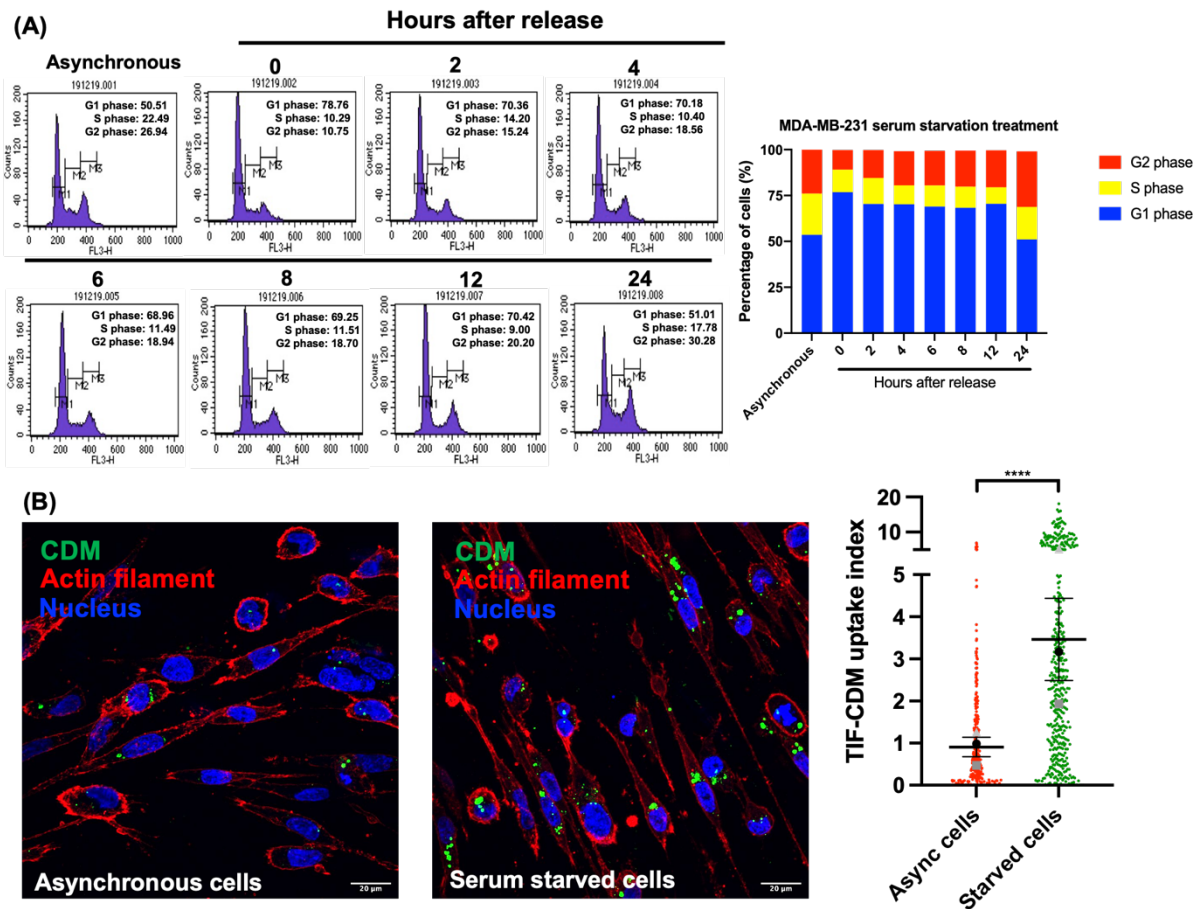


**Figure 4.3. CDM uptake is enhanced in serum starved MDA-MB-231 cells.** (A) MDA-MB-231 cells were synchronized by serum starvation for 24 hours and released in full medium. Cells were harvested at the indicated time points, fixed, and stained with Propidium Iodide (PI) before fluorescence-activated cell-sorting analysis (FACS) to determine DNA content. (B) Asynchronous and serum-starved MDA-MB-231 cells were plated in full growth medium on biotinylated CDM for an 8-hour incubation in the presence of 20 $\mu$ M E64d inhibitor. The extracellular biotin was removed by treatment with a cell-impermeable reducing agent (MesNa). Cells were fixed and stained for Streptavidin (green), actin (red) and nuclei (blue). Samples were imaged with a Nikon A1 confocal microscope and CDM uptake index was calculated with Image J. Bar=20 $\mu$ m. N=3 independent experiments. Mean  $\pm$  SEM, Mann-Whitney test (the big dots represent the mean of individual experiments). \*\*\*\*p<0.0001.

#### 4.2.2 Matrigel uptake is increased in G1 phase in invasive breast cancer cells

To characterize the internalization of which ECM components are specifically upregulated in MDA-MB-231 cells synchronized in G1 phase, the endocytosis of collagen I and Matrigel was measured in serum starved and non-starved MDA-MB-231 cells. The cells were serum starved for 24 hours, followed by 24 hours incubation on fluorescently labelled matrices in full growth medium. As shown in figure 4.4A, the internalization of collagen I was lower in the G1 population than in the asynchronous population as a result of fewer collagen I containing

vesicles inside the cells. By contrast, more and bigger Matrigel containing vesicles were visualized after serum starvation. Indeed, the statistical results illustrated that Matrigel, but not collagen I, internalization was significantly increased in G1 phase MDA-MB-231 cells compared to asynchronous cells (Figure 4.4B).

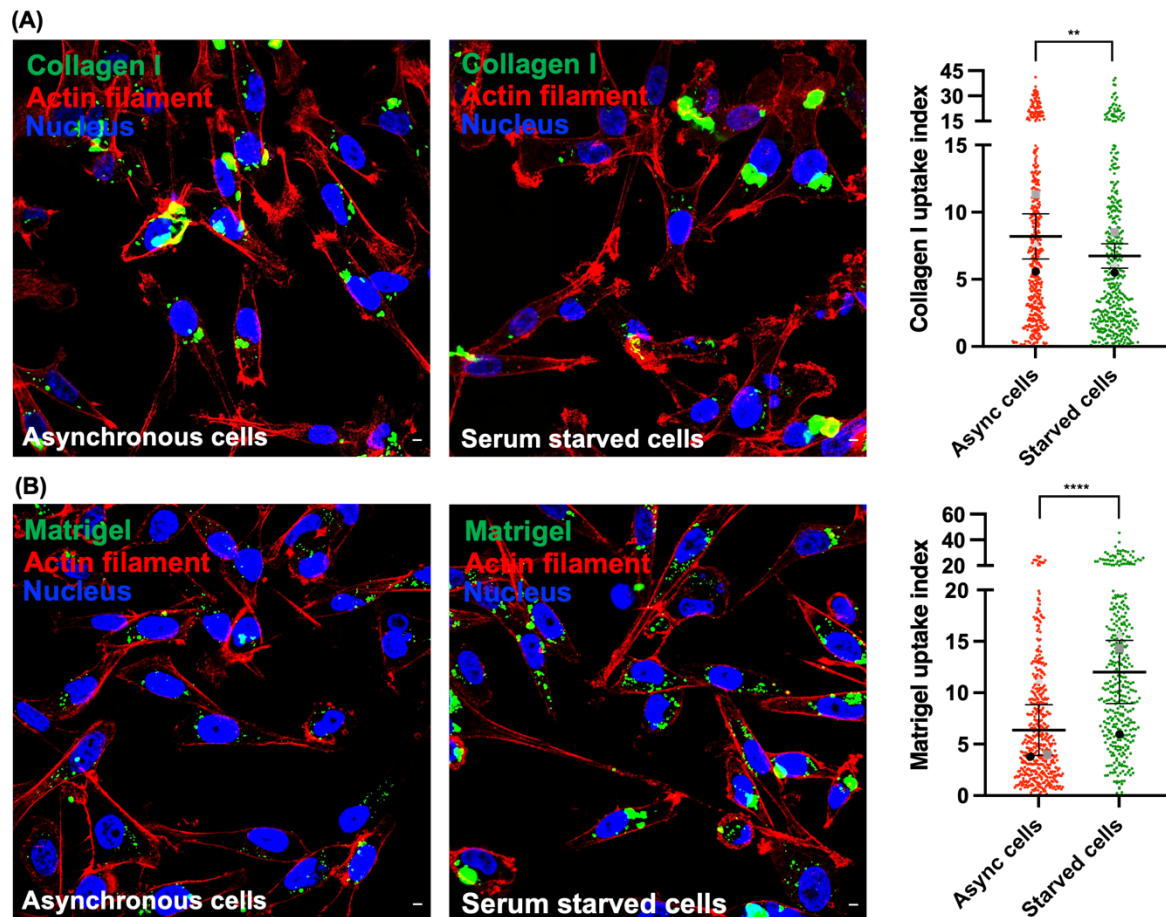


**Figure 4.4. Matrigel, but not collagen I, internalization is upregulated in serum starved MDA-MB-231 cells.** Asynchronous and serum starved MDA-MB-231 cells were plated in full growth medium on NHS-fluorescein labelled (A) 1mg/ml collagen I and (B) 1mg/ml Matrigel dishes for 24 hours in the presence of 20 $\mu$ M E64d. Cells were fixed and stained for actin (red) and nuclei (blue). Samples were imaged with a Nikon A1 confocal microscope, collagen I and Matrigel uptake index was calculated with Image J. Bar=20 $\mu$ m. N=3 independent experiments. Mean  $\pm$  SEM, Mann-Whitney test (the big dots represent the mean of individual experiments). \*\*p<0.01, \*\*\*\*p<0.0001 (Montserrat Llanses Martinez, Rainero lab).

In addition to MDA-MB-231 cells, we compared the internalization of collagen I and Matrigel between synchronized and asynchronous PyMT#1 cells as well. The cells were synchronized in G1 phase by serum starvation. As illustrated in figure 4.5A, a 24-hour serum starvation led to an efficient synchronization (around 80% cells in the G1) while PyMT#1 cells remained arrested in the G1 phase for about 8 hours after release from serum starvation, with less than

50% cells in the G1 phase at 12 hours. Here serum-starved and control non-starved cells were seeded on fluorescently labelled matrices in full growth medium for a 12-hour incubation. Consistent with our findings in MDA-MB-231 cells, increased number of Matrigel containing vesicles were visualized inside synchronized cells compared to the asynchronous cells (Figure 4.5C), The quantification demonstrated that Matrigel uptake was upregulated in G1 phase cells. However, there was no difference in collagen I internalization between the synchronized and asynchronous PyMT#1 cells (Figure 4.5B). Collectively, our results indicate that Matrigel, but not collagen I, uptake is promoted in G1 phase invasive breast cancer cells.

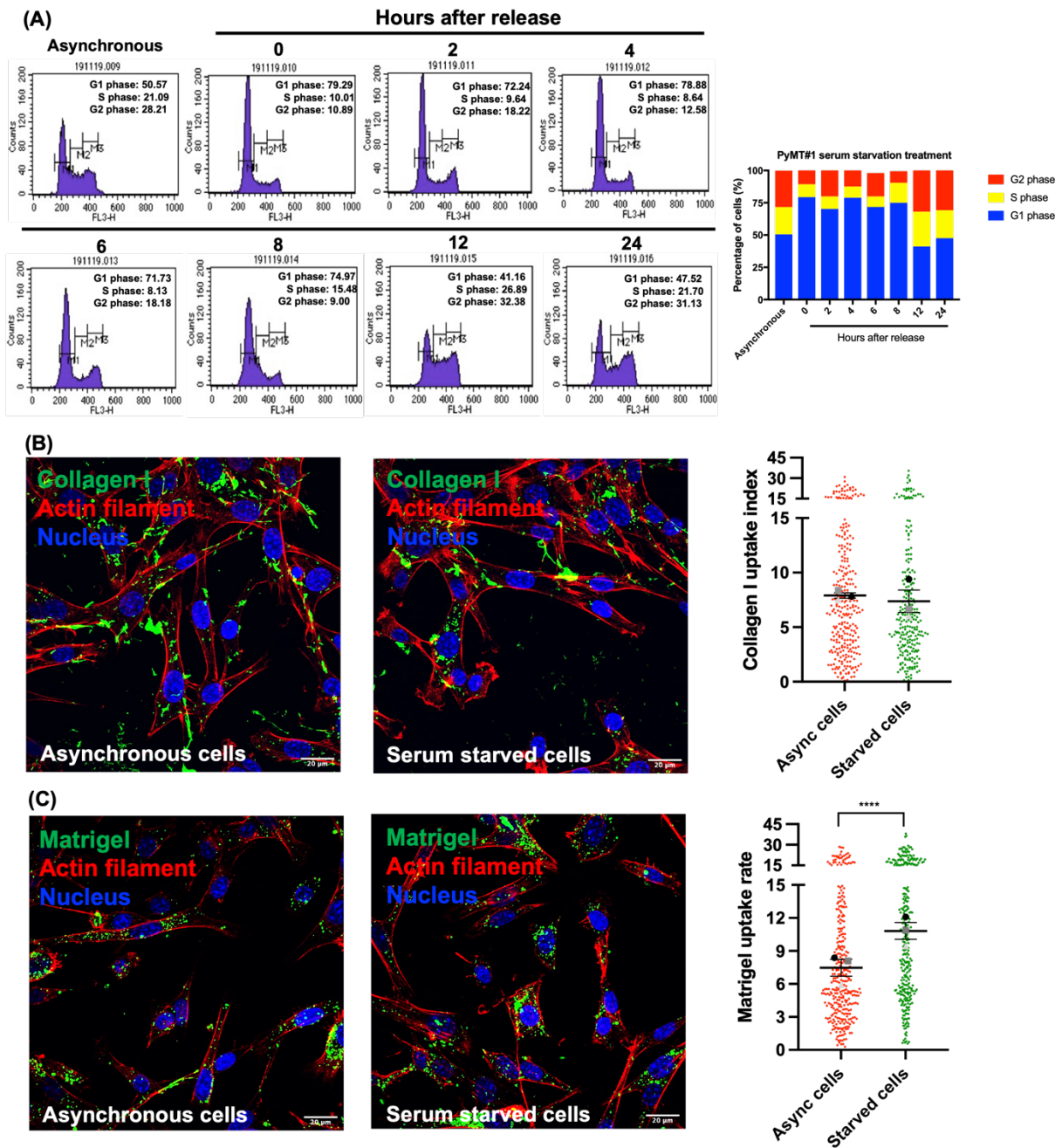


**Figure 4.5. Matrigel, but not collagen I, uptake is upregulated in serum starved PyMT#1 cells.** (A) PyMT#1 cells were synchronized at the G1 phase by serum starvation for 24 hours and released in full growth medium. Cells were harvested at the indicated time points, fixed, and stained with Propidium Iodide (PI) before fluorescence-activated cell-sorting analysis (FACS) to determine DNA content. (B-C) Asynchronous and serum starved PyMT#1 cells were plated on NHS-fluorescein labelled (B) 0.5mg/ml collagen I and (C) 1mg/ml Matrigel dishes for 12 hours in complete medium with 20 $\mu$ M E64d. Cells were fixed and stained for actin (red) and nuclei (blue). Samples were imaged with a Nikon A1 confocal microscope, collagen I and Matrigel uptake index was calculated with Image J. Bar=20 $\mu$ m. N=3 independent experiments. Mean  $\pm$  SEM, Mann-Whitney test (the big dots represent the mean of individual experiments). \*\*\*\*p<0.0001.

Serum starvation is widely used for synchronizing cells in the G1 phase of the cell cycle, but it often reduces cell survival and increases the DNA fragmentation (Baghdadchi, 2013). Thus, we then synchronized MDA-MB-231 cells in G1 by treating them with a CDK4/6 inhibitor, palbociclib (Pb). As expected, after Pb treatment around 85% of the cells were arrested in G1. At the same time, the cells remained in G1 for at least 8 hours after release from inhibition (Figure 4.6A). Pb treated and asynchronous MDA-MB-231 cells were seeded on fluorescently labelled collagen I and Matrigel for a 6-hour incubation. As demonstrated in figure 4.6B, there was no significant difference in collagen I endocytosis between the synchronized and asynchronous cells. By contrast, more Matrigel containing vesicles were visualized in the G1 population compared to what we observed in the total population (Figure 4.6C), which was consistent with the findings we obtained with serum starvation (Figure 4.4B). As apparent from the quantification, the internalization of Matrigel was significantly upregulated in G1 phase MDA-MB-231 cells.

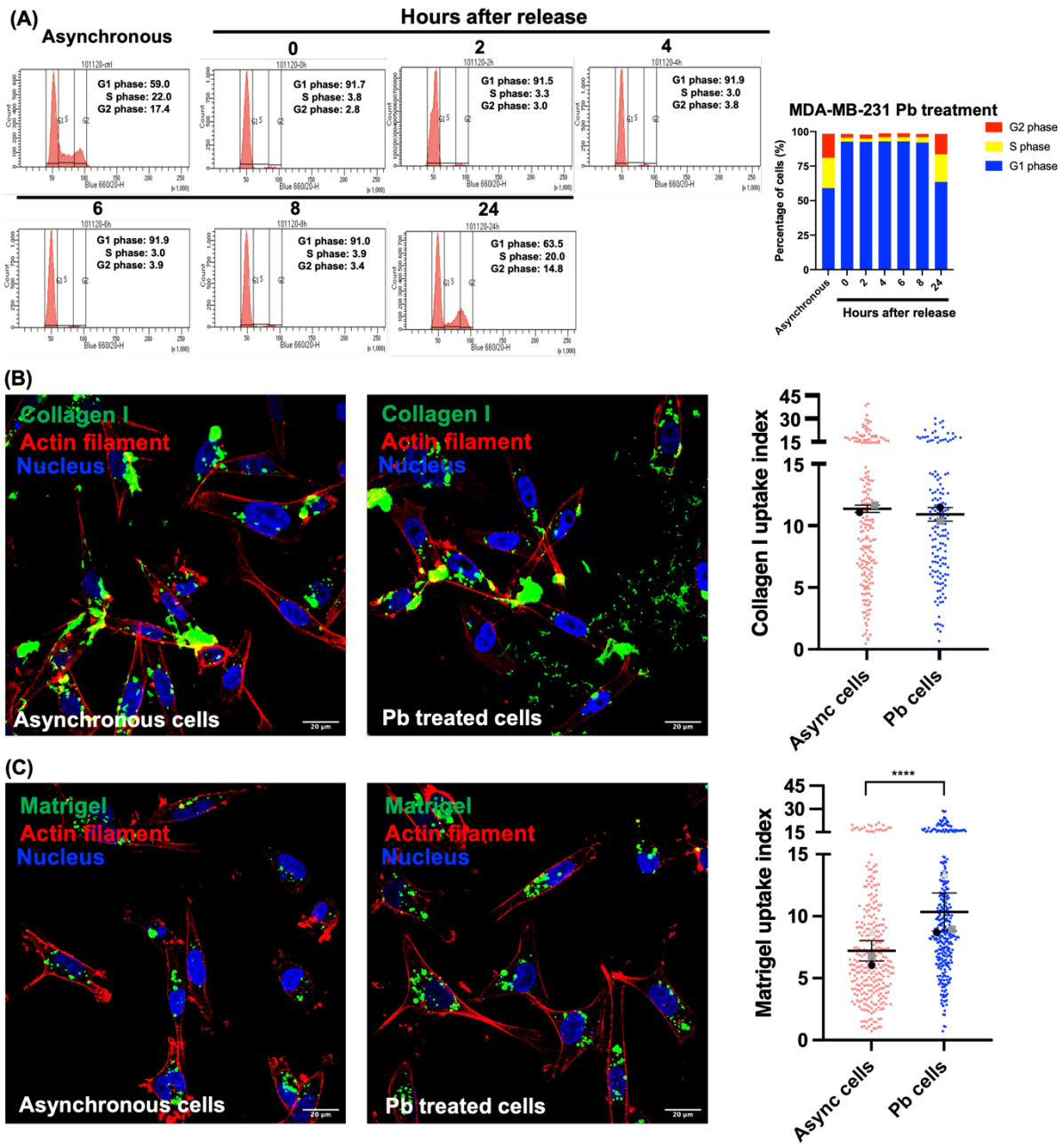


**Figure 4.6. Matrigel, but not collagen I, uptake is increased in Palbociclib (Pb) treated MDA-MB-231 cells.** (A) MDA-MB-231 cells were synchronized in the G1 phase by Pb treatment for 24 hours. Cells were harvested at the indicated time points after release from inhibition, fixed, and stained with Propidium Iodide (PI) before fluorescence-activated cell-sorting analysis (FACS) to determine DNA content. (B-C) Asynchronous and Pb treated MDA-MB-231 cells were plated on NHS-fluorescein labelled (B) 0.5mg/ml collagen I and (C) 1mg/ml Matrigel dishes for 6 hours in the presence of 20 $\mu$ M E64d. Cells were fixed and stained for actin (red) and nuclei (blue). Samples were imaged with a Nikon A1 confocal microscope, collagen I and Matrigel uptake index was calculated with Image J. Bar=20 $\mu$ m. For collagen internalization n=2 independent experiments. For Matrigel uptake n=3 independent experiments. Mean  $\pm$  SEM, Mann-Whitney test (the big dots represent the mean of individual experiments). \*\*\*\*p<0.0001.

Next, we synchronized MDA-MB-231 cells in G1 phase by DTB. The flow cytometry analysis illustrated that DTB resulted in an effective synchronization at the G1/S phase boundary while cells moved homogeneously through the cell cycle after removal of thymidine. More precisely, MDA-MB-231 cells went through the S phase at 2-4 hours and reached the G2 phase at 6-8 hours. Approximately 75% of the cells were in the G1 phase after 24 hours of post-release (Figure 4.7A). Collagen I and Matrigel internalization was compared between synchronized and asynchronous MDA-MB-231 cells by seeding the cells on labelled matrices for 24 hours after DTB release. Here no significant difference in the internalization of collagen I was observed between synchronized and asynchronous population of MDA-MB-231 cells (Figure 4.7B). In agreement with our findings upon serum starvation and CDK4/6 inhibitor Pb treatment (Figure 4.4B and 4.6C), there were more Matrigel positive vesicles in synchronized MDA-MB-231 cells compared to the asynchronous cells and the statistical analysis illustrated that the internalization of Matrigel was significantly increased in G1 phase MDA-MB-231 cells (Figure 4.7C).

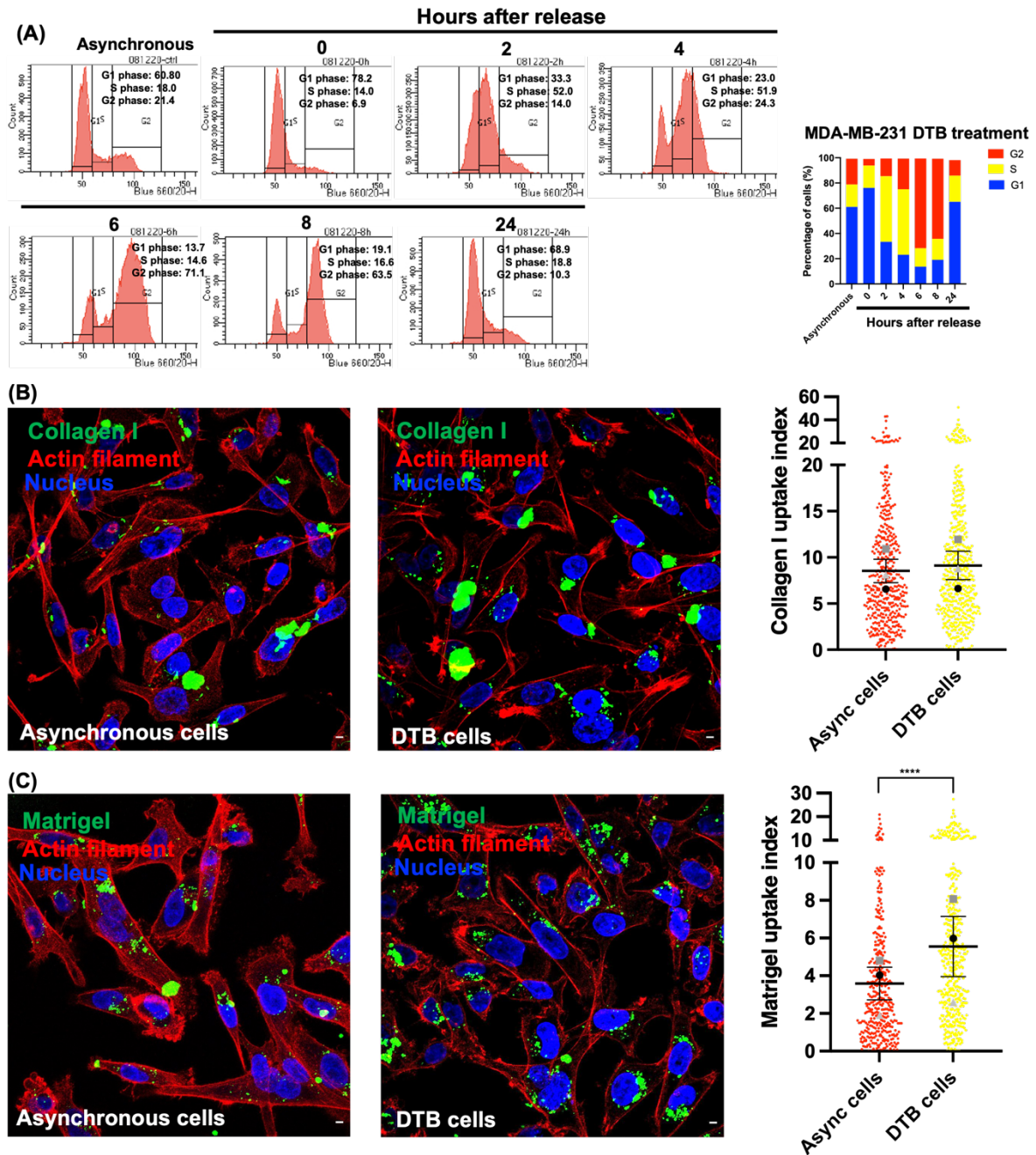


**Figure 4.7. Matrigel, but not collagen I, uptake is upregulated in DTB synchronized MDA-MB-231 cells.** (A) MDA-MB-231 cells were synchronized at the G1/S phase boarder by double thymidine block (DTB). Cells were harvested at the indicated time points after removal of thymidine, fixed, and stained with Propidium Iodide (PI) before fluorescence-activated cell-sorting analysis (FACS) to determine DNA content. (B-C) Asynchronous and synchronized MDA-MB-231 cells were plated on NHS-fluorescein labelled (B) 1mg/ml collagen I and (C) 1mg/ml Matrigel dishes for 24 hours in the presence of 20 $\mu$ M E64d. Cells were fixed and stained for actin (red) and nuclei (blue). Samples were imaged with a Nikon A1 confocal microscope, collagen I and Matrigel uptake index was calculated with Image J. Bar=20 $\mu$ m. N=3 independent experiments. Mean  $\pm$  SEM, Mann-Whitney test (the big dots represent the mean of individual experiments). \*\*\*\* $p$ <0.0001 (Montserrat Llanses Martinez, Rainero lab).

In order to visualize the cells in the different phases of cell cycle without interfering with cell cycle progression, we compared collagen and Matrigel internalization among G1, S and G2/M phase in FUCCI-MDA-MB-231 cells. The cells were seeded on fluorescently labelled matrices for an 8-hour incubation. As demonstrated in figure 4.8, FUCCI-MDA-MB-231 cells in the early G1, G1, S and G2/M phase appeared blue, red, yellow and green, respectively. We found that MDA-MB-231 cells were mostly in the G1 phase on both matrices. The cell cycle distribution was around 63% in the G1 phase on collagen I, and about 58% in the G1 phase on Matrigel. Additionally, we found that the cells in the S/G2/M phases were able to uptake more collagen I compared to those in the G1 phase of cell cycle (Figure 4.8A), which was consistent with our results obtained with serum starvation (Figure 4.4A). By contrast, more Matrigel containing vesicles were observed inside the cells in G1 compared to the cells in the S/G2/M and the statistical analysis showed that the internalization of Matrigel was significantly increased in G1 (Figure 4.8B). Furthermore, there was no difference in neither collagen I nor Matrigel internalization between the population in S phase and those in G2/M phase (Figure 4.8). Taken together, our findings demonstrate that Matrigel, but not collagen I, internalization is upregulated in G1 phase invasive breast cancer cells.

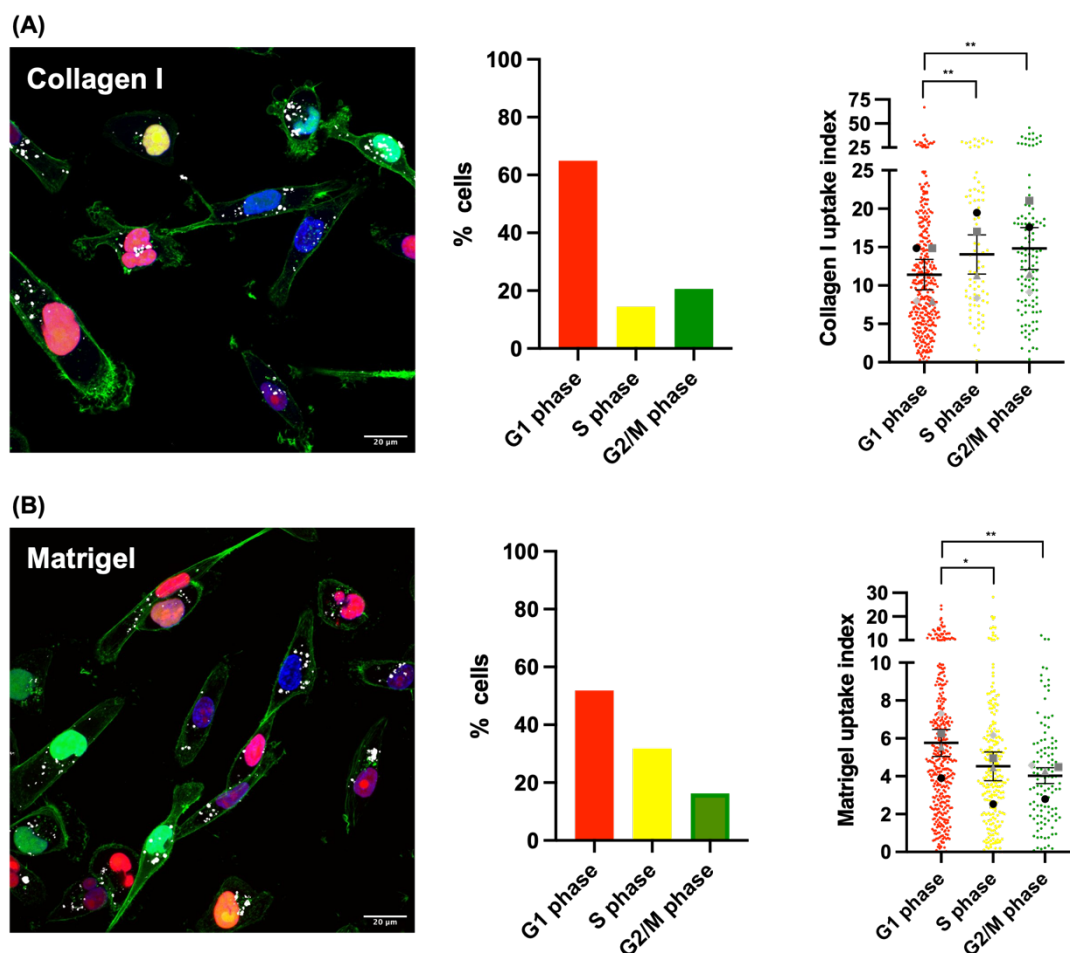


**Figure 4.8. Matrigel uptake is increased in the G1 phase Fucci-MDA-MB-231 cells.** Fucci-MDA-MB-231 cells were seeded on Alexa Fluor 647-labelled (A) 0.5mg/ml collagen I and (B) 1mg/ml Matrigel dishes for 8 hours. Cells were fixed and stained for actin (green). Fucci-MDA-MB-231 cells in the early G1, G1, S and G2/M phase appeared blue, red, yellow and green, respectively. Samples were imaged with a Nikon A1 confocal microscope, collagen I and Matrigel uptake index was calculated with Image J. Bar=20 $\mu$ m. N=4 independent experiments. Mean  $\pm$  SEM, Mann-Whitney test. \* $p$ <0.05, \*\* $p$ <0.01.

#### 4.2.3 Matrigel uptake is not affected by the cell cycle in normal mammary epithelial cells

We have showed that invasive breast cancer cells can uptake more Matrigel, but not collagen I, in the G1 phase of the cell cycle. To test whether the internalization of Matrigel in normal mammary epithelial cells is also upregulated in G1, we compared the endocytosis of Matrigel between NMuMG cells synchronized in G1 phase and the asynchronous population. Here we synchronized NMuMG cells using serum starvation. As illustrated in Figure 4.9A, 24 hours of serum starvation was sufficient to arrest NMuMG cells in G1 (more than 80%), and cells re-

entered the cell cycle around 12 hours after release from starvation. Next, serum starved cells and control non-starved cells were plated on fluorescently labelled Matrigel for 12 hours in complete medium. A similar number of Matrigel positive vesicles were visualized inside the cells between the serum starved and non-starved cells, and the quantification showed that there was no significant difference in Matrigel uptake between the synchronized and asynchronous populations (Figure 4.9B). Our findings suggest that Matrigel internalization is not cell cycle dependent in normal mammary epithelial cells.

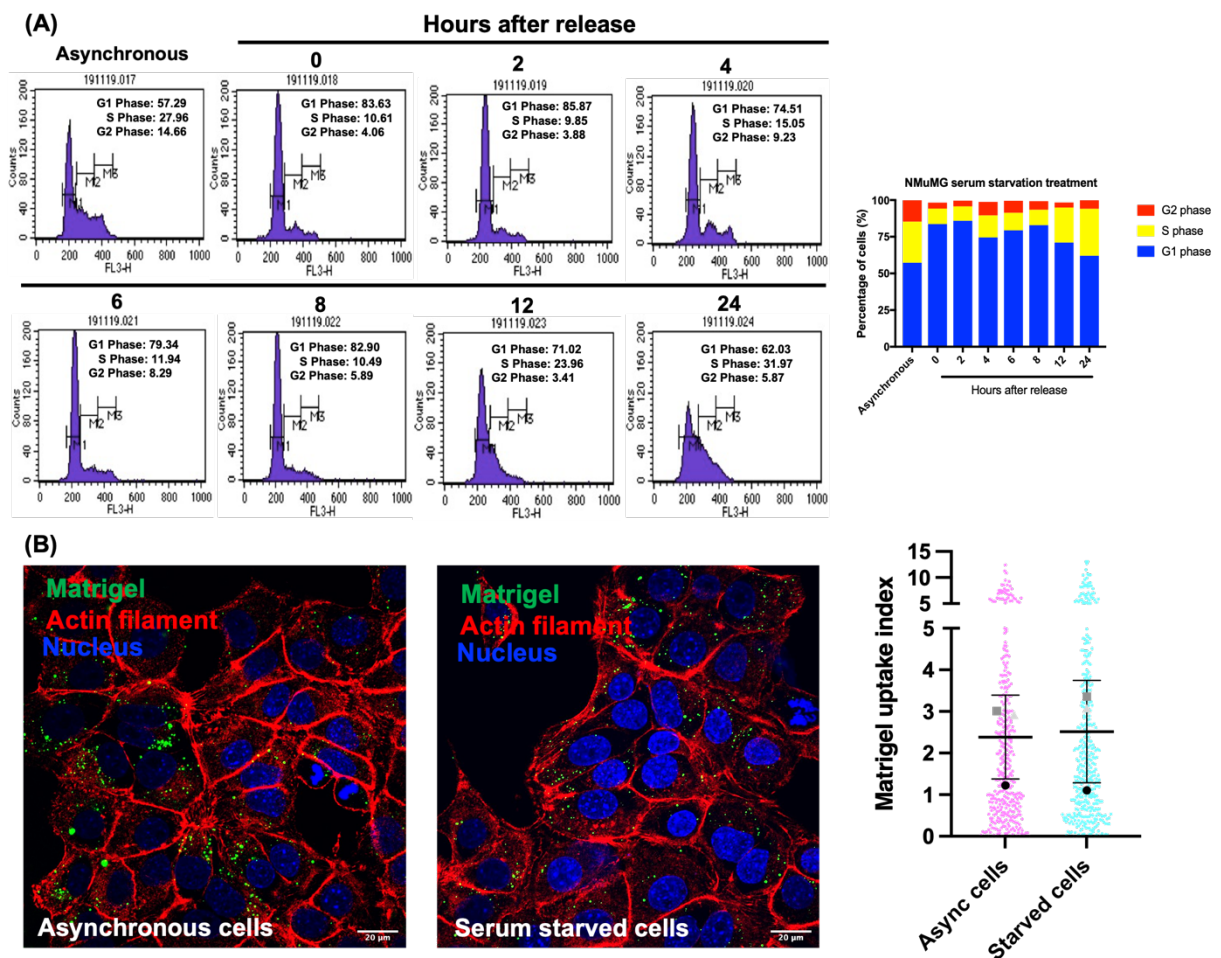


**Figure 4.9. Matrigel internalization is not cell cycle dependent in NMuMG cells.** **(A)** NMuMG cells were synchronized in the G1 phase using serum starvation for 24 hours. Cells were harvested at the indicated time points after release from starvation. The percentage of cells in different stages of the cell cycle was quantified by flow cytometric analysis of DNA content in fixed cells stained with propidium iodide (PI). **(B)** asynchronous and serum starved NMuMG cells were plated on NHS-fluorescein 1mg/ml Matrigel dishes for 12 hours in the presence of 20 $\mu$ M E64d. Cells were fixed and stained for actin (red) and nuclei (blue). Samples were imaged with a Nikon A1 confocal microscope, Matrigel uptake index was calculated with Image J. Bar=20 $\mu$ m. N=3 independent experiments. Mean  $\pm$  SEM, Mann-Whitney test (the big dots represent the mean of individual experiments).

#### **4.2.4 Laminin, but not collagen IV, uptake is upregulated in G1 invasive breast cancer cells**

We have illustrated that Matrigel, but not collagen I, uptake is upregulated in invasive breast cancer cells in the G1 phase of cell cycle. In order to characterise which component uptake is increased, we compared the internalization of the two major Matrigel (and BM) components between synchronized and asynchronous MDA-MB-231 cells: laminin/entactin (referred to as laminin thereafter) and collagen IV. The serum-starved and the control non-starved cells were plated on fluorescently labelled laminin or Matrigel containing dye-quenched collagen IV (DQ-collagen IV) in the full growth medium for an 8-hour incubation. As demonstrated in figure 4.10A, in asynchronous cells only few laminin positive vesicles were visualized in some cells, while most of serum starved cells displayed laminin containing vesicles inside the cells. As apparent from the quantification, the internalization of laminin was enhanced in synchronized MDA-MB-231 cells compared to the asynchronous population. By contrast, only a small, albeit statistically significant, increase in DQ-collagen IV internalization was observed in serum starved MDA-MB-231 cells compared to the control non-starved cells. However, the upregulated DQ-collagen IV internalization in synchronized MDA-MB-231 cells was not as significant as the difference we observed in the internalization of Matrigel and laminin (Figure 4.10B).

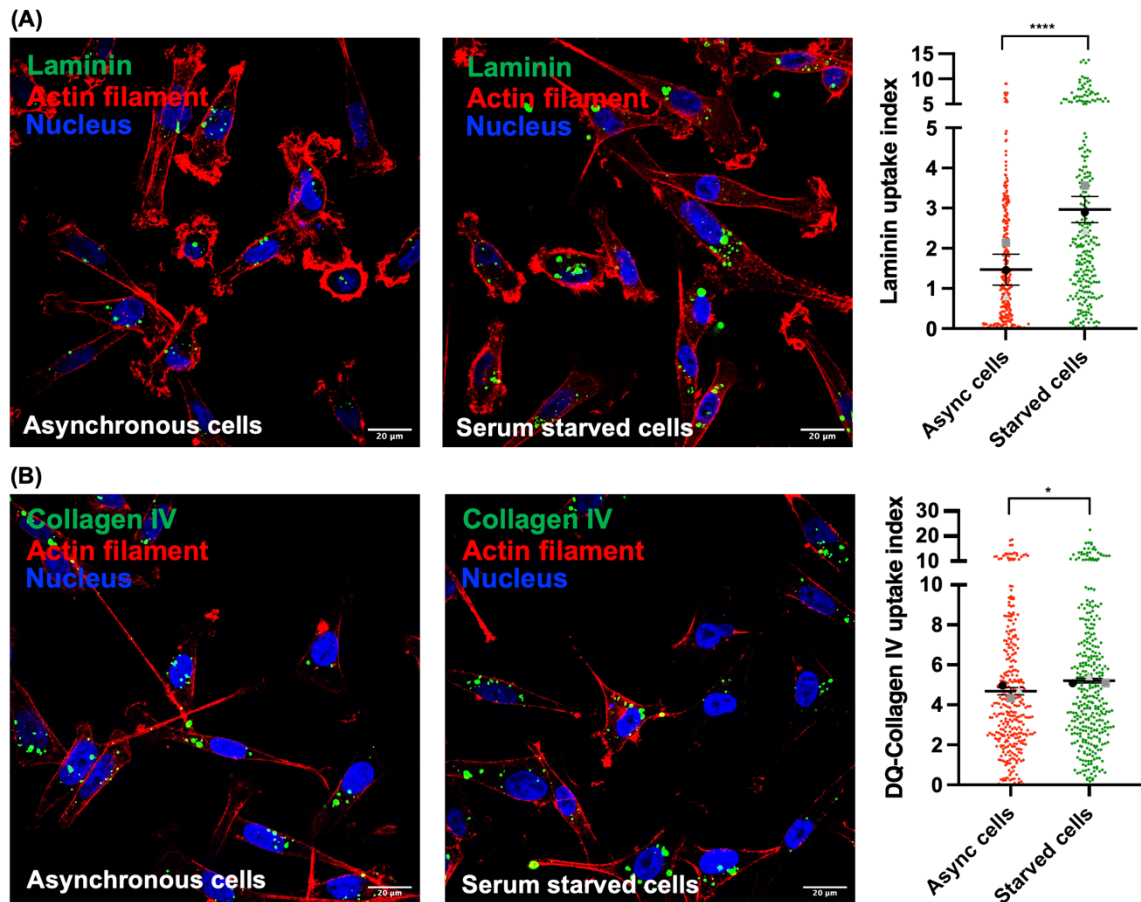


**Figure 4.10. Laminin and collagen IV internalization is enhanced in serum starved MDA-MB-231 cells.** (A-B) MDA-MB-231 cells were serum starved for 24 hours. Next, asynchronous and serum starved MDA-MB-231 cells were plated on NHS-fluorescein labelled (A) 2mg/ml laminin and (B) the mixture of 25 $\mu$ g/mL of DQ-collagen IV and 1mg/ml Matrigel dishes for 8 hours in the full growth medium in the presence of 20 $\mu$ M E64d. Cells were fixed and stained for actin (red) and nuclei (blue). Samples were imaged with a Nikon A1 confocal microscope. Laminin and DQ-collagen IV uptake index was calculated with Image J. Bar=20 $\mu$ m. N=3 independent experiments. Mean  $\pm$  SEM, Mann-Whitney test (the big dots represent the mean of individual experiments). \* $p$ <0.05, \*\*\*\* $p$ <0.0001.

Similar findings were observed in DTB synchronized MDA-MB-231 cells as well. In figure 4.11, more and bigger laminin positive vesicles were visualized in DTB synchronized cells compared to what we observed in asynchronous cells. Image quantification demonstrated that synchronized MDA-MB-231 cells were able to uptake more laminin (Figure 4.11). Altogether, our findings suggest that laminin, but not collagen IV, internalization is upregulated in G1 phase MDA-MB-231 cells.

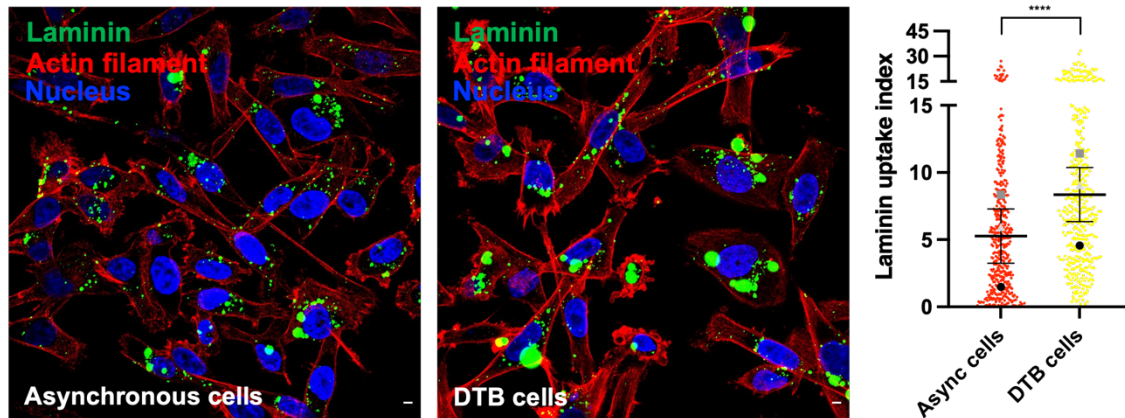


**Figure 4.11. The internalization of laminin is promoted in DTB synchronized MDA-MB-231 cells.** MDA-MB-231 cells were synchronized by DTB. Next, asynchronous and DTB synchronized MDA-MB-231 cells were plated on NHS-fluorescein labelled 2mg/ml laminin dishes for 24 hours in the presence of 20 $\mu$ M E64d. Cells were fixed and stained for actin (red) and nuclei (blue). Samples were imaged with a Nikon A1 confocal microscopy, laminin uptake index was calculated with Image J. Bar=20 $\mu$ m. N=3 independent experiments. Mean  $\pm$  SEM, Mann-Whitney test (the big dots represent the mean of individual experiments). \*\*\*\*p<0.0001 (Montserrat Llanses Martinez, Rainero lab).

#### 4.2.5 MMP inhibition might affect cell cycle-dependent ECM uptake

Both extracellular and intracellular degrading pathways are involved in the turnover of ECM, using either MMPs or lysosomal degradation, respectively (Rainero, 2016). MT1-MMP is a key MMP in regulating ECM proteolytic degradation (Jabłońska-Trypuć et al., 2016). A recent study demonstrated that the expression of MT1-MMP is upregulated in the G1 phase in MDA-MB-231 cells (Bayarmagnai et al., 2019b). Extracellular and intracellular ECM degradation pathways are considered to work collaboratively rather than mutually in regulating the turnover of ECM. Many ECM proteins form supramolecular complexes. Thus, extracellular degradation can partially breakdown large multimers or crosslinked molecules, promoting ECM internalization (Shi and Sottile, 2008b). In order to investigate whether increased Matrigel internalization is mediated by MMP activity in G1 phase, we treated synchronized and asynchronous MDA-MB-231 cells with a broad spectrum MMP inhibitor (GM6001).

We firstly compared the internalization of Matrigel between synchronized MDA-MB-231 cells using serum starvation and non-starved cells. The synchronized and asynchronous cells were plated on fluorescently labelled Matrigel with and without GM6001 for an 8-hour incubation. In agreement with our previous findings, a greater number of Matrigel containing vesicles were visualized in synchronized cells than what we observed in asynchronous cells in

both DMSO control condition and in the presence of GM6001. The quantification suggested that the uptake of Matrigel was significantly increased in serum starved cells compared to control non-starved cells (Figure 4.12). Interestingly, MMP inhibition did not affect Matrigel internalization in either synchronized or asynchronous cells (Figure 4.12).

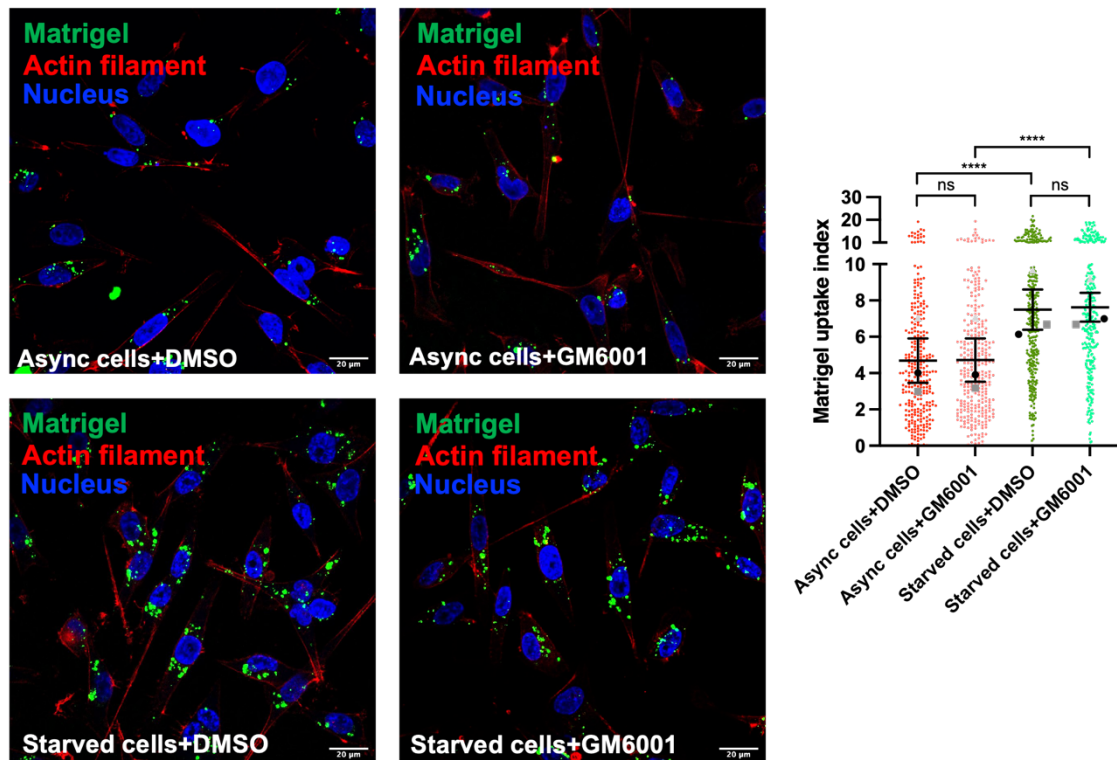


**Figure 4.12. MMP inhibition does not affect increased Matrigel uptake in serum starved MDA-MB-231 cells.** Asynchronous and serum starved MDA-MB-231 cells were plated on NHS-fluorescein labelled 1mg/ml Matrigel dishes for 8 hours in full growth medium in the presence of DMSO (control) or 10 $\mu$ M GM6001. At the same time, 20 $\mu$ M E64d was added in all conditions. Cells were fixed and stained for actin (red) and nuclei (blue). Samples were imaged with a Nikon A1 confocal microscope. Matrigel uptake index was calculated with Image J. Bar=20 $\mu$ m. N=3 independent experiments. Mean  $\pm$  SEM, Kruskal-wallis with multiple comparisons (the big dots represent the mean of individual experiments), \*\*\*\*p<0.0001.

We then examined the effect of MMP inhibition on Matrigel internalization in G1 by synchronizing cells with the CDK4/6 inhibitor Pb. Matrigel uptake was significantly higher in synchronized cells than in the total population of MDA-MB-231 cells in the DMSO control group (Figure 4.13), which was consistent with our previous data (Figure 4.6C). Additionally, GM6001 treatment did not affect Matrigel internalization in asynchronous cells (Figure 4.13). However, in synchronized MDA-MB-231 cells, MMP inhibition led to a significant reduction in Matrigel internalization compared to the DMSO control (Figure 4.13). Therefore, our results

suggest when MDA-MB-231 cells are synchronised in the G1 phase using a CDK4/6 inhibitor, but not with serum starvation, MMP activity contributes to upregulated Matrigel endocytosis.

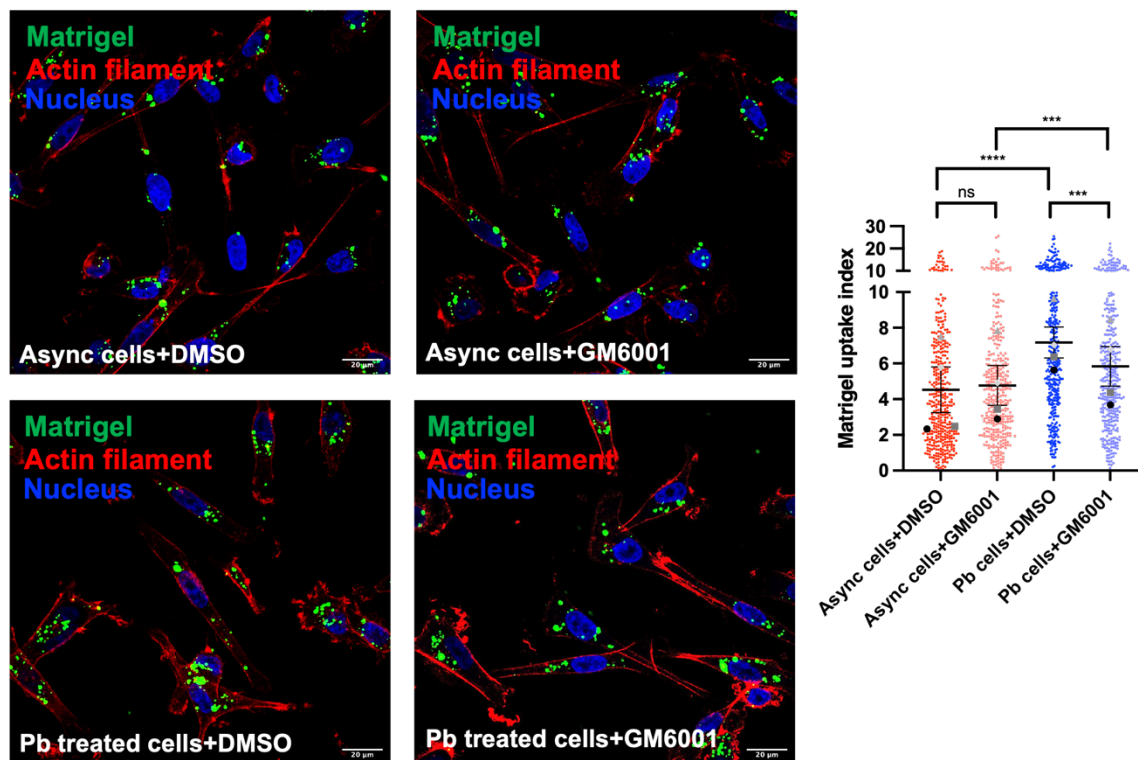


**Figure 4.13. MMP activity affects upregulated Matrigel internalization in Pb treated MDA-MB-231 cells.** Asynchronous and Pb treated MDA-MB-231 cells were seeded on NHS-fluorescein labelled 1mg/ml Matrigel dishes for 8 hours in the presence of DMSO (control) or 10 $\mu$ M GM6001. At the same time, 20 $\mu$ M E64d was added in all conditions. Cells were fixed and stained for actin (red) and nuclei (blue). Samples were imaged with a Nikon A1 confocal microscope. Matrigel uptake index was calculated with Image J. Bar=20 $\mu$ m. N=3 independent experiments. Mean  $\pm$  SEM, Kruskal-wallis with multiple comparisons (the big dots represent the mean of individual experiments), \*\*\*p<0.001, \*\*\*\*p<0.0001.

#### 4.2.6 Macropinocytosis is slightly affected by the cell cycle in invasive breast cancer cells

Macropinocytosis is an actin-dependent endocytic pathway by which extracellular fluids are engulfed via plasma membrane invagination. Unlike receptor-mediated endocytosis that can uptake specific ECM components via binding to a variety of receptors, macropinocytosis is a non-specific endocytic pathway which could uptake both integrins (Gu et al., 2011) and ECM components (Yhee et al., 2017). In pancreatic cancer cells, macropinocytosis is involved in nutrients uptake, contributing to metabolic needs and promoting tumor growth under nutrient starvation (Commisso et al., 2014). Here we measured macropinocytosis in G1 phase

by quantitating the endocytosis of fluorescently-labelled dextran, a standard marker of fluid-phase endocytosis (Commisso et al., 2013). Briefly, MDA-MB-231 cells were synchronized at the G1/S phase boundary by DTB, plated on 0.1mg/ml collagen I for 6 hours to fully adhere. 0.25mg/ml rhodamine-dextran was then added for a 1-hour incubation. Cells were fixed and stained for  $\beta 1$  integrin. As demonstrated in figure 4.14, a similar number of dextran containing vesicles were visualized inside both synchronized and asynchronous cells, and the quantification showed that there was only a small, albeit statistically significant, increase in dextran internalization in DTB synchronized MDA-MB-231 cells compared to the asynchronous cells. Therefore, our findings illustrate that, although macropinocytosis might be slightly affected by the cell cycle in breast cancer cells, the uptake of ECM components is specifically upregulated.

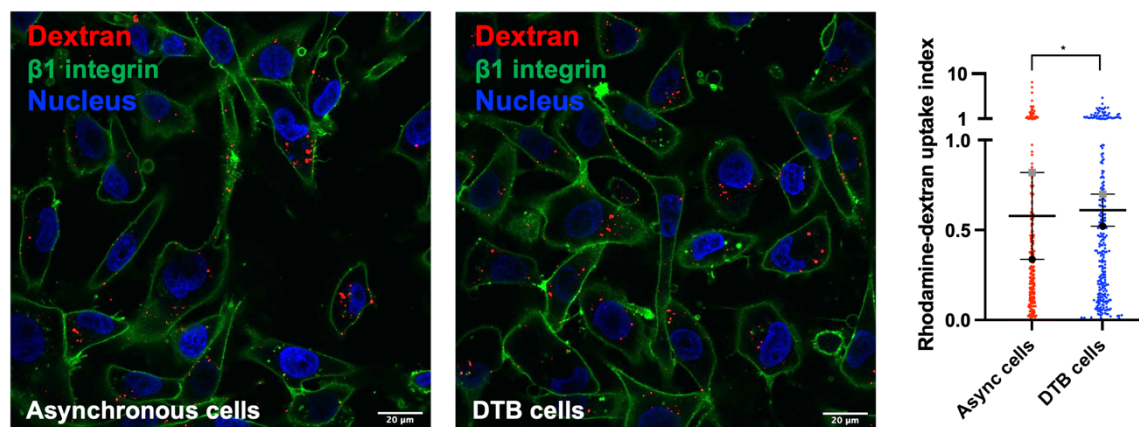


**Figure 4.14. Macropinocytosis is slightly upregulated in DTB synchronized MDA-MB-231 cells.** MDA-MB-231 cells were synchronized by DTB. Asynchronous and synchronized MDA-MB-231 cells were firstly plated on 0.1mg/ml of collagen I coated dishes for 6 hours to fully adhere. 0.25mg/ml Rhodamine-dextran (red) was then added for one hour uptake. Cells were fixed and stained for  $\beta 1$  (green) and nuclei (blue). Samples were imaged with a Nikon A1 confocal microscope; dextran uptake index was calculated with Image J. Bar=20 $\mu$ m. N=2 independent experiments. Mean  $\pm$  SEM, Mann-Whitney test (the big dots represent the mean of individual experiments). \* $p < 0.05$  (Montserrat Llanses Martinez, Rainero lab).

#### 4.2.7 $\beta 1$ Integrin traffic is upregulated in the G1 phase in invasive breast cancer cells

We have demonstrated that  $\beta 1$  integrin is required for ECM endocytosis in breast cancer cells. We then wanted to characterize whether  $\beta 1$  integrin traffic is also upregulated in G1 phase. As illustrated in figure 4.15, MDA-MB-231 cells, which were serum starved for 24 hours, and asynchronous cells were plated on 1mg/ml Matrigel for a 6-hour incubation, fixed and stained for  $\beta 1$  integrin. A significant increase in  $\beta 1$  integrin-positive vesicles was visualized in the

synchronized cells compared to asynchronous cells. The quantification of  $\beta 1$  integrin internal pool illustrated that  $\beta 1$  integrin internalization was significantly upregulated (Figure 4.15), suggesting a role of  $\beta 1$  integrin in regulating cell-cycle dependent Matrigel endocytosis.

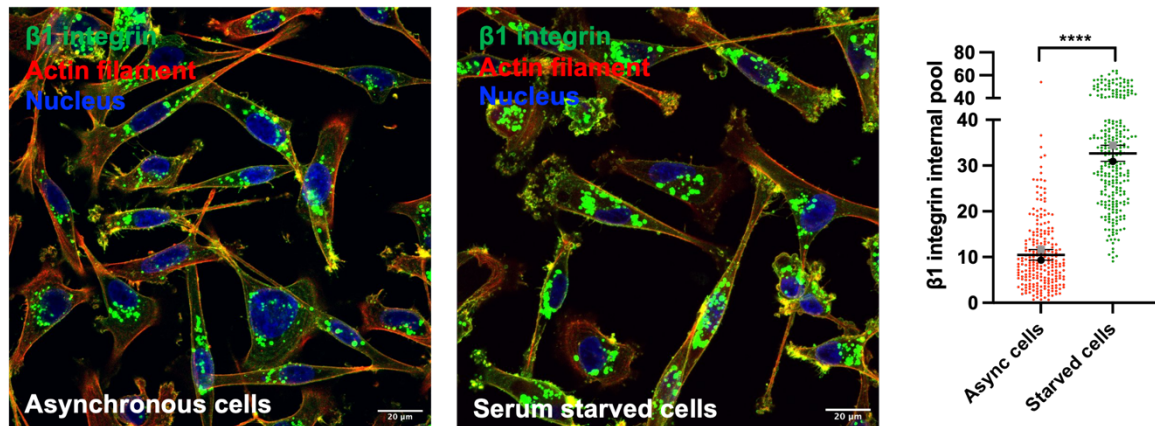


**Figure 4.15.  $\beta 1$  integrin endocytosis is upregulated in serum starved MDA-MB-231 cells.** Asynchronous and serum starved MDA-MB-231 cells were plated in full growth medium on 1mg/ml Matrigel dishes for 6 hours. Cells were fixed and stained for  $\beta 1$  integrin (green), actin (red) and nuclei (blue). Samples were imaged with a Nikon A1 confocal microscope,  $\beta 1$  integrin uptake was calculated with Image J. Bar=20 $\mu\text{m}$ . N=2 independent experiments. Mean  $\pm$  SEM, Mann-Whitney test (the big dots represent the mean of individual experiments). \*\*\*\* $p < 0.0001$ .

Next, we synchronized cells by treating them with the CDK4/6 inhibitor Pb. Synchronized and asynchronous MDA-MB-231 cells were seeded on Matrigel for a 6-hour incubation, fixed and stained for  $\beta 1$  integrin. Consistent with our data obtained with serum starvation, the presence of Pb led to more  $\beta 1$  integrin vesicles inside the cells (Figure 4.16). However, the increased  $\beta 1$  integrin internalization in Pb treated MDA-MB-231 cells was not as significant as the increase we observed in MDA-MB-231 cells synchronized by serum starvation (Figure 4.15). Altogether, our results suggest that  $\beta 1$  integrin might be required for the upregulated Matrigel uptake in G1 phase in MDA-MB-231 cells.

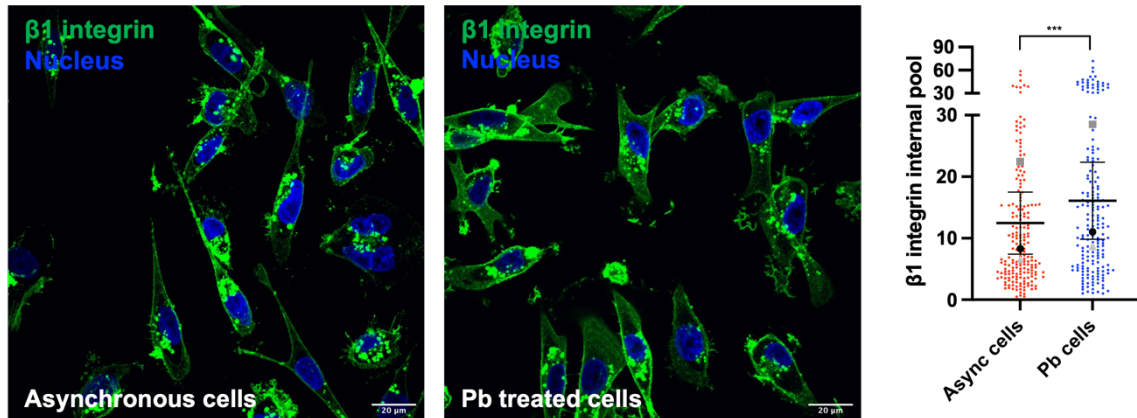


**Figure 4.16.  $\beta 1$  integrin endocytosis is upregulated in Pb treated MDA-MB-231 cells.** Asynchronous and Pb treated MDA-MB-231 cells were plated in full growth medium on 1mg/ml Matrigel dishes for 6 hours. Cells were fixed and stained for  $\beta 1$  integrin (green) and nuclei (blue). Samples were imaged with a Nikon A1 confocal microscope,  $\beta 1$  integrin uptake was calculated with Image J. Bar=20 $\mu$ m. N=3 independent experiments. Mean  $\pm$  SEM, Mann-Whitney test (the big dots represent the mean of individual experiments). \*\*\* $p < 0.001$ .

#### 4.2.8 Serum starvation regulates $\beta 1$ integrin trafficking

Both serum starved cells and Pb treated cells exhibited upregulated  $\beta 1$  integrin internalization compared to asynchronous cells. However, the upregulated  $\beta 1$  integrin internalization in Pb treated cells was not as significant as the increase we found in serum starved cells. Thus, we wanted to investigate whether serum starvation could regulate  $\beta 1$  integrin trafficking in a cell cycle-independent manner. Here MDA-MB-231 cells were incubated in serum free medium for 2 hours followed by seeding the cells on 0.1mg/ml collagen I in full growth medium for 6 hours. As demonstrated in figure 4.17, a significant upregulation of  $\beta 1$  integrin-positive vesicles was visualized in serum starved cells compared to non-starved cells. The quantification illustrated that  $\beta 1$  integrin endocytosis was promoted, indicating a role of serum starvation in regulating  $\beta 1$  integrin trafficking in a cell cycle-independent manner in MDA-MB-231 cells.

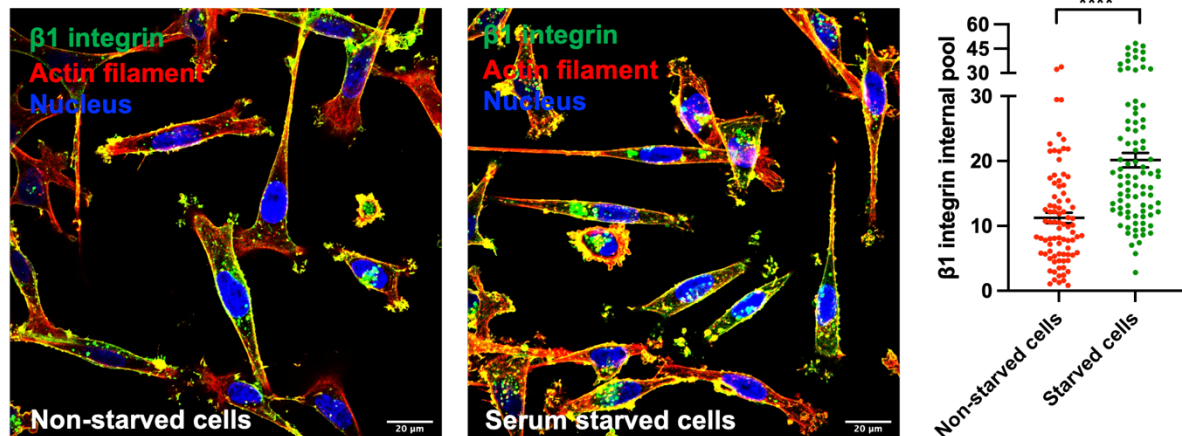


**Figure 4.17.  $\beta 1$  integrin endocytosis is increased in MDA-MB-231 cells after a 2-hour serum starvation.** MDA-MB-231 cells were firstly incubated in serum free medium for 2 hours. Afterward, non-starved and starved cells were plated in full growth medium on 0.1mg/ml collagen I dishes for 6 hours. Cells were fixed and stained for  $\beta 1$  integrin (green), actin (red) and nuclei (blue). Samples were imaged with a Nikon A1 confocal microscope,  $\beta 1$  integrin uptake was calculated with Image J. Bar=20 $\mu\text{m}$ . N=1. Mean  $\pm$  SEM, Mann-Whitney test. \*\*\*\*p<0.0001.

#### 4.2.9 Increased Matrigel uptake supports mTORC1 activity in G1 phase

The mTORC1 pathway is a pivotal regulator of the cell cycle. On the one hand, the inhibition of mTORC1 activity arrests mammalian cells in the G1 phase (Fingar et al., 2004). On the other hand, a recent study illustrated that CDK4/6 complexes promote mTORC1 activity in G1, which in turn contributes to cell growth (Romero-Pozuelo et al., 2020). Additionally, ligand-bound integrin endocytosis has been shown to promote mTORC1 activation in ovarian cancer cells (Rainero et al., 2015). Hence, we next investigated whether upregulated Matrigel uptake in G1 was linked to mTORC1 activity. Here we used phosphorylation of S6 (p-S6) as a marker of mTORC1 activation because its kinase (S6K) is itself directly phosphorylated by mTORC1 kinase activity (Ahmadiantehrani and London, 2017). As illustrated in figure 4.18, MDA-MB-231 cells, which were serum starved for 24 hours, and control non-starved cells were plated on either 1mg/ml or 0.1mg/ml Matrigel (as a thin coating to facilitate cell adhesion) for an 8-hour incubation, fixed and stained for p-S6. Previous work from the lab indicated that the ECM uptake is negligible in the presence of 0.1mg/ml Matrigel or collagen I (data not shown). Quantifying the intensity of p-S6, we found that serum starvation resulted in a significant increase in mTORC1 activity on high concentration Matrigel, while in the presence of 0.1mg/ml there was a much smaller induction of mTORC1 activity. Furthermore, there was

no significant difference in mTORC1 activity in the asynchronous cells on high Matrigel concentration compared to low concentration.

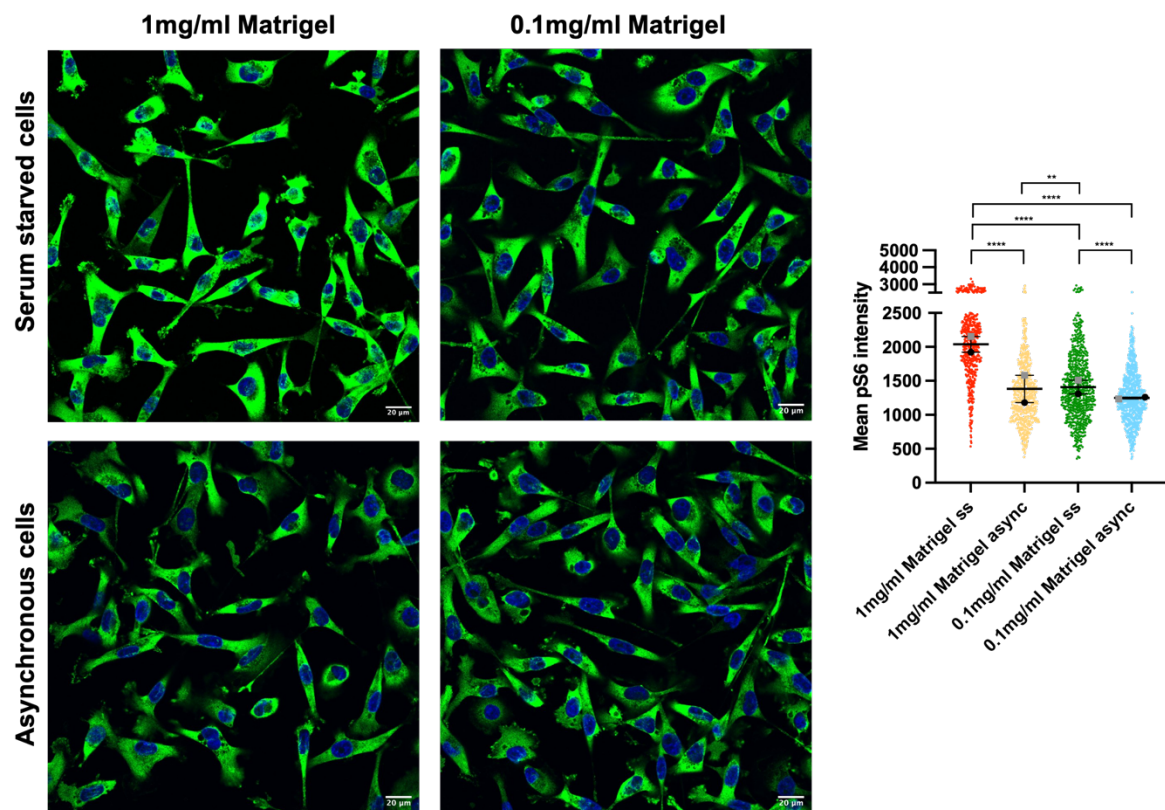


**Figure 4.18. mTORC1 activity is increased in serum starved MDA-MB-231 cells on Matrigel.** Asynchronous and serum starved MDA-MB-231 cells were seeded on 1mg/ml and 0.1mg/ml Matrigel dishes for an 8-hour incubation. Cells were then fixed and stained for p-S6 (green) and nuclei (blue). Samples were imaged with a Nikon A1 confocal microscope. The mean p-S6 intensity was calculated with Image J. Bar=20µm. N=2 independent experiments. Mean ± SEM, Kruskal-wallis with multiple comparisons (the big dots represent the mean of individual experiments), \*\*p<0.01, \*\*\*\*p<0.0001.

Next, we synchronized MDA-MB-231 cells in G1 by CDK4/6 inhibitor Pb treatment. The synchronized and asynchronous cells were plated on either 1mg/ml Matrigel or 0.1mg/ml collagen I (as a thin coating to facilitate cell adhesion), fixed and stained for p-S6. Consistent with our results obtained with serum starvation, Pb treatment led to higher mTORC1 activity on Matrigel. However, no difference in mTORC1 activity was observed between synchronized and asynchronous cells on 0.1mg/ml collagen I. Additionally, the activity of mTORC1 in the asynchronous cells on Matrigel was much higher compared to mTORC1 activity on 0.1mg/ml collagen I in both synchronized and asynchronous population of MDA-MB-231 cells (Figure 4.19). Collectively, our findings suggest that increased Matrigel uptake in the G1 phase might promote mTORC1 activity in MDA-MB-231 cells.

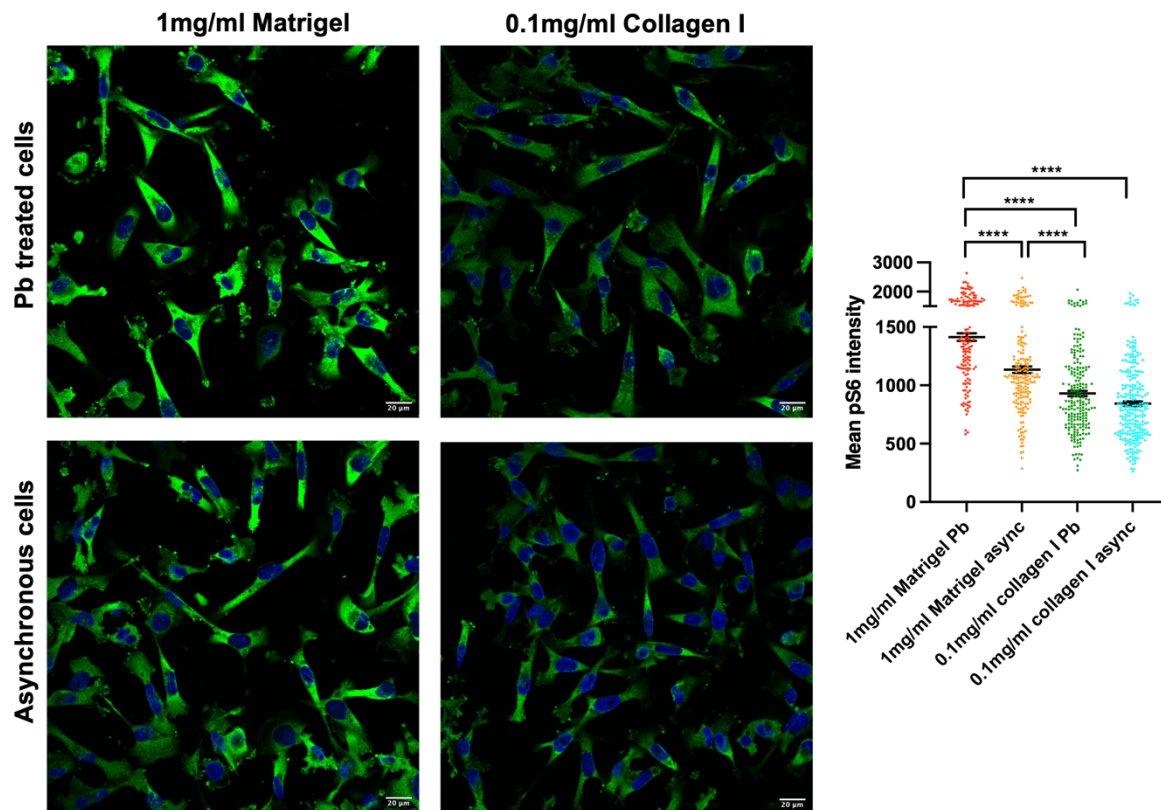


**Figure 4.19. mTORC1 activity is increased in Pb treated MDA-MB-231 cells on Matrigel.** Asynchronous and pb treated MDA-MB-231 cells were seeded on 1mg/ml Matrigel and 0.1mg/ml collagen I dishes for 6 hours incubation. Cells were then fixed and stained for p-S6 (green) and nuclei (blue). Samples were imaged with a Nikon A1 confocal microscope. The mean p-S6 intensity was calculated with Image J. Bar=20μm. N=1 experiment. Mean ± SEM, Kruskal-wallis with multiple comparisons, \*\*\*\*p<0.0001.

### 4.3 Discussion

Here we illustrated that Matrigel, but not collagen I, endocytosis is upregulated in the G1 phase in invasive breast cancer cells. Moreover, this cell cycle-dependent ECM uptake may be mediated by  $\beta$ 1 integrin. Furthermore, our findings suggest that increased Matrigel uptake might be required for mTORC1 activation in G1 (Figure 4.20).

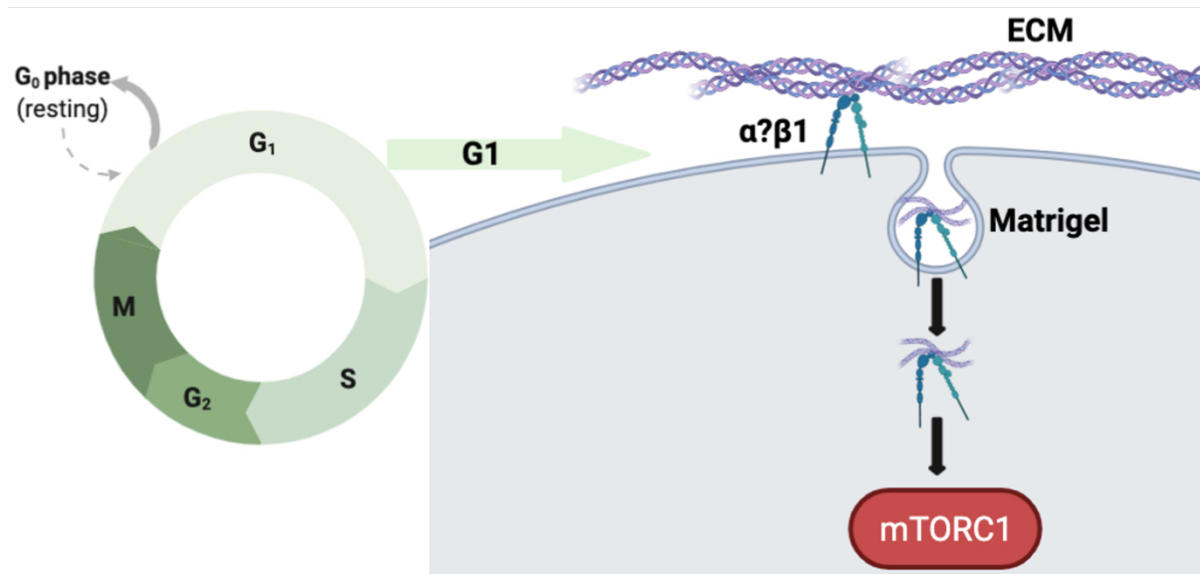


**Figure 4.20. Schematic to summarize the cell cycle-dependent ECM uptake.** Matrigel internalization is upregulated in G1 phase breast cancer cells.  $\beta 1$  integrin might be involved in this process. Increased Matrigel uptake may support mTORC1 activity in G1 phase. Image is 'Created with BioRender.com'.

Here we synchronized cells in G1 phase by serum starvation, double thymidine block (DTB) and Pb treatment. Although the endocytosis of collagen I is not altered in G1, our data from serum starvation suggest that collagen I internalization may be increased in G2. Similar results were also observed in FUCCI-MDA-MB-231 cells. CDK1/cyclin B complex is known to regulate the transition through G2 to M phase (Matthews et al., 2021). The inhibitor of CDK1, RO-3306, has been demonstrated to arrest cells in G2 phase (Vassilev, 2006). Thus, further studies can synchronize cancer cells in G2 phase by RO-3306 treatment, comparing the internalization of collagen I with asynchronous cells. In addition, our data illustrated that Matrigel endocytosis is upregulated in G1 phase in breast cancer cells. It has previously been illustrated that  $\alpha 6$  integrin knockdown arrests breast cancer cells in G1 phase by decreasing the expression of Cyclin E/CDK2 complexes (Wang et al., 2011). At the same time,  $\alpha 6 \beta 1$  integrin is known as a receptor for laminin (Humphries et al., 2006b). Therefore, one possible explanation is that breast cancer cells increase laminin internalization in G1 phase through a  $\alpha 6 \beta 1$  integrin-dependent pathway, promoting cell cycle progression. More work is needed to measure the expression and the endocytosis of laminin integrin receptors in the presence of Matrigel in G1 including  $\alpha 2$ ,  $\alpha 3$  and  $\alpha 6$  integrin subunits. Additionally, when cells proliferate, upregulated nucleotide synthesis in G1 phase is necessary for the replication of DNA and the production

of RNA, contributing to the synthesis of proteins in the following stages of the cell cycle (Lane and Fan, 2015). Nucleotide synthesis is known as an energy-intensive process that is regulated by different metabolic pathways and outside sources (Lopatkin and Yang, 2021). Recent data from the Rainero lab suggested that metabolites derived from ECM internalization and lysosomal degradation might feed into nucleotide synthesis pathways (Nazemi, data not shown). Hence, it is possible to speculate that increased Matrigel internalization in G1 phase may contribute to nucleotide synthesis in invasive breast cancer cells. Further studies are needed to verify this hypothesis.

MMPs are a proteolytic enzyme family that have a key role in ECM extracellular degradation. The expression of MT1-MMP in breast cancer cells is demonstrated to be upregulated in the G1 phase (Bayarmagnai et al., 2019b). Our findings revealed that MMP inhibition does not affect Matrigel endocytosis in MDA-MB-231 cells synchronized by serum starvation. However, when cells are synchronized by Pb treatment, MMP inhibition leads to a decreased Matrigel uptake in synchronized cells, suggesting the potential effects of different synchronization methods in regulating Matrigel uptake. Both serum starvation and Pb treatment can result in a reversible cell cycle arrest in G1 phase. However, serum starvation is also a common tool to investigate molecular mechanisms including protein degradation, cellular stress response and autophagy (Aghababazadeh and Kerachian, 2014). Additionally, serum starvation is a step in signal transduction studies as well as serum contains several important cytokines and growth factors that can confound signalling levels (Ahmadiankia, 2020). For example, it is illustrated that serum starvation facilitates the internalization of soluble laminin in mammary epithelial cells (Muranen et al., 2017). Therefore, we hypothesize that serum starvation might partially promote the endocytosis of Matrigel in invasive breast cancer cells.

Although our results indicated that serum starvation could regulate  $\beta 1$  integrin trafficking in a cell cycle-independent pathway, the internalization of  $\beta 1$  integrin is upregulated in G1 phase. There is increasing evidence suggesting that  $\beta 1$  integrin may be involved in the transition from G1 to S phase via two different pathways. Firstly, a recent study demonstrated that integrin-associated cell-ECM adhesion complexes are regulated in a cell cycle-dependent manner. They illustrated that the total focal adhesion area increased from G1 to S phase in HeLa cells. Moreover, the phosphorylation of formin-like 2 (FMNL2) in G1 and S phase was required for

the following redistribution of focal adhesions from periphery in G1 phase to both central area and cell periphery in S phase (Jones et al., 2018). Furthermore, it is suggested that the phosphorylated FMNL2 is a key regulator in  $\beta 1$  integrin internalization (Wang et al., 2015). In the previous chapter, we demonstrated that  $\beta 1$  integrin is required for the uptake of Matrigel. Thus, it is possible that the increased Matrigel internalization is induced by the endocytosis of Matrigel-bound  $\beta 1$  integrin focal adhesion in G1 phase. Secondly, the MEK-Erk is known as a main pathway mediated by  $\beta 1$  integrin (Moreno-Layseca and Streuli, 2014). A previous work illustrated that fibronectin activated  $\alpha 5 \beta 1$  integrin is required for the sustained Erk activity, contributing to the expression of cyclin D1 (Roovers et al., 1999). Therefore, we hypothesize that the interaction between Matrigel and  $\beta 1$  integrin can also promote cyclin D1 expression. At the same time, Matrigel is internalized in a  $\beta 1$  integrin-dependent pathway in this process. Further studies are needed to compare the expression of cyclin D1 between synchronized and asynchronous cells on Matrigel. Interestingly, we found a small increase in macropinocytosis in G1. Although it is shown that the stimulation of platelet-derived growth factor can induce the formation of circular dorsal ruffles, promoting the accumulation of  $\beta 1$  integrin from dorsal surface and the following internalization of  $\beta 1$  integrin by macropinocytosis (Gu et al., 2011). However, the upregulated macropinocytosis in synchronized cells is not as significant as the difference we observed in the internalization of  $\beta 1$  integrin in G1. Thus, our data suggest that upregulated ECM components internalization in G1 may be regulated by  $\beta 1$  integrin in breast cancer cells.

Our study revealed that the presence of Matrigel leads to a higher activity of mTORC1 in G1 phase. In parallel, another study showed that mTORC1 inhibition arrests MDA-MB-231 cells in G1 phase (Yellen et al., 2011). Thus, we hypothesis that the increased Matrigel uptake might contribute to cell division by increasing mTORC1 activity. Interestingly, our findings show that there is no significant difference in mTORC1 activity between the cells synchronized by Pb treatment and the asynchronous cells on 0.1mg/ml collagen I, whereas mTORC1 activity is higher in the serum-starved cells compared to the non-starved cells on 0.1mg/ml Matrigel. One possible explanation is that even low concentration Matrigel can trigger higher mTORC1 activity in G1 phase breast cancer cells compared to the asynchronous cells. At the same time, these results suggest that collagen I may be not specifically required in G1, which is consistent

with our findings from collagen I uptake assays. Further studies are required to investigate mTORC1 activity between synchronized and asynchronous cells on plastic. In another study, it was demonstrated that laminin internalization contributes to mTORC1 activation in normal mammary epithelial cells under serum starvation condition (Muranen et al., 2017), providing another explanation that the presence of low concentration Matrigel could promote mTORC1 activity in the serum starved cells via a metabolic pathway.

So far, pharmacologic inhibitors of CDK4/6 have changed the treatment landscape for breast cancer, showing promising anticancer effects and manageable toxicity. Here our study reveals an unexpected cell cycle-dependent ECM endocytosis in invasive breast cancer cells, which warrants further investigation. In addition, several key questions remain for future studies. Firstly, only NMuMG cells have been synchronized using serum starvation to measure the endocytosis of ECM in non-transformed epithelial cells in this work. More normal mammary epithelial cell lines and synchronization approaches should be employed in further work, characterizing whether cell cycle-dependent ECM internalization is specifically occurring on invasive breast cancer cells. Secondly, the expression of different  $\alpha$  subunits in G1 is required to be measured in the presence of Matrigel, elucidating the receptors for upregulated laminin endocytosis in G1. Thirdly, it has been illustrated that MDA-MB-231 cells in G1 display a higher invasive capacity compared to the cells in other cell cycle phases (Yano et al., 2014). Further studies are needed to understand whether this increased ECM uptake is required for MDA-MB-231 cell invasion in G1. Lastly, more work is necessary to characterize the contribution of increased mTORC1 activity in G1 for breast cancer development.

## 5 A proteomic approach to identify internalized ECM components

### 5.1 Introduction

The remarkably strong interaction between the small molecule biotin and the streptavidin is widely explored in biological research (Dundas et al., 2013). On the one hand, biotin is a small chemically inert and hydrophilic molecule. Biotinylation process does not disrupt biomolecule function of target molecule. On the other hand, the affinity interaction between streptavidin and biotin is highly selective, resulting in low non-specific binding (Chivers et al., 2010). A recent work from the Norman lab showed that the internalized proteomes could be identified using mass spectrometry proteomics. Briefly, the surface proteins were biotinylated followed by 20 minutes internalization. The internalized proteins were isolated by streptavidin-agarose beads and analysed by performing high-resolution mass spectrometry (Diaz-Vera et al., 2017). Here we developed a similar approach, combining mass spectrometry-based proteomics with a biotinylation-based method, to identify the ECM components that are internalized and their receptors.

In this chapter, we illustrate that our mass spectrometry approach led to the identification of core matrisome proteins internalized by MDA-MB-231 cells plated on biotinylated CDM. At the same time, several integrins were identified in the screen as well, suggesting that integrins are the main receptors responsible for the internalization of CDM in breast cancer cells. Taken together, we developed a novel proteomic approach that can characterize internalized ECM proteins and their receptors in an unbiased way.

## 5.2 Results

### 5.2.1 The detection of internalized CDM by western blotting

We have previously illustrated that internalized biotinylated-CDM could be visualized in MDA-MB-231 cells through binding to fluorescently labelled streptavidin. Here we firstly assessed whether internalized proteins can be detected by streptavidin western blotting. We labelled CDM with sulpho-NHS-SS-Biotin, which contains a reducible disulphide bond. Serum-starved and non-starved MDA-MB-231 cells were then seeded on CDM for a 16-hour incubation in the presence of the lysosomal inhibitor E64d. Afterwards, the extracellular biotin was removed by treating the cells with the membrane-impermeable reducing agent MESNA. The internalized biotinylated-CDM in the lysates were then assessed by western blotting using fluorescently conjugated streptavidin (Figure 5.1A). At the same time, to assess the specificity of the biotin-streptavidin binding, the non-biotinylated CDM was processed identically to the biotinylated ones and analysed by western blotting as well. As illustrated in figure 5.1B, three bands (220kDa, 110kDa and 72kDa) were detected in both biotinylated and non-biotinylated CDM, corresponding to the endogenously biotinylated proteins (most probably mitochondrial carboxylases) (Parrott and Barry, 2000). Additionally, more bands were detected in the lysates collected from biotinylated CDM compared to non-biotinylated CDM (Figure 5.1B). Moreover, the quantification suggested a higher band intensity in serum-starved cells compared to non-starved cells (Figure 5.1B), consistent with our previous data from imaging-based CDM uptake assays (Figure 4.3). Altogether, our findings show that internalized biotinylated CDM in MDA-MB-231 cells could be detected by western blotting.

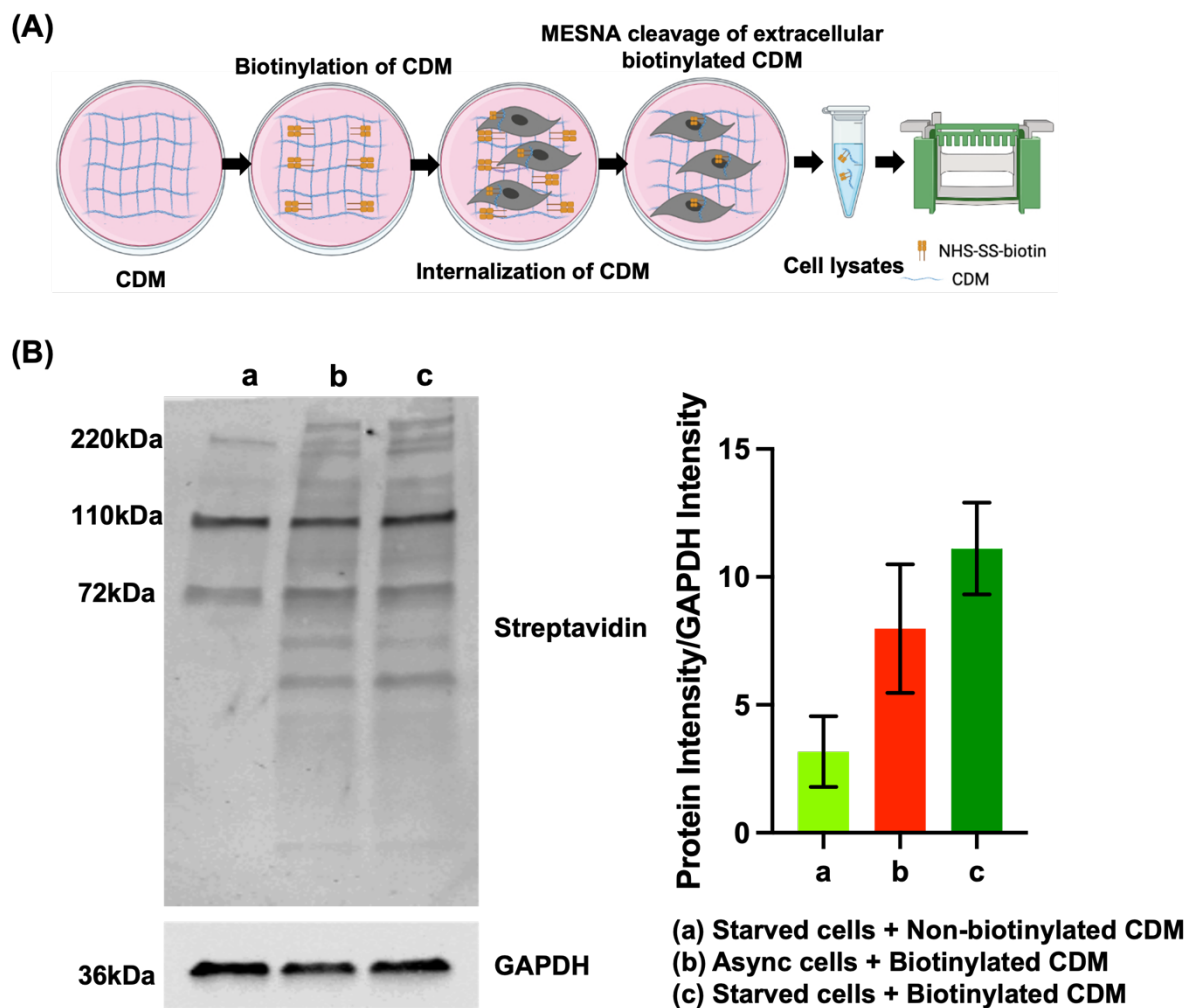


**Figure 5.1. Internalized CDM can be detected by western blotting using streptavidin.** (A) Workflow of western blotting used for detecting internalized CDM in MDA-MB-231 cells. Image is 'Created with BioRender.com'. (B) Serum starved cells were plated on biotinylated and non-biotinylated CDM for 16 hours in the presence 20 $\mu$ M E64d. Non-starved MDA-MB-231 cells were plated on biotinylated CDM with E64d. After MESNA treatment, cells were lysed and analyzed by western blotting using IR Dye 680LT streptavidin and antibody recognizing GAPDH. The intensity of the bands was quantified with Licor Odyssey system. N=2 independent experiments. Mean  $\pm$  SEM, Kruskal-wallis with multiple comparisons.

### **5.2.2 Detection of internalized proteins by streptavidin-agarose pulldown assay**

Prior to mass spectrometry analysis, we assessed the effectiveness of streptavidin-agarose pulldown assay (SAPA) using western blotting. The principle of the SAPA was to incubate biotinylated CDM with streptavidin-agarose beads. Here the total cell lysates were performed as described in the previous section. At the same time, the non-biotinylated CDM was also processed as a control. We then incubated some of total cell lysates with streptavidin-agarose beads at 4°C. For elution of proteins for western blotting, biotinylated proteins bound to streptavidin beads were boiled in SDS sample buffer for 10 minutes, referred to as pulldown lysates (Figure 5.2A).

In total cell lysates, three bands of endogenously biotinylated proteins were detected in both groups. Moreover, more bands were detected in the lysates collected from biotinylated CDM. These were consistent with what we observed in figure 5.1B. In pulldown lysates, we showed that biotinylated proteins in cells were enriched while no GAPDH was detected (Figure 5.2B), suggesting these samples were suitable for subsequent mass spectrometry assay.

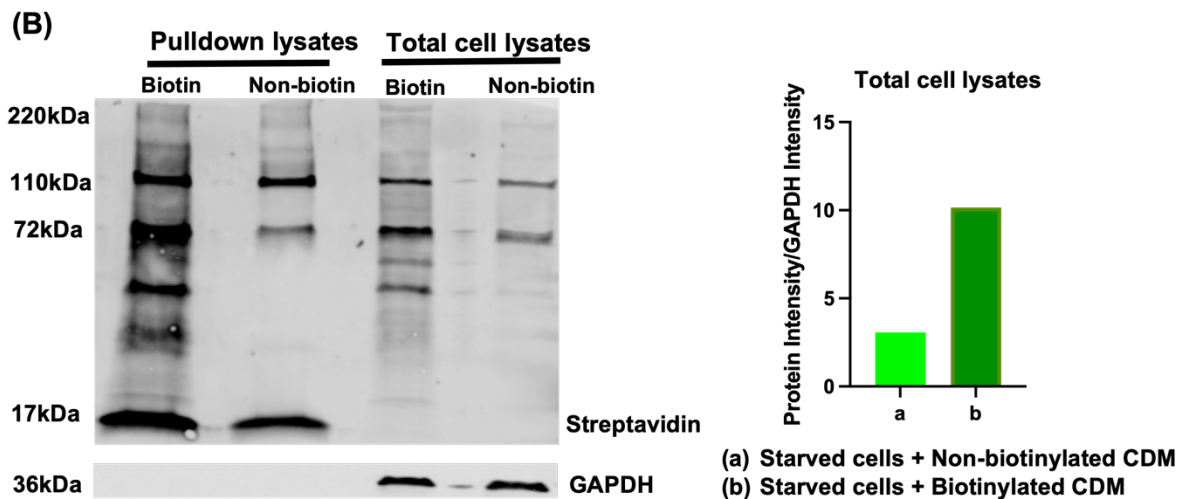
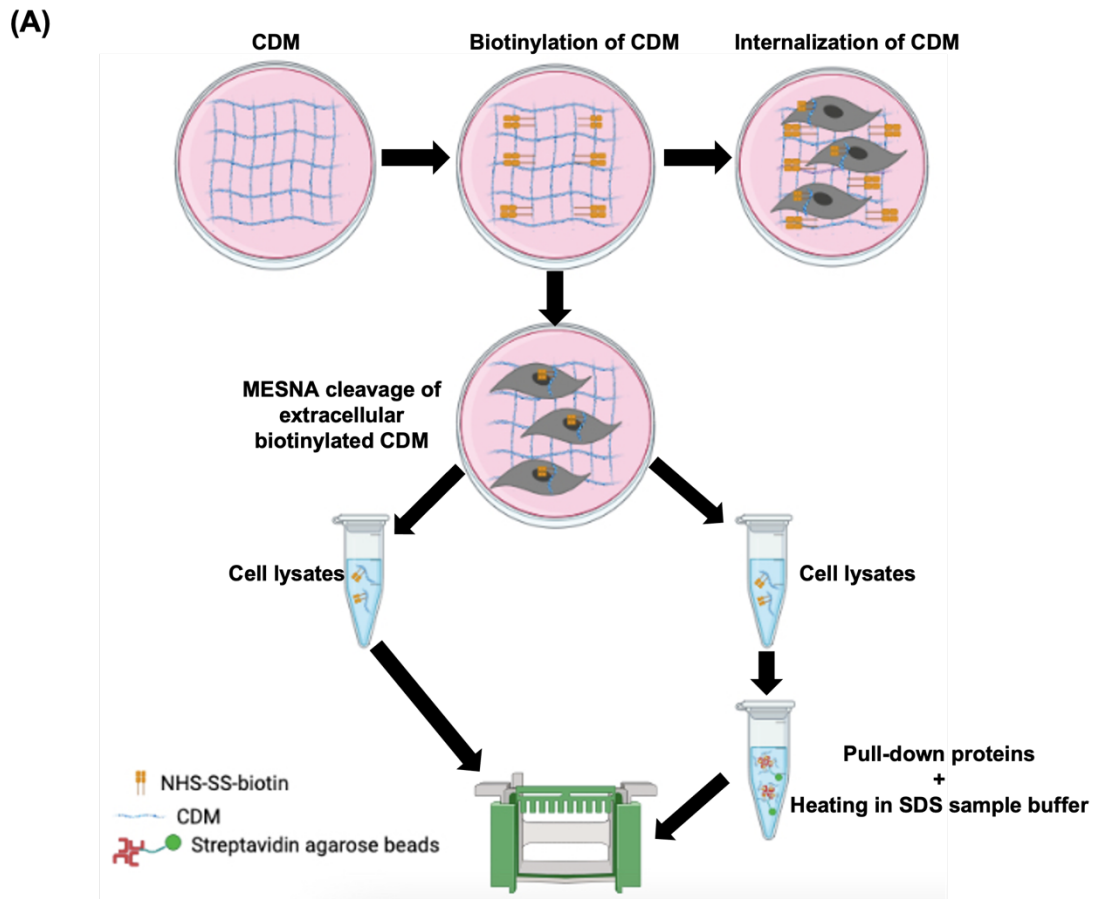


**Figure 5.2. Detection of internalized proteins using streptavidin-agarose pulldown assay (SAPA).** (A) Workflow of using western blotting detect internalized CDM in serum-starved MDA-MB-231 cells by SAPA. Image is 'Created with BioRender.com'. (B) Serum starved cells were plated on biotinylated and non-biotinylated CDM for 16 hours in the presence 20 $\mu$ M E64d. After MESNA treatment, cells were lysed and collected. Some lysates were analyzed by western blotting directly. The remaining lysates were incubated with streptavidin-agarose beads following by heating process and western blotting. The western blotting was performed using IR Dye 680LT streptavidin and antibody recognizing GAPDH. The intensity of the bands in the total cell lysates was quantified with Licor Odyssey system. N=1. A distinct band appeared around 17kDa corresponded to monomeric streptavidin.

### 5.2.3 Identification of internalized proteins by mass spectrometry

Because of the detection of internalized CDM components in MDA-MB-231 cells by western blotting, we used mass spectrometry to identify which proteins were internalized by MDA-MB-231 cells plated on biotinylated CDM, compared to non-biotinylated CDM. In-solution and in-gel digestion are two well-used approaches to prepare samples for mass spectrometry analysis. However, it was previously demonstrated that the extraction of peptides from a gel is less efficient, with estimates of 70%-80% of in-solution digest efficiency (Feist and Hummon, 2015). Therefore, the peptides were digested in-solution in this process (Figure 5.3).

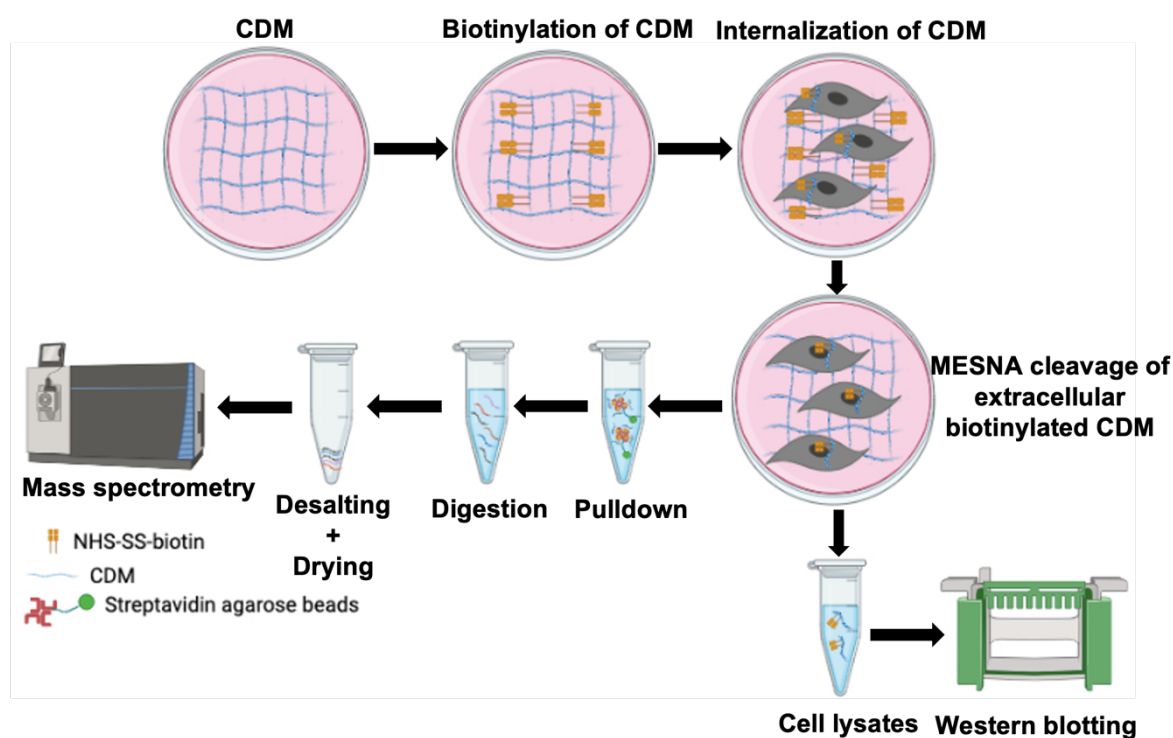


**Figure 5.3. Identification of internalized proteins and integrins using mass spectrometry.** Serum starved MDA-MB-231 cells were plated on biotinylated and nonbiotinylated CDM for 16 hours in the presence 20 $\mu$ M E64d. Cells were lysed after MESNA treatment. Some cell lysates were mixed in SDS sample buffer for western blotting, while the remaining lysates were used for mass spectrometry analysis. Image is 'Created with BioRender.com'.

Here serum starved MDA-MB-231 cells were plated onto biotinylated and non-biotinylated CDM for 16 hours in the presence of E64d. In order to quantify mass spectrometry data, the total cell lysates were split into two technical replicates before incubation with streptavidin-agarose beads. The intensity of GAPDH in western blotting results suggested that the number of cells collected from biotinylated and non-biotinylated CDM were similar (Figure 5.4A). Mass spectrometry data was analysed by Perseus and visualized by a volcano plot. Here 440

proteins were found (Table 5.2), and 304 proteins were upregulated in the pulldown lysates collected from biotinylated CDM (Figure 5.4B). As our aim is to identify the ECM components that are internalized by cancer cells, we annotate the list of upregulated proteins for hits identified by the matrisome project. The matrisome is a curated database of ECM components identified by mass spectrometry approaches. Matrisome proteins can be divided into 'core matrisome' and 'associated matrisome'. Core matrisome components contain collagens, proteoglycans and glycoproteins. Matrisome associated components include MMPs, ECM affiliated proteins and secreted factors (Hynes and Naba, 2012). The data demonstrated that 7 core matrisome proteins and 13 associated matrisome proteins were upregulated on biotinylated CDM based on the database of Matrisome project (<http://matrisomeproject.mit.edu/proteins/>) (Figure 5.4C & Table 5.1). Fibronectin is illustrated to be one of the most abundant proteins in the telomerase-immortalized fibroblast (TIF) CDM (Kaukonen et al., 2017b). Collagen VI is known to facilitate the assembly of CDM (Theocharidis et al., 2016). Fibrillin 1 and elastin microfibril interface-1 (EMILIN-1) are two structurally related glycoproteins, contributing to maintain the tissue homeostasis (Godwin et al., 2019; Schiavinato et al., 2016). Thrombospondin 1 (TSP-1) is a glycoprotein that participates in the organization of collagen fibril in ECM (Kim et al., 2015). The expression of tenascin-C (TNC) and TGFBI (transforming growth factor beta-induced) are tightly regulated, modifying numerous biological functions, such as cell adhesion and collagen I expression (Corona and Blobel, 2021; Ma et al., 2016). In chapter 3, our findings showed that MDA-MB-231 cells can internalize both collagen I and Matrigel. Consistently, in our raw mass spectrometry data, collagen alpha-2(I) chain, one of the chains for collagen I, was identified on biotinylated CDM specifically (Sałacińska et al., 2021) (data not shown). However, it was filtered by the statistical analysis due to the absence of collagen alpha-2(I) chain in one of the biotin groups.

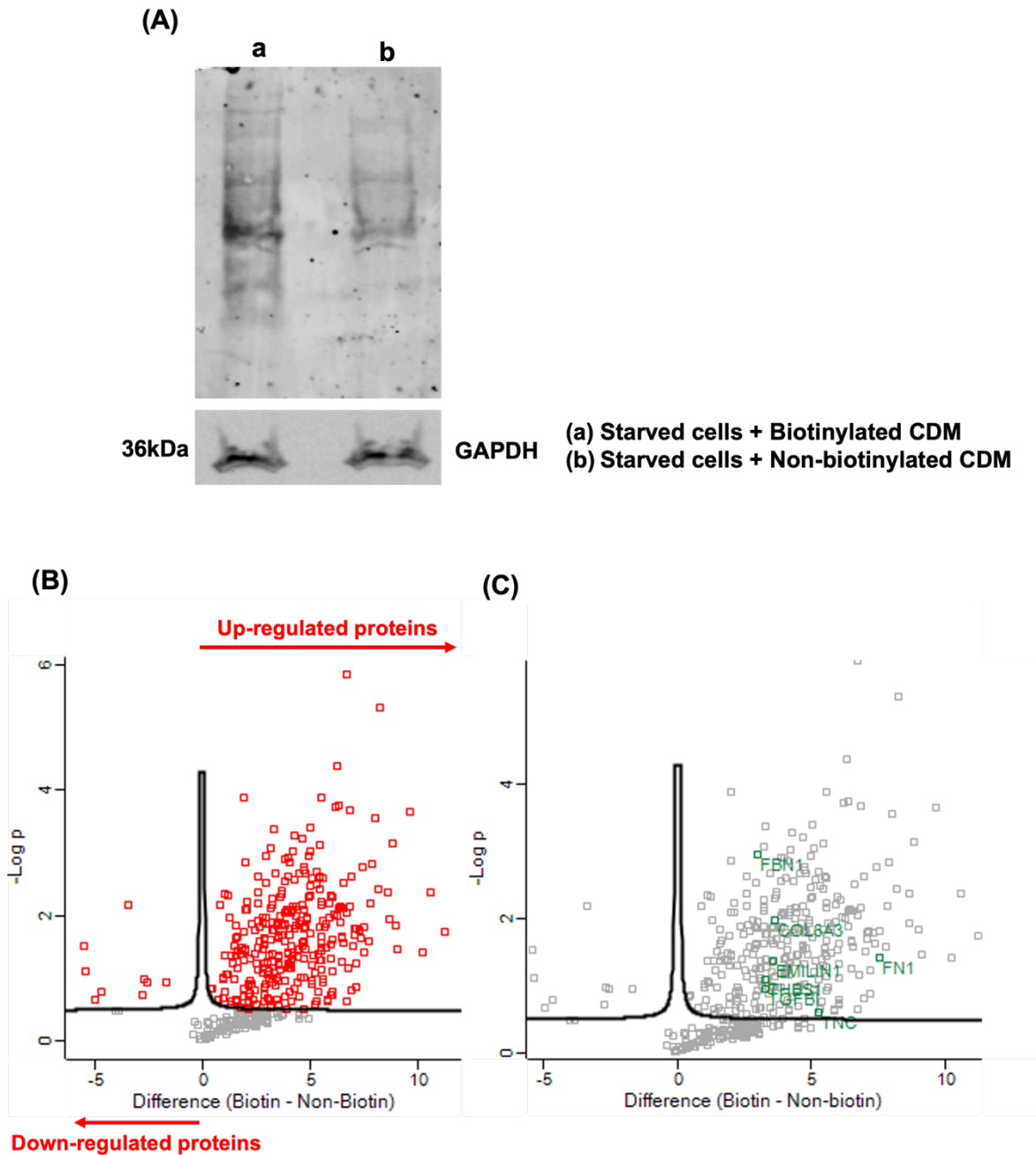


**Figure 5.4. Identification of internalized ECM proteins using mass spectrometry.** (A) Serum starved cells were plated on biotinylated CDM and non-biotinylated CDM for 16 hours in the presence 20 $\mu$ M E64d. After MESNA treatment, cells were lysed and analyzed by western blotting using IR Dye 680LT streptavidin and antibody recognizing GAPDH. Volcano plot illustrated (B) up-regulated and down-regulated components and (C) upregulated core matrisome proteins identified from biotinylated and non-biotinylated CDM in serum-starved MDA-MB-231 cells. T-test, p-value < 0.05.

**Table 5.1**      **List of upregulated ECM proteins in biotinylated CDM**

Name	Matrisome Division	Category
Elastin microfibril interface 1	Core matrisome	ECM Glycoproteins
Fibrillin 1	Core matrisome	ECM Glycoproteins
Fibronectin 1	Core matrisome	ECM Glycoproteins
Transforming growth factor-beta-induced protein	Core matrisome	ECM Glycoproteins
Thrombospondin 1	Core matrisome	ECM Glycoproteins
Tenascin C	Core matrisome	ECM Glycoproteins
Collage type VI, alpha 3	Core matrisome	Collagens
Annexin A1	Matrisome-associated	ECM-affiliated Proteins
Annexin A2	Matrisome-associated	ECM-affiliated Proteins
Annexin A4	Matrisome-associated	ECM-affiliated Proteins
Annexin A5	Matrisome-associated	ECM-affiliated Proteins
Annexin A6	Matrisome-associated	ECM-affiliated Proteins
Annexin A7	Matrisome-associated	ECM-affiliated Proteins
Collectin sub-family member 12	Matrisome-associated	ECM-affiliated Proteins
Chondroitin sulfate proteoglycan 4	Matrisome-associated	ECM-affiliated Proteins
Galectin-1	Matrisome-associated	ECM-affiliated Proteins
Protein ERGIC-53	Matrisome-associated	ECM-affiliated Proteins
ADAM metallopeptidase domain 9	Matrisome-associated	ECM Regulators
CD109 molecule	Matrisome-associated	ECM Regulators
Matrix metallopeptidase 14	Matrisome-associated	ECM Regulators

Several pieces of evidence from the literature and the data presented in chapter 3 illustrate a role of integrin in controlling ECM endocytosis. Therefore, we then wanted to characterize which integrins could be detected using mass spectrometry as interactors of biotinylated ECM components. The quantification illustrated that two  $\beta$  subunits ( $\beta 1$  and  $\beta 5$ ) and five  $\alpha$  subunits ( $\alpha 2$ ,  $\alpha 3$ ,  $\alpha 5$ ,  $\alpha V$  and  $\alpha 11$ ) were strongly upregulated on biotinylated CDM (Figure 5.5A). Among the hits, both  $\alpha 2\beta 1$  and  $\alpha 11\beta 1$  are known as collagen-binding integrins (Zeltz and Gullberg,

2016).  $\alpha 5\beta 1$  is a highly selective fibronectin receptor (Humphries et al., 2006a), whereas  $\alpha V\beta 1$  can bind to both fibronectin and vitronectin (Marshall et al., 1995).  $\alpha 3\beta 1$  is known as a highly selective receptor for laminin (Subbaram and DiPersio, 2011).  $\alpha V\beta 5$  is known to interact with various ECM components, including osteopontin, vitronectin and fibronectin (Bisanz et al., 2005; Park and Helfman, 2019) (Figure 5.5B).

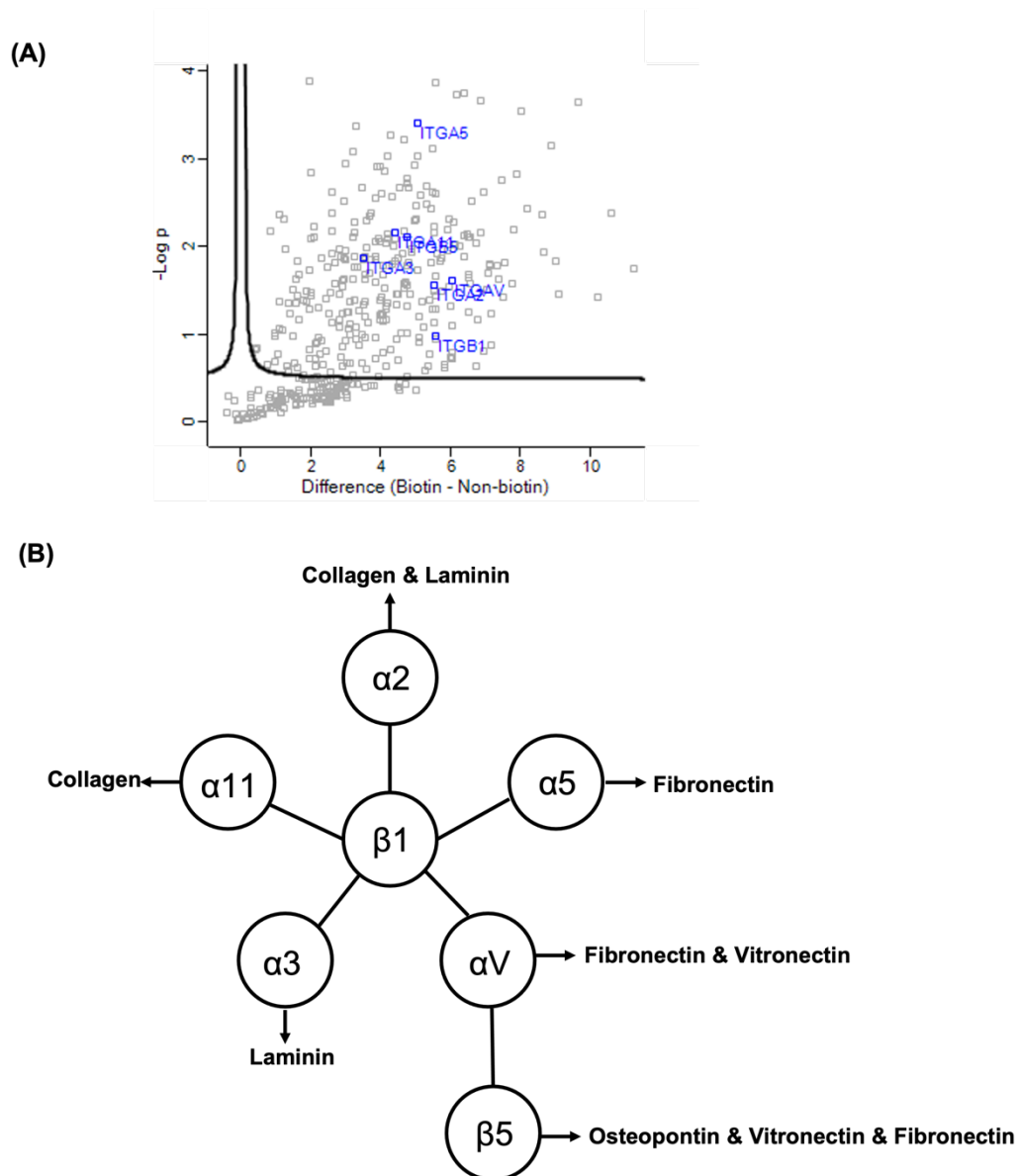


**Figure 5.5. Identification of integrins using mass spectrometry.** (A) Volcano plot illustrated upregulated integrins from biotinylated CDM (B) The ECM ligands of upregulated integrins from biotinylated CDM. T-test, p-value < 0.05.

Lastly, we have showed that most of internalized CDM were degraded inside the lysosomes in MDA-MB-231 cells. Here we illustrated that lysosomal-associated membrane glycoprotein 1 (LAMP1), lysosome integral membrane protein 2 (LIMP-2) and Ras-related protein Rab-7a (Rab7a) were upregulated on biotinylated CDM (Figure 5.6). LAMP1 is a major protein component of the lysosomal membrane and usually referred to as lysosomal marker (Cheng et al., 2018). LIMP-2 is a transmembrane glycoprotein mainly found in late endosomes and lysosomes, promoting endosomal and lysosomal function (Conrad et al., 2017). Rab7a is a key regulator of the endosomal-lysosomal system which is mainly located in the late endosomes (Sun et al., 2020). By contrast, early endosome antigen 1 (EEA1; a well-known marker of early endosomes) was not upregulated. Taken together, our data suggest that internalized CDM accumulated in the late endosomes/lysosomes in the presence of E64d.

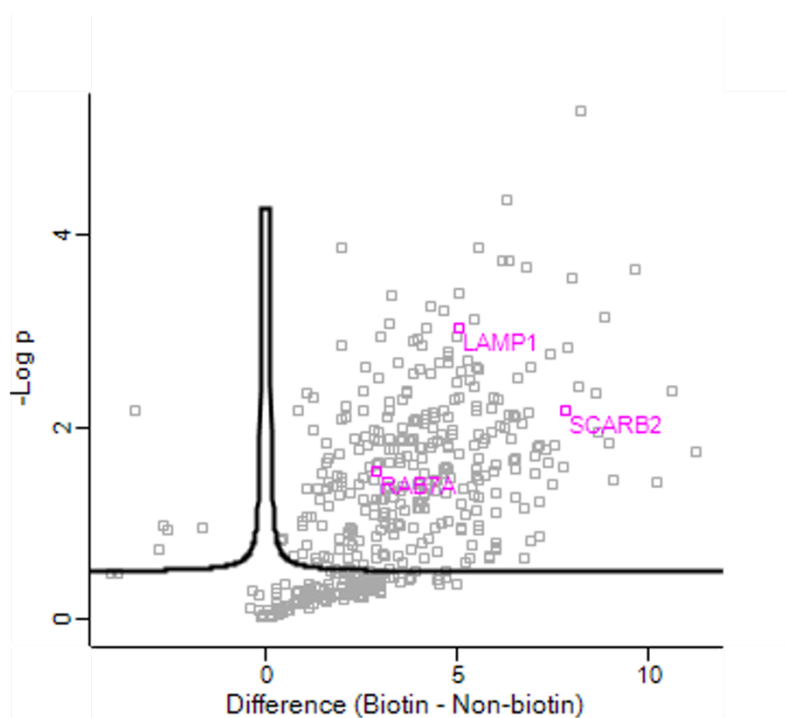


**Figure 5.6. Internalized CDM components are accumulated in the late endosomes/lysosomes.** Volcano plot illustrated the upregulation of lysosomal-associated membrane glycoprotein 1 (*LAMP1*), lysosome membrane protein 2 (*SCARB2*) and Ras-related protein Rab-7a (*RAB7A*) on biotinylated CDM. T-test, p-value < 0.05.

<b>Table 5.2</b>	<b>List of ECM proteins presented in the screen</b>
------------------	---

(+:upregulation; x: no different; -:downregulation)

Protein Name	T-test Bio-Nonbiotin
Myosin-9	+
Trifunctional enzyme subunit alpha, mitochondrial	+
Cytoskeleton-associated protein 4	+
Cytochrome b-c1 complex subunit 2, mitochondrial	+
Tenascin	+
Cytochrome b-c1 complex subunit 1, mitochondrial	+
Fatty acid synthase	+
Cytoplasmic dynein 1 heavy chain 1	+
Dolichyl-diphosphooligosaccharide-protein glycosyltransferase subunit DAD1	+
Myoferlin	+
Phosphate carrier protein, mitochondrial	+
Heat shock protein HSP 90-beta	+
Myosin light polypeptide 6	+
Mitochondrial carrier homolog 2	+
Clathrin heavy chain 1	+
Sideroflexin-1	+
Prolow-density lipoprotein receptor-related protein 1	+
ADP/ATP translocase 2	+
Myosin regulatory light chain 12A	+
Calcium-binding mitochondrial carrier protein Aralar1	+
Aminopeptidase N	+
Epoxide hydrolase 1	+
Annexin A2	+
Annexin A7	+
Prolyl endopeptidase FAP	+
Guanine nucleotide-binding protein G(I)/G(S)/G(T) subunit beta-1	+
Sideroflexin-3	+
Tubulin beta-4B chain	+
Heat shock protein HSP 90-alpha	+
Voltage-dependent anion-selective channel protein 1	+
Apolipoprotein B-100	+
Galectin-1	+
Transitional endoplasmic reticulum ATPase	+
Lysosome membrane protein 2	+
Dihydrolipoyl dehydrogenase, mitochondrial	+
Sarcoplasmic/endoplasmic reticulum calcium ATPase 2	+
Dipeptidyl peptidase 4	+
Calnexin	+
Sodium/potassium-transporting ATPase subunit alpha-1	+
Mitochondrial carnitine/acylcarnitine carrier protein	+
Voltage-dependent anion-selective channel protein 2 (Fragment)	+
Fibronectin	+
Prohibitin	+
Major facilitator superfamily domain-containing protein 10	+
Delta(24)-sterol reductase	+
MICOS complex subunit MIC60 (Fragment)	+
CAD protein	+
Dolichyl-diphosphooligosaccharide-protein glycosyltransferase subunit 2	+
Mitochondrial 2-oxoglutarate/malate carrier protein (Fragment)	+
Acyl-CoA 6-desaturase	+
Inhibitor of nuclear factor kappa-B kinase-interacting protein	+
Myosin-10	+
2-oxoglutarate dehydrogenase, mitochondrial	+
Eukaryotic initiation factor 4A-I	+
Annexin A1	+

Integrin beta-1	+
Alpha-actinin-1	+
E3 ubiquitin-protein ligase UBR4	+
Dolichyl-diphosphooligosaccharide-protein glycosyltransferase 48 kDa subunit	+
Annexin A5	+
Mitochondrial carrier homolog 1	+
Tricarboxylate transport protein, mitochondrial	+
Neutral alpha-glucosidase AB	+
Cytochrome c oxidase subunit 5A, mitochondrial	+
Cation-independent mannose-6-phosphate receptor	+
Glycogen phosphorylase, brain form	+
Importin-5	+
Prohibitin	+
Plectin	+
Cullin-associated NEDD8-dissociated protein 1	+
NPC intracellular cholesterol transporter 1	+
Vimentin	+
Endoplasmic reticulum metalloproteinase 1	+
Plasma membrane calcium-transporting ATPase 4	+
Endoplasmic reticulum chaperone protein	+
WD repeat-containing protein 1	+
Transmembrane protein 43	+
Myosin regulatory light polypeptide 9	+
eIF-2-alpha kinase activator GCN1	+
NAD(P) transhydrogenase, mitochondrial	+
ADP/ATP translocase 3	+
Propionyl-CoA carboxylase beta chain, mitochondrial	+
Transferrin receptor protein 1	+
Anoctamin-10	+
Exportin-2	+
Endoplasmic reticulum-Golgi intermediate compartment protein 1	+
Trifunctional enzyme subunit beta, mitochondrial	+
Vinculin	+
Peroxisomal membrane protein 11B	+
Microsomal glutathione S-transferase 3	+
Transforming growth factor-beta-induced protein ig-h3	+
Electron transfer flavoprotein-ubiquinone oxidoreductase, mitochondrial	+
Spectrin beta chain	+
Dolichyl-diphosphooligosaccharide-protein glycosyltransferase subunit 1	+
Nephrilysin	+
Leucine-rich PPR motif-containing protein, mitochondrial	+
Integrin alpha-V	+
Tropomyosin alpha-4 chain	+
Membrane-associated progesterone receptor component 1	+
Lysosome-associated membrane glycoprotein 1	+
Lysophospholipid acyltransferase 7	+
Membrane-associated progesterone receptor component 2	+
Protein kish-A	+
Copine-3	+
Calpain-2 catalytic subunit	+
Isoleucyl-tRNA synthetase 1	+
Acylglycerol kinase, mitochondrial	+
Importin-7	+
Collectin-12	+
HLA class I histocompatibility antigen, A alpha chain (Fragment)	+

E3 ubiquitin-protein ligase synoviolin	+
Unconventional myosin-1c	+
Cytochrome c oxidase subunit 4 isoform 1, mitochondrial	+
Elongation factor 1-gamma	+
FACT complex subunit SPT16	+
Transmembrane protein 33 (Fragment)	+
Spectrin alpha chain, non-erythrocytic 1	+
HLA class I histocompatibility antigen, B alpha chain (Fragment)	+
ATP synthase membrane subunit DAPIT, mitochondrial	+
ATP-citrate synthase	+
Thioredoxin-related transmembrane protein 1	+
Transportin-1	+
Syntaxin-7	+
Integrin beta-5	+
NADH-cytochrome b5 reductase 3	+
Proteasome adapter and scaffold protein ECM29	+
Importin subunit beta-1	+
Low-density lipoprotein receptor	+
CD109 antigen	+
Vesicular integral-membrane protein VIP36	+
E3 ubiquitin-protein ligase HUWE1	+
Protein RER1 (Fragment)	+
TMEM256-PLSCR3 readthrough (NMD candidate)	+
Protein ERGIC-53	+
Integrin alpha-2	+
ATP synthase subunit d, mitochondrial	+
Exportin-1	+
Integrin alpha-5	+
Heat shock protein 105 kDa	+
Solute carrier family 52, riboflavin transporter, member 2	+
Voltage-dependent anion-selective channel protein 3	+
Erythrocyte band 7 integral membrane protein	+
Reversion-inducing cysteine-rich protein with Kazal motifs	+
Nicotinamide phosphoribosyltransferase	+
EMILIN-1	+
Cytochrome P450 20A1	+
Claudin-11	+
Integrin alpha-11	+
Annexin A6	+
Putative heat shock protein HSP 90-beta 2	+
Golgi apparatus protein 1	+
CD63 antigen (Fragment)	+
Reactive oxygen species modulator 1	+
Guanine nucleotide-binding protein G(I)/G(S)/G(T) subunit beta-2	+
Splicing factor 3B subunit 1	+
Ubiquitin-like modifier-activating enzyme 1	+
CD166 antigen	+
26S proteasome non-ATPase regulatory subunit 2	+
Mitochondrial proton/calcium exchanger protein	+
Gelsolin	+
Transient receptor potential cation channel subfamily V member 2	+
Protein cornichon homolog 3	+
Sphingolipid delta(4)-desaturase DES1	+
Lysophosphatidylserine lipase ABHD12	+
Coatomer subunit beta	+

ATP synthase subunit beta, mitochondrial	+
Tetraspanin	+
T-complex protein 1 subunit alpha	+
Transmembrane 9 superfamily member 2	+
ATP synthase F(0) complex subunit B1, mitochondrial	+
Protein TMED7-TICAM2	+
Arginine-tRNA ligase, cytoplasmic	+
Eukaryotic translation initiation factor 3 subunit A	+
Extended synaptotagmin-1	+
Glycerol-3-phosphate dehydrogenase, mitochondrial	+
ATP synthase subunit f, mitochondrial	+
Microsomal glutathione S-transferase 1 (Fragment)	+
HLA class I histocompatibility antigen, B alpha chain	+
HLA class I histocompatibility antigen, C alpha chain	+
Serine/threonine-protein kinase mTOR	+
NADH dehydrogenase [ubiquinone] 1 beta subcomplex subunit 9	+
Thrombospondin-1	+
Transmembrane protein 168	+
Plastin-3	+
Matrix metalloproteinase-14	+
Integrin alpha-3	+
Protein disulfide-isomerase	+
PRA1 family protein	+
Neutral amino acid transporter B(0)	+
Lanosterol synthase	+
Epidermal growth factor receptor	+
4F2 cell-surface antigen heavy chain	+
Probable ubiquitin carboxyl-terminal hydrolase FAF-X	+
Vacuolar protein sorting-associated protein 35	+
Multidrug resistance-associated protein 4	+
Thy-1 membrane glycoprotein (Fragment)	+
Zinc transporter 7	+
Nurim	+
Solute carrier family 15 member 4	+
Threonine-tRNA ligase 1, cytoplasmic	+
Utrophin	+
Monocarboxylate transporter 4	+
Aspartate aminotransferase, mitochondrial	+
T-complex protein 1 subunit epsilon	+
Guanine nucleotide-binding protein G(i) subunit alpha-2	+
CAAX prenyl protease 1 homolog	+
14-3-3 protein epsilon	+
Collagen alpha-3(VI) chain	+
Chondroitin sulfate proteoglycan 4	+
Dynactin subunit 1	+
NADH-ubiquinone oxidoreductase 75 kDa subunit, mitochondrial	+
7-dehydrocholesterol reductase	+
Sodium-coupled neutral amino acid transporter 2	+
Hypoxia up-regulated protein 1	+
Actin-related protein 3	+
UPAR/Ly6 domain-containing protein	+
Coatmer subunit beta	+
Striatin-3	+
Cofilin-1 (Fragment)	+
Transmembrane protein 65	+

Anoctamin-6	+
Cytochrome c1, heme protein, mitochondrial	+
Trifunctional purine biosynthetic protein adenosine-3	+
Fibrillin-1	+
Ectonucleotide pyrophosphatase/phosphodiesterase family member 1	+
Beta-2-syntrophin	+
Ras-related protein Rab-7a	+
Cytochrome c oxidase subunit 5B, mitochondrial	+
T-complex protein 1 subunit theta	+
Nicastrin (Fragment)	+
LETM1 domain-containing protein 1	+
Exportin-5	+
26S proteasome non-ATPase regulatory subunit 1	+
ATP-dependent RNA helicase A	+
Calcium-binding mitochondrial carrier protein Aralar2	+
Kinesin-1 heavy chain	+
Cytochrome b5 type B	+
Copine-1 (Fragment)	+
60S ribosomal protein L30 (Fragment)	+
Inverted formin-2	+
Prenylcysteine oxidase 1	+
Syntenin-1	+
Alkyldihydroxyacetonephosphate synthase, peroxisomal	+
Tubulin beta-6 chain	+
Glycine-tRNA ligase	+
V-type proton ATPase catalytic subunit A	+
Protein transport protein Sec24C	+
Acyl-CoA (8-3)-desaturase (Fragment)	+
C-type mannose receptor 2	+
Fumarate hydratase, mitochondrial	+
Polypyrimidine tract binding protein 1, isoform CRA_b	+
Atlastin-3	+
Alpha-2-macroglobulin receptor-associated protein	+
Mitochondrial import receptor subunit TOM40 homolog	+
5-nucleotidase	+
Coatamer subunit gamma-1	+
Ephrin type-A receptor 2	+
Glucose-6-phosphate isomerase	+
Thioredoxin domain-containing protein 5	+
Annexin A4	+
DNA damage-binding protein 1	+
Tumor necrosis factor receptor superfamily member 6	+
Staphylococcal nuclease domain-containing protein 1	+
Paxillin (Fragment)	+
26S proteasome regulatory subunit 4	+
Alanine-tRNA ligase, cytoplasmic	+
Bcl-2-associated transcription factor 1	+
NADH-ubiquinone oxidoreductase chain 5	+
Perilipin-3	+
ATPase ASNA1	+
Cytoplasmic FMR1-interacting protein 1	+
Exportin-7	+
Estradiol 17-beta-dehydrogenase 11	+
Cleavage and polyadenylation-specificity factor subunit 6	+
Importin subunit alpha-1	+

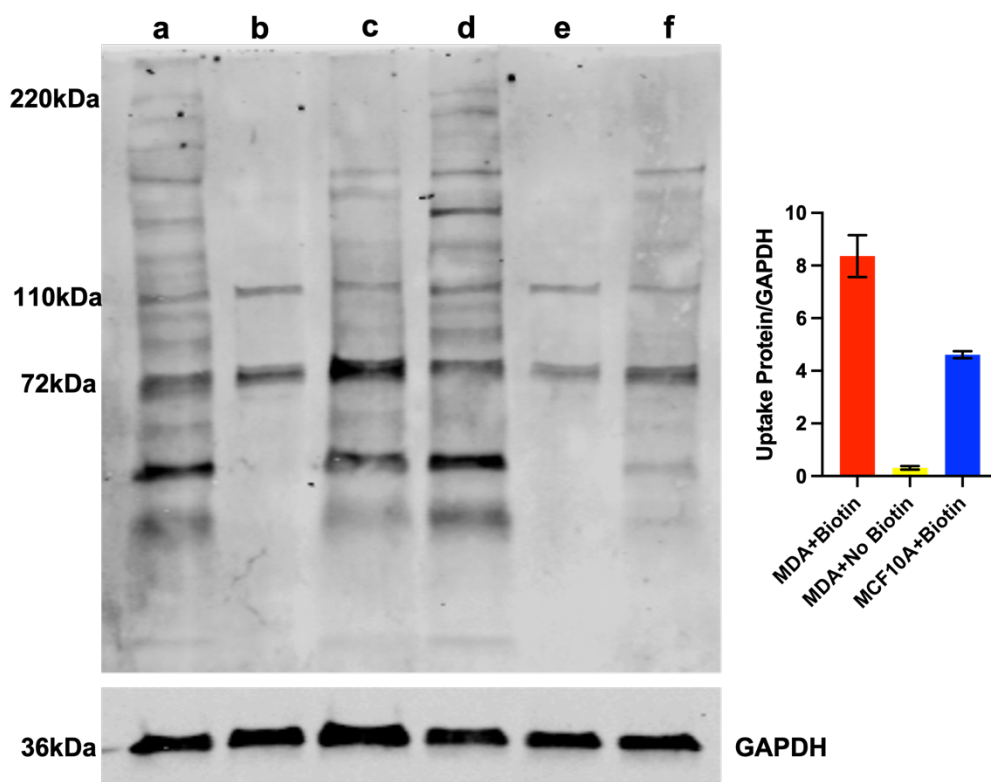
Glutamine-tRNA ligase	+
Chromodomain-helicase-DNA-binding protein 4 (Fragment)	+
Major vault protein	+
60S ribosomal protein L12	+
Transmembrane protein 11, mitochondrial	+
Stomatin-like protein 2, mitochondrial	+
Transmembrane 9 superfamily member 3	+
General vesicular transport factor p115	+
Delta-sarcoglycan	+
E3 ubiquitin-protein ligase MARCHF5	+
Leucine-rich repeat-containing protein 15	+
Large neutral amino acids transporter small subunit 1	+
Lipopolysaccharide-responsive and beige-like anchor protein	+
Transmembrane emp24 domain-containing protein 1	+
P2X purinoceptor 4	+
Disintegrin and metalloproteinase domain-containing protein 9	+
Glutamine-fructose-6-phosphate aminotransferase [isomerizing] 1	+
40S ribosomal protein S8	+
Large proline-rich protein BAG6	+
Heterogeneous nuclear ribonucleoprotein L (Fragment)	+
Ras GTPase-activating protein-binding protein 1	+
Neuropilin	+
Rho GTPase-activating protein 29	+
Ubiquitin carboxyl-terminal hydrolase 5	+
Succinate dehydrogenase [ubiquinone] flavoprotein subunit, mitochondrial	+
C-Jun-amino-terminal kinase-interacting protein 4	+
Gap junction alpha-1 protein	+
Condensin complex subunit 3	+
DnaJ homolog subfamily C member 13	+
Pyruvate carboxylase, mitochondrial	x
Acetyl-CoA carboxylase 1	x
Filamin-A	x
Actin, cytoplasmic 2	x
Collagen alpha-1(XII) chain	x
Filamin-B	x
Propionyl-CoA carboxylase alpha chain, mitochondrial	x
Methylcrotonoyl-CoA carboxylase subunit alpha, mitochondrial	x
Pyruvate kinase PKM	x
Putative elongation factor 1-alpha-like 3	x
Tubulin alpha-1A chain	x
Heat shock cognate 71 kDa protein	x
Glyceraldehyde-3-phosphate dehydrogenase	x
DNA-dependent protein kinase catalytic subunit	x
Ras GTPase-activating-like protein IQGAP1	x
Talin-1	x
Putative RNA-binding protein Luc7-like 2	x
Alpha-actinin-4	x
Alpha-enolase	x
RNA-binding protein 39	x
Filamin-C	x
Elongation factor 2	x
RNA-binding protein FUS	x
Endoplasmic reticulum chaperone BiP	x
L-lactate dehydrogenase A chain	x
Tubulin beta chain	x

C-1-tetrahydrofolate synthase, cytoplasmic	x
Probable ATP-dependent RNA helicase DDX46	x
Moesin	x
DNA (cytosine-5)-methyltransferase 1	x
Nucleolin	x
Coatamer subunit alpha	x
60 kDa heat shock protein, mitochondrial	x
Transketolase	x
CD44 antigen	x
Bifunctional glutamate/proline-tRNA ligase	x
Valine-tRNA ligase	x
Prelamin-A/C	x
Polyubiquitin-C	x
Microtubule-associated protein 1B	x
Eukaryotic translation initiation factor 4 gamma 1	x
Cytochrome b-c1 complex subunit 9	x
Serine/arginine-rich-splicing factor 2 (Fragment)	x
L-lactate dehydrogenase B chain	x
14-3-3 protein zeta/delta	x
Heat shock 70 kDa protein 1B	x
ATP synthase subunit alpha, mitochondrial	x
Stress-70 protein, mitochondrial	x
Phosphoglycerate kinase 1	x
T-complex protein 1 subunit gamma	x
Putative RNA-binding protein Luc7-like 1	x
Dihydropyrimidinase-related protein 2	x
Fructose-bisphosphate aldolase	x
Reticulon (Fragment)	x
Splicing factor U2AF 35 kDa subunit	x
Heterogeneous nuclear ribonucleoprotein K	x
Peroxiredoxin-1 (Fragment)	x
Serine/arginine-rich-splicing factor 7	x
Luc7-like protein 3	x
Very-long-chain enoyl-CoA reductase	x
T-complex protein 1 subunit zeta	x
Polyadenylate-binding protein 1	x
Y-box-binding protein 1	x
Calcium homeostasis endoplasmic reticulum protein	x
Cytoskeleton-associated protein 5	x
RNA-binding protein EWS	x
Far upstream element-binding protein 2	x
PDZ and LIM domain protein 5	x
GTP-binding nuclear protein Ran	x
Microtubule-associated protein 4	x
Cytochrome c oxidase subunit 2	x
Programmed cell death 6-interacting protein	x
Microtubule-actin cross-linking factor 1, isoforms 1/2/3/5	x
Transcription intermediary factor 1-beta	x
Splicing factor U2AF 65 kDa subunit	x
Leucine-tRNA ligase, cytoplasmic	x
Heterogeneous nuclear ribonucleoprotein M (Fragment)	x
Serine/arginine-rich-splicing factor 11 (Fragment)	x
Adenosylhomocysteinase	x
Arginine/serine-rich coiled-coil protein 2	x
Protein PRRC2C	x

Thyroid hormone receptor-associated protein 3	x
ATP-dependent 6-phosphofructokinase, platelet type	x
Eukaryotic translation initiation factor 3 subunit C	x
Eukaryotic translation initiation factor 5B	x
60S ribosomal protein L4	x
Heat shock 70 kDa protein 4	x
Adenylyl cyclase-associated protein 1	x
Serine/arginine repetitive matrix protein 2	x
Glutamate dehydrogenase 2, mitochondrial	x
T-complex protein 1 subunit eta	x
Receptor of-activated protein C kinase 1 (Fragment)	x
Keratinocyte proline-rich protein	x
Ribonuclease inhibitor	x
Peroxiredoxin-6	x
Heterogeneous nuclear ribonucleoprotein H	x
Heterogeneous nuclear ribonucleoprotein U-like protein 1 (Fragment)	x
Poly (ADP-ribose) polymerase 1	x
Long-chain-fatty-acid-CoA ligase 3	x
Dynamin-2	x
Rab GDP dissociation inhibitor beta	x
Cellular nucleic acid-binding protein	x
Elongation factor 1-delta	x
Heterogeneous nuclear ribonucleoprotein U	x
Eukaryotic translation initiation factor 4 gamma 2 (Fragment)	x
Phosphoglycerate mutase 1	x
Stress-induced-phosphoprotein 1	x
Pre-mRNA-processing-splicing factor 8	x
Torsin-1A-interacting protein 1 (Fragment)	x
Retinol dehydrogenase 11	x
Melanoma-associated antigen D2	x
ATP-binding cassette sub-family F member 1 (Fragment)	x
ATP synthase subunit gamma, mitochondrial	x
Nascent polypeptide-associated complex subunit alpha (Fragment)	x
Dystonin	x
Lamina-associated polypeptide 2, isoforms beta/gamma	x
F-actin-capping protein subunit alpha-1	x
Stimulator of interferon response cGAMP interactor 1	x
Phosphoglucomutase-1	x
Probable ATP-dependent RNA helicase DDX17	x
Laminin subunit beta-3	x
LIM domain only protein 7	x
Sister chromatid cohesion protein PDS5 homolog A	x
72 kDa type IV collagenase	x
Band 4.1-like protein 2	x
HCG2042749, isoform CRA_d	x
Catalase	x
Keratin, type II cytoskeletal 1	-
Neuroblast differentiation-associated protein AHNAK	-
Desmoplakin	-
Junction plakoglobin	-
Calmodulin-like protein 5	-
Dermcidin	-
Protein S100-A8	-
Keratin, type II cytoskeletal 78	-
Protein-glutamine gamma-glutamyltransferase E	-

## 5.2.4 Identification of internalized proteins in MDA-MB-231 and MCF10A cells

In section 5.2.3, we had two groups (biotin & non-biotin) that each contained two technical replicates. Here we set up two more biological replicates of MDA-MB-231 cells on biotinylated and non-biotinylated CDM. Additionally, we showed that MDA-MB-231 cells can uptake more CDM compared to MCF10A cells. Thus, MCF10A cells were seeded on biotinylated CDM for a 16-hour incubation in the presence of E64d, identifying potential differences in CDM uptake between MDA-MB-231 cells and MCF10A cells. As demonstrated in figure 5.7, endogenously biotinylated protein bands were detected in all three conditions. Moreover, more bands were detected on biotinylated CDM compared to control non-biotinylated CDM in MDA-MB-231 cells. Furthermore, the quantification suggested a higher band intensity in MDA-MB-231 cells compared to MCF10A cells, consistent with our previous findings from imaging-based CDM internalization assays (Figure 3.1).



(a) MDA-MB-231 cells + Biotinylated CDM (d) MDA-MB-231 cells + Biotinylated CDM  
(b) MDA-MB-231 cells + Non-biotinylated CDM (e) MDA-MB-231 cells + Non-biotinylated CDM  
(c) MCF10A cells + Biotinylated CDM (f) MCF10A cells + Biotinylated CDM

**Figure 5.7. Western blotting results of internalized CDM in MDA-MB-231 cells and MCF10A cells.** MDA-MB-231 cells were plated on biotinylated and non-biotinylated CDM for 16 hours in the presence 20 $\mu$ M E64d. MCF10A cells were plated on biotinylated CDM with E64d. After MESNA treatment, some cell lysates were analyzed by western blotting using IR Dye 680LT streptavidin and antibody recognizing GAPDH. The intensity of the bands was quantified with Licor Odyssey system. N=2 independent experiments. Mean  $\pm$  SEM, Kruskal-wallis with multiple comparisons. One replicate (d-f) was finished by Montserrat Llanses Martinez, Rainero lab.

### 5.3 Discussion

In this chapter, we used a proteomic approach to characterize internalized CDM components in breast cancer cells. Here 7 core matrisome proteins and 6 integrin heterodimers were found to be strongly upregulated on biotinylated CDM. Among the integrin hits, the ligand for  $\alpha 5\beta 1$  and  $\alpha v\beta 1$ , fibronectin, was identified to be upregulated as well. Collagen alpha-2(I) chain was detected on biotinylated CDM specifically. The ligand of  $\alpha 3\beta 1$  was detected both on biotinylated CDM and non-biotinylated CDM (Figure 5.8). These results suggest that integrins are the major receptors responsible for the endocytosis of CDM in breast cancer cells.

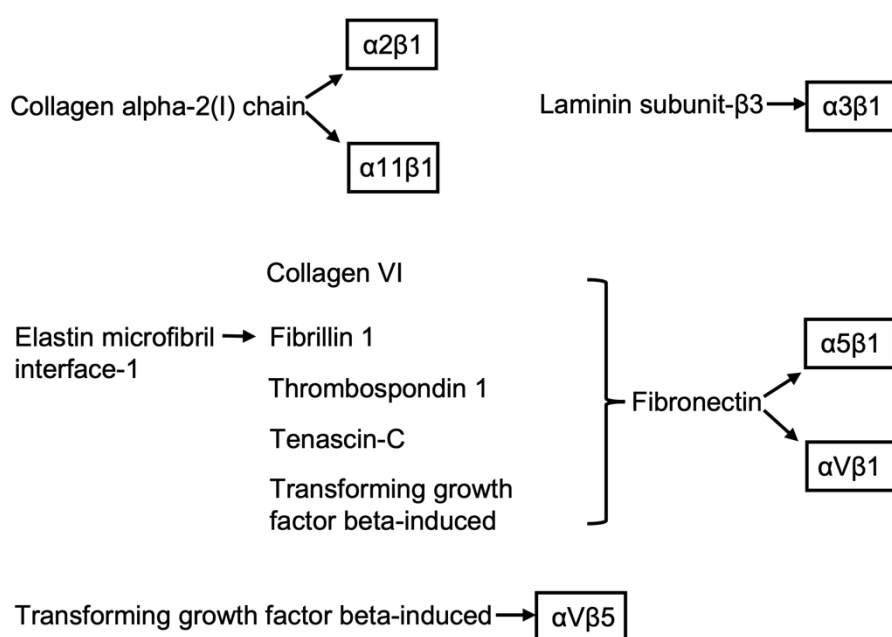


**Figure 5.8. Integrins may be the major receptors responsible for the endocytosis of CDM.** 6 integrins were identified to be upregulated on biotinylated CDM. In addition, 7 upregulated core matrisome proteins were listed as well.

Currently four endogenously biotinylated proteins have been detected in mammalian cells. Pyruvate carboxylase (130kDa), 3-methylcrotonyl coA carboxylase (75kDa) and propionyl coA carboxylase (72kDa) are located in the mitochondria, whereas acetyl coA carboxylase (220kDa) is found in the cytoplasm (Niers et al., 2011). The endogenously biotinylated protein bands in our samples are consistent with three of them. Furthermore, only these three endogenously biotinylated protein are detected on non-biotinylated CDM, suggesting the high specificity of the biotin-streptavidin binding. Here only proteins that are upregulated on biotinylated CDM and enriched over hits in matrisome database are selected.

Fibronectin is a large glycoprotein and mediates various cellular activities, including growth, adhesion, migration and differentiation (Erdogan et al., 2017). Our mass spectrometry results showed the upregulation of fibronectin in biotinylated CDM lysates, consistent with previous study that fibronectin is one of the most abundant components in TIF CDM (Kaukonen et al., 2017b). Interestingly, 5 of remaining upregulated core matrisome proteins can directly interact with fibronectin (Figure 5.8) (Choi et al., 2020; Corona and Blobe, 2021; Schiavinato et al., 2016). Collagen VI is a major ECM protein and contains of three genetically distinct  $\alpha$  chains:  $\alpha 1$  (VI),  $\alpha 2$  (VI) and  $\alpha 3$  (VI) (Cescon et al., 2015). Collagen VI is reported to bind to fibronectin directly by both  $\alpha 1$  (VI) and  $\alpha 2$  (VI) chains (Kuo et al., 1997; Tillet et al., 1994). Moreover, it has been previously shown that the binding between collagen VI and fibronectin contributes to the organization of fibronectin fibres (Sabatelli et al., 2001). The assembly of some ECM proteins has been demonstrated to be dependent on the presence of fibronectin, including collagen I, fibrillin 1 and TSP-1 (Sabatier et al., 2009; Sottile et al., 2007; Tan and Lawler, 2009). Fibrillin 1 and TSP-1 are two upregulated core matrisome proteins identified in the screen. Fibronectin has been shown to bind to the N-terminal domain of TSP-1, contributing to the incorporation of TSP-1 into ECM (Dardik and Lahav, 1999; Tan and Lawler, 2009). The C-terminal of fibrillin 1 is able to interact strongly with fibronectin, leading to the assembly of fibrillin 1 (Sabatier et al., 2009). Fibrillin 1 is known to be required for the deposition of EMILIN-1 by skin fibroblast. Moreover, a strong co-localization is also observed between fibrillin 1 and EMILIN-1 (Schiavinato et al., 2016). However, the binding sites between fibrillin 1 and EMILIN-1 have not been described yet. TNC contains an N-terminal association domain, epidermal growth factor (EGF)-like repeats, fibronectin type III-like repeats (TNfn), and a C-terminal fibrinogen-like globular domain (Choi et al., 2020). TNC has previously been shown to promote the expression of collagen I in foreskin fibroblasts and hepatic stellate cells (Bhattacharyya et al., 2016; Ma et al., 2016). The direct binding between fibronectin and TNfn of TNC has been well understood (To and Midwood, 2011). Lastly, the interaction between TGFBI and fibronectin has been shown to be required for the formation of pancreatic cancer cell-fibronectin adhesion. Although the binding sites between TGFBI and fibronectin are still not known, it is illustrated that the interaction between TGFBI in the ECM and  $\alpha V\beta 5$  can promote the migration of pancreatic cancer cells on fibronectin (Costanza et al., 2019). This may explain the upregulation of  $\alpha V\beta 5$  on biotinylated CDM. Taken together, it is possible that these CDM components are internalized in a complex with fibronectin.

Our findings illustrated that collagen alpha-2(I) chain is specifically detected in the lysates collected from biotinylated CDM. However, it was filtered in the analysis. It was shown that collagen I is present in low abundance in TIF CDM (Kutys et al., 2013b). Therefore, one possible explanation is that the low concentration in CDM results in less collagen I uptake. Kaukonen and colleagues demonstrated that collagen I in TIF CDM is much sparser compared to the corresponding cancer-associated fibroblast (CAF) CDM, which exhibits a denser and more uniform collagen I staining (Kaukonen et al., 2016), consistent with increased deposition and re-organization of collagen I in breast cancer (Insua-Rodríguez and Oskarsson, 2016). Thus, CAF CDM can be used to characterize internalized ECM components in breast cancer cells. In addition, ascorbic acid is known to promote the synthesis of collagen I (Herrmann et al., 2014). Therefore, ascorbic acid could be added every single day, increasing collagen content in TIF CDM. Independent studies have illustrated that fibronectin polymerization contributes to the deposition of collagen I (Li et al., 2003; Sottile et al., 2007). However, it has previously been demonstrated that the interaction between fibronectin and collagen I covers the enzymatic cleavage site on collagen I, protecting collagen I from enzymatic degradation (Paten et al., 2019). Increasing evidence suggests that enzymatic degradation may be an important step in regulating the internalization of collagen I. For example, E64d is known to inhibit extracellular cathepsins as well, whose exocytosis has been shown to be upregulated in breast cancer cells (Uhlman et al., 2017; Withana et al., 2012). Recent findings from the Rainero lab revealed a potential inhibitory effect of E64d on the uptake of high-concentration collagen I matrices. Therefore, the other possible explanation is that decreased extracellular collagen I degradation results in a slower collagen I internalization in TIF CDM.

As the main integrin receptor of fibronectin,  $\alpha 5\beta 1$  is significantly upregulated (Humphries et al., 2006a). The role of  $\alpha 5\beta 1$  in fibronectin internalization has been proved across multiple cell types. In migrating fibroblasts, ubiquitinated  $\alpha 5\beta 1$  is shown to be responsible for fibronectin internalization. Fibronectin-bound  $\alpha 5\beta 1$  complex is trafficked to lysosomes for degradation, contributing to the migration of fibroblasts (Lobert et al., 2010). In ovarian cancer cells,  $\alpha 5\beta 1$ -dependent fibronectin endocytosis is demonstrated to stimulate the activation of mTORC1 (Rainero et al., 2015). In addition to being degraded, internalized fibronectin could be re-secreted back to the plasma membrane, promoting fibrosarcoma cell migration (Sung et al., 2015). So far,  $\alpha 5\beta 1$  is known to be a key regulator in the development

of breast cancer. For example, MDA-MB-231 cells with high  $\alpha 5\beta 1$  expression elevated a 3-fold invasive capacity compared with the cells exhibiting low  $\alpha 5\beta 1$  levels in a 3D system containing fibronectin and collagen I (Mierke et al., 2011). At the same time, we detected significantly higher fibronectin internalization in PyMT#1 cells compared to NMuMG cells (data not shown). Taken together, further studies are required to characterise the role of  $\alpha 5\beta 1$  in controlling fibronectin uptake in breast cancer cells and the contribution of fibronectin uptake in the development of breast cancer. Interestingly, we found that  $\alpha V\beta 1$  is upregulated as well.  $\alpha V\beta 1$  is a receptor for both vitronectin and fibronectin (Marshall et al., 1995). It is suggested that cells preferentially use  $\alpha 5\beta 1$ , rather than  $\alpha V\beta 1$ , to bind to fibronectin (Danen et al., 2002). However, there is increasing evidence suggesting that  $\alpha V\beta 1$  may act as a co-operator with  $\alpha 5\beta 1$ , promoting cell spreading on fibronectin (Bharadwaj et al., 2017; Marshall et al., 1995). Similarly, It has been previously demonstrated that  $\alpha V\beta 5$  contributes to the adhesion and spreading of breast cancer cells on fibronectin (Bartsch et al., 2003; Park and Helfman, 2019). Altogether, it is possible that the high abundance fibronectin in TIF CDM can induce  $\alpha V\beta 1$  and  $\alpha V\beta 5$  activation and internalization, facilitating the formation of  $\alpha 5\beta 1$ -dependent cell adhesion. More studies are needed to check the expression of  $\alpha V\beta 1$   $\alpha V\beta 5$  in MDA-MB-231 cells on TIF CDM. Both  $\alpha 2\beta 1$  and  $\alpha 11\beta 1$  are known as collagen-binding integrins (Humphries et al., 2006a). Ligands for  $\alpha 2\beta 1$  integrin include collagen I, III, IV, V and XI, as well as collagens XVI and XXIII (Zeltz and Gullberg, 2016). It has been demonstrated that  $\alpha 2\beta 1$  contributes to the uptake of collagen I in fibroblasts (Arora et al., 2000). Moreover, our results in chapter 3 suggest a role of  $\alpha 2\beta 1$  in controlling collagen I internalization in MDA-MB-231 cells. These may explain the upregulation of  $\alpha 2\beta 1$  on biotinylated CDM. At the same time, these data also support our hypothesis that upregulated collagen VI on biotinylated CDM is internalized by binding to fibronectin instead of by an integrin-dependent pathway. Currently, the role of  $\alpha 11\beta 1$  in breast cancer is poorly understood because its expression is primarily restricted to stromal cells such as fibroblasts and mesenchymal stem cells (Saby et al., 2019). Further work is needed to find the reason why  $\alpha 11\beta 1$  integrin is upregulated on biotinylated CDM in MDA-MB-231 cells. Laminin subunit- $\beta 3$ , one of the chains for laminin-332 (Baba et al., 2008), is detected in our mass spectrometry results. At the same time, its main receptor,  $\alpha 3\beta 1$ , is upregulated on biotinylated CDM. So far, our findings in chapter 3 suggest a role of  $\alpha 2\beta 1$  in regulating laminin-111 uptake. Further studies are required to characterize the mechanisms of laminin-332 internalization in breast cancer cells.

It has been previously shown that  $\beta 1$  integrin could be internalized via a clathrin-dependent pathway (Arjonen et al., 2012). At the same time, there is increasing evidence suggesting that clathrin-dependent  $\beta 1$  integrin endocytosis contributes to the disassembly of focal adhesions (FAs) (Chao and Kunz, 2009; Ezratty et al., 2009). Consistently, our mass spectrometry results illustrated that three of the most important scaffold proteins in FAs, vinculin, paxillin and actinin, are strongly upregulated in the lysates collected from biotinylated CDM (Nagano et al., 2012). Moreover, calpain is identified to be upregulated as well, which can promote the turnover of FAs by cleaving multiple FA-related proteins including talin and paxillin (Nagano et al., 2012). Furthermore, the AP-2 complex is detected on biotinylated CDM specifically; AP-2 has been shown to be an essential adaptor for the disassembly of FAs, mediated by clathrin-dependent integrin endocytosis (Ezratty et al., 2009). Interestingly, the Ivaska lab illustrated that AP-2 was required for the internalization of  $\alpha 2\beta 1$  (De Franceschi et al., 2016), supporting the upregulation of  $\alpha 2\beta 1$  on biotinylated CDM. Collectively, our findings suggest that integrins are the major receptors responsible for the internalization of CDM in breast cancer cells via a clathrin-mediated pathway accompanying the turnover of FAs.

Label-free approach to relative quantification in proteomics have been widely used since no additional chemistries or sample preparation steps are needed. However, this is an inherently non-quantitative method (Asara et al., 2008). Thus, at least three more biological replicates are required in the future. Moreover, it is possible to assess the internalized CDM components quantitatively combining stable isotope amino acids (SILAC) in cell culture-based proteomics with a biotinylation-based method to identify internalized proteins (Diaz-Vera et al., 2017; Pappireddi et al., 2019). Furthermore, upregulated ECM components and integrins identified in proteomic analysis should be confirmed by either western blotting or immunofluorescence.

## 6 General Discussion

### 6.1 Summary of key findings

The ECM is one of the most important components of the TME and it is in direct contact with tumour cells (Cox, 2021). Increasing evidence illustrates that the uptake of ECM and lysosomal degradation is significantly linked to higher tumor initiation, invasiveness and growth across multiple cancer cells. For example, recent findings from the Rainero lab showed that under amino acid starvation, MDA-MB-231 cells can internalize and degrade CDM, collagen I and Matrigel, contributing to the growth of breast cancer cells (Nazemi et al., 2021). Additionally, the uptake of fibronectin has been shown to stimulate the activation of mTORC1 and promote ovarian cancer cell invasion (Rainero et al., 2015). In this study, we characterized ECM components internalization in breast cancer cells and the receptors involved in this process using two different but complementary techniques. We demonstrated that collagen I and laminin can be internalized in breast cancer cells in a  $\alpha 2\beta 1$ -dependent manner. At the same time, internalized ECM components were delivered to late endosomes/lysosomes for degradation, as the presence of the lysosomal inhibitor E64d led to significant accumulation of internalized ECM. These findings were confirmed by imaging-based ECM internalization assays and mass spectrometry-based proteomics. Moreover, we revealed that the interactions between ECM components and  $\alpha 2\beta 1$  led to the endocytosis of  $\alpha 2\beta 1$  in breast cancer cells. Furthermore, we illustrated the potential effects of this  $\alpha 2\beta 1$  integrin-dependent ECM uptake in regulating breast cancer cell migration and invasion. We found that the inhibition of  $\alpha 2\beta 1$  resulted in a significant decrease both in breast cancer cell migration on CDM and invasion in through a 3D mixture of collagen I and Matrigel. Hence, we hypothesized that the endocytosis of collagen I and laminin might be able to promote the migration and invasion of breast cancer cells either by regulating the activation of  $\alpha 2\beta 1$  integrin-specific signalling or  $\alpha 2\beta 1$  trafficking (Figure 6.1). On the one hand, it has been illustrated that the cytoplasmic domain of collagen I-bound  $\alpha 2$  subunit is able to mediate the activation p38 MAPK signalling (Ivaska et al., 1999b), leading to a migratory phenotype (Klekotka et al., 2001). Similarly, a recent study illustrated that the activation of p38 MAPK signalling mediated by collagen I binding is necessary for the invasion of prostate cancer cells (Ojalill et al., 2018). Interestingly, recent findings from the Rainero lab implicated p38 MAPK signalling in the

regulation of ECM internalization, suggesting the existence of a potential feedforward loop supporting ECM internalization and cell migration. On the other hand,  $\alpha 2\beta 1$  endocytosis may promote focal adhesion turnover, thereby stimulating cell migration and invasion. In addition, increased active  $\alpha 2\beta 1$  in cells might be recycled to the cell front, facilitating the migration and invasion of breast cancer cells. Finally, the endocytosis and degradation of ECM components may be involved in promoting nutrient signalling and energy production, required to support invasion cell migration. More studies are required to elucidate the mechanism through which  $\alpha 2\beta 1$ -dependent pathway contributes to the migration and invasion of breast cancer cells. In addition, we revealed that the internalization of laminin, but not collagen I, was promoted in G1 phase in breast cancer cells. This cell cycle-dependent ECM endocytosis might be mediated by  $\beta 1$  integrin, contributing to the activation of mTORC1 in G1. However, further studies are necessary to characterise this process.

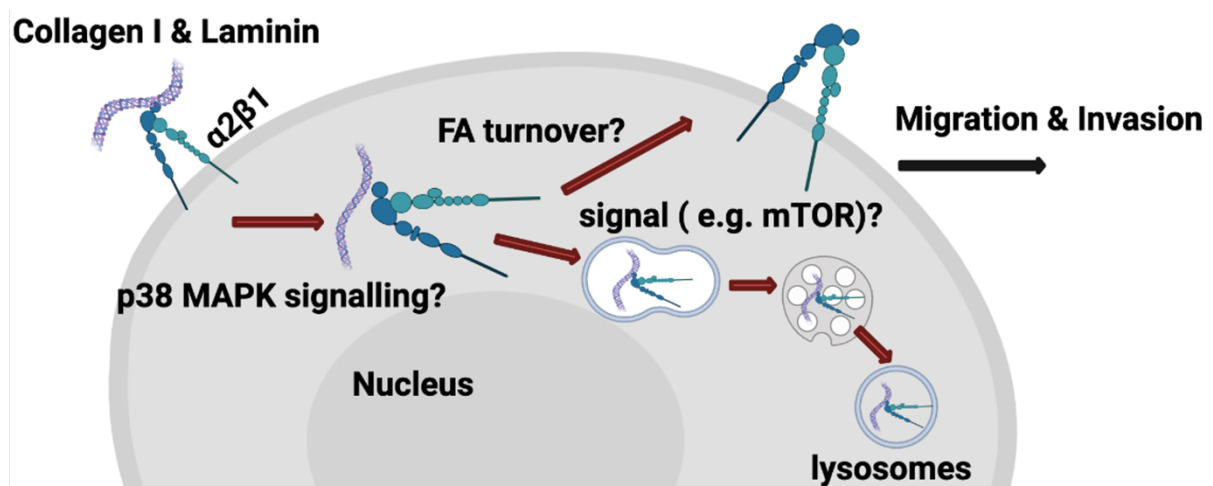


**Figure 6.1. Mechanism of  $\alpha 2\beta 1$ -dependent ECM internalization in regulating breast cancer cell migration and invasion.**  $\alpha 2\beta 1$  is responsible for the internalization collagen I and Matrigel/laminin. Internalized ECM components are delivered to lysosomes for degradation. This process contributes to the migration and invasion of breast cancer cells either by inducing  $\alpha 2\beta 1$  trafficking or p38 signaling activation. Image is 'Created with BioRender.com'.

## 6.2 The identification of internalized ECM components in breast cancer cells

We used imaging-based approaches in chapter 3 to compare the endocytosis of different ECM components between normal mammary epithelial cells and invasive breast cancer cells. We showed that in the presence of E64d, the internalization of Matrigel/laminin, but not collagen

I, was upregulated in breast cancer cells. In chapter 5, we also used mass spectrometry-based proteomics to identify internalized CDM components in MDA-MB-231 cells and MCF10A cells. Here more biotinylated bands were detected in the total cell lysates collected from MDA-MB-231 cells using western blotting, suggesting that more CDM components were internalized in invasive breast cancer cells compared to normal mammary epithelial cells. At the same time, SILAC-based or isotope-coded affinity tags (ICAT)-based proteomics could be used to confirm the upregulated laminin internalization in breast cancer cells in the future.

Integrin  $\alpha 2\beta 1$  has been implicated as a key regulator in the development and progression of different cancer types (Adorno-Cruz and Liu, 2019). However, there is conflicting evidence for the role of  $\alpha 2\beta 1$  in breast cancer. Some studies suggest that the loss of  $\alpha 2\beta 1$  facilitates breast cancer metastasis (Ramirez et al., 2011), whereas other studies show that high expression of  $\alpha 2\beta 1$  correlates with a metastatic phenotype (Zuo et al., 2019). For example, It has been illustrated that  $\alpha 2\beta 1$  integrin-mediated activation of p38 MAPK can enhance the production of MMP-13, contributing to the migration of MDA-MB-231 cells (Ibaragi et al., 2011). Our data demonstrated that the inhibition of  $\alpha 2\beta 1$  or decreased  $\alpha 2\beta 1$  expression strongly reduced the internalization of collagen I and Matrigel. At the same time, integrin  $\alpha 2\beta 1$  was detected to be upregulated on biotinylated CDM as well. These findings indicate that  $\alpha 2\beta 1$  is required for the endocytosis of ECM components in MDA-MB-231 cells. Additionally, our results suggest that the binding between  $\alpha 2\beta 1$  and collagen I/Matrigel promotes the activation and uptake of  $\alpha 2\beta 1$  integrin. However, we were not able to check whether internalized  $\alpha 2\beta 1$  was in active conformation due to the lack of an antibody specifically recognizing activated  $\alpha 2$  integrin only. However, it would be possible to measure the co-localization between internalized  $\alpha 2$  and active  $\beta 1$  in the presence of collagen I or Matrigel in MDA-MB-231 cells. In addition,  $\alpha 5\beta 1$  was detected to be significantly upregulated on biotinylated CDM as well. Consistently, its main ECM ligand, fibronectin, was found in the screen as well. Interestingly, we measured the internalization of fibronectin using imaging-based approaches in normal mouse mammary epithelial cells and invasive breast cancer PyMT#1 cells, and we detected significantly higher fibronectin internalization in PyMT#1 cells (data not shown). Collectively, further studies are necessary to elucidate the  $\alpha 5\beta 1$  and the contribution of fibronectin uptake in breast cancer cells.

In this study, TIF CDM was used to perform CDM endocytosis assays and mass spectrometry-based proteomics. However, CAFs are considered as the main cell type in the TME contributing to the synthesis and remodelling of the ECM that surround breast tumours. The composition of TIF CDM and CAF CDM has been identified by mass spectrometry (Hernandez-Fernaud et al., 2017), demonstrating that the expression of collagens and LOX proteins were upregulated in CAF CDM, contributing to the cross-linking and re-alignment of collagen (Pankova et al., 2016). In addition, fibronectin derived from CAFs is known to be organized in parallel lines aligned with each other, whereas fibronectin in TIF CDM is like a mesh (Erdogan et al., 2017). These findings suggest that CDM derived from CAFs can mimic more features of *in vivo* matrices around breast cancers. Hence, further studies are needed to characterize the internalized CAF CDM components in breast cancer cells. However, it is key to note that several factors, including ECM structure and stiffness, may affect ECM uptake. For example, increased proteolytic degradation may be required for the internalization of CAF CDM.

We performed imaging-based ECM internalization assays and proteomics in the presence of E64d. We found that internalized ECM proteins accumulated in late endosomes/lysosomes. However, it is important to consider that the presence of E64d may affect cellular functions. For example, the extracellular degradation of collagen I may be decreased, leading to a slower collagen I internalization rate (Podgorski et al., 2005). Thus, cell migration and invasion assays were performed without E64d treatment. Our data show that  $\alpha 2\beta 1$  is an important regulator in breast cancer cell migration and invasion. However, we did not link the  $\alpha 2\beta 1$ -dependent ECM endocytosis with the migration and invasion of breast cancer cells directly. One possible explanation is that  $\alpha 2\beta 1$ -dependent ECM intracellular degradation results in extracellular ECM remodelling, in a similar mechanism to MMP-mediated ECM extracellular degradation thereby regulating the migration and invasion of breast cancer cells, upon breaking the BM structure and forming 'micro-tracks' (Das et al., 2017; Li et al., 2017). Moreover, it is possible that ECM binding leads to the activation of p38 MAPK signalling (Ivaska et al., 1999b), which in turn contributes to ECM uptake. Furthermore, a recent study illustrated that MDA-MB-231 cells on higher ECM density display higher ATP production, since more energy are needed for their migration (Zanotelli et al., 2018). Therefore, these data raise the possibility that collagen I and Matrigel are internalized and degraded to be used as a fuel source in the tricarboxylic

acid (TCA) cycle, contributing to the production of ATP. Recently, invasion assays in the presence of pHrodo-labelled ECM have been developed in an attempt to bridge the gap between ECM internalization and breast cancer cell invasion. Additionally, we found that green cell tracker at the concentration used in this study exhibited an inhibitory effect on the invasion of breast cancer cell invasion. Thus, GFP-expressing MDA-MB-231 cells have been generated. Moreover, we tried to image DQ-collagen I internalization in invading breast cancer cells using confocal microscopy. However, the concentration of gel mixture we used in this study is too thick to image single cells in a high resolution (60X NA 1.4 oil immersion objective). Hence, Airyscan microscopy can be used in the following studies to measure the uptake of pHrodo-labelled ECM components and GFP-expressing breast cancer cells invasion in 3D system.

### **6.3 Cell cycle-dependent ECM uptake in breast cancer cells**

In order to confirm that what we observed was cell cycle-dependent, we used three different approaches to synchronize cells in G1 since the potential side effects induced by each method (Ligasová and Koberna, 2021). For example, our findings demonstrate that even a short-term serum starvation could affect  $\beta 1$  integrin trafficking. Moreover, FUCCI-MDA-MB-231 cells, a powerful model in cell cycle study, were used in this work as well. However, we noticed that the growth of FUCCI-MDA-MB-231 cells was slower than MDA-MB-231 cells in general, one potential factor which might affect ECM uptake. Here we illustrated that the uptake of laminin, but not collagen I, was promoted in G1 in both human and mouse invasive breast cancer cells. At the same time, we showed that in the presence of Matrigel, the internalization of  $\beta 1$  was upregulated in G1, suggesting the role of  $\beta 1$  in this cell cycle-dependent laminin endocytosis process. However, we did not measure the expression of different  $\alpha$  integrin subunits in G1 in breast cancer cells. We have illustrated that  $\alpha 2\beta 1$  is required for the endocytosis of laminin and collagen I. Interestingly, a recent study illustrated that the inhibition of  $\alpha 2\beta 1$  in prostate cancer cells resulted in G1 cell cycle arrest (Salemi et al., 2021). Therefore, more studies are necessary to characterize the potential contribution of  $\alpha 2\beta 1$  in controlling the cell cycle of breast cancer cells in the presence of Matrigel/laminin.

We have illustrated that integrin-dependent ECM internalization is a key player in regulating breast cancer cell migration and invasion. At the same time, increasing evidence suggests that cancer cells in G1 have a higher invasive capacity compared to the cells in other cell cycle stages (Yano et al., 2014), particularly breast cancer cells. Using FUCCI-MDA-MB-231 cells, the Gligorijevic lab recently illustrated the coordination of cell cycle progression with the ECM extracellular degradation. They showed that MT1-MMP is preferentially recruited to invadopodia in G1, promoting invadopodia maturation and collagen I degradation, as well as increasing MDA-MB-231 cell invasion (Bayarmagnai et al., 2019b). Thus, it is possible that not only upregulated ECM extracellular degradation, but also intracellular degradation in G1 can contribute to the invasion of breast cancer cells. In addition, there is a large body of evidence revealing the role of mTOR in regulating cell growth as a checkpoint in the late G1. The mTOR-dependent checkpoint that can sense whether there is sufficient nutrition for a cell to double size prior to committing to replicate the genome and divide. Increased mTOR signalling is able to suppress TGF $\beta$  signals, which suppress cell cycle progression in late G1 and increase the levels of cyclin E-CDK2 inhibitor p27 (Cuyàs et al., 2014). The studies from Blenis lab showed that inhibiting mTOR leads to arrest in late G1. Moreover, arrested cells are smaller than the control cells (Fingar et al., 2004, 2002), consistent with a role of mTOR as a nutritional sensor that restricts cell growth without sufficient nutrients (Foster et al., 2010). Furthermore, it has been demonstrated that internalized ECM components could enhance mTORC1 activity (Muranen et al., 2017; Nazemi et al., 2021; Rainero et al., 2015). Therefore, it is possible to speculate that the high proliferation rate of breast cancer cells leads to increased laminin uptake in G1 to sustain mTOR signalling and progress through the late G1 checkpoint. Consistently, we showed that the endocytosis of Matrigel in normal mammary epithelial is not affected by the cell cycle. In addition, increased synthesis of nucleotide in G1 phase is required for cell proliferation (Lane and Fan, 2015). Recent data from the Rainero lab showed that metabolites derived from ECM internalization and degradation may feed into nucleotide synthesis pathways (Nazemi, data not shown). Hence, these findings raise the possibility that increased Matrigel endocytosis in G1 may contribute to the synthesis of nucleotide in invasive breast cancer cells.

To date, three CDK4/6 inhibitors, Palbociclib and abemaciclib, have received FDA approval for the treatment of metastatic breast cancers (Du et al., 2020). At the same time, since

CDK4/6 pathway could intersect with several key mitogenic signalling pathways, the combination of CDK4/6 inhibitors with other therapies has been tested as well. For example, the combination of Pd and endocrine therapy has been used in the treatment of ER-positive breast cancers (Goel et al., 2018). However, a number of side effects have been observed after CDK4/6 inhibitor treatment, such as increased autophagy (Valenzuela et al., 2017; Vijayaraghavan et al., 2017) and upregulated anti-tumor immune response (Goel et al., 2017). Here we demonstrated that the internalization of ECM is upregulated in G1, suggesting a potential role of this cell cycle-dependent ECM endocytosis in regulating the activation of mTORC1. Although the contribution of mTOR signalling in these unexpected biological phenotypes is still poorly understood, our results suggest that the ECM might be one of the factors to be considered in breast cancer therapy targeted to the cell cycle.

## 6.4 Therapeutic opportunities

Increasing evidence from experimental studies on the contribution of the ECM in breast cancer development and progression suggests that ECM components and their receptors may be promising therapeutic targets in the treatment of breast cancer. For example, increased collagen crosslinking and remodelling is known to promote breast cancer metastatic spread. Inhibitors targeting to collagen crosslinking enzymes of the LOX family have been developed for clinical use (Cox and Epler, 2011). Moreover, MMPs are considered as therapeutic targets against breast cancer as well. DX-2400, an inhibitor of MMP14, has been tested in a murine model of breast cancer. DX-2400 not only can inhibit the growth of primary tumour but also impairs the growth when combined with radiotherapy (Ager et al., 2015). Furthermore, several inhibitors targeting integrins have been tested in breast cancer treatment. For instance, Intetumumab, a  $\alpha v\beta 3$  integrin blocking antibody, has been demonstrated to inhibit metastasis and increases survival in a rat model of breast cancer metastasis to the brain (Wu et al., 2012).

Although  $\alpha 2\beta 1$  integrin is illustrated to be a key receptor for metastasis of breast cancer cells to the liver and bone (Moritz et al., 2021; Naci, 2015), no  $\alpha 2\beta 1$  inhibitor has been proved for clinical use. Additionally, increasing studies demonstrate that  $\alpha 2\beta 1$  could be involved in chemoresistance. For example, adhesion of MDA-MB-231 cells to collagen I via  $\alpha 2\beta 1$  has been

proved to inhibit apoptosis induced by both paclitaxel and vincristine, two chemotherapeutic agents which have been used in the clinical treatment of breast cancer (Aoudjit and Vuori, 2001). We demonstrated that  $\alpha 2\beta 1$  integrin is an important player in regulating breast cancer cell migration and invasion, suggesting that  $\alpha 2\beta 1$  can be one of the novel therapeutic targets in the treatment of breast cancer in the future.

## 6.5 Conclusion and future directions

This study reveals the role of ECM internalization on breast cancer cell migration and invasion, as well as an unexpected cell cycle-dependent ECM endocytosis. At the same time, this work has raised a number of questions about the contribution of ECM uptake which are important for further studies. Here I suggest the following experiments for the continuation of this work:

### Related to Chapter 3:

- Characterize whether  $\alpha 2\beta 1$  integrin can regulate the migration and invasion of breast cancer cells on ECM by triggering p38 MAPK activation. For this, the activation of p38 MAPK could be analysed by western blotting in MDA-MB-231 cells seeded on both collagen I and Matrigel. The cell migration and invasion assays could be performed in the presence of p38 inhibitor (SB203580).
- Fully understand the role of  $\alpha 2\beta 1$ -dependent ECM internalization in the activation of p38 MAPK by decreasing the endocytosis of ECM (e.g., Rab21 knockdown). In addition, assess the internalization of ECM with p38 inhibitor in MDA-MB-231 cells.
- Optimise cell migration and invasion assays on pHrodo-labelled CDM/matrix. This can be used to bridge the endocytosis of ECM and breast cancer cell migration/invasion in a direct manner.

### Related to Chapter 4:

- The distribution of focal adhesion complexes should be investigated in synchronized breast cancer cells on Matrigel, which allows us to assess whether upregulated laminin endocytosis in G1 phase is induced by the turnover of focal adhesions.
- The expression of different  $\alpha$  integrin subunits could be validated in synchronized cells on Matrigel, defining the receptors controlling cell cycle-dependent ECM uptake.

- Understand the related role of cell cycle-dependent ECM endocytosis in breast cancer through sorting different stages of FUCCI-MDA-MB-231 cells by FACS and performing migration assay on CDM.

**Related to Chapter 5:**

- Compare the internalization of CDM between normal mammary epithelial cells and invasive breast cancer cells to investigate whether breast cancer cells could uptake different ECM components.
- Assess the internalized CDM components in normal mammary epithelial and invasive breast cancer cells quantitatively through combining SILAC-based proteomics with a biotinylated-based method. This could be further compared to our findings in chapter 3 in this study.
- Perform mass spectrometry-based proteomics on CAF CDM to assess whether breast cancer cells can uptake different components due to the remodelling of ECM.

Taken together, the findings presented in this study suggest that  $\alpha 2\beta 1$ -dependent collagen I and laminin endocytosis contribute to breast cancer cell migration and invasion. Additionally, we characterize that the uptake of ECM is cell cycle dependent. This process may be required for the activation of mTORC1 in G1 breast cancer cells. The ECM is one of the most important components in TME. For this reason, studies that target to the ECM in breast cancer research are necessary and poised to become the norm of the field. I hope the findings in this work will be beneficial for the development of breast cancer therapy in the future.

## 7 References

- Adorno-Cruz, V., Liu, H., 2019. Regulation and functions of integrin  $\alpha 2$  in cell adhesion and disease. *Genes & Diseases* 6, 16–24. <https://doi.org/10.1016/j.gendis.2018.12.003>
- Ager, E.I., Kozin, S.V., Kirkpatrick, N.D., Seano, G., Kodack, D.P., Askoxylakis, V., Huang, Y., Goel, S., Snuderl, M., Muzikansky, A., Finkelstein, D.M., Dransfield, D.T., Devy, L., Boucher, Y., Fukumura, D., Jain, R.K., 2015. Blockade of MMP14 Activity in Murine Breast Carcinomas: Implications for Macrophages, Vessels, and Radiotherapy. *JNCI: Journal of the National Cancer Institute* 107. <https://doi.org/10.1093/jnci/djv017>
- Aghababazadeh, M., Kerachian, M.A., 2014. Cell Fasting: Cellular Response and Application of Serum Starvation. *Journal of Nutrition, Fasting and Health* 2, 147–150. <https://doi.org/10.22038/jfh.2014.3928>
- Ahmadiankia, N., 2020. In vitro and in vivo studies of cancer cell behavior under nutrient deprivation. *Cell Biol Int* 44, 1588–1597. <https://doi.org/10.1002/cbin.11368>
- Ahmadiantehrani, S., London, S.E., 2017. Bidirectional manipulation of mTOR signaling disrupts socially mediated vocal learning in juvenile songbirds. *Proc Natl Acad Sci USA* 114, 9463–9468. <https://doi.org/10.1073/pnas.1701829114>
- Akram, M., Iqbal, M., Daniyal, M., Khan, A.U., 2017. Awareness and current knowledge of breast cancer. *Biol Res* 50, 33. <https://doi.org/10.1186/s40659-017-0140-9>
- Albregues, J., Shields, M.A., Ng, D., Park, C.G., Ambrico, A., Poindexter, M.E., Upadhyay, P., Uyeminami, D.L., Pommier, A., Küttner, V., Bružas, E., Maiorino, L., Bautista, C., Carmona, E.M., Gimotty, P.A., Fearon, D.T., Chang, K., Lyons, S.K., Pinkerton, K.E., Trotman, L.C., Goldberg, M.S., Yeh, J.T.-H., Egeblad, M., 2018. Neutrophil extracellular traps produced during inflammation awaken dormant cancer cells in mice. *Science* 361, eaao4227. <https://doi.org/10.1126/science.aao4227>
- Amin, M.B., Greene, F.L., Edge, S.B., Compton, C.C., Gershenwald, J.E., Brookland, R.K., Meyer, L., Gress, D.M., Byrd, D.R., Winchester, D.P., 2017. The Eighth Edition AJCC Cancer Staging Manual: Continuing to build a bridge from a population-based to a more “personalized” approach to cancer staging. *CA: A Cancer Journal for Clinicians* 67, 93–99. <https://doi.org/10.3322/caac.21388>
- Aoudjit, F., Vuori, K., 2001. Integrin signaling inhibits paclitaxel-induced apoptosis in breast cancer cells. *Oncogene* 20, 4995–5004. <https://doi.org/10.1038/sj.onc.1204554>
- Apostolou, P., Papatotiriou, I., 2017. Current perspectives on CHEK2 mutations in breast cancer. *Breast Cancer (Dove Med Press)* 9, 331–335. <https://doi.org/10.2147/BCTT.S111394>
- Arjonen, A., Alanko, J., Veltel, S., Ivaska, J., 2012. Distinct Recycling of Active and Inactive  $\beta 1$  Integrins. *Traffic* 13, 610–625. <https://doi.org/10.1111/j.1600-0854.2012.01327.x>
- Arora, P.D., Manolson, M.F., Downey, G.P., Sodek, J., McCulloch, C.A.G., 2000. A Novel Model System for Characterization of Phagosomal Maturation, Acidification, and Intracellular Collagen Degradation in Fibroblasts. *J. Biol. Chem.* 275, 35432–35441. <https://doi.org/10.1074/jbc.M003221200>
- Arora, P.D., Wang, Y., Bresnick, A., Dawson, J., Janmey, P.A., McCulloch, C.A., 2013. Collagen remodeling by phagocytosis is determined by collagen substrate topology and calcium-dependent interactions of gelsolin with nonmuscle myosin IIA in cell adhesions. *MBoC* 24, 734–747. <https://doi.org/10.1091/mbc.e12-10-0754>
- Asara, J.M., Christofk, H.R., Freimark, L.M., Cantley, L.C., 2008. A label-free quantification method by MS/MS TIC compared to SILAC and spectral counting in a proteomics screen. *PROTEOMICS* 8, 994–999. <https://doi.org/10.1002/pmic.200700426>
- Baba, Y., Iyama, K., Hirashima, K., Nagai, Y., Yoshida, N., Hayashi, N., Miyanari, N., Baba, H., 2008. Laminin-332 promotes the invasion of oesophageal squamous cell carcinoma via PI3K activation. *Br J Cancer* 98, 974–980. <https://doi.org/10.1038/sj.bjc.6604252>
- Baghdadchi, N., 2013. The Effects of Serum Starvation on Cell Cycle Synchronization 10.

- Balanis, N., Wendt, M.K., Schiemann, B.J., Wang, Z., Schiemann, W.P., Carlin, C.R., 2013. Epithelial to Mesenchymal Transition Promotes Breast Cancer Progression via a Fibronectin-dependent STAT3 Signaling Pathway. *J. Biol. Chem.* 288, 17954–17967. <https://doi.org/10.1074/jbc.M113.475277>
- Ballabeni, A., Zamponi, R., Moore, J.K., Helin, K., Kirschner, M.W., 2013. Geminin deploys multiple mechanisms to regulate Cdt1 before cell division thus ensuring the proper execution of DNA replication. *PNAS* 110, E2848–E2853. <https://doi.org/10.1073/pnas.1310677110>
- Barczyk, M., Carracedo, S., Gullberg, D., 2010. Integrins. *Cell Tissue Res* 339, 269–280. <https://doi.org/10.1007/s00441-009-0834-6>
- Barkan, D., Kleinman, H., Simmons, J.L., Asmussen, H., Kamaraju, A.K., Hoenorhoff, M.J., Liu, Z., Costes, S.V., Cho, E.H., Lockett, S., Khanna, C., Chambers, A.F., Green, J.E., 2008. Inhibition of Metastatic Outgrowth From Single Dormant Tumor Cells by Targeting the Cytoskeleton. *Cancer Res* 68, 6241–6250. <https://doi.org/10.1158/0008-5472.CAN-07-6849>
- Barroso-Sousa, R., Metzger-Filho, O., 2016. Differences between invasive lobular and invasive ductal carcinoma of the breast: results and therapeutic implications. *Ther Adv Med Oncol* 8, 261–266. <https://doi.org/10.1177/1758834016644156>
- Bartsch, J.E., Staren, E.D., Appert, H.E., 2003. Adhesion and migration of extracellular matrix-stimulated breast cancer. *Journal of Surgical Research* 110, 287–294. [https://doi.org/10.1016/S0022-4804\(03\)00004-0](https://doi.org/10.1016/S0022-4804(03)00004-0)
- Bass, M.D., Williamson, R.C., Nunan, R.D., Humphries, J.D., Byron, A., Morgan, M.R., Martin, P., Humphries, M.J., 2011. A Syndecan-4 Hair Trigger Initiates Wound Healing through Caveolin- and RhoG-Regulated Integrin Endocytosis. *Developmental Cell* 21, 681–693. <https://doi.org/10.1016/j.devcel.2011.08.007>
- Bayarmagnai, B., Perrin, L., Esmaeili Pourfarhangi, K., Graña, X., Tüzel, E., Gligorijevic, B., 2019a. Invadopodia-mediated ECM degradation is enhanced in the G1 phase of the cell cycle. *J Cell Sci* 132, jcs227116. <https://doi.org/10.1242/jcs.227116>
- Bayarmagnai, B., Perrin, L., Esmaeili Pourfarhangi, K., Graña, X., Tüzel, E., Gligorijevic, B., 2019b. Invadopodia-mediated ECM degradation is enhanced in the G1 phase of the cell cycle. *Journal of Cell Science* 132, jcs227116. <https://doi.org/10.1242/jcs.227116>
- Bharadwaj, M., Strohmeier, N., Colo, G.P., Helenius, J., Beerenwinkel, N., Schiller, H.B., Fässler, R., Müller, D.J., 2017.  $\alpha$ V-class integrins exert dual roles on  $\alpha$ 5 $\beta$ 1 integrins to strengthen adhesion to fibronectin. *Nat Commun* 8, 14348. <https://doi.org/10.1038/ncomms14348>
- Bhattacharyya, S., Wang, W., Morales-Nebreda, L., Feng, G., Wu, M., Zhou, X., Lafyatis, R., Lee, J., Hinchcliff, M., Feghali-Bostwick, C., Lakota, K., Budinger, G.R.S., Raparia, K., Tamaki, Z., Varga, J., 2016. Tenascin-C drives persistence of organ fibrosis. *Nat Commun* 7, 11703. <https://doi.org/10.1038/ncomms11703>
- Bierie, B., Pierce, S.E., Kroeger, C., Stover, D.G., Pattabiraman, D.R., Thiru, P., Liu Donaher, J., Reinhardt, F., Chaffer, C.L., Keckesova, Z., Weinberg, R.A., 2017. Integrin- $\beta$ 4 identifies cancer stem cell-enriched populations of partially mesenchymal carcinoma cells. *Proc Natl Acad Sci USA* 114, E2337–E2346. <https://doi.org/10.1073/pnas.1618298114>
- Bisanz, K., Yu, J., Edlund, M., Spohn, B., Hung, M.-C., Chung, L.W.K., Hsieh, C.-L., 2005. Targeting ECM–Integrin Interaction with Liposome-Encapsulated Small Interfering RNAs Inhibits the Growth of Human Prostate Cancer in a Bone Xenograft Imaging Model. *Molecular Therapy* 12, 634–643. <https://doi.org/10.1016/j.ymthe.2005.05.012>
- Bombonati, A., Sgroi, D.C., 2011. The molecular pathology of breast cancer progression. *J. Pathol.* 223, 308–318. <https://doi.org/10.1002/path.2808>
- Bonnans, C., Chou, J., Werb, Z., 2014. Remodelling the extracellular matrix in development and disease. *Nat Rev Mol Cell Biol* 15, 786–801. <https://doi.org/10.1038/nrm3904>
- Boopathy, G.T.K., Hong, W., 2019. Role of Hippo Pathway-YAP/TAZ Signaling in Angiogenesis. *Front. Cell Dev. Biol.* 7. <https://doi.org/10.3389/fcell.2019.00049>

- Bridgewater, R.E., Norman, J.C., Caswell, P.T., 2012. Integrin trafficking at a glance. *Journal of Cell Science* 125, 3695–3701. <https://doi.org/10.1242/jcs.095810>
- Carbognin, L., Miglietta, F., Paris, I., Dieci, M.V., 2019. Prognostic and Predictive Implications of PTEN in Breast Cancer: Unfulfilled Promises but Intriguing Perspectives. *Cancers (Basel)* 11. <https://doi.org/10.3390/cancers11091401>
- Castro, G.D., Castro, J.A., 2014. Alcohol drinking and mammary cancer: Pathogenesis and potential dietary preventive alternatives. *World J Clin Oncol* 5, 713–729. <https://doi.org/10.5306/wjco.v5.i4.713>
- Caswell, P., Norman, J., 2008. Endocytic transport of integrins during cell migration and invasion. *Trends in Cell Biology* 18, 257–263. <https://doi.org/10.1016/j.tcb.2008.03.004>
- Caswell, P.T., Chan, M., Lindsay, A.J., McCaffrey, M.W., Boettiger, D., Norman, J.C., 2008. Rab-coupling protein coordinates recycling of  $\alpha 5\beta 1$  integrin and EGFR1 to promote cell migration in 3D microenvironments. *The Journal of Cell Biology* 183, 143–155. <https://doi.org/10.1083/jcb.200804140>
- Cavo, M., Fato, M., Peñuela, L., Beltrame, F., Raiteri, R., Scaglione, S., 2016. Microenvironment complexity and matrix stiffness regulate breast cancer cell activity in a 3D in vitro model. *Sci Rep* 6, 35367. <https://doi.org/10.1038/srep35367>
- Cerami, E., Gao, J., Dogrusoz, U., Gross, B.E., Sumer, S.O., Aksoy, B.A., Jacobsen, A., Byrne, C.J., Heuer, M.L., Larsson, E., Antipin, Y., Reva, B., Goldberg, A.P., Sander, C., Schultz, N., 2012. The cBio Cancer Genomics Portal: An open platform for exploring multidimensional cancer genomics data. *Cancer Discovery* 2, 401–404. <https://doi.org/10.1158/2159-8290.CD-12-0095>
- Cescon, M., Gattazzo, F., Chen, P., Bonaldo, P., 2015. Collagen VI at a glance. *Journal of Cell Science* jcs.169748. <https://doi.org/10.1242/jcs.169748>
- Chang, J., Chaudhuri, O., 2019. Beyond proteases: Basement membrane mechanics and cancer invasion. *Journal of Cell Biology* 218, 2456–2469. <https://doi.org/10.1083/jcb.201903066>
- Chao, W.-T., Kunz, J., 2009. Focal adhesion disassembly requires clathrin-dependent endocytosis of integrins. *FEBS Letters* 583, 1337–1343. <https://doi.org/10.1016/j.febslet.2009.03.037>
- Chen, G., Deng, X., 2018. Cell Synchronization by Double Thymidine Block. *Bio Protoc* 8. <https://doi.org/10.21769/BioProtoc.2994>
- Cheng, X.-T., Xie, Y.-X., Zhou, B., Huang, N., Farfel-Becker, T., Sheng, Z.-H., 2018. Revisiting LAMP1 as a marker for degradative autophagy-lysosomal organelles in the nervous system. *Autophagy* 14, 1472–1474. <https://doi.org/10.1080/15548627.2018.1482147>
- Chivers, C.E., Crozat, E., Chu, C., Moy, V.T., Sherratt, D.J., Howarth, M., 2010. A streptavidin variant with slower biotin dissociation and increased mechanostability. *Nat Methods* 7, 391–393. <https://doi.org/10.1038/nmeth.1450>
- Choi, Y.E., Song, M.J., Hara, M., Imanaka-Yoshida, K., Lee, D.H., Chung, J.H., Lee, S.-T., 2020. Effects of Tenascin C on the Integrity of Extracellular Matrix and Skin Aging. *Int J Mol Sci* 21, 8693. <https://doi.org/10.3390/ijms21228693>
- Christoforides, C., Rainero, E., Brown, K.K., Norman, J.C., Toker, A., 2012. PKD Controls  $\alpha v\beta 3$  Integrin Recycling and Tumor Cell Invasive Migration Through its Substrate Rabaptin-5. *Dev Cell* 23, 560–572. <https://doi.org/10.1016/j.devcel.2012.08.008>
- Ciruelos Gil, E.M., 2014. Targeting the PI3K/AKT/mTOR pathway in estrogen receptor-positive breast cancer. *Cancer Treatment Reviews* 40, 862–871. <https://doi.org/10.1016/j.ctrv.2014.03.004>
- Commisso, C., Davidson, S.M., Soydaner-Azeloglu, R.G., Parker, S.J., Kamphorst, J.J., Hackett, S., Grabocka, E., Nofal, M., Drebin, J.A., Thompson, C.B., Rabinowitz, J.D., Metallo, C.M., Vander Heiden, M.G., Bar-Sagi, D., 2013. Macropinocytosis of protein is an amino acid supply route in Ras-transformed cells. *Nature* 497, 633–637. <https://doi.org/10.1038/nature12138>
- Commisso, C., Flinn, R.J., Bar-Sagi, D., 2014. Determining the macropinocytic index of cells through a quantitative image-based assay. *Nat Protoc* 9, 182–192. <https://doi.org/10.1038/nprot.2014.004>

- Conklin, M.W., Eickhoff, J.C., Riching, K.M., Pehlke, C.A., Eliceiri, K.W., Provenzano, P.P., Friedl, A., Keely, P.J., 2011. Aligned Collagen Is a Prognostic Signature for Survival in Human Breast Carcinoma. *The American Journal of Pathology* 178, 1221–1232. <https://doi.org/10.1016/j.ajpath.2010.11.076>
- Conrad, K.S., Cheng, T.-W., Ysselstein, D., Heybrock, S., Hoth, L.R., Chrunyk, B.A., am Ende, C.W., Krainc, D., Schwake, M., Saftig, P., Liu, S., Qiu, X., Ehlers, M.D., 2017. Lysosomal integral membrane protein-2 as a phospholipid receptor revealed by biophysical and cellular studies. *Nat Commun* 8, 1908. <https://doi.org/10.1038/s41467-017-02044-8>
- Coopman, P.J., Thomas, D.M., Gehlsen, K.R., Mueller, S.C., 1996. Integrin alpha 3 beta 1 participates in the phagocytosis of extracellular matrix molecules by human breast cancer cells. *Mol Biol Cell* 7, 1789–1804.
- Corona, A., Globe, G.C., 2021. The role of the extracellular matrix protein TGFBI in cancer. *Cellular Signalling* 84, 110028. <https://doi.org/10.1016/j.cellsig.2021.110028>
- Costa, E.C., Moreira, A.F., de Melo-Diogo, D., Gaspar, V.M., Carvalho, M.P., Correia, I.J., 2016. 3D tumor spheroids: an overview on the tools and techniques used for their analysis. *Biotechnology Advances* 34, 1427–1441. <https://doi.org/10.1016/j.biotechadv.2016.11.002>
- Costanza, B., Rademaker, G., Tiamiou, A., De Tullio, P., Leenders, J., Blomme, A., Bellier, J., Bianchi, E., Turtoi, A., Delvenne, P., Bellahcène, A., Peulen, O., Castronovo, V., 2019. Transforming growth factor beta-induced, an extracellular matrix interacting protein, enhances glycolysis and promotes pancreatic cancer cell migration. *Int. J. Cancer* 145, 1570–1584. <https://doi.org/10.1002/ijc.32247>
- Cox, T.R., 2021. The matrix in cancer. *Nat Rev Cancer* 21, 217–238. <https://doi.org/10.1038/s41568-020-00329-7>
- Cox, T.R., Erler, J.T., 2011. Remodeling and homeostasis of the extracellular matrix: implications for fibrotic diseases and cancer. *Disease Models & Mechanisms* 4, 165–178. <https://doi.org/10.1242/dmm.004077>
- Curino, A.C., Engelholm, L.H., Yamada, S.S., Holmbeck, K., Lund, L.R., Molinolo, A.A., Behrendt, N., Nielsen, B.S., Bugge, T.H., 2005. Intracellular collagen degradation mediated by uPARAP/Endo180 is a major pathway of extracellular matrix turnover during malignancy. *Journal of Cell Biology* 169, 977–985. <https://doi.org/10.1083/jcb.200411153>
- Cuyàs, E., Corominas-Faja, B., Joven, J., Menendez, J.A., 2014. Cell Cycle Regulation by the Nutrient-Sensing Mammalian Target of Rapamycin (mTOR) Pathway, in: Noguchi, E., Gadaleta, M.C. (Eds.), *Cell Cycle Control: Mechanisms and Protocols, Methods in Molecular Biology*. Springer, New York, NY, pp. 113–144. [https://doi.org/10.1007/978-1-4939-0888-2\\_7](https://doi.org/10.1007/978-1-4939-0888-2_7)
- Dai, X., Li, T., Bai, Z., Yang, Y., Liu, X., Zhan, J., Shi, B., 2015. Breast cancer intrinsic subtype classification, clinical use and future trends. *Am J Cancer Res* 5, 2929–2943.
- Danen, E.H.J., Sonneveld, P., Brakebusch, C., Fässler, R., Sonnenberg, A., 2002. The fibronectin-binding integrins  $\alpha 5\beta 1$  and  $\alpha v\beta 3$  differentially modulate RhoA–GTP loading, organization of cell matrix adhesions, and fibronectin fibrillogenesis. *Journal of Cell Biology* 159, 1071–1086. <https://doi.org/10.1083/jcb.200205014>
- Dao, L., Blaue, C., Franz, C.M., 2021. Integrin  $\alpha 2\beta 1$  as a negative regulator of the laminin receptors  $\alpha 6\beta 1$  and  $\alpha 6\beta 4$ . *Micron* 148, 103106. <https://doi.org/10.1016/j.micron.2021.103106>
- Dardik, R., Lahav, J., 1999. Functional Changes in the Conformation of Thrombospondin-1 during Complexation with Fibronectin or Heparin. *Experimental Cell Research* 248, 407–414. <https://doi.org/10.1006/excr.1999.4415>
- Das, A., Monteiro, M., Barai, A., Kumar, S., Sen, S., 2017. MMP proteolytic activity regulates cancer invasiveness by modulating integrins. *Sci Rep* 7, 14219. <https://doi.org/10.1038/s41598-017-14340-w>
- Davidenko, N., Schuster, C.F., Bax, D.V., Farndale, R.W., Hamaia, S., Best, S.M., Cameron, R.E., 2016. Evaluation of cell binding to collagen and gelatin: a study of the effect of 2D and 3D

- architecture and surface chemistry. *J Mater Sci: Mater Med* 27, 148. <https://doi.org/10.1007/s10856-016-5763-9>
- Davis, P.K., Ho, A., Dowdy, S.F., 2001. Biological Methods for Cell-Cycle Synchronization of Mammalian Cells. *BioTechniques* 30, 1322–1331. <https://doi.org/10.2144/01306rv01>
- de Bernabé, D.B.-V., Inamori, K., Yoshida-Moriguchi, T., Weydert, C.J., Harper, H.A., Willer, T., Henry, M.D., Campbell, K.P., 2009. Loss of  $\alpha$ -Dystroglycan Laminin Binding in Epithelium-derived Cancers Is Caused by Silencing of LARGE. *Journal of Biological Chemistry* 284, 11279–11284. <https://doi.org/10.1074/jbc.C900007200>
- De Franceschi, N., Arjonen, A., Elkhatib, N., Denessiouk, K., Wrobel, A.G., Wilson, T.A., Pouwels, J., Montagnac, G., Owen, D.J., Ivaska, J., 2016. Selective integrin endocytosis is driven by interactions between the integrin  $\alpha$ -chain and AP2. *Nat Struct Mol Biol* 23, 172–179. <https://doi.org/10.1038/nsmb.3161>
- De Franceschi, N., Hamidi, H., Alanko, J., Sahgal, P., Ivaska, J., 2015. Integrin traffic - the update. *Journal of Cell Science* 128, 839–852. <https://doi.org/10.1242/jcs.161653>
- DeSantis, C.E., Ma, J., Gaudet, M.M., Newman, L.A., Miller, K.D., Goding Sauer, A., Jemal, A., Siegel, R.L., 2019. Breast cancer statistics, 2019. *CA: A Cancer Journal for Clinicians* 69, 438–451. <https://doi.org/10.3322/caac.21583>
- Diaz-Vera, J., Palmer, S., Hernandez-Fernaud, J.R., Dornier, E., Mitchell, L.E., Macpherson, I., Edwards, J., Zanivan, S., Norman, J.C., 2017. A proteomic approach to identify endosomal cargoes controlling cancer invasiveness. *Journal of Cell Science* 130, 697–711. <https://doi.org/10.1242/jcs.190835>
- Dix, C.L., Matthews, H.K., Uroz, M., McLaren, S., Wolf, L., Heatley, N., Win, Z., Almada, P., Henriques, R., Boutros, M., Trepap, X., Baum, B., 2018. The Role of Mitotic Cell-Substrate Adhesion Remodeling in Animal Cell Division. *Developmental Cell* 45, 132-145.e3. <https://doi.org/10.1016/j.devcel.2018.03.009>
- Dobrokhotov, O., Samsonov, M., Sokabe, M., Hirata, H., 2018. Mechanoregulation and pathology of YAP/TAZ via Hippo and non-Hippo mechanisms. *Clin Trans Med* 7, 23. <https://doi.org/10.1186/s40169-018-0202-9>
- Donaldson, J.G., Johnson, D.L., Dutta, D., 2016. Rab and Arf G proteins in endosomal trafficking and cell surface homeostasis. *Small GTPases* 7, 247–251. <https://doi.org/10.1080/21541248.2016.1212687>
- Dozynkiewicz, M.A., Jamieson, N.B., MacPherson, I., Grindlay, J., van den Berghe, P.V.E., von Thun, A., Morton, J.P., Gourley, C., Timpson, P., Nixon, C., McKay, C.J., Carter, R., Strachan, D., Anderson, K., Sansom, O.J., Caswell, P.T., Norman, J.C., 2012. Rab25 and CLIC3 Collaborate to Promote Integrin Recycling from Late Endosomes/Lysosomes and Drive Cancer Progression. *Developmental Cell* 22, 131–145. <https://doi.org/10.1016/j.devcel.2011.11.008>
- Du, Q., Guo, X., Wang, M., Li, Y., Sun, X., Li, Q., 2020. The application and prospect of CDK4/6 inhibitors in malignant solid tumors. *Journal of Hematology & Oncology* 13, 41. <https://doi.org/10.1186/s13045-020-00880-8>
- Duffy, M.J., Maguire, T.M., Hill, A., McDermott, E., O'Higgins, N., 2000. Metalloproteinases: role in breast carcinogenesis, invasion and metastasis. *Breast Cancer Res* 2, 252. <https://doi.org/10.1186/bcr65>
- Dundas, C.M., Demonte, D., Park, S., 2013. Streptavidin-biotin technology: improvements and innovations in chemical and biological applications. *Appl Microbiol Biotechnol* 97, 9343–9353. <https://doi.org/10.1007/s00253-013-5232-z>
- Elizalde, P.V., Russo, R.I.C., Chervo, M.F., Schillaci, R., 2016. ErbB-2 nuclear function in breast cancer growth, metastasis and resistance to therapy. *Endocrine-Related Cancer* 23, T243–T257. <https://doi.org/10.1530/ERC-16-0360>
- Erdogan, B., Ao, M., White, L.M., Means, A.L., Brewer, B.M., Yang, L., Washington, M.K., Shi, C., Franco, O.E., Weaver, A.M., Hayward, S.W., Li, D., Webb, D.J., 2017. Cancer-associated fibroblasts

- promote directional cancer cell migration by aligning fibronectin. *Journal of Cell Biology* 216, 3799–3816. <https://doi.org/10.1083/jcb.201704053>
- Ezratty, E.J., Bertaux, C., Marcantonio, E.E., Gundersen, G.G., 2009. Clathrin mediates integrin endocytosis for focal adhesion disassembly in migrating cells. *Journal of Cell Biology* 187, 733–747. <https://doi.org/10.1083/jcb.200904054>
- Fallahpour, S., Navaneelan, T., De, P., Borgo, A., 2017. Breast cancer survival by molecular subtype: a population-based analysis of cancer registry data. *CMAJ Open* 5, E734–E739. <https://doi.org/10.9778/cmajo.20170030>
- Feist, P., Hummon, A., 2015. Proteomic Challenges: Sample Preparation Techniques for Microgram-Quantity Protein Analysis from Biological Samples. *IJMS* 16, 3537–3563. <https://doi.org/10.3390/ijms16023537>
- Feng, Y., Spezia, M., Huang, S., Yuan, C., Zeng, Z., Zhang, L., Ji, X., Liu, W., Huang, B., Luo, W., Liu, B., Lei, Y., Du, S., Vuppalapati, A., Luu, H.H., Haydon, R.C., He, T.-C., Ren, G., 2018. Breast cancer development and progression: Risk factors, cancer stem cells, signaling pathways, genomics, and molecular pathogenesis. *Genes & Diseases* 5, 77–106. <https://doi.org/10.1016/j.gendis.2018.05.001>
- Fingar, D.C., Richardson, C.J., Tee, A.R., Cheatham, L., Tsou, C., Blenis, J., 2004. mTOR Controls Cell Cycle Progression through Its Cell Growth Effectors S6K1 and 4E-BP1/Eukaryotic Translation Initiation Factor 4E. *Mol Cell Biol* 24, 200–216. <https://doi.org/10.1128/MCB.24.1.200-216.2004>
- Fingar, D.C., Salama, S., Tsou, C., Harlow, E., Blenis, J., 2002. Mammalian cell size is controlled by mTOR and its downstream targets S6K1 and 4EBP1/eIF4E. *Genes Dev.* 16, 1472–1487. <https://doi.org/10.1101/gad.995802>
- Foster, D.A., Yellen, P., Xu, L., Saqcena, M., 2010. Regulation of G1 Cell Cycle Progression: Distinguishing the Restriction Point from a Nutrient-Sensing Cell Growth Checkpoint(s). *Genes & Cancer* 1, 1124–1131. <https://doi.org/10.1177/1947601910392989>
- Friedl, P., Gilmour, D., 2009. Collective cell migration in morphogenesis, regeneration and cancer. *Nat Rev Mol Cell Biol* 10, 445–457. <https://doi.org/10.1038/nrm2720>
- Gao, N., Flynn, D.C., Zhang, Z., Zhong, X.-S., Walker, V., Liu, K.J., Shi, X., Jiang, B.-H., 2004. G<sub>1</sub> cell cycle progression and the expression of G<sub>1</sub> cyclins are regulated by PI3K/AKT/mTOR/p70S6K1 signaling in human ovarian cancer cells. *American Journal of Physiology-Cell Physiology* 287, C281–C291. <https://doi.org/10.1152/ajpcell.00422.2003>
- Godwin, A.R.F., Singh, M., Lockhart-Cairns, M.P., Alanazi, Y.F., Cain, S.A., Baldock, C., 2019. The role of fibrillin and microfibril binding proteins in elastin and elastic fibre assembly. *Matrix Biology* 84, 17–30. <https://doi.org/10.1016/j.matbio.2019.06.006>
- Goel, S., DeCristo, M.J., McAllister, S.S., Zhao, J.J., 2018. CDK4/6 Inhibition in Cancer: Beyond Cell Cycle Arrest. *Trends in Cell Biology* 28, 911–925. <https://doi.org/10.1016/j.tcb.2018.07.002>
- Goel, S., DeCristo, M.J., Watt, A.C., BrinJones, H., Sceneay, J., Li, B.B., Khan, N., Ubellacker, J.M., Xie, S., Metzger-Filho, O., Hoog, J., Ellis, M.J., Ma, C.X., Ramm, S., Krop, I.E., Winer, E.P., Roberts, T.M., Kim, H.-J., McAllister, S.S., Zhao, J.J., 2017. CDK4/6 inhibition triggers anti-tumour immunity. *Nature* 548, 471–475. <https://doi.org/10.1038/nature23465>
- González-Tarragó, V., Elosegui-Artola, A., Bazellières, E., Oria, R., Pérez-González, C., Roca-Cusachs, P., 2017. Binding of ZO-1 to  $\alpha 5\beta 1$  integrins regulates the mechanical properties of  $\alpha 5\beta 1$ –fibronectin links. *Mol Biol Cell* 28, 1847–1852. <https://doi.org/10.1091/mbc.E17-01-0006>
- Gu, Z., Noss, E.H., Hsu, V.W., Brenner, M.B., 2011. Integrins traffic rapidly via circular dorsal ruffles and macropinocytosis during stimulated cell migration. *Journal of Cell Biology* 193, 61–70. <https://doi.org/10.1083/jcb.201007003>
- Gucalp, A., Traina, T.A., Eisner, J.R., Parker, J.S., Selitsky, S.R., Park, B.H., Elias, A.D., Baskin-Bey, E.S., Cardoso, F., 2019. Male breast cancer: a disease distinct from female breast cancer. *Breast Cancer Res Treat* 173, 37–48. <https://doi.org/10.1007/s10549-018-4921-9>

- Han, Y., Yu, X., Li, S., Tian, Y., Liu, C., 2020. New Perspectives for Resistance to PARP Inhibitors in Triple-Negative Breast Cancer. *Frontiers in Oncology* 10.
- Hanahan, D., Weinberg, R.A., 2011. Hallmarks of Cancer: The Next Generation. *Cell* 144, 646–674. <https://doi.org/10.1016/j.cell.2011.02.013>
- Harbeck, N., Gnant, M., 2017. Breast cancer. *The Lancet* 389, 1134–1150. [https://doi.org/10.1016/S0140-6736\(16\)31891-8](https://doi.org/10.1016/S0140-6736(16)31891-8)
- Harbeck, N., Penault-Llorca, F., Cortes, J., Gnant, M., Houssami, N., Poortmans, P., Ruddy, K., Tsang, J., Cardoso, F., 2019. Breast cancer. *Nat Rev Dis Primers* 5, 66. <https://doi.org/10.1038/s41572-019-0111-2>
- Hernandez-Fernaund, J.R., Ruengeler, E., Casazza, A., Neilson, L.J., Puelleine, E., Santi, A., Ismail, S., Lilla, S., Dhayade, S., MacPherson, I.R., McNeish, I., Ennis, D., Ali, H., Kugeratski, F.G., Al Khamici, H., van den Biggelaar, M., van den Berghe, P.V.E., Cloix, C., McDonald, L., Millan, D., Hoyle, A., Kuchnio, A., Carmeliet, P., Valenzuela, S.M., Blyth, K., Yin, H., Mazzone, M., Norman, J.C., Zanivan, S., 2017. Secreted CLIC3 drives cancer progression through its glutathione-dependent oxidoreductase activity. *Nature Communications* 8. <https://doi.org/10.1038/ncomms14206>
- Herrmann, D., Conway, J.R.W., Vennin, C., Magenau, A., Hughes, W.E., Morton, J.P., Timpson, P., 2014. Three-dimensional cancer models mimic cell–matrix interactions in the tumour microenvironment. *Carcinogenesis* 35, 1671–1679. <https://doi.org/10.1093/carcin/bgu108>
- Hohenester, E., Yurchenco, P.D., 2013. Laminins in basement membrane assembly. *Cell Adhesion & Migration* 7, 56–63. <https://doi.org/10.4161/cam.21831>
- Horejs, C.-M., 2016. Basement membrane fragments in the context of the epithelial-to-mesenchymal transition. *European Journal of Cell Biology* 95, 427–440. <https://doi.org/10.1016/j.ejcb.2016.06.002>
- Horwitz, R., Webb, D., 2003. Cell migration. *Current Biology* 13, R756–R759. <https://doi.org/10.1016/j.cub.2003.09.014>
- Hou, S., Isaji, T., Hang, Q., Im, S., Fukuda, T., Gu, J., 2016. Distinct effects of  $\beta 1$  integrin on cell proliferation and cellular signaling in MDA-MB-231 breast cancer cells. *Sci Rep* 6, 18430. <https://doi.org/10.1038/srep18430>
- Humphries, J.D., Byron, A., Humphries, M.J., 2006a. Integrin ligands at a glance. *Journal of Cell Science* 119, 3901–3903. <https://doi.org/10.1242/jcs.03098>
- Humphries, J.D., Byron, A., Humphries, M.J., 2006b. Integrin ligands at a glance. *Journal of Cell Science* 119, 3901–3903. <https://doi.org/10.1242/jcs.03098>
- Huth, H.W., Santos, D.M., Gravina, H.D., Resende, J.M., Goes, A.M., De Lima, M.E., Ropert, C., 2017. Upregulation of p38 pathway accelerates proliferation and migration of MDA-MB-231 breast cancer cells. *Oncology Reports* 37, 2497–2505. <https://doi.org/10.3892/or.2017.5452>
- Hynes, R., 1987. Integrins: A family of cell surface receptors. *Cell* 48, 549–554. [https://doi.org/10.1016/0092-8674\(87\)90233-9](https://doi.org/10.1016/0092-8674(87)90233-9)
- Hynes, R.O., Naba, A., 2012. Overview of the Matrisome--An Inventory of Extracellular Matrix Constituents and Functions. *Cold Spring Harbor Perspectives in Biology* 4, a004903–a004903. <https://doi.org/10.1101/cshperspect.a004903>
- Ibaragi, S., Shimo, T., Hassan, N.M.M., Isowa, S., Kurio, N., Mandai, H., Kodama, S., Sasaki, A., 2011. Induction of MMP-13 Expression in Bone-metastasizing Cancer Cells by Type I Collagen through Integrin  $\alpha 1\beta 1$  and  $\alpha 2\beta 1$ -p38 MAPK Signaling. *ANTICANCER RESEARCH* 7.
- Insua-Rodríguez, J., Oskarsson, T., 2016. The extracellular matrix in breast cancer. *Advanced Drug Delivery Reviews* 97, 41–55. <https://doi.org/10.1016/j.addr.2015.12.017>
- Iqbal, Nida, Iqbal, Naveed, 2014. Human Epidermal Growth Factor Receptor 2 (HER2) in Cancers: Overexpression and Therapeutic Implications. *Molecular Biology International* 2014, 1–9. <https://doi.org/10.1155/2014/852748>

- Itoh, Y., 2018. Discoidin domain receptors: Microenvironment sensors that promote cellular migration and invasion. *Cell Adhesion & Migration* 1–8. <https://doi.org/10.1080/19336918.2018.1460011>
- Ivaska, J., Käpylä, J., Pentikäinen, O., Hoffrén, A.-M., Hermonen, J., Huttunen, P., Johnson, M.S., Heino, J., 1999a. A Peptide Inhibiting the Collagen Binding Function of Integrin  $\alpha 21$  Domain. *Journal of Biological Chemistry* 274, 3513–3521. <https://doi.org/10.1074/jbc.274.6.3513>
- Ivaska, J., Reunanen, H., Westermarck, J., Koivisto, L., Kähäri, V.-M., Heino, J., 1999b. Integrin  $\alpha 21$  Mediates Isoform-specific Activation of p38 and Upregulation of Collagen Gene Transcription by a Mechanism Involving the  $\alpha 2$  Cytoplasmic Tail. *The Journal of Cell Biology* 147, 15.
- Jabłońska-Trypuć, A., Matejczyk, M., Rosochacki, S., 2016. Matrix metalloproteinases (MMPs), the main extracellular matrix (ECM) enzymes in collagen degradation, as a target for anticancer drugs. *Journal of Enzyme Inhibition and Medicinal Chemistry* 31, 177–183. <https://doi.org/10.3109/14756366.2016.1161620>
- Jacob, A., Prekeris, R., 2015. The regulation of MMP targeting to invadopodia during cancer metastasis. *Front Cell Dev Biol* 3. <https://doi.org/10.3389/fcell.2015.00004>
- Jacquemet, G., Green, D.M., Bridgewater, R.E., von Kriegsheim, A., Humphries, M.J., Norman, J.C., Caswell, P.T., 2013. RCP-driven  $\alpha 5\beta 1$  recycling suppresses Rac and promotes RhoA activity via the RacGAP1–IQGAP1 complex. *J Cell Biol* 202, 917–935. <https://doi.org/10.1083/jcb.201302041>
- Jaskolski, F., Mulle, C., Manzoni, O.J., 2005. An automated method to quantify and visualize colocalized fluorescent signals. *Journal of Neuroscience Methods* 146, 42–49. <https://doi.org/10.1016/j.jneumeth.2005.01.012>
- Jedezsko, C., Sameni, M., Olive, M., Moin, K., Sloane, B.F., 2013. Visualizing Protease Activity in Living Cells: From Two Dimensions to Four Dimensions 19.
- Jevnikar, Z., Obermajer, N., Bogyo, M., Kos, J., 2008. The role of cathepsin X in the migration and invasiveness of T lymphocytes. *Journal of Cell Science* 121, 2652–2661. <https://doi.org/10.1242/jcs.023721>
- Johnson, M.B., Pang, B., Gardner, D.J., Niknam-Benia, S., Soundarajan, V., Bramos, A., Perrault, D.P., Banks, K., Lee, G.K., Baker, R.Y., Kim, G.H., Lee, S., Chai, Y., Chen, M., Li, W., Kwong, L., Hong, Y.-K., Wong, A.K., 2017. Topical Fibronectin Improves Wound Healing of Irradiated Skin. *Sci Rep* 7. <https://doi.org/10.1038/s41598-017-03614-y>
- Jones, M.C., Askari, J.A., Humphries, J.D., Humphries, M.J., 2018. Cell adhesion is regulated by CDK1 during the cell cycle. *The Journal of Cell Biology* 217, 3203–3218. <https://doi.org/10.1083/jcb.201802088>
- Jones, M.C., Zha, J., Humphries, M.J., 2019. Connections between the cell cycle, cell adhesion and the cytoskeleton. *Phil. Trans. R. Soc. B* 374, 20180227. <https://doi.org/10.1098/rstb.2018.0227>
- Jung, M., Lee, J., Seo, H.-Y., Lim, J.S., Kim, E.-K., 2015. Cathepsin Inhibition-Induced Lysosomal Dysfunction Enhances Pancreatic Beta-Cell Apoptosis in High Glucose. *PLoS ONE* 10, e0116972. <https://doi.org/10.1371/journal.pone.0116972>
- Kai, F., Drain, A.P., Weaver, V.M., 2019. The Extracellular Matrix Modulates the Metastatic Journey. *Developmental Cell* 49, 332–346. <https://doi.org/10.1016/j.devcel.2019.03.026>
- Kai, F., Laklai, H., Weaver, V.M., 2016. Force Matters: Biomechanical Regulation of Cell Invasion and Migration in Disease. *Trends in Cell Biology* 26, 486–497. <https://doi.org/10.1016/j.tcb.2016.03.007>
- Kamińska, M., Ciszewski, T., Łopacka-Szatan, K., Miotła, P., Starosławska, E., 2015. Breast cancer risk factors. *Prz Menopauzalny* 14, 196–202. <https://doi.org/10.5114/pm.2015.54346>
- Kaplan, R.N., Riba, R.D., Zacharoulis, S., Bramley, A.H., Vincent, L., Costa, C., MacDonald, D.D., Jin, D.K., Shido, K., Kerns, S.A., Zhu, Z., Hicklin, D., Wu, Y., Port, J.L., Altorki, N., Port, E.R., Ruggero, D., Shmelkov, S.V., Jensen, K.K., Rafii, S., Lyden, D., 2005. VEGFR1-positive haematopoietic bone marrow progenitors initiate the pre-metastatic niche. *Nature* 438, 820–827. <https://doi.org/10.1038/nature04186>

- Kaukonen, R., Jacquemet, G., Hamidi, H., Ivaska, J., 2017a. Cell-derived matrices for studying cell proliferation and directional migration in a complex 3D microenvironment. *Nature Protocols* 12, 2376–2390. <https://doi.org/10.1038/nprot.2017.107>
- Kaukonen, R., Jacquemet, G., Hamidi, H., Ivaska, J., 2017b. Cell-derived matrices for studying cell proliferation and directional migration in a complex 3D microenvironment. *Nat Protoc* 12, 2376–2390. <https://doi.org/10.1038/nprot.2017.107>
- Kaukonen, R., Mai, A., Georgiadou, M., Saari, M., De Franceschi, N., Betz, T., Sihto, H., Ventelä, S., Elo, L., Jokitalo, E., Westermarck, J., Kellokumpu-Lehtinen, P.-L., Joensuu, H., Grenman, R., Ivaska, J., 2016. Normal stroma suppresses cancer cell proliferation via mechanosensitive regulation of JMJD1a-mediated transcription. *Nat Commun* 7, 12237. <https://doi.org/10.1038/ncomms12237>
- Kaushik, S., Pickup, M.W., Weaver, V.M., 2016. From transformation to metastasis: deconstructing the extracellular matrix in breast cancer. *Cancer Metastasis Rev* 35, 655–667. <https://doi.org/10.1007/s10555-016-9650-0>
- Kerrisk, M.E., Cingolani, L.A., Koleske, A.J., 2014. ECM receptors in neuronal structure, synaptic plasticity, and behavior, in: *Progress in Brain Research*. Elsevier, pp. 101–131. <https://doi.org/10.1016/B978-0-444-63486-3.00005-0>
- Kharitidi, D., Apaja, P.M., Manteghi, S., Suzuki, K., Malitskaya, E., Roldan, A., Gingras, M.-C., Takagi, J., Lukacs, G.L., Pause, A., 2015. Interplay of Endosomal pH and Ligand Occupancy in Integrin  $\alpha 5\beta 1$  Ubiquitination, Endocytic Sorting, and Cell Migration. *Cell Reports* 13, 599–609. <https://doi.org/10.1016/j.celrep.2015.09.024>
- Kim, D.J., Christofidou, E.D., Keene, D.R., Hassan Milde, M., Adams, J.C., 2015. Intermolecular interactions of thrombospondins drive their accumulation in extracellular matrix. *MBoC* 26, 2640–2654. <https://doi.org/10.1091/mbc.E14-05-0996>
- Kim, M.-S., Lee, E.-J., Kim, H.-R.C., Moon, A., n.d. p38 Kinase Is a Key Signaling Molecule for H-Ras-induced Cell Motility and Invasive Phenotype in Human Breast Epithelial Cells 9.
- Kimura, F., Ueda, A., Sato, E., Akimoto, J., Kaise, H., Yamada, K., Hosonaga, M., Kawai, Y., Teraoka, S., Okazaki, M., Ishikawa, T., 2017. Hereditary breast cancer associated with Cowden syndrome-related PTEN mutation with Lhermitte-Duclos disease. *surg case rep* 3, 83. <https://doi.org/10.1186/s40792-017-0355-6>
- Kinbara, K., Goldfinger, L.E., Hansen, M., Chou, F.-L., Ginsberg, M.H., 2003. Ras GTPases: integrins' friends or foes? *Nat Rev Mol Cell Biol* 4, 767–777. <https://doi.org/10.1038/nrm1229>
- Kirkbride, K.C., Sung, B.H., Sinha, S., Weaver, A.M., 2011. Cortactin. *Cell Adh Migr* 5, 187–198. <https://doi.org/10.4161/cam.5.2.14773>
- Kjøller, L., Engelholm, L.H., Høyer-Hansen, M., Danø, K., Bugge, T.H., Behrendt, N., 2004. uPARAP/endo180 directs lysosomal delivery and degradation of collagen IV. *Experimental Cell Research* 293, 106–116. <https://doi.org/10.1016/j.yexcr.2003.10.008>
- Klekotka, P.A., Santoro, S.A., Zutter, M.M., 2001.  $\alpha 2$  Integrin Subunit Cytoplasmic Domain-dependent Cellular Migration Requires p38 MAPK. *Journal of Biological Chemistry* 276, 9503–9511. <https://doi.org/10.1074/jbc.M006286200>
- Kuo, H.-J., Maslen, C.L., Keene, D.R., Glanville, R.W., 1997. Type VI Collagen Anchors Endothelial Basement Membranes by Interacting with Type IV Collagen\*. *Journal of Biological Chemistry* 272, 26522–26529. <https://doi.org/10.1074/jbc.272.42.26522>
- Kutys, M.L., Doyle, A.D., Yamada, K.M., 2013a. Regulation of cell adhesion and migration by cell-derived matrices. *Experimental Cell Research* 319, 2434–2439. <https://doi.org/10.1016/j.yexcr.2013.05.030>
- Kutys, M.L., Doyle, A.D., Yamada, K.M., 2013b. Regulation of cell adhesion and migration by cell-derived matrices. *Exp Cell Res* 319, 2434–2439. <https://doi.org/10.1016/j.yexcr.2013.05.030>
- Lahlou, H., Muller, W.J., 2011.  $\beta 1$ -integrins signaling and mammary tumor progression in transgenic mouse models: implications for human breast cancer. *Breast Cancer Res* 13, 229. <https://doi.org/10.1186/bcr2905>

- Lane, A.N., Fan, T.W.-M., 2015. Regulation of mammalian nucleotide metabolism and biosynthesis. *Nucleic Acids Research* 43, 2466–2485. <https://doi.org/10.1093/nar/gkv047>
- Lauffenburger, D.A., Horwitz, A.F., 1996. Cell Migration: A Physically Integrated Molecular Process. *Cell* 84, 359–369. [https://doi.org/10.1016/S0092-8674\(00\)81280-5](https://doi.org/10.1016/S0092-8674(00)81280-5)
- Lebert, J.M., Lester, R., Powell, E., Seal, M., McCarthy, J., 2018. Advances in the Systemic Treatment of Triple-Negative Breast Cancer. *Current Oncology* 25, 142–150. <https://doi.org/10.3747/co.25.3954>
- Leonoudakis, D., Huang, G., Akhavan, A., Fata, J.E., Singh, M., Gray, J.W., Muschler, J.L., 2014. Endocytic trafficking of laminin is controlled by dystroglycan and is disrupted in cancers. *Journal of Cell Science* 127, 4894–4903. <https://doi.org/10.1242/jcs.152728>
- Li, C.H., Karantza, V., Aktan, G., Lala, M., 2019. Current treatment landscape for patients with locally recurrent inoperable or metastatic triple-negative breast cancer: a systematic literature review. *Breast Cancer Res* 21, 1–14. <https://doi.org/10.1186/s13058-019-1210-4>
- Li, H., Qiu, Z., Li, F., Wang, C., 2017. The relationship between MMP-2 and MMP-9 expression levels with breast cancer incidence and prognosis. *Oncol Lett* 14, 5865–5870. <https://doi.org/10.3892/ol.2017.6924>
- Li, S., Van Den Diepstraten, C., D'Souza, S.J., Chan, B.M.C., Pickering, J.G., 2003. Vascular Smooth Muscle Cells Orchestrate the Assembly of Type I Collagen via  $\alpha 2\beta 1$  Integrin, RhoA, and Fibronectin Polymerization. *Am J Pathol* 163, 1045–1056.
- Li, Y.R., Ro, V., Tchou, J.C., 2018. Obesity, Metabolic Syndrome, and Breast Cancer: From Prevention to Intervention. *Curr Surg Rep* 6. <https://doi.org/10.1007/s40137-018-0204-y>
- Ligasová, A., Koberna, K., 2021. Strengths and Weaknesses of Cell Synchronization Protocols Based on Inhibition of DNA Synthesis. *IJMS* 22, 10759. <https://doi.org/10.3390/ijms221910759>
- Lin, E.Y., Jones, J.G., Li, P., Zhu, L., Whitney, K.D., Muller, W.J., Pollard, J.W., 2003. Progression to Malignancy in the Polyoma Middle T Oncoprotein Mouse Breast Cancer Model Provides a Reliable Model for Human Diseases. *The American Journal of Pathology* 163, 2113–2126. [https://doi.org/10.1016/S0002-9440\(10\)63568-7](https://doi.org/10.1016/S0002-9440(10)63568-7)
- Liu, M., Liu, H., Chen, J., 2018. Mechanisms of the CDK4/6 inhibitor palbociclib (PD 0332991) and its future application in cancer treatment (Review). *Oncology Reports* 39, 901–911. <https://doi.org/10.3892/or.2018.6221>
- Liu, X., Wu, K., Zheng, D., Luo, C., Fan, Y., Zhong, X., Zheng, H., 2021. Efficacy and Safety of PARP Inhibitors in Advanced or Metastatic Triple-Negative Breast Cancer: A Systematic Review and Meta-Analysis. *Frontiers in Oncology* 11.
- Liu, Y., Nguyen, N., Colditz, G.A., 2015. Links between alcohol consumption and breast cancer: a look at the evidence. *Womens Health (Lond Engl)* 11, 65–77. <https://doi.org/10.2217/whe.14.62>
- Lobert, V.H., Brech, A., Pedersen, N.M., Wesche, J., Oppelt, A., Malerød, L., Stenmark, H., 2010. Ubiquitination of  $\alpha 5\beta 1$  Integrin Controls Fibroblast Migration through Lysosomal Degradation of Fibronectin-Integrin Complexes. *Developmental Cell* 19, 148–159. <https://doi.org/10.1016/j.devcel.2010.06.010>
- Lopatkin, A.J., Yang, J.H., 2021. Digital Insights Into Nucleotide Metabolism and Antibiotic Treatment Failure. *Frontiers in Digital Health* 3.
- Lu, P., Takai, K., Weaver, V.M., Werb, Z., 2011. Extracellular Matrix Degradation and Remodeling in Development and Disease. *Cold Spring Harbor Perspectives in Biology* 3, a005058–a005058. <https://doi.org/10.1101/cshperspect.a005058>
- Lu, P., Weaver, V.M., Werb, Z., 2012. The extracellular matrix: A dynamic niche in cancer progression. *The Journal of Cell Biology* 196, 395–406. <https://doi.org/10.1083/jcb.201102147>
- Lu, S., Simin, K., Khan, A., Mercurio, A.M., 2008. Analysis of Integrin 4 Expression in Human Breast Cancer: Association with Basal-like Tumors and Prognostic Significance. *Clinical Cancer Research* 14, 1050–1058. <https://doi.org/10.1158/1078-0432.CCR-07-4116>
- Lundgren, K., Brown, M., Pineda, S., Cuzick, J., Salter, J., Zabaglo, L., Howell, A., Dowsett, M., Landberg, G., 2012. Effects of cyclin D 1 gene amplification and protein expression on time to recurrence

- in postmenopausal breast cancer patients treated with anastrozole or tamoxifen: A TransATAC study. *Breast Cancer Research* 14. <https://doi.org/10.1186/bcr3161>
- Ma, J.-C., Huang, X., Shen, Y.-W., Zheng, C., Su, Q.-H., Xu, J.-K., Zhao, J., 2016. Tenascin-C promotes migration of hepatic stellate cells and production of type I collagen. *Bioscience, Biotechnology, and Biochemistry* 80, 1470–1477. <https://doi.org/10.1080/09168451.2016.1165600>
- Madsen, D.H., Engelholm, L.H., Ingvarsen, S., Hillig, T., Wagenaar-Miller, R.A., Kjølner, L., Gårdsvoll, H., Høyer-Hansen, G., Holmbeck, K., Bugge, T.H., Behrendt, N., 2007. Extracellular Collagenases and the Endocytic Receptor, Urokinase Plasminogen Activator Receptor-associated Protein/Endo180, Cooperate in Fibroblast-mediated Collagen Degradation. *J. Biol. Chem.* 282, 27037–27045. <https://doi.org/10.1074/jbc.M701088200>
- Maemura, M., Akiyama, S.K., Woods, V.L., Dickson, R.B., 1995. Expression and ligand binding of  $\alpha 2\beta 1$  integrin on breast carcinoma cells. *Clin Exp Metast* 13, 223–235. <https://doi.org/10.1007/BF00133478>
- Mai, A., Veltel, S., Pellinen, T., Padzik, A., Coffey, E., Marjomäki, V., Ivaska, J., 2011. Competitive binding of Rab21 and p120RasGAP to integrins regulates receptor traffic and migration. *Journal of Cell Biology* 194, 291–306. <https://doi.org/10.1083/jcb.201012126>
- Mak, K.M., Mei, R., 2017. Basement Membrane Type IV Collagen and Laminin: An Overview of Their Biology and Value as Fibrosis Biomarkers of Liver Disease. *The Anatomical Record* 300, 1371–1390. <https://doi.org/10.1002/ar.23567>
- Malik, G., Knowles, L.M., Dhir, R., Xu, S., Yang, S., Ruoslahti, E., Pilch, J., 2010. Plasma fibronectin promotes lung metastasis by contributions to fibrin clots and tumor cell invasion. *Cancer Res* 70, 4327–4334. <https://doi.org/10.1158/0008-5472.CAN-09-3312>
- Marshall, J.F., Rutherford, D.C., McCartney, A.C., Mitjans, F., Goodman, S.L., Hart, I.R., 1995. Alpha v beta 1 is a receptor for vitronectin and fibrinogen, and acts with alpha 5 beta 1 to mediate spreading on fibronectin. *J Cell Sci* 108 ( Pt 3), 1227–1238. <https://doi.org/10.1242/jcs.108.3.1227>
- Matthews, H.K., Bertoli, C., de Bruin, R.A.M., 2021. Cell cycle control in cancer. *Nat Rev Mol Cell Biol*. <https://doi.org/10.1038/s41580-021-00404-3>
- Maughan, K.L., Lutterbie, M.A., Ham, P.S., 2010. Treatment of Breast Cancer. *Breast Cancer* 81, 8.
- Melander, M.C., Jürgensen, H.J., Madsen, D.H., Engelholm, L.H., Behrendt, N., 2015. The collagen receptor uPARAP/Endo180 in tissue degradation and cancer (Review). *International Journal of Oncology* 47, 1177–1188. <https://doi.org/10.3892/ijo.2015.3120>
- Mierke, C.T., Frey, B., Fellner, M., Herrmann, M., Fabry, B., 2011. Integrin  $\alpha 5\beta 1$  facilitates cancer cell invasion through enhanced contractile forces. *J Cell Sci* 124, 369–383. <https://doi.org/10.1242/jcs.071985>
- Mogilner, A., Oster, G., 1996. Cell motility driven by actin polymerization. *Biophysical Journal* 71, 3030–3045. [https://doi.org/10.1016/S0006-3495\(96\)79496-1](https://doi.org/10.1016/S0006-3495(96)79496-1)
- Montgomery, N., Hill, A., McFarlane, S., Neisen, J., O’Grady, A., Conlon, S., Jirstrom, K., Kay, E.W., Waugh, D.J., 2012. CD44 enhances invasion of basal-like breast cancer cells by upregulating serine protease and collagen-degrading enzymatic expression and activity. *Breast Cancer Res* 14, R84. <https://doi.org/10.1186/bcr3199>
- Moreno-Layseca, P., Icha, J., Hamidi, H., Ivaska, J., 2019. Integrin trafficking in cells and tissues. *Nat Cell Biol* 21, 122–132. <https://doi.org/10.1038/s41556-018-0223-z>
- Moreno-Layseca, P., Streuli, C.H., 2014. Signalling pathways linking integrins with cell cycle progression. *Matrix Biology* 34, 144–153. <https://doi.org/10.1016/j.matbio.2013.10.011>
- Morgan, M.R., Humphries, M.J., Bass, M.D., 2007. Synergistic control of cell adhesion by integrins and syndecans. *Nat Rev Mol Cell Biol* 8, 957–969. <https://doi.org/10.1038/nrm2289>
- Morini, M., Mottolèse, M., Ferrari, N., Ghiorzo, F., Buglioni, S., Mortarini, R., Noonan, D.M., Natali, P.G., Albini, A., 2000. The  $\alpha 3\beta 1$  integrin is associated with mammary carcinoma cell metastasis, invasion, and gelatinase B (mmp-9) activity. *International Journal of Cancer* 87, 336–342. [https://doi.org/10.1002/1097-0215\(20000801\)87:3<336::AID-IJC5>3.0.CO;2-3](https://doi.org/10.1002/1097-0215(20000801)87:3<336::AID-IJC5>3.0.CO;2-3)

- Moritz, M.N.O., Merkel, A.R., Feldman, E.G., Selistre-de-Araujo, H.S., Rhoades (Sterling), J.A., 2021. Biphasic  $\alpha 2\beta 1$  Integrin Expression in Breast Cancer Metastasis to Bone. *International Journal of Molecular Sciences* 22, 6906. <https://doi.org/10.3390/ijms22136906>
- Mouw, J.K., Ou, G., Weaver, V.M., 2014. Extracellular matrix assembly: a multiscale deconstruction. *Nat Rev Mol Cell Biol* 15, 771–785. <https://doi.org/10.1038/nrm3902>
- Mukhopadhyay, R., Theriault, R.L., Price, J.E., n.d. Increased levels of  $\alpha 6$  integrins are associated with the metastatic phenotype of human breast cancer cells 8.
- Muller, P.A.J., Caswell, P.T., Doyle, B., Iwanicki, M.P., Tan, E.H., Karim, S., Lukashchuk, N., Gillespie, D.A., Ludwig, R.L., Gosselin, P., Cromer, A., Brugge, J.S., Sansom, O.J., Norman, J.C., Vousden, K.H., 2009. Mutant p53 Drives Invasion by Promoting Integrin Recycling. *Cell* 139, 1327–1341. <https://doi.org/10.1016/j.cell.2009.11.026>
- Muller, P.A.J., Trinidad, A.G., Timpson, P., Morton, J.P., Zanivan, S., van den Berghe, P.V.E., Nixon, C., Karim, S.A., Caswell, P.T., Noll, J.E., Coffill, C.R., Lane, D.P., Sansom, O.J., Neilsen, P.M., Norman, J.C., Vousden, K.H., 2013. Mutant p53 enhances MET trafficking and signalling to drive cell scattering and invasion. *Oncogene* 32, 1252–1265. <https://doi.org/10.1038/onc.2012.148>
- Muranen, T., Iwanicki, M.P., Curry, N.L., Hwang, J., DuBois, C.D., Coloff, J.L., Hitchcock, D.S., Clish, C.B., Brugge, J.S., Kalaany, N.Y., 2017. Starved epithelial cells uptake extracellular matrix for survival. *Nat Commun* 8, 13989. <https://doi.org/10.1038/ncomms13989>
- Naba, A., Clauser, K.R., Hoersch, S., Carr, S.A., Hynes, R.O., n.d. The Matrisome: In Silico Definition and In Vivo Characterization by Proteomics of Normal and Tumor Extracellular Matrices\* □S 18.
- Naci, D., 2015. Alpha2beta1 integrin in cancer development and chemoresistance. *Seminars in Cancer Biology* 9.
- Nagano, M., Hoshino, D., Koshikawa, N., Akizawa, T., Seiki, M., 2012. Turnover of Focal Adhesions and Cancer Cell Migration. *International Journal of Cell Biology* 2012, 1–10. <https://doi.org/10.1155/2012/310616>
- Nazemi, M., Yanes, B., Martinez, M.L., Walker, H., Bard, F., Rainero, E., 2021. The extracellular matrix promotes breast cancer cell growth under amino acid starvation by promoting tyrosine catabolism (preprint). *Cancer Biology*. <https://doi.org/10.1101/2021.06.09.447520>
- Niehoff, N.M., Nichols, H.B., Zhao, S., White, A.J., Sandler, D.P., 2019. Adult Physical Activity and Breast Cancer Risk in Women with a Family History of Breast Cancer. *Cancer Epidemiol Biomarkers Prev* 28, 51–58. <https://doi.org/10.1158/1055-9965.EPI-18-0674>
- Niers, J.M., Chen, J.W., Weissleder, R., Tannous, B.A., 2011. Enhanced in vivo imaging of metabolically biotinylated cell surface reporters. *Anal Chem* 83, 994–999. <https://doi.org/10.1021/ac102758m>
- Nissinen, L., Koivunen, J., Käpylä, J., Salmela, M., Nieminen, J., Jokinen, J., Sipilä, K., Pihlavisto, M., Pentikäinen, O.T., Marjamäki, A., Heino, J., 2012. Novel  $\alpha 2\beta 1$  Integrin Inhibitors Reveal That Integrin Binding to Collagen under Shear Stress Conditions Does Not Require Receptor Preactivation. *Journal of Biological Chemistry* 287, 44694–44702. <https://doi.org/10.1074/jbc.M111.309450>
- Obr, A., Edwards, D.P., 2012. The Biology of Progesterone Receptor in the Normal Mammary gland and in Breast Cancer. *Mol Cell Endocrinol* 357, 4–17. <https://doi.org/10.1016/j.mce.2011.10.030>
- Ojalill, M., Parikainen, M., Rappu, P., Aalto, E., Jokinen, J., Virtanen, N., Siljamäki, E., Heino, J., 2018. Integrin  $\alpha 2\beta 1$  decelerates proliferation, but promotes survival and invasion of prostate cancer cells. *Oncotarget* 9, 32435–32447. <https://doi.org/10.18632/oncotarget.25945>
- Orr, K.S., Savage, K.I., 2015. The BRCA1 and BRCA2 Breast and Ovarian Cancer Susceptibility Genes — Implications for DNA Damage Response, DNA Repair and Cancer Therapy. *Advances in DNA Repair*. <https://doi.org/10.5772/59996>
- Ortega, M.A., Fraile-Martínez, O., Asúnsolo, Á., Buján, J., García-Honduvilla, N., Coca, S., 2020. Signal Transduction Pathways in Breast Cancer: The Important Role of PI3K/Akt/mTOR. *Journal of Oncology* 2020, 1–11. <https://doi.org/10.1155/2020/9258396>

- Oskarsson, T., 2013. Extracellular matrix components in breast cancer progression and metastasis. *The Breast* 22, S66–S72. <https://doi.org/10.1016/j.breast.2013.07.012>
- Ottini, L., Rizzolo, P., Silvestri, V., Falchetti, M., 2011. Inherited and acquired alterations in development of breast cancer. *TACG* 145. <https://doi.org/10.2147/TACG.S13226>
- Pankova, D., Chen, Y., Terajima, M., Schliekelman, M.J., Baird, B.N., Fahrenholtz, M., Sun, L., Gill, B.J., Vadakkan, T.J., Kim, M.P., Ahn, Y.-H., Roybal, J.D., Liu, X., Parra Cuentas, E.R., Rodriguez, J., Wistuba, I.I., Creighton, C.J., Gibbons, D.L., Hicks, J.M., Dickinson, M.E., West, J.L., Grande-Allen, K.J., Hanash, S.M., Yamauchi, M., Kurie, J.M., 2016. Cancer-Associated Fibroblasts Induce a Collagen Cross-link Switch in Tumor Stroma. *Mol Cancer Res* 14, 287–295. <https://doi.org/10.1158/1541-7786.MCR-15-0307>
- Pappireddi, N., Martin, L., Wühr, M., 2019. A Review on Quantitative Multiplexed Proteomics. *ChemBioChem* 20, 1210–1224. <https://doi.org/10.1002/cbic.201800650>
- Park, H.-J., Helfman, D.M., 2019. Up-regulated fibronectin in 3D culture facilitates spreading of triple negative breast cancer cells on 2D through integrin  $\beta$ -5 and Src. *Sci Rep* 9, 19950. <https://doi.org/10.1038/s41598-019-56276-3>
- Park, J., Schwarzbauer, J.E., 2014. Mammary epithelial cell interactions with fibronectin stimulate epithelial-mesenchymal transition. *Oncogene* 33, 1649–1657. <https://doi.org/10.1038/onc.2013.118>
- Parrott, M.B., Barry, M.A., 2000. Metabolic Biotinylation of Recombinant Proteins in Mammalian Cells and in Mice. *Molecular Therapy* 1, 96–104. <https://doi.org/10.1006/mthe.1999.0011>
- Paten, J.A., Martin, C.L., Wanis, J.T., Siadat, S.M., Figueroa-Navedo, A.M., Ruberti, J.W., Deravi, L.F., 2019. Molecular Interactions between Collagen and Fibronectin: A Reciprocal Relationship that Regulates De Novo Fibrillogenesis. *Chem* 5, 2126–2145. <https://doi.org/10.1016/j.chempr.2019.05.011>
- Paul, N.R., Jacquemet, G., Caswell, P.T., 2015. Endocytic Trafficking of Integrins in Cell Migration. *Current Biology* 25, R1092–R1105. <https://doi.org/10.1016/j.cub.2015.09.049>
- Pellinen, T., Arjonen, A., Vuoriluoto, K., Kallio, K., Fransén, J.A.M., Ivaska, J., 2006. Small GTPase Rab21 regulates cell adhesion and controls endosomal traffic of  $\beta$ 1-integrins. *Journal of Cell Biology* 173, 767–780. <https://doi.org/10.1083/jcb.200509019>
- Pellinen, T., Tuomi, S., Arjonen, A., Wolf, M., Edgren, H., Meyer, H., Grosse, R., Kitzing, T., Rantala, J.K., Kallioniemi, O., Fässler, R., Kallio, M., Ivaska, J., 2008. Integrin Trafficking Regulated by Rab21 Is Necessary for Cytokinesis. *Developmental Cell* 15, 371–385. <https://doi.org/10.1016/j.devcel.2008.08.001>
- Pernas, S., Tolaney, S.M., Winer, E.P., Goel, S., 2018. CDK4/6 inhibition in breast cancer: current practice and future directions. *Ther Adv Med Oncol* 10, 1758835918786451. <https://doi.org/10.1177/1758835918786451>
- Petrie, R.J., Doyle, A.D., Yamada, K.M., 2009. Random versus directionally persistent cell migration. *Nat Rev Mol Cell Biol* 10, 538–549. <https://doi.org/10.1038/nrm2729>
- Pickup, M.W., Mouw, J.K., Weaver, V.M., 2014. The extracellular matrix modulates the hallmarks of cancer. *EMBO Rep* 15, 1243–1253. <https://doi.org/10.15252/embr.201439246>
- Podgorski, I., Linebaugh, B.E., Sameni, M., Jedeszko, C., Bhagat, S., Cher, M.L., Sloane, B.F., 2005. Bone Microenvironment Modulates Expression and Activity of Cathepsin B in Prostate Cancer. *Neoplasia* 7, 207–223.
- Prasedya, E.S., Miyake, M., Kobayashi, D., Hazama, A., 2016. Carrageenan delays cell cycle progression in human cancer cells in vitro demonstrated by FUCCI imaging. *BMC Complement Altern Med* 16, 270. <https://doi.org/10.1186/s12906-016-1199-5>
- Provenzano, P.P., Inman, D.R., Eliceiri, K.W., Keely, P.J., 2009. Matrix density-induced mechanoregulation of breast cell phenotype, signaling and gene expression through a FAK–ERK linkage. *Oncogene* 28, 4326–4343. <https://doi.org/10.1038/onc.2009.299>
- Quail, D.F., Joyce, J.A., 2013. Microenvironmental regulation of tumor progression and metastasis. *Nature Medicine* 19, 1423–1437. <https://doi.org/10.1038/nm.3394>

- Rainero, E., 2016. Extracellular matrix endocytosis in controlling matrix turnover and beyond: emerging roles in cancer. *Biochemical Society Transactions* 44, 1347–1354. <https://doi.org/10.1042/BST20160159>
- Rainero, E., Caswell, P.T., Muller, P.A.J., Grindlay, J., McCaffrey, M.W., Zhang, Q., Wakelam, M.J.O., Vousden, K.H., Graziani, A., Norman, J.C., 2012. Diacylglycerol kinase  $\alpha$  controls RCP-dependent integrin trafficking to promote invasive migration. *The Journal of Cell Biology* 196, 277–295. <https://doi.org/10.1083/jcb.201109112>
- Rainero, E., Howe, J.D., Caswell, P.T., Jamieson, N.B., Anderson, K., Critchley, D.R., Machesky, L., Norman, J.C., 2015. Ligand-Occupied Integrin Internalization Links Nutrient Signaling to Invasive Migration. *Cell Reports* 10, 398–413. <https://doi.org/10.1016/j.celrep.2014.12.037>
- Rainero, E., Norman, J.C., 2013. Late endosomal and lysosomal trafficking during integrin-mediated cell migration and invasion: Cell matrix receptors are trafficked through the late endosomal pathway in a way that dictates how cells migrate. *BioEssays* 35, 523–532. <https://doi.org/10.1002/bies.201200160>
- Ramirez, N.E., Zhang, Z., Madamanchi, A., Boyd, K.L., O’Rear, L.D., Nashabi, A., Li, Z., Dupont, W.D., Zijlstra, A., Zutter, M.M., 2011. The  $\alpha 2\beta 1$  integrin is a metastasis suppressor in mouse models and human cancer. *J Clin Invest* 121, 226–237. <https://doi.org/10.1172/JCI42328>
- Rebustini, I.T., Myers, C., Lassiter, K.S., Surmak, A., Szabova, L., Holmbeck, K., Pedchenko, V., Hudson, B.G., Hoffman, M.P., 2009. MT2-MMP-dependent release of collagen IV NC1 domains regulates submandibular gland branching morphogenesis. *Dev Cell* 17, 482–493. <https://doi.org/10.1016/j.devcel.2009.07.016>
- Riento, K., Ridley, A.J., 2003. ROCKs: multifunctional kinases in cell behaviour. *Nat Rev Mol Cell Biol* 4, 446–456. <https://doi.org/10.1038/nrm1128>
- Rintanen, N., Karjalainen, M., Alanko, J., Paavolainen, L., Mäki, A., Nissinen, L., Lehkonen, M., Kallio, K., Cheng, R.H., Upla, P., Ivaska, J., Marjomäki, V., 2012. Calpains promote  $\alpha 2\beta 1$  integrin turnover in nonrecycling integrin pathway. *MBoC* 23, 448–463. <https://doi.org/10.1091/mbc.e11-06-0548>
- Riso, E.-M., Kaasik, P., Seene, T., 2016. Remodelling of Skeletal Muscle Extracellular Matrix: Effect of Unloading and Reloading. *Composition and Function of the Extracellular Matrix in the Human Body*. <https://doi.org/10.5772/62295>
- Roignot, J., Peng, X., Mostov, K., 2013. Polarity in Mammalian Epithelial Morphogenesis. *Cold Spring Harbor Perspectives in Biology* 5, a013789–a013789. <https://doi.org/10.1101/cshperspect.a013789>
- Romero-Pozuelo, J., Figlia, G., Kaya, O., Martin-Villalba, A., Teleanu, A.A., 2020. Cdk4 and Cdk6 Couple the Cell-Cycle Machinery to Cell Growth via mTORC1. *Cell Reports* 31, 107504. <https://doi.org/10.1016/j.celrep.2020.03.068>
- Roovers, K., Davey, G., Zhu, X., Bottazzi, M.E., Assoian, R.K., 1999.  $\alpha 5\beta 1$  Integrin Controls Cyclin D1 Expression by. *Molecular Biology of the Cell* 10, 8.
- Sabatelli, P., Bonaldo, P., Lattanzi, G., Braghetta, P., Bergamin, N., Capanni, C., Mattioli, E., Columbaro, M., Ognibene, A., Pepe, G., Bertini, E., Merlini, L., Maraldi, N.M., Squarzone, S., 2001. Collagen VI deficiency affects the organization of fibronectin in the extracellular matrix of cultured fibroblasts. *Matrix Biology* 20, 475–486. [https://doi.org/10.1016/S0945-053X\(01\)00160-3](https://doi.org/10.1016/S0945-053X(01)00160-3)
- Sabatier, L., Chen, D., Fagotto-Kaufmann, C., Hubmacher, D., McKee, M.D., Annis, D.S., Mosher, D.F., Reinhardt, D.P., 2009. Fibrillin Assembly Requires Fibronectin. *MBoC* 20, 846–858. <https://doi.org/10.1091/mbc.e08-08-0830>
- Saby, C., Collin, G., Sinane, M., Buache, E., Van Gulick, L., Saltel, F., Maquoi, E., Morjani, H., 2019. DDR1 and MT1-MMP Expression Levels Are Determinant for Triggering BIK-Mediated Apoptosis by 3D Type I Collagen Matrix in Invasive Basal-Like Breast Carcinoma Cells. *Front. Pharmacol.* 10, 462. <https://doi.org/10.3389/fphar.2019.00462>
- Sakaue-Sawano, A., Kurokawa, H., Morimura, T., Hanyu, A., Hama, H., Osawa, H., Kashiwagi, S., Fukami, K., Miyata, T., Miyoshi, H., Imamura, T., Ogawa, M., Masai, H., Miyawaki, A., 2008. Visualizing

- Spatiotemporal Dynamics of Multicellular Cell-Cycle Progression. *Cell* 132, 487–498. <https://doi.org/10.1016/j.cell.2007.12.033>
- Sałacińska, K., Pinkier, I., Rutkowska, L., Chlebna-Sokół, D., Jakubowska-Pietkiewicz, E., Michałus, I., Kępczyński, Ł., Salachna, D., Jamsheer, A., Bukowska-Olech, E., Jaszczuk, I., Jakubowski, L., Gach, A., 2021. Novel Mutations Within Collagen Alpha1(I) and Alpha2(I) Ligand-Binding Sites, Broadening the Spectrum of Osteogenesis Imperfecta – Current Insights Into Collagen Type I Lethal Regions. *Frontiers in Genetics* 12.
- Salemi, Z., Azizi, R., Fallahian, F., Aghaei, M., 2021. Integrin  $\alpha 2\beta 1$  inhibition attenuates prostate cancer cell proliferation by cell cycle arrest, promoting apoptosis and reducing epithelial–mesenchymal transition. *Journal of Cellular Physiology* 236, 4954–4965. <https://doi.org/10.1002/jcp.30202>
- Sameni, M., Doseescu, J., Moin, K., Sloane, B.F., 2003. Functional Imaging of Proteolysis: Stromal and Inflammatory Cells Increase Tumor Proteolysis 2, 17.
- Saqcena, M., Menon, D., Patel, D., Mukhopadhyay, S., Chow, V., Foster, D.A., 2013. Amino Acids and mTOR Mediate Distinct Metabolic Checkpoints in Mammalian G1 Cell Cycle. *PLoS ONE* 8, e74157. <https://doi.org/10.1371/journal.pone.0074157>
- Scales, T.M.E., Jayo, A., Obara, B., Holt, M.R., Hotchin, N.A., Berditchevski, F., Parsons, M., 2013.  $\alpha 3\beta 1$  integrins regulate CD151 complex assembly and membrane dynamics in carcinoma cells within 3D environments. *Oncogene* 32, 3965–3979. <https://doi.org/10.1038/onc.2012.415>
- Schiavinato, A., Keene, D.R., Wohl, A.P., Corallo, D., Colombatti, A., Wagener, R., Paulsson, M., Bonaldo, P., Sengle, G., 2016. Targeting of EMILIN-1 and EMILIN-2 to Fibrillin Microfibrils Facilitates their Incorporation into the Extracellular Matrix. *Journal of Investigative Dermatology* 136, 1150–1160. <https://doi.org/10.1016/j.jid.2016.02.021>
- Schindelin, J., Arganda-Carreras, I., Frise, E., Kaynig, V., Longair, M., Pietzsch, T., Preibisch, S., Rueden, C., Saalfeld, S., Schmid, B., Tinevez, J.-Y., White, D.J., Hartenstein, V., Eliceiri, K., Tomancak, P., Cardona, A., 2012. Fiji: an open-source platform for biological-image analysis. *Nat Methods* 9, 676–682. <https://doi.org/10.1038/nmeth.2019>
- Senbanjo, L.T., Chellaiah, M.A., 2017. CD44: A Multifunctional Cell Surface Adhesion Receptor Is a Regulator of Progression and Metastasis of Cancer Cells. *Front Cell Dev Biol* 5. <https://doi.org/10.3389/fcell.2017.00018>
- Sharma, P., Ng, C., Jana, A., Padhi, A., Szymanski, P., Lee, J.S.H., Behkam, B., Nain, A.S., 2017. Aligned fibers direct collective cell migration to engineer closing and nonclosing wound gaps. *MBoC* 28, 2579–2588. <https://doi.org/10.1091/mbc.e17-05-0305>
- Sherr, C.J., Bartek, J., 2017. Cell Cycle–Targeted Cancer Therapies. *Annu. Rev. Cancer Biol.* 1, 41–57. <https://doi.org/10.1146/annurev-cancerbio-040716-075628>
- Shi, F., Sottile, J., 2011. MT1-MMP regulates the turnover and endocytosis of extracellular matrix fibronectin. *Journal of Cell Science* 124, 4039–4050. <https://doi.org/10.1242/jcs.087858>
- Shi, F., Sottile, J., 2008a. Caveolin-1-dependent  $\alpha 1$  integrin endocytosis is a critical regulator of fibronectin turnover. *Journal of Cell Science* 121, 2360–2371. <https://doi.org/10.1242/jcs.014977>
- Shi, F., Sottile, J., 2008b. Caveolin-1-dependent  $\alpha 1$  integrin endocytosis is a critical regulator of fibronectin turnover. *Journal of Cell Science* 121, 2360–2371. <https://doi.org/10.1242/jcs.014977>
- Shi, M., Pedchenko, V., Greer, B.H., Van Horn, W.D., Santoro, S.A., Sanders, C.R., Hudson, B.G., Eichman, B.F., Zent, R., Pozzi, A., 2012. Enhancing Integrin  $\alpha 1$  Inserted (I) Domain Affinity to Ligand Potentiates Integrin  $\alpha 1\beta 1$ -mediated Down-regulation of Collagen Synthesis. *Journal of Biological Chemistry* 287, 35139–35152. <https://doi.org/10.1074/jbc.M112.358648>
- Shield, K., Riley, C., Quinn, M.A., Rice, G.E., Ackland, M.L., Ahmed, N., 2007.  $\alpha 2\beta 1$  integrin affects metastatic potential of ovarian carcinoma spheroids by supporting disaggregation and proteolysis. *J Carcinog* 6, 11. <https://doi.org/10.1186/1477-3163-6-11>

- Shimoi, T., Hamada, A., Yamagishi, M., Hirai, M., Yoshida, M., Nishikawa, T., Sudo, K., Shimomura, A., Noguchi, E., Yunokawa, M., Yonemori, K., Shimizu, C., Kinoshita, T., Fukuda, T., Fujiwara, Y., Tamura, K., 2018. PIK3CA mutation profiling in patients with breast cancer, using a highly sensitive detection system. *Cancer Sci* 109, 2558–2566. <https://doi.org/10.1111/cas.13696>
- Shiovitz, S., Korde, L.A., 2015. Genetics of breast cancer: a topic in evolution. *Annals of Oncology* 26, 1291–1299. <https://doi.org/10.1093/annonc/mdv022>
- Singh, P., Carraher, C., Schwarzbauer, J.E., 2010. Assembly of Fibronectin Extracellular Matrix. *Annual Review of Cell and Developmental Biology* 26, 397–419. <https://doi.org/10.1146/annurev-cellbio-100109-104020>
- Sökeland, G., Schumacher, U., 2019. The functional role of integrins during intra- and extravasation within the metastatic cascade. *Molecular Cancer* 18, 12. <https://doi.org/10.1186/s12943-018-0937-3>
- Sottile, J., Chandler, J., 2005. Fibronectin Matrix Turnover Occurs through a Caveolin-1-dependent Process. *MBoC* 16, 757–768. <https://doi.org/10.1091/mbc.e04-08-0672>
- Sottile, J., Shi, F., Rublyevska, I., Chiang, H.-Y., Lust, J., Chandler, J., 2007. Fibronectin-dependent collagen I deposition modulates the cell response to fibronectin. *American Journal of Physiology-Cell Physiology* 293, C1934–C1946. <https://doi.org/10.1152/ajpcell.00130.2007>
- Subbaram, S., DiPersio, C.M., 2011. Integrin  $\alpha 3\beta 1$  as a breast cancer target. *Expert Opinion on Therapeutic Targets* 15, 1197–1210. <https://doi.org/10.1517/14728222.2011.609557>
- Sun, M., Luong, G., Plastikwala, F., Sun, Y., 2020. Control of Rab7a activity and localization through endosomal type Igamma PIP 5-kinase is required for endosome maturation and lysosome function. *The FASEB Journal* 34, 2730–2748. <https://doi.org/10.1096/fj.201901830R>
- Sung, B.H., Ketova, T., Hoshino, D., Zijlstra, A., Weaver, A.M., 2015. Directional cell movement through tissues is controlled by exosome secretion. *Nat Commun* 6, 7164. <https://doi.org/10.1038/ncomms8164>
- Sung, B.H., Weaver, A.M., 2011. Regulation of lysosomal secretion by cortactin drives fibronectin deposition and cell motility. *Bioarchitecture* 1, 257–260. <https://doi.org/10.4161/bioa.1.6.19197>
- Sung, B.H., Zhu, X., Kaverina, I., Weaver, A.M., 2011. Cortactin Controls Cell Motility and Lamellipodial Dynamics by Regulating ECM Secretion. *Current Biology* 21, 1460–1469. <https://doi.org/10.1016/j.cub.2011.06.065>
- Swain, S.M., Baselga, J., Kim, S.-B., Ro, J., Semiglazov, V., Campone, M., Ciruelos, E., Ferrero, J.-M., Schneeweiss, A., Heeson, S., Clark, E., Ross, G., Benyunes, M.C., Cortés, J., 2015. Pertuzumab, Trastuzumab, and Docetaxel in HER2-Positive Metastatic Breast Cancer. *N Engl J Med* 372, 724–734. <https://doi.org/10.1056/NEJMoa1413513>
- Tan, K., Lawler, J., 2009. The interaction of Thrombospondins with extracellular matrix proteins. *J Cell Commun Signal* 3, 177–187. <https://doi.org/10.1007/s12079-009-0074-2>
- Tang, P., Tse, G.M., 2016. Immunohistochemical Surrogates for Molecular Classification of Breast Carcinoma: A 2015 Update. *Archives of Pathology & Laboratory Medicine* 140, 806–814. <https://doi.org/10.5858/arpa.2015-0133-RA>
- Taubenberger, A.V., Baum, B., Matthews, H.K., 2020. The Mechanics of Mitotic Cell Rounding. *Front. Cell Dev. Biol.* 8, 687. <https://doi.org/10.3389/fcell.2020.00687>
- Teckchandani, A., Toida, N., Goodchild, J., Henderson, C., Watts, J., Wollscheid, B., Cooper, J.A., 2009. Quantitative proteomics identifies a Dab2/integrin module regulating cell migration. *Journal of Cell Biology* 186, 99–111. <https://doi.org/10.1083/jcb.200812160>
- Theisen, U., Straube, E., Straube, A., 2012. Directional Persistence of Migrating Cells Requires Kif1C-Mediated Stabilization of Trailing Adhesions. *Developmental Cell* 23, 1153–1166. <https://doi.org/10.1016/j.devcel.2012.11.005>
- Theocharidis, G., Drymoussi, Z., Kao, A.P., Barber, A.H., Lee, D.A., Braun, K.M., Connelly, J.T., 2016. Type VI Collagen Regulates Dermal Matrix Assembly and Fibroblast Motility. *Journal of Investigative Dermatology* 136, 74–83. <https://doi.org/10.1038/JID.2015.352>

- Theocharis, A.D., Skandalis, S.S., Gialeli, C., Karamanos, N.K., 2016. Extracellular matrix structure. *Advanced Drug Delivery Reviews* 97, 4–27. <https://doi.org/10.1016/j.addr.2015.11.001>
- Thu, K., Soria-Bretones, I., Mak, T., Cescon, D., 2018. Targeting the cell cycle in breast cancer: towards the next phase. *Cell Cycle* 17, 1871–1885. <https://doi.org/10.1080/15384101.2018.1502567>
- Tian, T., Li, X., Zhang, J., 2019. mTOR Signaling in Cancer and mTOR Inhibitors in Solid Tumor Targeting Therapy. *International Journal of Molecular Sciences* 20, 755. <https://doi.org/10.3390/ijms20030755>
- Tillet, E., Wiedemann, H., Golbik, R., Pan, T.-C., Zhang, R.-Z., Mann, K., Chu, M.-L., Timpl, R., 1994. Recombinant expression and structural and binding properties of alpha1(VI) and alpha2(VI) chains of human collagen type VI. *Eur J Biochem* 221, 177–187. <https://doi.org/10.1111/j.1432-1033.1994.tb18727.x>
- To, W.S., Midwood, K.S., 2011. Identification of Novel and Distinct Binding Sites within Tenascin-C for Soluble and Fibrillar Fibronectin. *Journal of Biological Chemistry* 286, 14881–14891. <https://doi.org/10.1074/jbc.M110.189019>
- Trotter, E.W., Hagan, I.M., 2020. Release from cell cycle arrest with Cdk4/6 inhibitors generates highly synchronized cell cycle progression in human cell culture. *Open Biol.* 10, 200200. <https://doi.org/10.1098/rsob.200200>
- Uhler, C., Shivashankar, G.V., 2017. Regulation of genome organization and gene expression by nuclear mechanotransduction. *Nat Rev Mol Cell Biol* 18, 717–727. <https://doi.org/10.1038/nrm.2017.101>
- Uhlman, A., Folkers, K., Liston, J., Pancholi, H., Hinton, A., 2017. Effects of Vacuolar H<sup>+</sup>-ATPase Inhibition on Activation of Cathepsin B and Cathepsin L Secreted from MDA-MB231 Breast Cancer Cells. *Cancer Microenvironment* 10, 49–56. <https://doi.org/10.1007/s12307-017-0196-7>
- Upla, P., Marjomaki, V., Kankaanpaa, P., Ivaska, J., Hyypia, T., 2004. Clustering Induces a Lateral Redistribution of  $\alpha_2\beta_1$  Integrin from Membrane Rafts to Caveolae and Subsequent Protein Kinase C– dependent Internalization. *Molecular Biology of the Cell* 15, 12.
- Valenzuela, C.A., Vargas, L., Martinez, V., Bravo, S., Brown, N.E., 2017. Palbociclib-induced autophagy and senescence in gastric cancer cells. *Experimental Cell Research* 360, 390–396. <https://doi.org/10.1016/j.yexcr.2017.09.031>
- Vassilev, L.T., 2006. Cell Cycle Synchronization at the G<sub>2</sub>/M Phase Border by Reversible Inhibition of CDK1. *Cell Cycle* 5, 2555–2556. <https://doi.org/10.4161/cc.5.22.3463>
- Vijayaraghavan, S., Karakas, C., Doostan, I., Chen, X., Bui, T., Yi, M., Raghavendra, A.S., Zhao, Y., Bashour, S.I., Ibrahim, N.K., Karuturi, M., Wang, J., Winkler, J.D., Amaravadi, R.K., Hunt, K.K., Tripathy, D., Keyomarsi, K., 2017. CDK4/6 and autophagy inhibitors synergistically induce senescence in Rb positive cytoplasmic cyclin E negative cancers. *Nat Commun* 8, 15916. <https://doi.org/10.1038/ncomms15916>
- Wagner, V., Gil, J., 2020. Senescence as a therapeutically relevant response to CDK4/6 inhibitors. *Oncogene* 39, 5165–5176. <https://doi.org/10.1038/s41388-020-1354-9>
- Waks, A.G., Winer, E.P., 2019. Breast Cancer Treatment: A Review. *JAMA* 321, 288. <https://doi.org/10.1001/jama.2018.19323>
- Walker, C., Mojares, E., del Río Hernández, A., 2018. Role of Extracellular Matrix in Development and Cancer Progression. *IJMS* 19, 3028. <https://doi.org/10.3390/ijms19103028>
- Wang, Y., Arjonen, A., Pouwels, J., Ta, H., Pausch, P., Bange, G., Engel, U., Pan, X., Fackler, O.T., Ivaska, J., Grosse, R., 2015. Formin-like 2 Promotes  $\beta_1$ -Integrin Trafficking and Invasive Motility Downstream of PKC $\alpha$ . *Developmental Cell* 34, 475–483. <https://doi.org/10.1016/j.devcel.2015.06.015>
- Wang, Y., Shenouda, S., Baranwal, S., Rathinam, R., Jain, P., Bao, L., Hazari, S., Dash, S., Alahari, S.K., 2011. Integrin subunits alpha5 and alpha6 regulate cell cycle by modulating the chk1 and Rb/E2F pathways to affect breast cancer metastasis. *Molecular Cancer* 10, 84. <https://doi.org/10.1186/1476-4598-10-84>

- Wang, Z., 2021. Regulation of Cell Cycle Progression by Growth Factor-Induced Cell Signaling. *Cells* 10, 3327. <https://doi.org/10.3390/cells10123327>
- Wewer, U.M., Shaw, L.M., Albrechtsen, R., Mercuriot, A.M., 1997. The Integrin  $\alpha 6\beta 1$  Promotes the Survival of Metastatic Human Breast Carcinoma Cells in Mice 151, 8.
- Whatcott, C.J., Diep, C.H., Jiang, P., Watanabe, A., LoBello, J., Sima, C., Hostetter, G., Shepard, H.M., Von Hoff, D.D., Han, H., 2015. Desmoplasia in Primary Tumors and Metastatic Lesions of Pancreatic Cancer. *Clin Cancer Res* 21, 3561–3568. <https://doi.org/10.1158/1078-0432.CCR-14-1051>
- Wienke, D., Davies, G.C., Johnson, D.A., Sturge, J., Lambros, M.B.K., Savage, K., Elsheikh, S.E., Green, A.R., Ellis, I.O., Robertson, D., Reis-Filho, J.S., Isacke, C.M., 2007. The Collagen Receptor Endo180 (CD280) Is Expressed on Basal-like Breast Tumor Cells and Promotes Tumor Growth In vivo. *Cancer Res* 67, 10230–10240. <https://doi.org/10.1158/0008-5472.CAN-06-3496>
- Wienke, D., MacFadyen, J.R., Isacke, C.M., 2003. Identification and Characterization of the Endocytic Transmembrane Glycoprotein Endo180 as a Novel Collagen Receptor. *MBoC* 14, 3592–3604. <https://doi.org/10.1091/mbc.e02-12-0814>
- Williams, C., Lin, C.-Y., 2013. Oestrogen receptors in breast cancer: basic mechanisms and clinical implications. *Ecancermedicalscience* 7. <https://doi.org/10.3332/ecancer.2013.370>
- Willumsen, N., Ali, S.M., Leitzel, K., Drabick, J.J., Yee, N., Polimera, H.V., Nagabhairu, V., Krecko, L., Ali, Ayesha, Maddukuri, A., Moku, P., Ali, Aamnah, Poulouse, J., Menon, H., Pancholy, N., Costa, L., Karsdal, M.A., Lipton, A., 2019. Collagen fragments quantified in serum as measures of desmoplasia associate with survival outcome in patients with advanced pancreatic cancer. *Sci Rep* 9, 19761. <https://doi.org/10.1038/s41598-019-56268-3>
- Wilson, B.J., Allen, J.L., Caswell, P.T., 2018. Vesicle trafficking pathways that direct cell migration in 3D matrices and in vivo. *Traffic* 19, 899–909. <https://doi.org/10.1111/tra.12605>
- Winkler, J., Abisoye-Ogunniyan, A., Metcalf, K.J., Werb, Z., 2020. Concepts of extracellular matrix remodelling in tumour progression and metastasis. *Nat Commun* 11, 5120. <https://doi.org/10.1038/s41467-020-18794-x>
- Withana, N.P., Blum, G., Sameni, M., Slaney, C., Anbalagan, A., Olive, M.B., Bidwell, B.N., Edgington, L., Wang, L., Moin, K., Sloane, B.F., Anderson, R.L., Bogyo, M.S., Parker, B.S., 2012. Cathepsin B Inhibition Limits Bone Metastasis in Breast Cancer. *Cancer Res* 72, 1199–1209. <https://doi.org/10.1158/0008-5472.CAN-11-2759>
- Withana, N.P., Blum, G., Sameni, M., Slaney, C., Anbalagan, A., Olive, M.B., Bidwell, B.N., Edgington, L., Wang, L., Moin, K., Sloane, B.F., Anderson, R.L., Bogyo, M.S., Parker, B.S., n.d. Cathepsin B Inhibition Limits Bone Metastasis in Breast Cancer. *Cancer Research* 12.
- Wu, Y.J., Muldoon, L.L., Gahramanov, S., Kraemer, D.F., Marshall, D.J., Neuwelt, E.A., 2012. Targeting  $\alpha V$ -integrins decreased metastasis and increased survival in a nude rat breast cancer brain metastasis model. *J Neurooncol* 110, 27–36. <https://doi.org/10.1007/s11060-012-0942-0>
- Xu, S., Xu, H., Wang, W., Li, S., Li, H., Li, T., Zhang, W., Yu, X., Liu, L., 2019. The role of collagen in cancer: from bench to bedside. *J Transl Med* 17, 309. <https://doi.org/10.1186/s12967-019-2058-1>
- Yang, J., Nie, J., Ma, X., Wei, Y., Peng, Y., Wei, X., 2019. Targeting PI3K in cancer: mechanisms and advances in clinical trials. *Mol Cancer* 18, 26. <https://doi.org/10.1186/s12943-019-0954-x>
- Yano, S., Miwa, S., Mii, S., Hiroshima, Y., Uehara, F., Yamamoto, M., Kishimoto, H., Tazawa, H., Bouvet, M., Fujiwara, T., Hoffman, R.M., 2014. Invading cancer cells are predominantly in  $G_0/G_1$  resulting in chemoresistance demonstrated by real-time FUCCI imaging. *Cell Cycle* 13, 953–960. <https://doi.org/10.4161/cc.27818>
- Yao, E.S., Zhang, H., Chen, Y.-Y., Lee, B., Chew, K., Moore, D., Park, C., 2007. Increased  $\beta 1$  Integrin Is Associated with Decreased Survival in Invasive Breast Cancer. *Cancer Res* 67, 659–664. <https://doi.org/10.1158/0008-5472.CAN-06-2768>
- Yellen, P., Saqcena, M., Salloum, D., Feng, J., Preda, A., Xu, L., Rodrik-Outmezguine, V., Foster, D.A., 2011. High-dose rapamycin induces apoptosis in human cancer cells by dissociating mTOR

- complex 1 and suppressing phosphorylation of 4E-BP1. *Cell Cycle* 10, 3948–3956. <https://doi.org/10.4161/cc.10.22.18124>
- Yersal, O., Barutca, S., 2014. Biological subtypes of breast cancer: Prognostic and therapeutic implications. *World J Clin Oncol* 5, 412–424. <https://doi.org/10.5306/wjco.v5.i3.412>
- Yhee, J.Y., Yoon, H.Y., Kim, H., Jeon, S., Hergert, P., Im, J., Panyam, J., Kim, K., Nho, R.S., 2017. The effects of collagen-rich extracellular matrix on the intracellular delivery of glycol chitosan nanoparticles in human lung fibroblasts. *Int J Nanomedicine* 12, 6089–6105. <https://doi.org/10.2147/IJN.S138129>
- Yue, B., 2014. Biology of the Extracellular Matrix: An Overview. *J Glaucoma* S20–S23. <https://doi.org/10.1097/IJG.0000000000000108>
- Zanotelli, M.R., Goldblatt, Z.E., Miller, J.P., Bordeleau, F., Li, J., VanderBurgh, J.A., Lampi, M.C., King, M.R., Reinhart-King, C.A., 2018. Regulation of ATP utilization during metastatic cell migration by collagen architecture. *MBoC* 29, 1–9. <https://doi.org/10.1091/mbc.E17-01-0041>
- Zeltz, C., Gullberg, D., 2016. The integrin–collagen connection – a glue for tissue repair? *Journal of Cell Science* 129, 1284–1284. <https://doi.org/10.1242/jcs.188672>
- Zielke, N., Edgar, B.A., 2015. Fucci sensors: powerful new tools for analysis of cell proliferation. *WIREs Developmental Biology* 4, 469–487. <https://doi.org/10.1002/wdev.189>
- Zuo, X., Yang, Y., Zhang, Y., Zhang, Z., Wang, X., Shi, Y., 2019. Platelets promote breast cancer cell MCF-7 metastasis by direct interaction: surface integrin  $\alpha 2\beta 1$ -contacting-mediated activation of Wnt- $\beta$ -catenin pathway. *Cell Commun Signal* 17, 142. <https://doi.org/10.1186/s12964-019-0464-x>